RADIAL GAS HOLDUP PROFILE AND MIXING IN THE COLLECTION ZONE OF FLOTATION COLUMNS

Manqiu Xu

A thesis submitted to the
Faculty of Graduate Studies and Research
in partial fulfilment of the requirements for
the degree of
Doctor of Philosophy

Dept. of Mining and Metallurgical Engineering
McGill University
Montreal, Canada

To those people who lost their lives fighting for the democratization of human society.

In particular, to those young people who lost their lives in Taianmen Square, Beijing, in 1989.

ABSTRACT

Radial gas holdup profiles were determined in 50cm and 91cm dia. flotation columns. The local gas holdup was measured using an electrical conductivity technique, which is described in detail. The effect of gas rate and axial location on the profiles was investigated. The relative variation in gas holdup was about 20%. The profiles were axially symmetric but of complex shape: parabolic, saddle and 'W' shapes were observed. For the case of a parabolic profile, the shear stress model was solved to give liquid circulation velocity profiles; no solution was found for the other gas holdup profile shapes.

Measurement of radial gas holdup profiles may prove useful in evaluating sparger systems. For example, in the pilot column, one off-centre sparger gave a non-symmetrical shape but nevertheless did distribute the gas relatively evenly.

Liquid residence time distributions (RTD) were measured for various operating and design conditions using the pulse tracer technique. Application of the one-dimensional plug flow axial dispersion model and the use of the vessel dispersion number N_d to quantify the degree of mixing was evaluated. A numerical solution to the axial dispersion model with closed-closed boundary conditions using the finite difference method is recommended for column RTD studies. Compartment models were also evaluated: the N perfect tanks-in-series model did not fit the data but a backflow compartment model was successful.

The effect of gas rate, liquid rate, column length, feed percent solids and column verticality on N_d was studied. It was found that N_d increased with gas rate and decreased with liquid rate and column length. Percent solids and verticality had a minor effect on N_d. New correlations to predict N_d were developed and compared with previous correlations.

PROFIL DE RÉTENTIONS RADIALES DE GAZ ET EFFET DE MÉLANGE DANS LA ZONE DE COLLECTION POUR DES COLONNES DE FLOTTATION

RÉSUMÉ

On a établi les profils de rétention radiales de gaz dans une colonne de flottation de laboratoire de grande dimension et dans une colonne de flottation d'usine pilote. On a mesuré la rétention de gaz localisé en utilisant la technique basée sur la conductivité électrique, technique qui y est décrite en détails. L'effet dû à la variation du volume du gaz et de différents systèmes générateurs de bulles a été étudié en profondeur. La forme des profils est complexe. Ces derniers varient de la forme parabolique, au 'W', en passant par une courbe en forme de selle à cheval. A l'aide d'un profil parabolique de rétention radiale, des profils de vélocité de circulation du liquide furent calculés en utilisant le modèle de contrainte en cisaillement.

Connaissant les profils de rétentions radiales du gaz, le rendement des systèmes générateurs de bulles peuvent être évalués. Les résultats ont montré que ces profils de rétentions radiales du gaz n'étaient pas symétriques si un ou plusieurs gicleurs d'air étaient fermés ou inopérants.

On a mesuré les distributions des temps de séjour du liquide pour différentes conditions d'opération et de design en utilisant la technique d'un traceur injecté instantanément. L'utilisation du modèle uni-dimensionnel de dispersion axiale à écoulement bouchon fut rigoureusement étudiée et décrite. En général, cinq méthodes expérimentales sont disponibles et il y a cinq solutions correspondant au modèle de dispersion axiale. En utilisant la méthode des différences finies, on a développé un modèle de dispersion uniaxiale avec coefficient de diffusion nul aux deux extrémités. On

suggère cette solution pour des études de distribution des temps de séjour. Le modèle de dispersion axiale a été rigoureusement comparée avec un modèle de réservoirs en série et un modèle de reflux compartimenté. On a découvert qu'il n'y a pas beaucoup de différences entre un modèle de dispersion axiale et un modèle de reflux compartimenté quoique le premier n'utilise qu'un seul paramètre, i.e. le nombre de dispersion en réacteur N_d, pour décrire le degré de mélange alors que l'autre utilise deux paramètres, i.e. le ratio de reflux λ et le nombre de compartiments n. Le modèle de réservoirs en série ne concorde pas avec la distribution des temps de séjour de la présente étude.

On a étudié l'effet du débit du gaz, du débit du liquide, de la hauteur de la colonne, du pourcentage de solides et de la verticalité de la colonne sur le nombre de dispersion du réacteur liquide. On a trouvé que ce nombre s'accroît avec le débit du gaz mais décroît avec le débit du liquide. La présence de particules solides dans l'alimentation réduit légèrement le mélange du liquide. Une nouvelle corrélation entre le nombre de dispersion du réacteur et le débit du gaz, du liquide, le pourcentage de solides et le ratio longueur versus diamètre de la colonne a été proposée et comparée aux corrélations précédentes. On nota que d'autres chercheurs lors de recherches précédentes n'ont pas inclus l'effet du débit du liquide et de la longueur de la colonne.

ACKNOWLEDGEMENTS

This work would not be completed without recognizing the essential contributions of many people whose names do not appear on the title page. First of all, I am indebted to two people:

My wife, Lilan, for her support, understanding throughout the past three years, and for sharing the excitement of raising our daughter, Lisha.

My supervisor, Prof. J.A. Finch, for his enthusiasm, generosity, keen interest, excellent advice and constant encouragement throughout the research program.

As well, I gratefully acknowledge Prof. A.R. Laplante for helpful discussion and advice. Discussions with Prof. G.S. Dobby, Dr. C.O. Gomez, Dr. J.B. Yianatos, Dr. R. Espinosa and Dr. S.R. Rao is also acknowledged.

I like to thank my colleagues at McGill Mineral Processing group for discussion and help. The assistance of M. Leroux in some test work and M. Knoepfel in building the experimental apparatus is also gratefully acknowledged.

I am sincerely grateful to Dr. B.J. Huls, Falconbridge Limited, for providing me the chance to do pilot plant test work.

TABLE OF CONTENTS

ABSTRACT i
RÉSUMÉ ii
ACKNOWLEDGEMENTS iv
TABLE OF CONTENTS v
NOMENCLATURE x
LIST OF FIGURES xiv
LIST OF TABLES xxii
LIST OF APPENDICES xxiii

CHAPTER 1 INTRODUCTION

1.1 Flotation Column Development 1
1.2 Description and Advantages of Flotation Columns 2
1.3 Bubble Generation and Modification in Flotation Columns 4
1.4 Objectives of the Present Work 8
1.7 Structure of the Thesis 12

CHAPTER 2 HYDRODYNAMICS OF GAS/WATER SYSTEM

2.1 General Observations 14
2.2 Gas and Gas Holdup 17
2.2.1 Measurement of Gas Holdup 18
2.2.2 Effect of Operating Variables 18
2.3 Bubble Diameter 19
2.4 Bubbly Flow Model Development 20
2.4.1 Slip Velocity in A Bubble Swarm 20
2.4.2 Terminal Velocity of A Single Bubble 22

2.4.3 Bubbly Flow Model 23
2.5 Applications of Bubbly Flow Model 25
2.5.1 Correlating Gas Holdup vs. Gas Rate 25
2.5.2 Correlating Bias rate vs. Gas Rate 26
2.5.3 Estimating Bubble Size 26
2.5.4 Effect of Solids on Gas Holdup 29
2.6 Column Limiting Operating Conditions 31

CHAPTER 3 HOLDUP DISTRIBUTION AND LIQUID CIRCULATION

3.1 General Observations 32
3.2 Radial Gas Holdup Variation 34
3.2.1 Parabolic Radial Gas Holdup Profile 35
3.2.2 Saddle-Shaped Radial Gas Holdup Profile 36
3.3 Liquid Circulation Models 38
3.3.1 Model 1: Shear Stress Model 39
3.3.2 Model 2: Momentum Balance 46
3.3.4 Model 3: Energy Balance 48

CHAPTER 4 MIXING

4.1 Significance of Mixing in Column Flotation 49
4.2 Phase Mixing Theories 50
4.2.1 Liquid Phase Radial Mixing 51
4.2.2 Gas Phase Mixing 53
4.2.3 Solid Phase Mixing 55
4.3 Mixing Models 56
4.3.1 Axial Dispersion Models 56
Solution 1: A Batch System 62
Solution 2: An Open Vessel 63

Solution 3: A Closed Vessel 65
Solution 4: Step Tracer Injection 74
Solution 5: Steady-State Backmixing 76
4.3.2 Tanks-in-Series Model 78
4.3.3 Backflow Compartment Model 80
4.4 Comparison between Axial Dispersion Model and Compartment Model 84
4.5 Fitting RTD to Mixing Models 86
4.5.1 Moments Matching 87
4.5.2 Direct Search (Least Squares) 87

CHAPTER 5 EXPERIMENTAL SET-UP AND TECHNIQUES

5.1 Experimental Columns 89
5.2 Sparger System Design and Gas Distribution 92
5.2.1 Sparger System Design 92
5.2.2 Gas Distribution 94
5.3 Theory and Application of Electrical Conductivity Measurement . . . 95
5.3.1 Background Principle 95
5.3.2 Conductivity of Liquid with Dispersed Gas Bubbles 96
5.3.3 Local Gas Holdup Measurement 99
5.3.4 Local Gas Holdup Measuring Probes 104
5.4 Axial Gas Holdup Measurement 107
5.5 Measurement of Liquid RTD 109
5.5.1 Experimental Techniques 109
5.5.2 Tracer Selection 111
5.6 Data Acquisition and Processing 113

CHAPTER 6 RESULTS: GAS HOLDUP DISTRIBUTION

6.1 Axial Gas Holdup Profiles 116

6.2 Radial Gas Holdup profiles 122
6.2.1 No Frother Addition 125
6.2.2 10ppm Frother Concentration 130
6.2.3 In the Pilot Flotation Column 133
6.3 Liquid Circulation Velocity Profiles 139

CHAPTER 7 RESULTS: MIXING

7.1 Testing Model Fit 141
7.1.1 Closed Vessel Numerical Solution with Open Vessel Analytical Solution 141
7.1.2 Age Distributions 146
7.1.3 Comparison between Axial Dispersion and Compartment Models 148
7.2 Effect of Variables on N_d 150
7.2.1 Batch Operation: Effect of Gas Rate 150
7.2.2 Continuous Operation. Effect of Gas and Liquid Rates . . . 151
7.2.3 Continuous Operation: Effect of Column Length 156
7.2.4 Continuous Operation: Effect of Column Verticality 158
7.2.5 Effect of Feed Solid Particles 159
7.3 Dispersion of Solid Particles 161
7.4 Data Analysis: Predicting N_d 162
7.4.1 Data Analysis 162
7.4.2 Estimating Vessel Dispersion Number 169

CHAPTER 8 DISCUSSION

8.1 Gas Holdup Distribution 172
8.1.1 Axial Gas Holdup Distribution 172
8.1.2 Radial Gas Holdup Distribution 173
8.2 Liquid Circulation Velocity Profile 175

8.3 Mixing Models 176
8.3.1 Axial Dispersion Model 176
8.3.2 Compartment Models 179
8.4 Liquid Dispersion 180
8.4.1 Experimental Results 180
8.4.2 Predicting Vessel Dispersion Number 181
8.5 Solid Dispersion 184

CHAPTER 9 CONCLUSIONS

9.1 Conclusions 185
9.2 Claims for Original Research 188
9.3 Suggestions for Future Work 189

REFERENCES 190
APPENDICES 201

NOMENCLATURE

A,B,C	coefficients or constants
$C(Z,t)$	tracer concentration at Z, t
C_f	tracer concentration in feed stream
C_0	initial tracer equilibrium concentration
d_c	column diameter, cm
d_b	bubble diameter, cm
d_p	particle diameter, μm
E_0	Eötvos number
E_l	liquid dispersion coefficient, cm^2/s
$E_{l,\alpha}$	liquid dispersion coefficient with an inclination (rad.)
$E_{l,S}$	liquid dispersion coefficient with feed solid percentage (wt.%)
E_{zg}	gas phase axial dispersion coefficient, cm^2/s
E_{rl}	radial dispersion coefficient of liquid phase, cm^2/s
$E(\theta,x)$	dimensionless tracer concentration at θ,x
$Erf(z)$	error function
$Erfc(z)$	complementary error function
$F_e(\theta_i)$	experimental dimensionless RTD
$F_m(\theta_i)$	model prediction of dimensionless RTD
g	acceleration due to gravity, cm/s^2
H_c	column collection zone height, cm
J_b	superficial bias rate, cm/s
J_f	superficial feed rate, cm/s
J_g	superficial gas rate, cm/s
J_l	superficial liquid downward rate, cm/s
K_c	conductance of continuous phase, siemens
K_e	conductance of gas/liquid mixture, siemens
k_c	flotation rate constant, min^{-1}; or conductivity of continuous phase, siemens/cm
k_e	conductivity of gas/liquid mixture, siemens/cm

L	length between two opposite electrodes, cm
M_o	Morton number
m	constant given by Equations (2.7) and (2.8) or $m=2$
n	constant or number of compartments in tanks-in-series model and in backflow compartment model
N_d	liquid vessel dispersion number, dimensionless and general usage
$N_{dcc}{}^{L}$	liquid vessel dispersion number for closed-closed boundary conditions, least squares fit (numerical solution to the axial dispersion model)
$N_{dcc}{}^{M}$	the same as $N_{dcc}{}^{L}$ but using the moments match fit.
$N_{doo}{}^{L}$	liquid vessel dispersion number for open-open boundary conditions, least squares fit (the analytical solution to the axial dispersion model)
$N_{doo}{}^{M}$	the same as $N_{doo}{}^{M}$ but using the moments match fit
N_{dt}	the vessel dispersion number obtained from tanks-in-series model
N_{dbc}	the vessel dispersion number obtained from backflow compartment model
ΔP	pressure drop between two levels ($\epsilon_g=0$)
ΔP_c	pressure drop between two levels ($\epsilon_g\neq 0$)
p	constant
Pe	Peclet number ($1/N_d$)
Q_g	volumetric gas flowrate, cm^3/s
Q_l	volumetric liquid flowrate, cm^3/s
Re_b	bubble Reynolds number
Re_p	particle Reynolds number
r	column radial distance from the centre, cm
R	column radius, cm
R_c	column collection zone recovery
S	solid percentage by weight
$T_l(\phi)$	axial shear stress at radius r from column centre, $g\cdot cm/s^2$
T_{lw}	axial shear stress at column wall, $g\cdot cm/s^2$

t	time, seconds
u_l	interstitial liquid rate [$=J_l/(1-\epsilon_g)$], cm/s
U_{sb}	bubble slip velocity, cm/s
U_{sl}	slurry interstitial velocity, cm/s
U_{sp}	particle slip velocity, cm/s
U_T	terminal rising velocity of a bubble, cm/s
$V_l(\phi)$	liquid circulation velocity at $\phi=r/R$, cm/s
V_{lc}	liquid circulation velocity at column centre $\phi=0$, cm/s
V_{lw}	liquid circulation velocity at column wall $\phi=1$, cm/s
V_r	bubble radial or lateral velocity, cm/s
x	dimensionless axial or vertical position, Z/H_c
Z	axial distance from tracer injection position to tracer detection position, cm

Greek Symbols

α	tilt angle in rad.
β	constant (Eq.5.3)
$\Gamma(n)$	gamma function
γ	relative conductivity, dimensionless
γ^*	relative conductance, dimensionless
δ	pulse tracer input, Dirac delta function
ϵ_g	fractional gas holdup
ϵ_{gf}	fractional gas holdup in the froth zone
ϵ_{gc}	local gas holdup at column centre
ϵ_{gw}	local gas holdup at wall ($\epsilon_{gw}=0$)
$\epsilon_g(\phi)$	local gas holdup at $\phi=r/R$
ϵ_s	fractional solids holdup
$\epsilon_g(t)$	gas holdup measured as a function of time
θ	dimensionless time (t/τ)
λ	backflow ratio in backflow compartment model

λ_n	*nth* positive root of Equation (4.23)
μ_l	liquid viscosity, g/cm·s
μ_{sl}	slurry viscosity, g/cm·s
ν_l	liquid kinematic viscosity (μ_l/ρ_l), cm^2/s
ν_T	turbulent kinematic viscosity, cm^2/s
π	pi (=3.1415926)
ρ_l	liquid density, g/cm^3
ρ_{sl}	slurry density, g/cm^3
ρ_b	density of bubble/particle aggregate, g/cm^3
ρ_g	gas density (=0)
$\rho(\phi)$	local density of gas/liquid mixture, g/cm^3
ρ_{gl}	average density of gas/liquid mixture, g/cm^3
σ_θ^2	dimensionless variance of RTD
τ	mean residence time, minutes
τ_p	particle mean residence time, minutes
Φ	sum of the squares of the deviations between experimental RTD and model RTD
ϕ	dimensionless radial position (r/R)
ω_b	gas eddy diffusivity
ℓ^2	mixing length used in Equation (3.22)

LIST OF FIGURES

Figure 1.1 Schematic illustration of a flotation column 3
Figure 1.2 Bubble generation by a porous sparger 4
Figure 1.3 Bubble generation in static shear contacting 5
Figure 1.4 Cominco's bubble generator 6
Figure 1.5 Schematic illustration of the Jameson cell 7
Figure 1.6 Packed flotation column (after Yang, 1988) 8
Figure 1.7 Hydrodynamics of the column collection zone 9
Figure 1.8 Mixing of the column collection zone 10
Figure 1.9 Four steps in the mixing studies of the column collection zone 11

Figure 2.1 Gas holdup as a function of gas rate: a general relationship (after Finch and Dobby, 1990) 15
Figure 2.2 Approximate dependence of flow regime on gas rate and column diameter (after Shah et al., 1982) 16
Figure 2.3 Methods of gas holdup measurement (after Finch and Dobby, 1990) 19
Figure 2.4 Bubbly flow model fit of gas holdup as a function of gas rate with m=2 (dashed line is model result where U_T=21cm/s) 25
Figure 2.5 Bias rate as a function of gas rate (curve c is plotted using the equation of Pal and Masliyah, 1990) 27
Figure 2.6 Illustration of bubble size estimation using the bubbly flow model 27
Figure 2.7 Effect of solids particles on gas holdup calculated using the bubbly flow model 30
Figure 2.8 Comparison of measured maximum gas rates for three phenomena (feed is used to control level; data from Xu et al., 1990a) 31

Figure 3.1 Induction of liquid circulation in a column 33
Figure 3.2 Gulf-stream liquid circulation 34
Figure 3.3 Parabolic radial gas holdup profiles calculated using Eq.(3.1) with various n values 35
Figure 3.4 Saddle-shaped radial gas holdup profiles (from Drew and Lahey, 1981; data from Serizawa et al., 1976) 37

Figure 3.5 Development of radial gas holdup profile as a function of axial distance from the initial profile (after Beyerlein et al., 1985) 38
Figure 3.6 Recirculation flow velocity profiles 39
Figure 3.7 Circulation velocity profiles calculated using shear stress model for Newtonian fluid 42
Figure 3.8 Circulation velocity profiles calculated from shear stress model: effect of gas holdup 43
Figure 3.9 Scheme for calculating circulation velocity profile using the shear stress model concern both viscosity and turbulence effect 45
Figure 3.10 Circulation velocity profiles for non-Newtonian fluid calculated using the shear stress model 47
Figure 3.11 Circulation velocity profile calculated using the momentum balance model 48

Figure 4.1 Comparison of liquid dispersion coefficient estimated from various correlations 54
Figure 4.2 Closed-closed boundaries 59
Figure 4.3 Open-open boundaries 60
Figure 4.4 Closed-open or open-closed boundaries 60
Figure 4.5 Schematic illustration of commonly employed experimental techniques for studying liquid axial dispersion in bubble columns 61

Figure 4.6 Tracer response curves calculated from the solution to the axial dispersion model in a batch system with a pulse tracer injection 63
Figure 4.7 RTD curves calculated from the analytical solution to the axial dispersion model for an open vessel 64
Figure 4.8 Integration domain fro the numerical solution to the dimensionless axial dispersion model (closed boundaries) 67
Figure 4.9 Computational molecule for explicit approximation of 'marching' ahead in time 69
Figure 4.10 Effect of increasing the number of sections (M) on the accuracy of the computation for intermediate mixing 72
Figure 4.11 A pulse tracer dispersion at different dimensionless location (Z/H_c) for intermediate mixing 72

Figure 4.12 A pulse tracer dispersion in a three dimensional plot for intermediate mixing 73
Figure 4.13 RTD curves in a closed vessel for various extent of mixing as predicted from the numerical solution to the axial dispersion model 73
Figure 4.14 RTD curves calculated from the solution to the axial dispersion model (inverse step tracer input) 76
Figure 4.15 Concentration profiles indicating liquid backmixing calculated by the axial dispersion model 77
Figure 4.16 RTD curves predicted by the tanks-in-series model 79
Figure 4.17 Backflow compartment model for the representation of a flotation column 81
Figure 4.18 RTD curves calculated from the backflow compartment model: effect of the backflow ratio 83
Figure 4.19 RTD curves calculated from the backflow compartment model: effect of the number of compartments 84
Figure 4.20 Comparison of the axial dispersion model with compartment models for a relatively low extent of mixing 85
Figure 4.21 Comparison of the axial dispersion model with compartment models for a relatively high extent of mixing 86

Figure 5.1 Small laboratory flotation column set-up 90
Figure 5.2 Large-scale laboratory flotation column set-up 91
Figure 5.3 Filter cloth sparger design 92
Figure 5.4 Arrangement of multiple-sparger system 93
Figure 5.5 Gas regulation system for large-scale flotation column 94
Figure 5.6 An ideal conductivity cell 96
Figure 5.7 Physical representation of Maxwell Model (1873) 97
Figure 5.8 Cell design used in the present study 100
Figure 5.9 Calibrating the electrode cell of local gas holdup measurement 101
Figure 5.10 Relative conductance vs. gas holdup 101
Figure 5.11 Comparison of gas holdup estimated from relative conductance and measured from water manometers 102
Figure 5.12 Ideal signal of cell type #4 103
Figure 5.13 An example of response curve of cell type #4 in this work . 104
Figure 5.14 Conductance probe for measuring radial gas holdup profiles in the 50cm laboratory flotation column 105

Figure 5.15 Probe structure and electrodes arrangement for the pilot flotation column 106
Figure 5.16 Supporting frame of the Probe for measuring local gas holdup in the pilot flotation column 107
Figure 5.17 Axial gas holdup measurement using pressure transducer . . 108
Figure 5.18 RTD measurement set-up 110
Figure 5.19 Voltage-time response for electrodes inside the column: effect of gas bubbles 111
Figure 5.20 A typical calibration curve of KCl concentration (wt. %) vs. relative voltage (voltage of solution - voltage of water alone) 113
Figure 5.21 Computer data acquisition system 114
Figure 5.22 Flowchart of computer data acquisition Program : 115

Figure 6.1 Voltage signal from pressure transducer at different levels over a period of 200s (8 spargers in equal operation) 117
Figure 6.2 Voltage signal from pressure transducer vs. distance from the top of the collection zone (no froth) for various gas rates 118
Figure 6.3a Vertical gas holdup profiles at J_g=0.62cm/s 120
Figure 6.3b Vertical gas holdup profiles at J_g=1.33cm/s 121
Figure 6.3c Vertical gas holdup profiles at J_g=2.03cm/s 122
Figure 6.4 Local gas holdup as a function of time at the location 2.0m above the bottom 123
Figure 6.5 Radial gas holdup profiles at the different levels and the reproducibility 125
Figure 6.6 Radial gas holdup distribution at various gas rates near the bottom level 126
Figure 6.7 Radial gas holdup distribution at various gas rates at 150cm above sparger level 126
Figure 6.8 Radial gas holdup distribution at various gas rates at 200cm above the sparger level 127
Figure 6.9 Radial gas holdup distribution at various gas rates near the interface level 127
Figure 6.10 Radial gas holdup distribution at various gas rates near the bottom level 128
Figure 6.11 Radial gas holdup distribution at various gas rates at 200cm above sparger level 128
Figure 6.12 Radial gas holdup distribution at various gas rates

near the sparger level when only one sparger in operation (off-centre,no frother addition) 129
Figure 6.13 Radial gas holdup distribution at various gas rates near the interface level when only one sparger in operation (off-centre, no frother addition) 129
Figure 6.14 Radial gas holdup distribution at three different levels at J_g=1.33cm/s 130
Figure 6.15 Radial gas holdup distribution at three different levels at J_g=2.03cm/s 131
Figure 6.16 Radial gas holdup distribution at three different levels at J_g=2.70cm/s 131
Figure 6.17 Radial gas holdup distribution at three different levels at J_g=0.66cm/s 132
Figure 6.18 Radial gas holdup distribution at three different levels at J_g=2.04cm/s 132
Figure 6.19 Radial gas holdup distribution at three different levels in the pilot flotation column (J_g=0.6cm/s, 15ppm) 134
Figure 6.20 Radial gas holdup distribution at three different levels in a pilot flotation column (J_g=0.9cm/s, 15ppm) 135
Figure 6.21 Radial gas holdup distribution at three different levels in the pilot flotation column (J_g=2.15cm/s, 15ppm) 136
Figure 6.22 Radial gas holdup distribution at three different levels in the pilot flotation column (J_g=0.6cm/s, 15ppm, one sparger at centre) 137
Figure 6.23 Radial gas holdup distribution at three different levels in a pilot flotation column (J_g=0.6cm/s, 15ppm, one sparger off centre) 138
Figure 6.24 Liquid circulation velocity profiles at 100cm above the bottom calculated from shear stress model 140
Figure 6.25 Liquid circulation velocity profiles at 200cm above the bottom calculated from shear stress model 140

Figure 7.1 Closed vessel case: comparison of model fitting between moments matching and least squares (a) at a low gas rate (b) at a high gas rate 142
Figure 7.2 Effect of the cut-off τ_{max} point on RTD tail on calculated vessel dispersion number 144
Figure 7.3 Comparison of the fitting to experimental data between open vessel analytical and closed vessel numerical

solutions (a) at a laboratory column (d_c=10.16cm), (b) at an industrial column (d_c=250cm, raw data supplied by Espinosa et al., 1988) 144
Figure 7.4 Experimental age distributions in a laboratory column and comparison with model fit (1:feed, 2:middle, 3: exit). (a) at a low gas rate, (b) at a high gas rate 146
Figure 7.5 Experimental age distributions in industrial flotation columns and comparison with model fit. (a) column size 45×45×9500 cm (data from Yianatos et al., 1988), (b) column size 250×1300 cm (data from Espinosa et al., 1989) 147
Figure 7.6 Fitting to experimental RTD: comparison between axial dispersion model and compartment models (1: experimental data; 2: closed vessel numerical solution to axial dispersion model; 3: backflow compartment model; 4: tanks-in-series model) (a) at a low gas rate, (b) at a high gas rate (also see Table 7.4 for N_d values) 149
Figure 7.7 Tracer response curve and model fits in batch operation: the effect of gas rate (see also Table 7.5) 150
Figure 7.8 Dimensionless RTD curves: the effect of gas and liquid rates (see also Table 7.7 for N_d values) 152
Figure 7.9 RTD curves at zero gas rate: the effect of liquid rates . . . 154
Figure 7.10 RTD and model fit in the pilot column 155
Figure 7.11 RTD curves: the effect of column length 157
Figure 7.12 RTD curves: the effect of column verticality 159
Figure 7.13 RTD curves: the feed solid percentage 160
Figure 7.14 Normalized inverse step response curve for solid mixing . . 161
Figure 7.15 Liquid axial dispersion coefficient as a function of gas rate for various liquid rates 163
Figure 7.16 Liquid axial dispersion coefficient vs. gas rate (log-log scale) 163
Figure 7.17 liquid vessel dispersion number vs. gas rate (log-log scale) 164
Figure 7.18 liquid axial dispersion coefficient vs. liquid rate (log-log scale) 164
Figure 7.19 Liquid vessel dispersion number vs. liquid rate (log-log scale) 165
Figure 7.20 Liquid axial dispersion coefficient:

the effect of column length 166
Figure 7.21 Liquid vessel dispersion number vs. column length to diameter ratio (log-log scale) 166
Figure 7.22 I 'quid axial dispersion coefficient: the effect of column verticality (solid lines are the prediction of the correlation of Tinge and Drinkenburg, 1986) 167
Figure 7.23 Liquid dispersion number: the effect of feed solid percentage (solid line is the prediction of the correlation of Laplante et al., 1988) 168
Figure 7.24 A proposed correlation between vessel dispersion number and design operating variables 170

Figure 8.1 Correlation between vessel dispersion number and design and operating variable (Eq.8.3) 182
Figure 8.2 Correlation between vessel dispersion number and design and operating variables, considering the possible effect of gas rate (Eq.8.4) 183

LIST OF TABLES

Table 2.1 Approximate maximum gas rates observed in practice 17
Table 2.2 Various expressions of slip velocity 21
Table 2.3 Bubble diameters measured and predicted 29

Table 4.1 Correlations for liquid phase axial dispersion coefficient . . . 52
Table 4.2 Correlations for gas phase axial dispersion coefficient 55
Table 4.3 Moments for three boundary conditions 87

Table 6.1 Gas holdup calculation from pressure measurements 119

Table 7.1 Comparison of N_d values obtained between moments matching and least squares in closed vessel case 143
Table 7.2 Comparison of N_d values between open and closed solutions 145
Table 7.3 Summary of N_d values 145
Table 7.4 N_d values obtained from different model fits 148
Table 7.5 E_t values obtained in batch operation 151
Table 7.6 Vessel dispersion number obtained at various gas and liquid rates 153
Table 7.7 Vessel dispersion number obtained in the pilot flotation column 156
Table 7.8 Vessel dispersion number obtained at different column lengths 157
Table 7.9 Vessel dispersion number obtained at different verticality 158
Table 7.10 Vessel dispersion number obtained at different feed solid percentage 160
Table 7.11 Summary of previous data from other investigators 171

Table 8.1 Comparison of N_d values 177

LIST OF APPENDICES

Appendix 1	Gas holdup calculation using bubbly flow model	201
Appendix 2	Estimation of bubble size using bubbly flow model	203
Appendix 3	Calculation of solids effect on gas holdup	204
Appendix 4	Calculation of circulation velocity profiles for Newtonian fluid	206
Appendix 5	Calculation of circulation velocity profiles for non-Newtonian fluid	208
Appendix 6	Numerical solution to axial dispersion model using finite difference method	211
Appendix 7	Calculation of RTD curves using the solution to step tracer injection under steady-state	213
Appendix 8	Solution to the tanks-in-series model	215
Appendix 9	Numerical solution to backflow compartment model	217
Appendix 10	Example of moments and dimensionless RTD calculation from the voltage-time response data	218
Appendix 11	Function minimization (least squares fit to experimental RTD)	226
Appendix 12	Computer data acquisition program	230
Appendix 13	Computer data processing and reduction program	238

CHAPTER 1

INTRODUCTION

In this chapter, the history of flotation column development, column operation and the advantages of the column over mechanical flotation cells are briefly described. The methods of bubble generation and recent developments related to flotation columns are reviewed. The objectives of the research work are presented, with a detailed description of the thesis structure.

1.1 Flotation Column Development

The flotation column studied in this thesis was invented in Canada in the early 1960s. Early descriptions of the column were given by Wheeler (1966) and Boutin and Wheeler (1967). Industrial applications and fundamental studies of the flotation column progressed slowly in the 1970s in the Western world, while large-scale flotation columns have been extensively used in China since 1961 but the experience was very poorly documented (Hu and Liu, 1988). Applications and fundamental studies have been growing very fast since 1980 (Wheeler, 1988; Finch and Dobby, 1990a). Some of the work has been documented in a book (Finch and Dobby, 1990a). In this book, the operating and design features of flotation columns were extensively illustrated with data from the laboratory and industrial scale.

In 1981, the first commercial flotation column was installed at Les Mines Gaspé (Québéc, Canada) by the Column Flotation Company of Canada. The duty of the column was Mo cleaning (Coffin and Miszczak, 1982). The column proved very effective, a single column stage replacing several stages of Mo cleaning. The final circuit in 1987 was two stages (a 36" square column followed by an 18" square column) compared with the original circuit which had comprised up to 13 stages of conventional cells. The circuit simplifications and improved metallurgy at Les Mines Gaspé attracted the Canadian Mo producers, notably Gibraltar Mines. Columns rapidly became standard for

Mo cleaning through out North and South America. Gibraltar Mines extended the application of columns to bulk Cu/Mo cleaning and commissioned a 3 stage column circuit, each column being 7ft. in diameter by 40ft. in height. This has led to commercial application away from just Mo cleaning, for example: matte separation at Inco (Feeley et al, 1987), Pb/Zn middlings cleaning at Mt. Isa Mines (Johnson, 1988) and a coarse Pb circuit at Cominco's Polaris plant (Kosick et al., 1988). Worldwide applications now (Sastry, 1988) include Cu, Mo, Pb, Zn and Sn cleaning, bulk sulphide roughing of Au ores, and coal, graphite and phosphate flotation.

Fundamental research work is continuing to increase. Early studies were given by Sastry and Fuerstenau (1970), Flint and Howarth (1971) and Rice et al. (1974). Dobby and Finch (1985a; 1985b; 1986a; 1986b; 1987; 1988) established the basic requirements for flotation column modelling and scale-up. Subsequently, Yianatos et al. (1985, 1988a, 1988b), Pal and Masliyah (1990) and Falutsu and Dobby (1990) directed attention to flotation column froth behaviour. Four aspects were stressed: froth hydrodynamics, cleaning action (rejection of hydraulically entrained particles), selectivity (separation between particles of different hydrophobicity) and froth drop back (recycle of material from froth to collection zone). Espinosa et al. (1988a, 1988b, 1988c), conducting work on fines flotation by columns, found that the column froth has a carrying capacity limitation. Fundamental research concerning flotation kinetics, scale-up, modelling and control of flotation columns are now being conducted worldwide. Modifications to the conventional column are now in practice, for example, the Packed column (Yang, 1988), the Jameson cell (Jameson, 1988) and the microbubble column (Yoon et al., 1987).

1.2 Description and Advantages of Flotation Columns

A typical flotation column is illustrated schematically in Figure 1.1. Commercial units are typically 9-15m in height and 0.5 to 3.0m in diameter, the larger ones often being baffled vertically. The largest unbaffled column appears to be 2.5m in diameter (Espinosa et al., 1989). The cross-section of the column may be square (supplied by Column Flotation Company of Canada) or circular (favoured in most home-made units). The side of a square column or the diameter of a circular column is used to designate column size. The column consists of two distinct zones: the collection zone (also known as slurry or pulp or recovery zone) and above it the froth zone (also known as cleaning zone). A distinct interface between the two zones is usually established. Feed is

introduced to the collection zone below the interface. Solid particles, settling downwards due to gravity from the feed slurry, are contacted countercurrently with a bubble swarm, rising upwards from the bubble generators (spargers) located near the bottom. Hydrophobic particles collide with and attach to the bubbles and are transported to the froth zone. Hydrophillic and less hydrophobic particles are removed from the bottom. In the froth zone, wash water is added near the top of the froth to prevent the hydraulic entrainment of fine hydrophillic particles into the concentrate (Dobby and Finch, 1985b; Yianatos, 1987). Usually a net downward flow of water through the froth is maintained, called a positive bias.

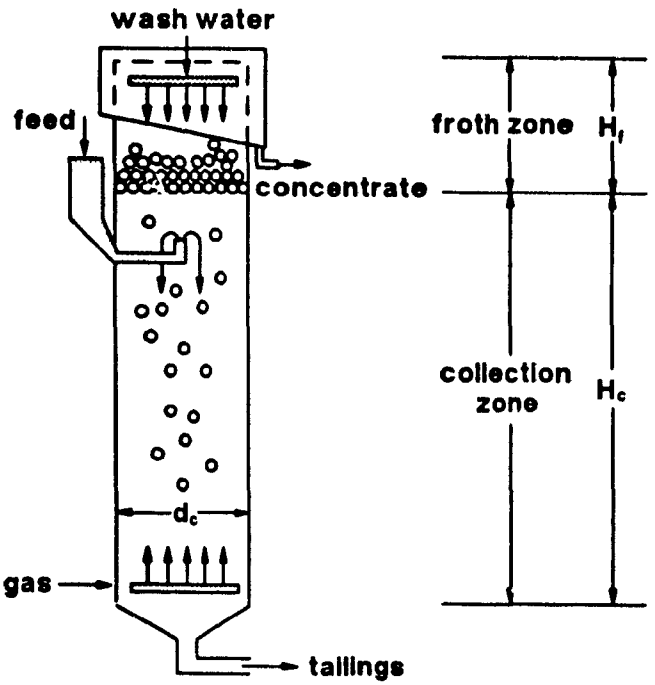

Figure 1.1 Schematic illustration of a flotation column

The flotation column has proved particulary attractive for fine particle flotation and can achieve upgrading in a single stage comparable to that in several stages of mechanical flotation machines, often with improved recoveries (Cienski and Coffin, 1982; Amelunxen and Redfern, 1985 and Egan, et al., 1988). The main reason appears to be the rejection of hydrophillic particles through the wash water/bias action.

Three principal features distinguish the flotation column from a mechanical flotation machine: the wash water, the bubble generation system and the absence of mechanical agitation.

The addition of wash water reduces recovery of fine gangue particles by reducing the recovery of feed water to the concentrate. Gangue is recovered by entrainment in feed water, thus gangue recovery depends on feed water recovery. Entrainment can significantly reduce separation performance. Therefore, a rational solution to gangue recovery is to eliminate the feed water from entering the concentrate. Wash water helps

achieve this, even when used in mechanical flotation machines (Kaya, 1989).

The bubble generation system in flotation columns needs to produce small bubbles preferably at controllable sizes without mechanical agitation. In flotation, the role of bubble size is not completely understood. Some investigators have used microbubbles ($< 100\ \mu m$) and found that the flotation recovery can be improved by decreasing bubble size (Ahmed and Jameson, 1985; Szatkowski, 1985, 1987; Luttrell et al., 1988), while Dobby and Finch (1986b), Xu et al. (1987, 1989b, 1990a), Yianatos and Finch (1990) and more recently, Luttrell and Yoon (1990) have argued that the benefit of using microbubbles is limited due to the interrelation of bubble size, gas rate and downward liquid rate. In general, the bubble size range in flotation columns is about 0.5 to 1.5 mm at superficial gas rates from 0.5 cm/s to 2.5 cm/s.

1.3 Bubble Generation and Modification in Flotation Columns

The bubble generation techniques in flotation columns are quite different from the methods used in mechanical flotation machines, where bubbles are formed behind a rotating impeller. Small bubbles can be produced at a relatively low gas rate. Gas holdup obtained in this case is quite small (typically from 8 - 14%, Jameson and Allum, 1984).

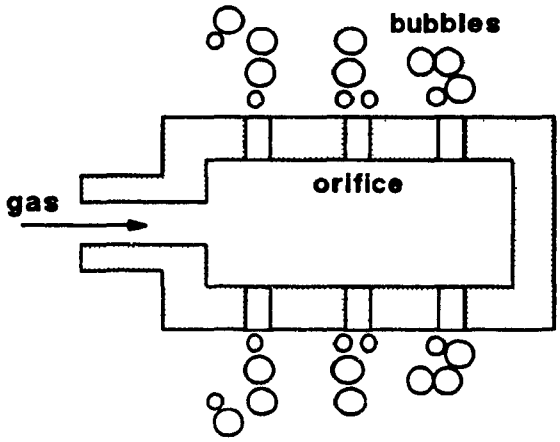

Figure 1.2 Bubble generation by a porous sparger

In the conventional (or Canadian) flotation column, porous spargers (Figure 1.2) are often used. Metallurgical performance of flotation column is not affected to a great degree whether using rubber or cloth spargers (Huls et al, 1991). Nonflexible media (e.g. porous glass, steel and plastic) spargers are only used in laboratory flotation columns due to the problem of plugging with solid particles. Mersmann (1978) observed that a good generation of uniform bubbles can be achieved only if the gas passes all the holes on the surface of porous type spargers. It has been found in the laboratory flotation column that not all the sparger surface is active at the same time. For example, with vertical spargers bubbles emerge initially from the top section of the spargers, and as gas rate is increased the bubble producing surface expands

downwards.

Figure 1.3 shows the bubble formation using static shear contacting. In general, the slurry or water rate is extremely high and bubble size decreases as the slurry or water rate increases. Plugging of the orifices by fine particles tends to occur, but high gas content and fine bubbles can be achieved.

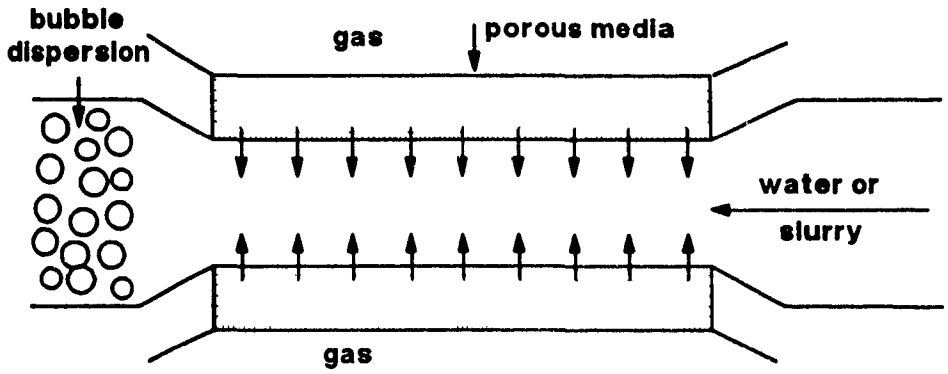

Figure 1.3 Bubble generation in static shear contacting

Bubbles are also generated using orifice pressure drop (gas and water injected through orifices, e.g. USBM and Cominco spargers). Figure 1.4 shows schematically the Cominco sparger. Bubbles are generated using the combination of orifices and water injection. Bubble size in this case increases with gas rate and decreases as the water rate and frother concentration increase (Huls et al, 1991).

Mechanical agitation, used for generating air bubbles in mechanical flotation cells, has been used in the Hydrochem Column (Schneider and Weert, 1988). Mechanical agitation is not only energy-consuming but also produces turbulence. Turbulence may be required to suspend solid particles in mechanical cells. In flotation columns and the new derived flotation cells (e.g. Jameson cell, Packed column), particles suspension is not a prerequisite.

A wide range of flotation machine designs is available. The basic design and operating principles of the mechanical flotation machines are well known (Harris, 1976). Young (1982) presented an extensive review on the various flotation machines.

The flotation column has been progressively modified since its invention. Among these modifications, the Jameson cell, the Packed flotation columns and the microbubble column are most significant.

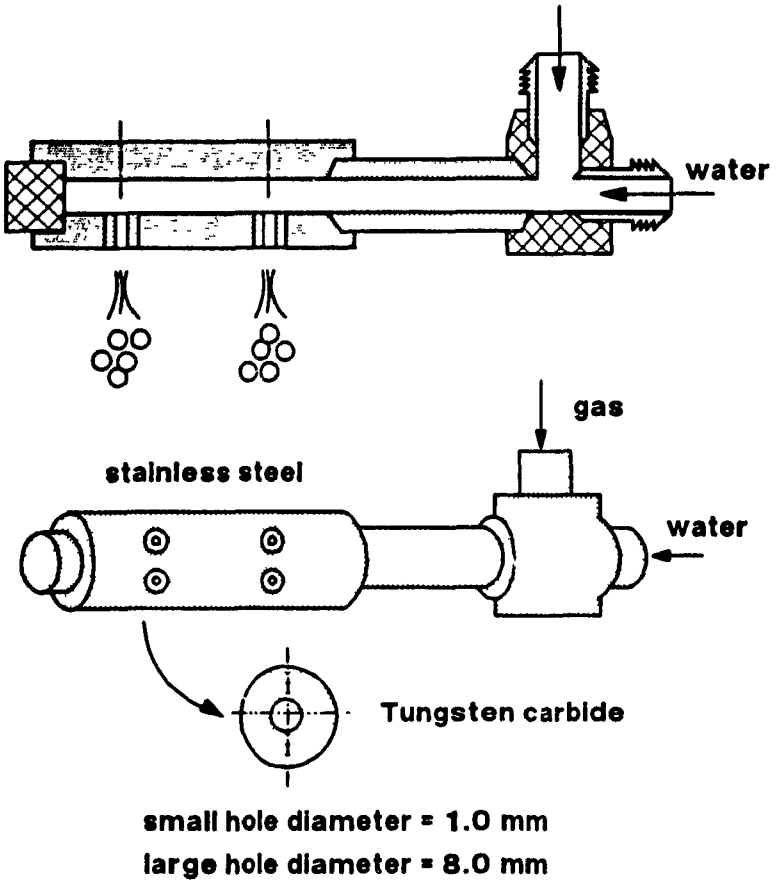

Figure 1.4 Cominco's bubble generator

Figure 1.5 shows a Jameson flotation column. This cell was designed by Prof. Jameson in collaboration with Mount Isa Mines Ltd. The major differences between this cell and the column are the bubble generation and volume of the slurry zone. Bubbles are generated by aspirating air using a downward flow of slurry. The intense mixing between bubbles and slurry occurs in the downcomer, which effectively is the collection zone. The advantages of this cell are the reduced slurry zone volume and increased flotation rate (Jameson, 1988).

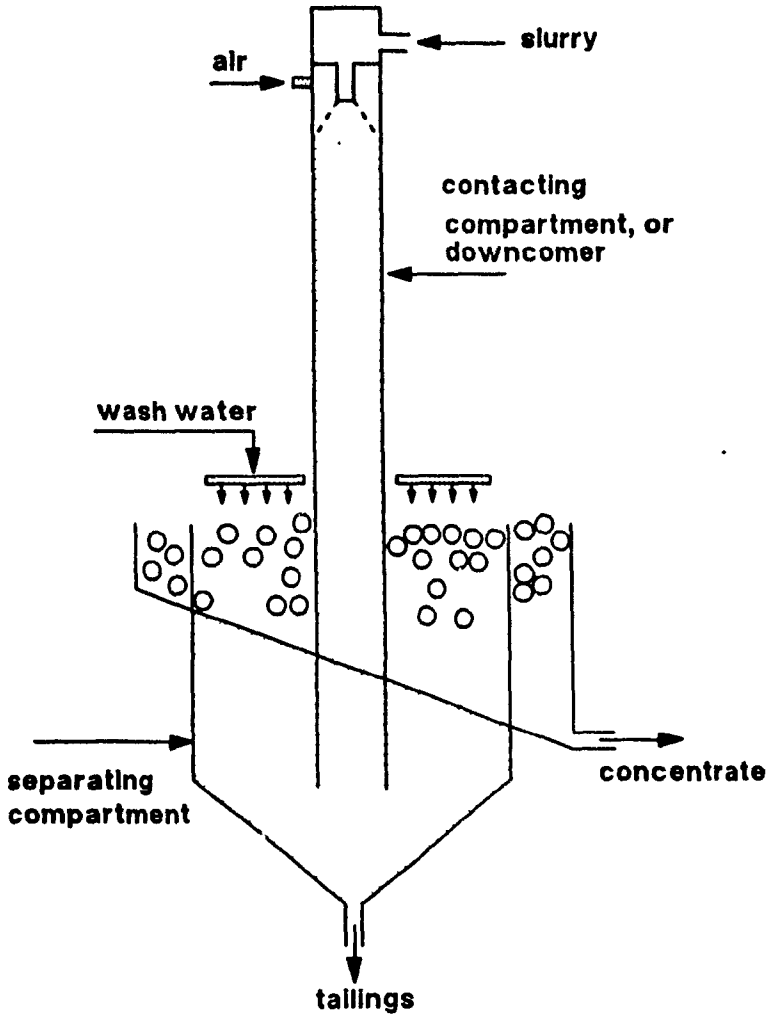

Figure 1.5 Schematic diagram of the Jameson cell

Packed flotation column (Figure 1.6) was developed at Michigan Technological University, U.S.A. (Yang, 1988). The key feature of this column is the packing, which reduces slurry mixing and breaks air into small bubble. It seems that the packing pattern and materials are the important factors. The packing elements are arranged in blocks positioned at right angles to each other. Air is broken into fine bubbles upon passing the packing elements. Thus, no bubble sparger is needed, which is an advantage. Spargers continue to cause problems in conventional columns.

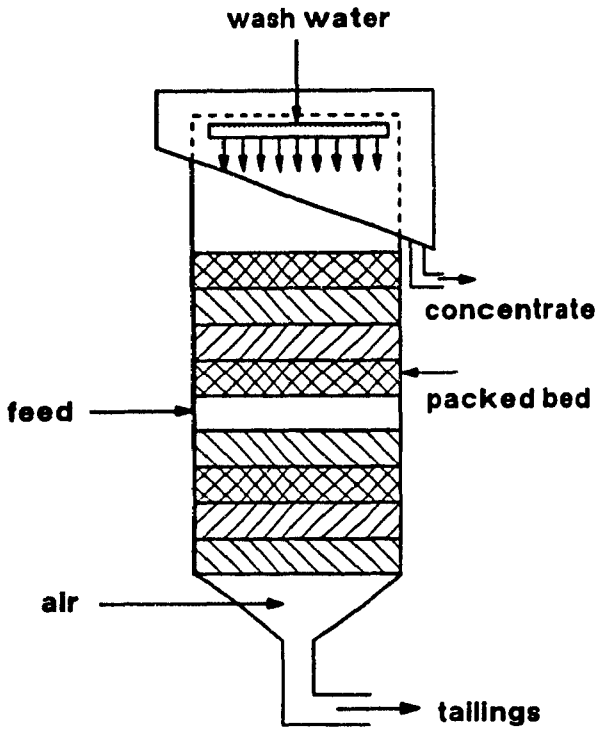

Figure 1.6 Packed flotation column (after Yang, 1988)

1.4 Objectives of the Present Work

To understand the behaviour of the collection zone of a flotation column, the hydrodynamics and mixing characteristics must be studied.

The hydrodynamics (Figure 1.7) is defined by the interrelation between bubble diameter, gas holdup and gas and liquid rates. The flow regime usually encountered in a countercurrent flotation column is bubbly flow. Bubbly flow is characterized by the relatively uniform rising of bubbles of relatively uniform size, and hence a relatively uniform radial gas holdup profile. Beyond bubbly flow (Figure 1.9), churn-turbulent flow is characterized by liquid circulation resulting from non-uniform bubbles and non-uniform radial gas holdup distribution. The interrelation between bubble size, gas holdup and gas and liquid rates determines the transition from bubbly to churn-turbulent flow. One objective of the present work is to determine radial gas holdup profiles.

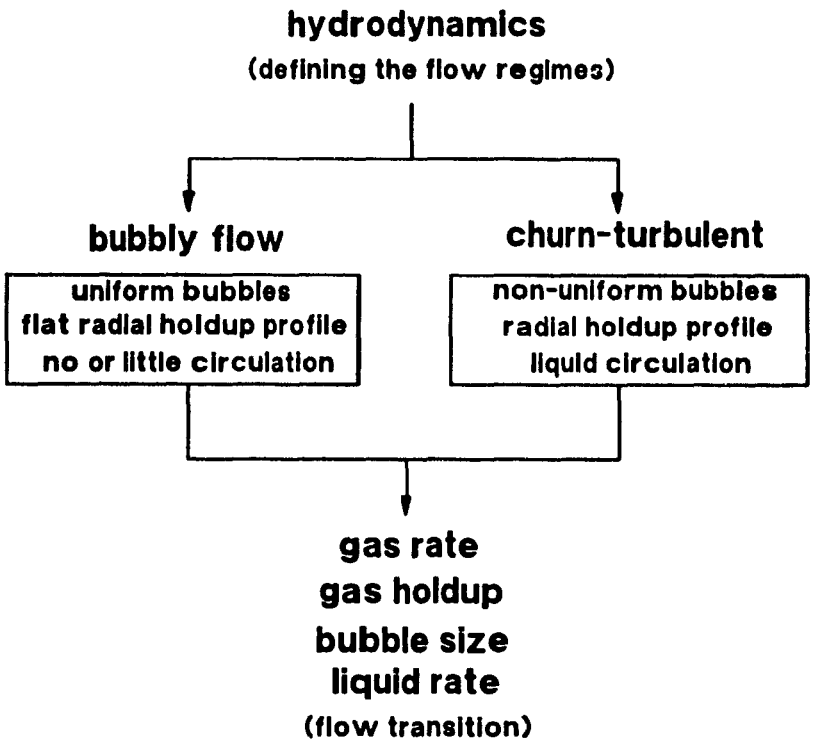

Figure 1.7 Hydrodynamics of the column collection zone

The mixing —— or more specifically the particle transport —— characteristics of the collection zone (Figure 1.8) in a flotation column have a direct impact on grade and recovery (Dobby, 1984; Finch and Dobby, 1990a; Luttrell and Yoon, 1988). Particle mixing in the collection zone must be estimated, for example, for column scale-up. The degree of the axial mixing is denoted by a dimensionless variable, N_d, the vessel dispersion number, which is estimated from the experimental residence time distribution (RTD) curves. It is important to consider the problem of determining N_d (Figure 1.9): First, the experimental method for measuring residence time distribution requires a choice of the mode of tracer addition and of column operation. For example, batch or continuous operations are feasible. Tracer addition can be either pulse or step. Tracer concentration can be measured either continuously using conductivity (e.g. for salt type of tracers) or by sampling small volumes of liquid and then off-line analyzing the tracer concentration (e.g. for dye tracers); Second, the mixing models used to describe the RTD data can be, for example, the one-dimensional plug flow axial dispersion model, compartment models or some others. The selection of a particular model is judged on its fit to the experimental RTD. Analytical and numerical solutions to these models are available for given initial and boundary conditions; Third, the RTD data analysis for

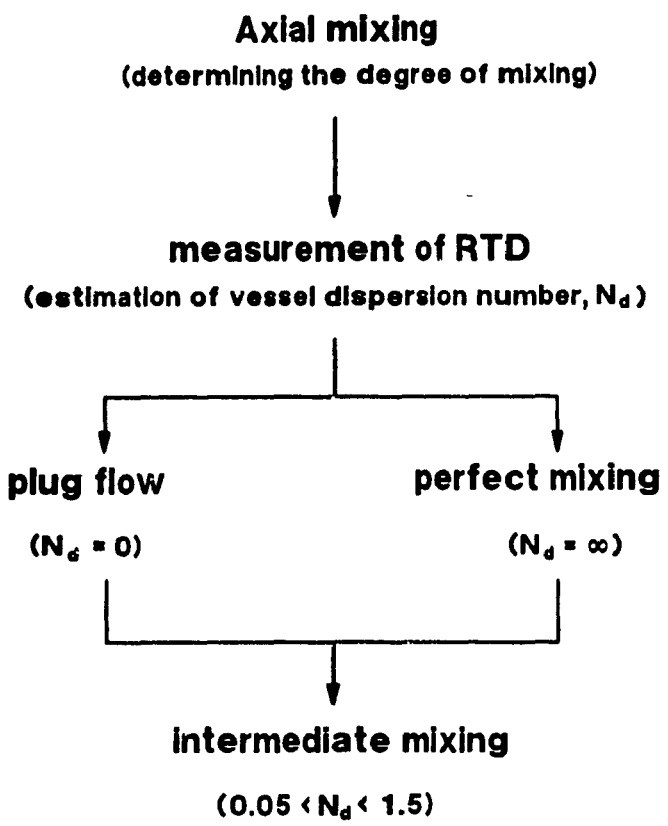

Figure 1.8 Mixing of the column collection zone

fitting the models and estimating the mixing parameters are either moments matching or least-squares techniques. These two methods of data analysis give different results; Last, after the above three steps have been established, the effect of the operating and design variables on the degree of mixing can then be investigated. One objective of this work is to establish the appropriate method of determining N_d. With this established, a second objective is to determine N_d for various operating (e.g. gas and liquid rates) and design (e.g. size of column) conditions.

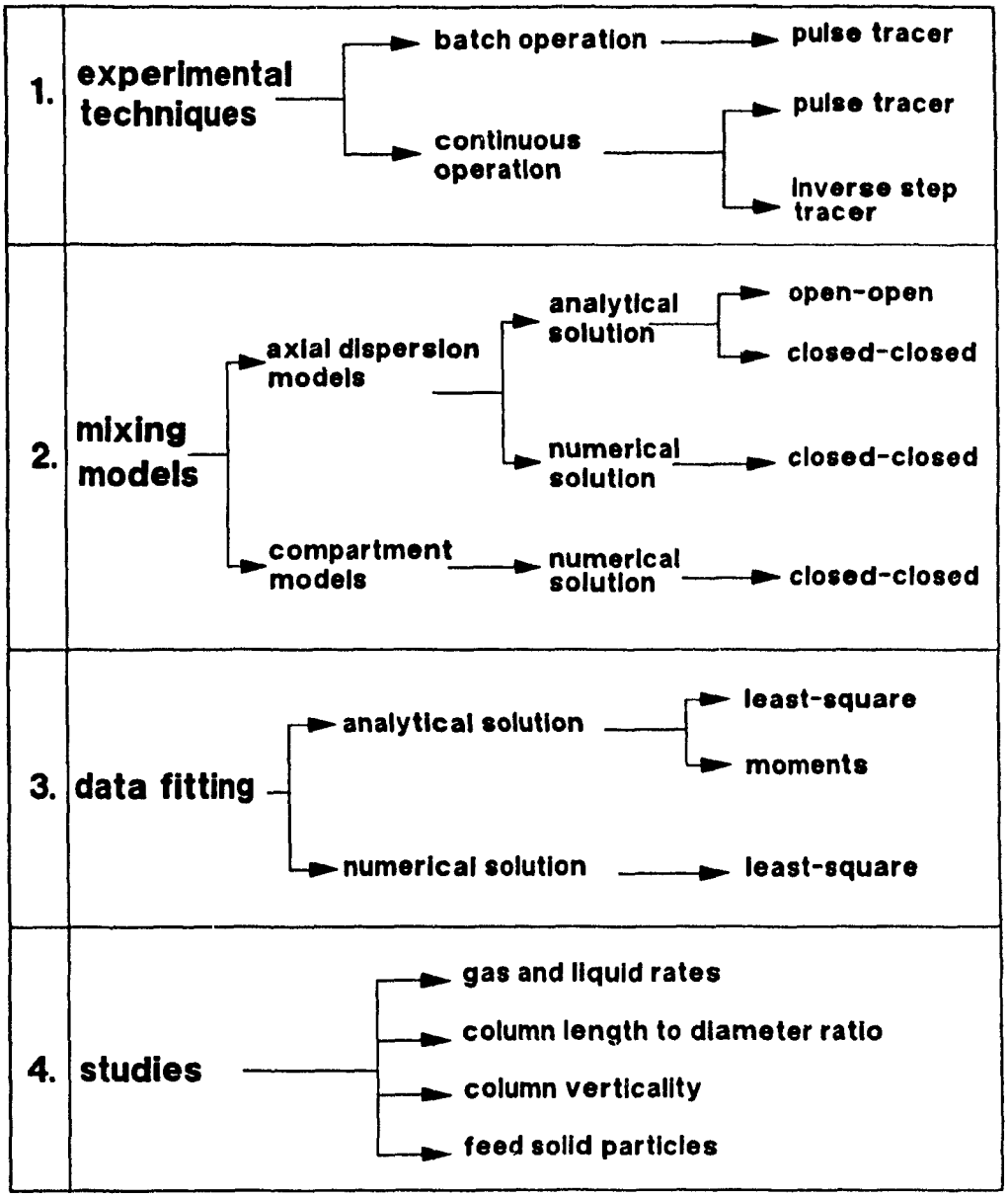

Figure 1.9 Four steps of mixing studies in the collection zone

1.5 Structure of the Thesis

The thesis consists of nine chapters. At the beginning of each chapter, a summary is given. It is hoped that in this way the reader can locate information easily that may be of interest. A large number of figures of both experimental set-up and results is presented inside the main text. Numerical results are provided in tables for the convenience of other investigators.

Chapter 1 is the introduction in which column development, bubble generation and major modification to conventional flotation columns are described, along with the objectives of the present work and the structure of the thesis.

Chapter 2 reviews the hydrodynamics of the water/gas two-phase system along with the model development to describe the bubbly flow regime.

Chapter 3 reviews the radial gas holdup distribution literature. Methods of calculating liquid circulation velocity profiles from the parabolic radial gas holdup distribution are then described.

Chapter 4 describes the mixing models and data analysis for estimating mixing parameters. In particular, the axial dispersion model, the tanks-in-series model and the backflow compartment model are described in detail. Analytical and numerical solutions to the axial dispersion model are presented. Methods of fitting the model to experimental RTD are described and discussed.

Chapter 5 describes the experimental set-up and techniques. The laboratory flotation columns, sparger design and computer data acquisition system are presented in detail. Background of measuring conductivity of liquid is reviewed. Local gas holdup measurement using the electrical conductivity technique and design of the conductance cells are investigated, and gas holdup obtained using this method are compared with the measurement using pressure manometers. The residence time distribution determination using an electrical conductivity technique with Kcl as a tracer is described.

Chapter 6 presents the results of axial and radial gas holdup distributions measured in a large laboratory flotation column (50cm in diameter) and a pilot flotation column (91cm in diameter).

Chapter 7 presents the data on liquid dispersion: the effect of gas and liquid rates, column length, column verticality and feed solid percentages are described. A new correlation for predicting vessel dispersion number, N_d, is developed.

Chapter 8 discusses the models developed in the present work and the significance of the present experimental results. This chapter is in two main parts: local gas holdup distribution and mixing characteristics of the collection zone of a flotation column.

Chapter 9 concludes the present work and suggests future research.

CHAPTER 2

HYDRODYNAMICS OF GAS/LIQUID SYSTEMS

In this chapter, the hydrodynamics of gas/liquid two-phase systems is reviewed, with model development to describe the bubbly flow. The applications of the bubbly flow model for correlating gas holdup with gas rate, correlating bias rate with gas rate, estimating bubble size and determining the possible effect of solid particles on gas holdup are investigated. The limiting conditions (maximum gas rate or minimum bubble size) for flotation column operation to remain in the bubbly flow regime are also considered.

2.1 General Observation

The hydrodynamics, transport and mixing properties of the collection zone of a flotation column are strongly dependent on the prevailing flow regime. Many investigators (e.g. Wallis, 1969; Lockett and Kirkpatrick, 1975; Hills, 1976; Miller, 1980) have proposed different criteria to differentiate flow regimes. The definitions of Wallis (1969) for characterizing flow regimes have been commonly accepted (Shah, et al., 1982). Wallis (1969) classified the upward movement of the bubble swarm into three separate flow regimes. These flow regimes, in the order of increasing gas rate, are,

Bubbly flow or quiescent flow: This regime is characterized by almost uniformly sized bubbles with equal radial distribution. This regime usually is limited to a gas rate less than 5 cm/s (Fair, 1962). The theory of bubbly flow was originally developed by Lapidus and Elgin (1957), Richardson and Zaki (1954) and Wallis (1962). The theory gives satisfactory correlations of the liquid/gas bubbly flow only if the bubbles are of equal size and are uniformly distributed over the column cross-section. Using stagnant bubble clouds in a flowing liquid, Lockett and Kirkpatrick (1975) showed that the bubbly flow regime can be realized up to a gas holdup of 66%; in general the bubbly flow theory fails if the gas holdup is larger than about 15% (Shah, et al., 1982; Whalley and Davidson, 1974). In a

flotation column where frother is added, the bubbly flow can be maintained up to a gas holdup of 35% (Xu et al., 1989b; Yianatos and Finch, 1990).

Churn-turbulent flow or heterogeneous regime: At higher gas rate, the homogeneous dispersion of gas inside the liquid can no longer be maintained and an unsteady flow pattern with channelling occurs. This flow regime is characterized by large bubbles rising with high velocities in the presence of small bubbles (Hills and Darton, 1976). The gas bubbles may even take the form of spherical caps with a very mobile and flexible interface and the diameter can grow up to about 15 cm. Usually, the bubbles coalesce and break up repeatedly as they rise up.

Slug flow: In small diameter columns, at high gas rates, large bubbles are stabilized by the column wall leading to the formation of bubble slugs. Bubble slugs can be observed in columns of diameter up to 15 cm (Hills, 1976; Miller, 1980).

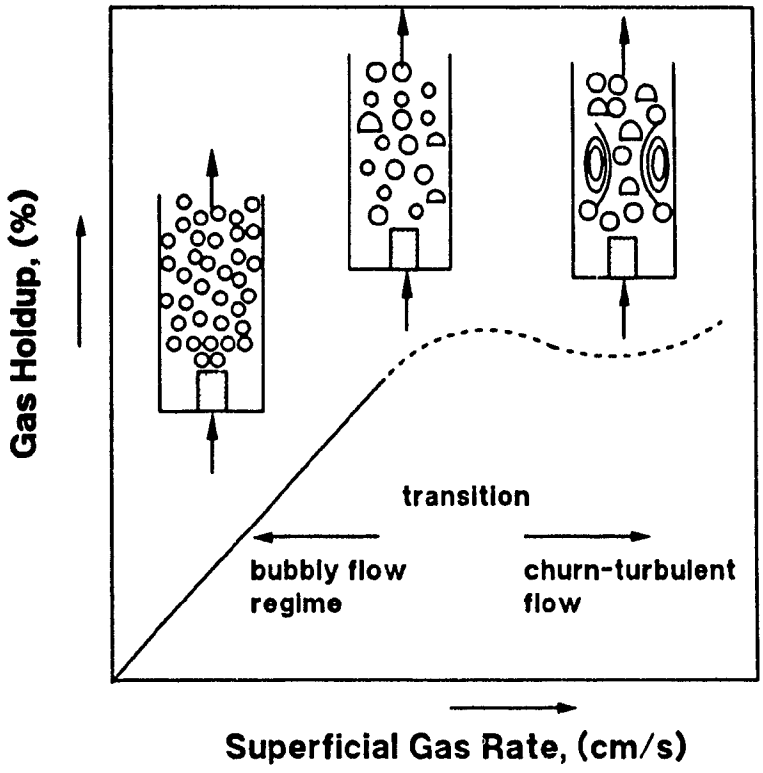

Figure 2.1 Gas holdup as a function of gas rate: a general relationship (after Finch and Dobby, 1990)

A flow regime map is schematically represented in Figure 2.1. Gas holdup increases approximately linearly with gas rate and then deviates above a certain range of gas rates. The exact values of the gas rate and gas holdup at this transition are difficult to obtain. Iordache and Jinescu (1986) presented a kinetic model to describe the stochastic motion of bubbles in gas/liquid dispersion. According to the kinetic model, there exists a transition zone between the bubbly and churn turbulent flow regimes. The dependence of the flow regimes on column diameter and gas rate is roughly presented in Figure 2.2. The types of gas spargers, the physical-chemical properties of the liquid and liquid rate can affect the transition between flow regimes (Shah and Deckwer, 1981; Xu et al., 1989b, 1990a).

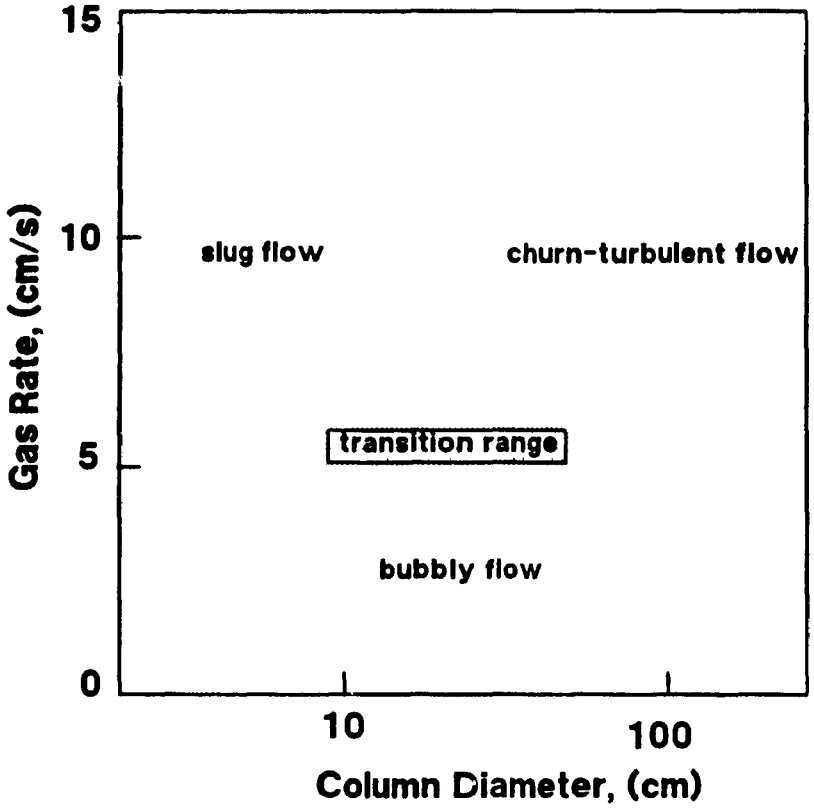

Figure 2.2 Approximate dependence of flow regimes on gas rate and column diameter (after Shah et al., 1982)

Each flow regime has its particular applications. For example, bubbly flow is the desired flow regime in the operation of flotation columns, while churn-turbulent flow is desired in the thermal cracking of heavy oils (Ueyama et al., 1989). A general observation in industrial flotation column operation is that the column performance deteriorates above a certain gas rate. Some examples of reported 'maximum' gas rates are given in Table 2.1. The decrease in recovery may have its origin in the collection process (Dobby and Finch, 1986b), but the loss of grade and certainly the reference to the loss of interface, loss of positive bias and instability in level measurement have their origin in the properties of the gas/liquid system. Xu et al. (1989b, 1990a) identified three distinct phenomena in water-gas two-phase system which could dictate a maximum in the gas rate: loss of bubbly flow, loss of slurry/froth interface, or loss of positive bias. These are all related to the transport upwards of water by bubbles. Consequently bubble size as well as gas rate becomes a factor. Gas rate and bubble size can be combined by considering bubble surface area rate.

Table 2.1 Approximate Maximum Gas Rates Observed in Practice *

location	duty	d_c (cm)	max. J_g (cm/s)	comments	reference
Niobec	$CaCo_3$ flo.	6.35	2~2.5	loss of interface	field observation
Kidd Greek	Cu/Zn sep.	20.3	3.0	negative bias	field observation
Mount Isa	Cu clnr.	5.08	3.5	loss of recovery	field observation
Mount Isa	Pb/Zn bulk clnr.	250	1.0	loss of grade	Espinosa et al., 1989
Gibraltar	Cu clnr.	92.4	4.0	unstable level	Dobby et al., 1985
INCO	Cu/Ni sep.	180	3.2	loss of recovery	private com., 1988

* taken from Finch and Dobby (1990b)

2.2 Gas Rate and Gas Holdup

A very important feature of volumetric gas flow rate or superficial gas rate (often simplified as gas rate) is that it varies with the static head pressure along the column. The gas rate used in the thesis, unless noted otherwise, is the value referring to standard conditions (i.e. at 1 atmosphere) which are at the top of the column.

When introduced into a column through a sparger, gas is dispersed as small bubbles which move upwards due to buoyancy. The volumetric fraction occupied by bubbles is called gas holdup ϵ_g. Gas holdup is one of the most important parameters characterizing the hydrodynamics of the flotation column.

2.2.1 Measurement of Gas Holdup

Gas holdup can be measured in a number of ways. Figure 2.3 shows the common approaches used in bubble and flotation column studies. Method (a) is bed expansion in which the increase in level is due to the injection of gas. This method gives the average gas holdup for the whole vessel. Method (b) is usually applied in laboratory column studies using the pressure drop between two positions. Gas holdup is given by the pressure difference over the distance between the pressure tapping points. This method can measure gas holdup for a specific section and thus gives local gas holdup. Method (c) measures gas holdup by using some properties such as electrical conductivity. Method (c) can usually be modified to measure gas holdup at a specific point within the column. The bed expansion method is usually in good agreement with the pressure drop method (relative difference less than 3%, Xu, 1987). However, the bed expansion method will not be accurate if there is a layer of froth on the top, making the surface difficult to define. Point gas holdup measurement using a conductivity technique will be described in the experimental part.

2.2.2 Effect of Operating Variables

Gas holdup is mainly dependent on the superficial gas rate and is very sensitive to the physical properties of the liquid (e.g., frother concentration) and it is difficult to predict. In bubbly flow, gas holdup is approximately linearly proportional to gas rate. At a given gas rate, increasing the downward liquid rate and frother concentration increases the gas holdup. The effect of sparger surface area on gas holdup and bubble size has been studied (Xu, 1987; Xu and Finch, 1989). In general for internal porous spargers, the relative size of spargers to column cross-section plays an important role (Clingan and McGregor, 1987; Xu and Finch, 1989).

Kulkarni et al. (1987) recently derived a theoretical model to predict gas holdup in a bubble column which contains some surfactant. They first obtained a single bubble rising velocity from the Navier-Stokes equation and related it to bubble swarm velocity

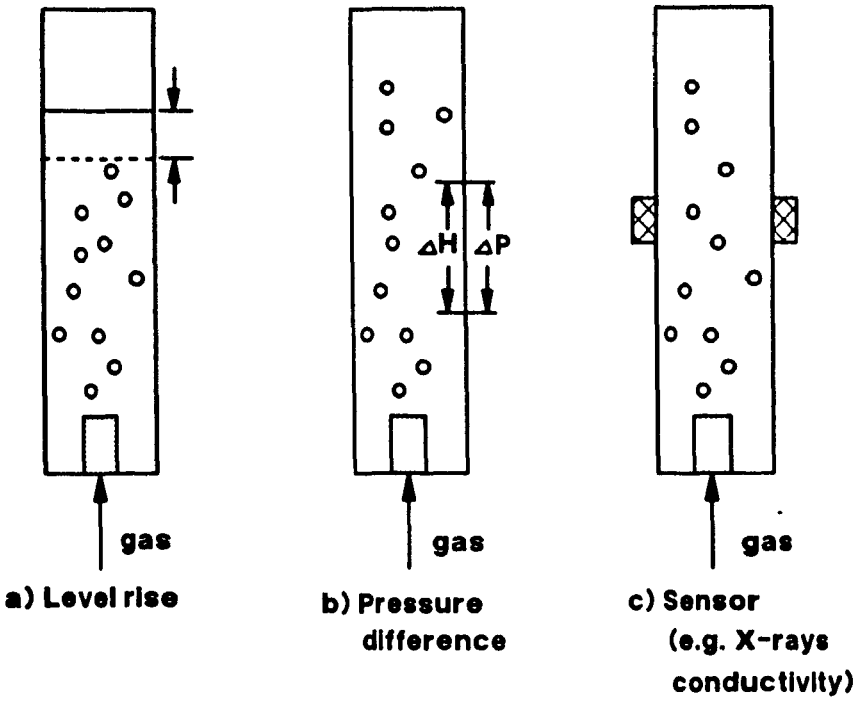

Figure 2.3 Methods of gas holdup measurement (after Finch and Dobby, 1990a)

(Marrucci, 1965) which includes gas holdup. However, the application of the model requires a knowledge of the liquid properties, such as density, viscosity, bubble size and a retardation parameter which must be experimentally determined.

The effect of solid particles is complicated. The presence of solids in the liquid does not affect the gas holdup significantly (Shah et al., 1982). The attachment of hydrophobic particles onto the surface of bubbles increases the gas holdup due to the reduced rising velocity or the increased residence time of bubbles (Yianatos et al., 1988a; Finch and Dobby, 1990a).

2.3 Bubble Diameter

A bubble is a dispersed volume of liquid occupied by gas and enclosed by a gas/liquid interface. The equilibrium shape of the bubble is determined by the stress balance at the gas/liquid interface. The hydrostatic pressure, always acting on a bubble, causes a bubble to rise, change shape or expand. Bubble size, rising velocity and bubble size distribution in a flotation column have a direct influence on the performance of the column, mainly through affecting the hydrodynamics of the system, and the particle

collection rate (Dobby, 1984; Finch and Dobby, 1990).

Many methods are available to determine bubble size. Photographic techniques are used most widely and often as a reference to any newly developed technique. Other methods include light scattering and reflection, and various optical and electrical probes. Though the bubble size distributions obtained from various techniques are often markedly different, the volume to surface mean bubble diameter (sometimes called the Sauter mean diameter, d_{vs}) are usually in good agreement (Shah et al., 1982). Various correlations have been developed to correlate bubble size with gas rate, gas holdup and liquid surface tension, viscosity. However, none of these correlations is widely used (Shah et al., 1982). In general, bubble size depends on gas rate, liquid properties (in particular, frother concentration) and probably bubble generation system.

2.4 Bubbly Flow Model Development

The theory of bubbly flow (also called drift flux analysis) is based on the hydrodynamic behaviour of bubbles in the liquid. The applications of this bubbly flow theory include: the estimation of bubble size from given gas rate, liquid rate and gas holdup; the correlation of gas holdup with gas rate and liquid rate; and the effect of bubble loading on gas holdup.

2.4.1 Slip Velocity in a Bubble Swarm

The slip velocity U_{sb} is the velocity of the gas phase relative to the liquid phase, and is defined as,

$$U_{sb} = \frac{J_g}{\varepsilon_g} \pm \frac{J_l}{(1-\varepsilon_g)} \tag{2.1}$$

The $\pm$ sign refers to countercurrent flow and concurrent flow, respectively. Superficial gas rate J_g is positive upwards and superficial liquid rate J_l positive downwards.

The slip velocity is related to gas holdup ϵ_g and the terminal rise velocity of a single bubble U_T. Various expressions for this are reported by Lockett and Kirkpatrick (1975). An updated list is given Table 2.2.

Table 2.2 Various Expressions of Slip Velocity

equations	eq. number	constant	reference
$U_{sb} = U_T$	(2.2)		Turner (1966)
$U_{sb} = U_T(1-\varepsilon_g)^{-1}$	(2.3)		Davidson and Harrison (1966)
$U_{sb} = U_T(1-\varepsilon_g)^{m-1}$	(2.4)	$m=2$ $m=2.39$	Wallis (1962) Bridge et al. (1964)
$U_{sb} = U_T\frac{1-\varepsilon_g}{1-\varepsilon_g^{5/3}}$	(2.5)		Marrucci (1965)
$U_{sb} = U_T(1-\varepsilon_g)^{1.39}(1+2.55\varepsilon_g^3)$	(2.6)		Lockett and Kirkpatrick (1975)

In Equation (2.4), Wallis (1962) used $m=2$ for small bubbles and $m=0$ for large bubbles. For $m=0$, Equation (2.4) reduces to Equation (2.3). Bridge et al. (1964) used $m=2.39$ for small air bubbles in water following the relationship of Richardson and Zaki (1954),

$$m = [4.45 + 18(\frac{d_b}{d_c})]Re_b^{-0.1} \quad (1<Re_b<200) \tag{2.7}$$

$$m=4.45Re_b^{-0.1} (200<Re_b<500) \tag{2.8}$$

where Re_b is the bubble Reynolds number based on the terminal velocity of a bubble and given by,

$$Re_b = \frac{d_b U_T \rho_l}{\mu_l} \tag{2.9}$$

Generally speaking, all the above proposed correlations for slip velocity have the

following form,

$$U_{sb} = U_T F(\varepsilon_g) \tag{2.10}$$

The most frequently used relation for $F(\epsilon_g)$ is,

$$F(\varepsilon_g) = (1-\varepsilon_g)^{m-1} \tag{2.11}$$

which gives Equation (2.4).

Various values of m have been used, ranging from a constant m (e.g. $m=2$, Wallis, 1962) to m being a function of Reynolds number (Dobby and Finch, 1986b; Dobby et al., 1988; Yianatos et al, 1988a) based on the relation of Richardson and Zaki (1954).

2.4.2 Terminal Velocity of a Single Bubble

The terminal velocity of a single bubble U_T is often used as a correlating parameter. It can be calculated by the method of Clift et al. (1978),

$$U_T = \frac{\mu_l}{\rho_l d_b} Mo^{-0.149}(J-0.857) \tag{2.12}$$

where Mo is the Morton number given by,

$$Mo = \frac{g\mu_l^4(\rho_l-\rho_g)}{\rho_l^2\delta^3} \tag{2.13}$$

and J is a correlating constant given by,

$$J = 0.94H^{0.747} \quad (2<H<59.3) \tag{2.14}$$

and

$$J = 3.42H^{0.441} \quad (H>59.3) \tag{2.15}$$

where H is given by,

$$H = \frac{4}{3} Eo Mo^{-0.149} \left(\frac{\mu_\ell}{\mu_w}\right)^{-0.14} \tag{2.16}$$

where Eo is Eötvos number defined as,

$$Eo = \frac{g d_b^2 (\rho_\ell - \rho_g)}{\delta} \tag{2.17}$$

The above correlation of bubble terminal velocity is for a system where some surface-active contamination is inevitable and for the range, $Mo < 10^{-3}$, $Eo < 40$, $Re_b > 0.1$.

A simpler expression can be used for $d_b < 2$mm, given by Schiller and Naumann (1933),

$$U_T = \frac{g d_b^2 (\rho_\ell - \rho_g)}{18 \mu_\ell (1 + 0.15 Re_b^{0.687})} \quad (d_b < 2mm) \tag{2.18}$$

There is little difference between the above two correlations for $d_b < 2$mm. For $2\text{mm} < d_b < 10\text{mm}$, U_T is independent of bubble size, with a value close to 21 cm/s (Clift et al., 1978). For water at 20°C and a surface tension of 65 dynes/cm (a reasonable approximation for flotation systems), Equation (2.18) is simplified to (Dobby et al. 1988),

$$U_T = 48.9 d_b^{0.514} - 0.309 d_b^{-1} \tag{2.19}$$

2.4.3 Bubbly Flow Model

The bubbly flow model developed here gives a relationship between slip velocity and terminal velocity and gas holdup, modified by an empirical dependency of bubble size on gas rate.

For the range of bubble sizes ($d_b < 2$mm) of interest in flotation, an empirical relationship has been developed for correlating bubble size with gas rate (Dobby and

Finch, 1986b; Xu and Finch, 1989a; Yianatos and Finch, 1990), namely,

$$d_b = C \cdot J_g^{0.25} \tag{2.20}$$

where C (i.e. d_b at J_t = 1.0cm/s), is mainly dependent on frother concentration and sparger size. A consequence is that U_T becomes a function of gas rate.

Equations (2.1) and (2.4) can be combined to give various forms of 'drift flux equations'. Two forms of use here are,

$$J_g = U_T \varepsilon_g (1-\varepsilon_g)^{m-1} - J_t \frac{\varepsilon_g}{1-\varepsilon_g} \tag{2.21}$$

and,

$$J_t = U_T (1-\varepsilon_g)^m - J_g \frac{1-\varepsilon_g}{\varepsilon_g} \tag{2.22}$$

The drift flux equations are usually applied at relatively low gas holdup (e.g. $\epsilon_g \leq 0.25$), but Lockett and Kirkpatrick (1975) showed they apply up to at least $\epsilon_g = 0.66$. Pal and Masliyah (1990) have recently shown they apply to the froth zone of a flotation column where $\epsilon_g > 0.8$. Substituting J_b for J_t in Equation (2.22) gives (Pal and Masliyah, 1990),

$$J_b = U_T (1-\varepsilon_{gf})^m - J_g \frac{1-\varepsilon_{gf}}{\varepsilon_{gf}} \tag{2.23}$$

where ϵ_{gf} represents the gas holdup at froth zone. Pal and Masliyah (1990) have recently suggested an empirical correlation for J_b which is slightly improved over Equation (2.23),

$$J_b = U_T (1-\varepsilon_{gf}) \exp(0.1 - 2.5\,\varepsilon_{gf}) - J_g \frac{1-\varepsilon_{gf}}{\varepsilon_{gf}} \tag{2.24}$$

2.5 Applications of Bubbly Flow Model

The bubbly flow model can be used mainly for correlating gas holdup as a function of gas rate, correlating bias rate as a function of gas rate, estimating bubble size and determining the effect of bubble loading on gas holdup.

2.5.1 Correlating Gas Holdup vs Gas Rate

To illustrate the applications of the bubbly flow model, gas holdup as a function of gas rate (Xu et al., 1990) is presented in Figure 2.4 (A program written in FORTRAN for this calculation is presented in Appendix 1). Solid curves are the bubbly flow model fits with m=2 and U_T as a function of bubble size. The dashed line is also the bubbly flow model fit with m=2 but U_T=21cm/s, which is for bubbling in surfactant-free water. In general the model fit is very good. The important point here is that there is a maximum in gas rate both theoretically and experimentally, for bubbly flow to exist under the given conditions (Xu et al., 1990a).

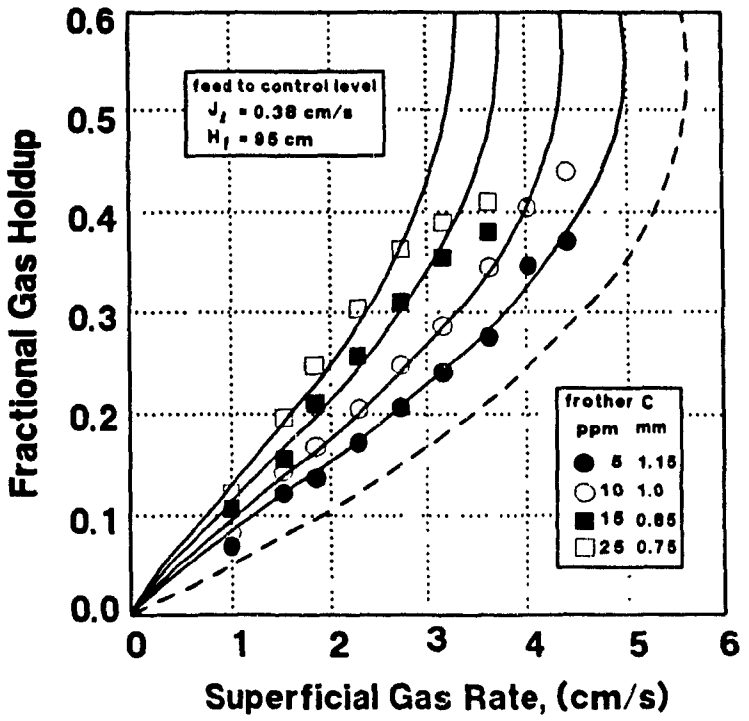

Figure 2.4 Bubbly Model fit of gas holdup as a function of gas rate with m=2 (dashed line is model result where U_T=21cm/s)

2.5.2 Correlating Bias Rate vs. Gas Rate

To calculate bias rate as a function of gas rate, the gas holdup and bubble size in the froth zone need to be known. Gas holdup in the froth zone, according to Yianatos (1987), varies with gas rate and varies with height in the froth bed. Recent work by Pal and Masliyah (1990) suggests that gas holdup is independent of these two factors. An average value of gas holdup for given conditions can be assumed. Bubble size in the froth zone is probably different from that in the collection zone and changes with gas rate (Finch and Dobby, 1990a). Pal and Masliyah (1990) assumed that bubble size is the same in both zones. Adopting this assumption and assuming bubble size in the froth also follows the empirical correlation with respect to the effect of gas rate, a solution for J_b can be obtained.

Figure 2.5, taken from Xu et al. (1990a) (C=0.15cm, ϵ_{gf}=0.75; Eq.2.23 for curve a m=2, curve b $m=4.45Re_b^{-0.1}$, Eq.2.24 for curve c), shows that increasing gas rate decreases the positive bias and at a certain gas rate bias rate becomes zero. The different values of m give quite different gas rates where J_b=0, and Eq.2.24 gives a different value of J_g for J_b=0 from Eq.2.23. The equation of Pal and Masliyah approximately fits the experimental data. However, the work of Xu et al. (1990a) demonstrated that the gas rate at which bias rate is zero is dependent on the froth depth.

2.5.3 Estimating Bubble Size: d_b vs. J_g

In correlating gas holdup as a function of gas rate, bubble size needs to be known and is assumed to be a function of gas rate. Inversely, if gas holdup, gas and liquid rates are known, bubble size can be estimated. The procedure is to repeatedly substitute estimates of d_b into Equations (2.18) and (2.4) until the calculated U_{sb} from Equation (2.4) equals the measured U_{sb} from Equation (2.1).

This can be illustrated using Figure 2.6 where curve a is the definition equation of slip velocity (eq.2.1) and curves b, c, d are given by the relation between slip velocity and terminal velocity for various bubble sizes. In plotting Figure 2.6, m=2.0 is used (using $m=4.45Re_b^{-0.1}$ does not make a large difference). As an example, suppose the measured gas holdup is 12%, then for the given conditions the estimated bubble size is about 1mm (a QuickBASIC program is presented in Appendix 2 for estimating bubble size). It is noted here that there are two intercepts between curve a and the others. This

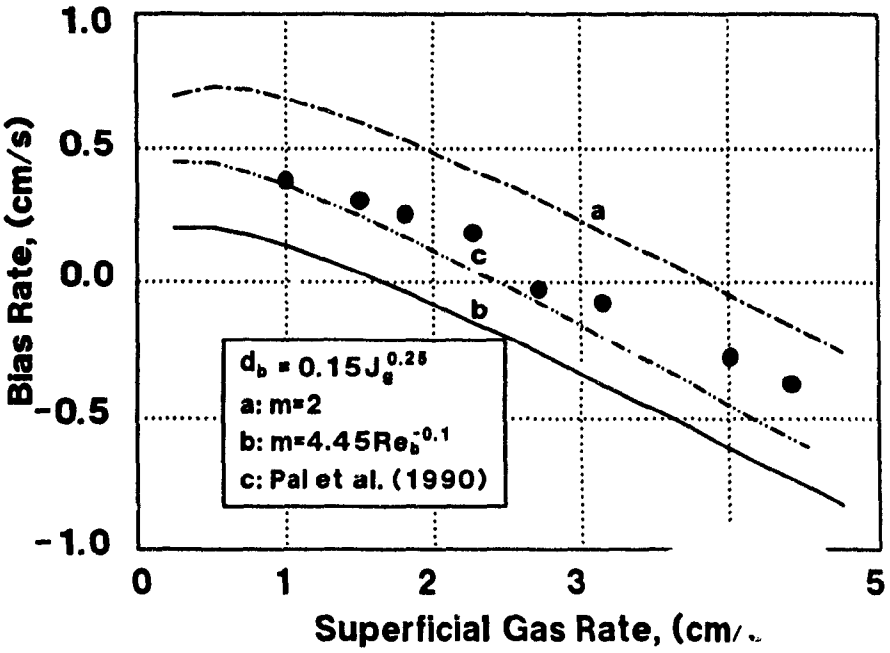

Figure 2.5 Bias rate as a function of gas rate (curve c is plotted using the equation of Pal and Masliyah, 1990; data from Xu et al , 1990a)

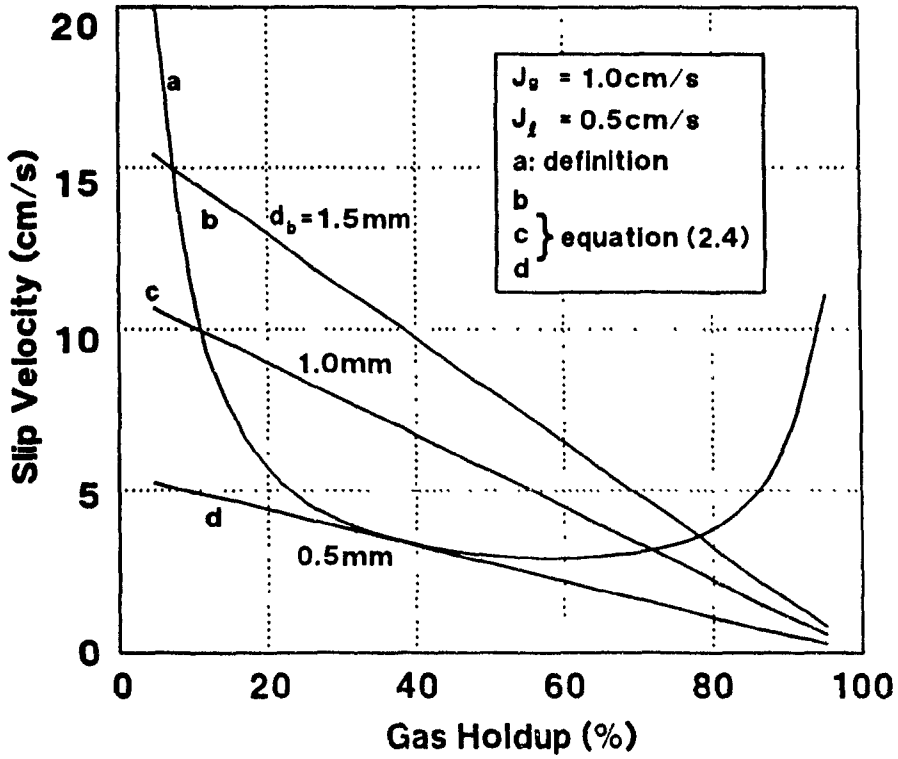

Figure 2.6 Illustration of bubble size estimation using the bubbly flow model

implies that there are two solutions: the one at higher gas holdup is interpreted to refer to the froth zone. There is a particular case where only one intercept is achieved. Below that bubble size, there is no longer an intercept. This bubble size is the minimum bubble size for the bubbly flow model to apply. The minimum bubble size represents the limiting conditions for flotation column operation in the bubbly flow regime.

In previous approach (Yianatos et al., 1988a), m was taken as function of Reynolds number, by analogy with the result for settling of solid particles derived by Richardson and Zaki (1954), and U_{sb} was related to bubble diameter by analogy with the hindered settling equation used by Masliyah (1979).

In the present case, m is fixed at 2.0, following the suggestion of Wallis (1969) for fine bubbles ($d_b < 2.0$mm), and the Schiller and Naumann (1933) expression is used for bubble terminal velocity, U_T (eq.2.18).

The routine now is to measure U_{sb} (by measuring J_g, J_l and ϵ_g), to estimate U_T from Equation (2.18) (with $m=2$) and iteratively solve for d_b in Equations (2.18) and (2.21).

Other expressions for U_T provided $d_b \leq 1.5$mm, could be substituted (Dobby et al., 1988). One simplification that becomes apparent on use is there is now only one definition for Re_b instead of, as before, one for the determination of m and another for the determination of U_{sb}.

Using this new routine the data of Yianatos et al. (1988a) was re-examined (Xu and Finch, 1990b); an extract of the results, selected to cover the full range in d_b, is given in Table 2.3. Essentially no difference with the previous result is found.

Table 2.3 Bubble Diameters Measured and Predicted

frother[1] ppm	J_g (cm/s)	J_l (cm/s)	ϵ_g (%)	Re	d_b^2 (cm)	d_b^3 (cm)	d_b^4 (cm)
5	1.0	0.91	9.5	157	1.20	1.11	1.11
10	1.0	0.85	12.9	97	0.86	0.87	0.87
15	1.0	0.82	15.8	77	0.77	0.75	0.76
20	1.0	0.85	15.5	79	0.69	0.77	0.77
25	1.0	0.77	16.2	74	0.73	0.74	0.74
10	2.1	0.30	15.7	265	1.51	1.40	1.40
15	1.5	0.30	14.0	165	1.13	1.11	1.11
15	0.5	1.00	12.3	37	0.62	0.55	0.55
15	0.5	1.00	17.0	55	0.67	0.64	0.64

1. Dowfroth 250C
2. bubble size measured using photography
3. bubble size predicted following Yianatos et al. (1988)
4. bubble size predicted using present approach

2.5.4 Effect of Solids on Gas Holdup

The effect of solid particles on the gas holdup in the collection zone of flotation columns can be predicted using the bubbly flow model. Hydrophobic solids loading on bubbles reduces the rising velocity of the bubbles leading to an increase in gas holdup. On the other hand, hydrophillic particles remain in the liquid, increasing both the slurry density and viscosity. These increases have opposite effects on gas holdup. An increase in slurry density increases the driving force leading to a higher rising velocity of bubbles and less gas holdup, while an increase in slurry viscosity decreases the rising velocity of bubbles leading to higher gas holdup. To simplify the situation, change in slurry viscosity due to solid particles is not considered.

Bubble-particle aggregate density ρ_s can be estimated assuming that: particles are small relative to bubbles, each particle occupies d_p^2 surface of the bubble (Szatkowski and Freyberger, 1985), and bubble loads to 50% of a monolayer (Jameson, 1986). Then,

$$\rho_b = \frac{\pi d_p \rho_p}{2 d_b} \tag{2.25}$$

This is equivalent to the mass of solids per unit volume of gas. Figure 2.7 presents gas holdup as a function of bubble size. Curve a is the case where 50% of the bubble surface is loaded with solid particles with no solids in suspension; curve b is the case where no solid particles are added; curve c is the case where the slurry density increases to $\rho_{sl}=1.20$ g/cm^3 with no solids attached on bubble surface (A FORTRAN program is written for these calculations and is included in Appendix 3). This plot suggests that at small bubble size gas holdup can increase by more that 50% due to bubble loading while it may decrease by 20% due solids in suspension. The effect at large bubble size is small.

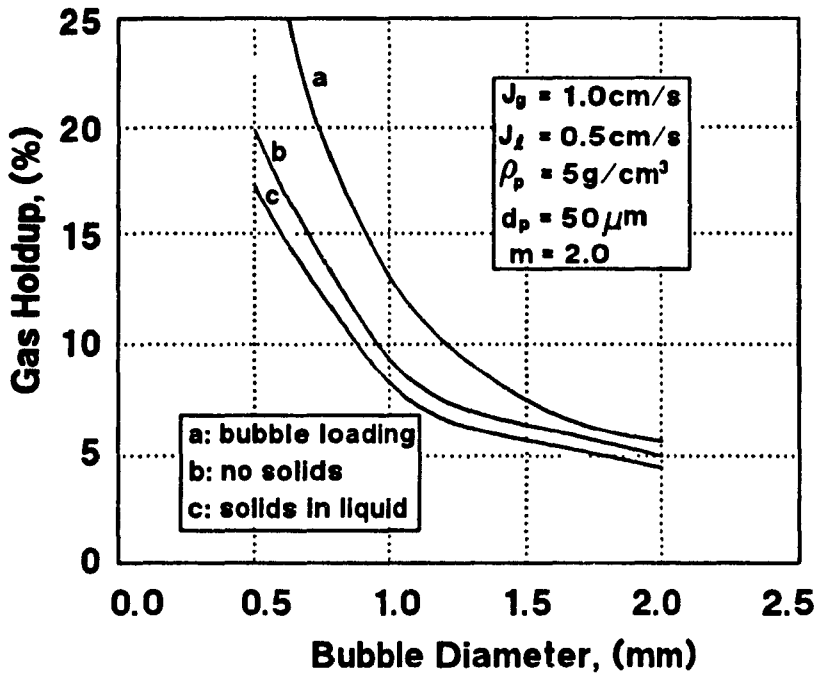

Figure 2.7 Effect of solid particles on gas holdup calculated from bubbly flow model

2.6 Column Limiting Operating Conditions

A flotation column is probably best operated with the following three conditions: bubbly flow, a distinct froth/slurry interface and a positive bias. It is observed that the gas rate can modify these conditions.

Xu et al. (1989, 1990a) have determined the gas rates at which loss of bubbly flow, loss of interface or loss of positive bias occurs. Figure 2.8 presents the measured maximum gas rate for the three phenomena. They also derived the theoretical maximum in gas rate using the bubbly flow model (Xu et al., 1990a). The measured and theoretical maximum gas rates are in good agreement. Kasireddy and Al Taweel (1989) have recently made theoretical estimates of maximum gas rate for loss of bubbly flow and the values are in agreement with the results of Xu et al. (1990a).

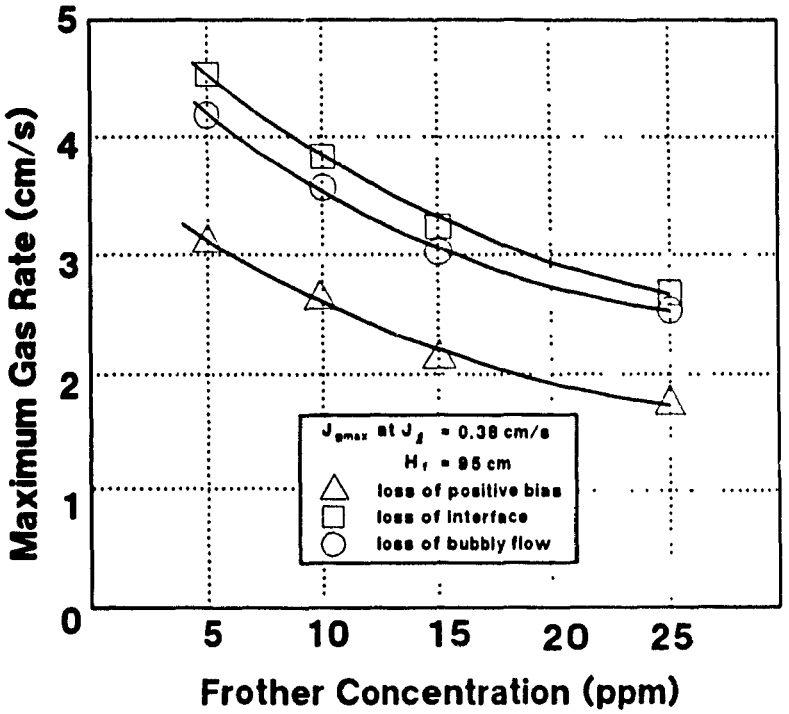

Figure 2.8 Comparison of measured maximum gas rates for the three defined phenomena (feed is used to control level; data from Xu et al., 1990)

CHAPTER 3

GAS HOLDUP DISTRIBUTION AND LIQUID CIRCULATION

Radial gas holdup distribution is examined in this chapter. Various theoretical models for describing radial gas holdup profiles and calculating liquid circulation velocity profiles are reviewed, and the liquid circulation velocity profiles for the case of parabolic radial gas holdup profiles are calculated from the shear stress model.

3.1 General Observations

For the development and application of the bubbly flow model, a homogeneous bubble swarm uniformly distributed throughout the column cross-section is assumed with a single bubble size and a single terminal rising velocity for all bubbles. This assumption usually holds for relative small bubbles, low gas rates, and in particular for gas distributed evenly over the entire column cross-section. However, a survey of published work reveals that gas holdup in columns is not uniform over the column cross-section (Freedman and Davidson, 1969; Nassos and Bankoff, 1966; Hills, 1974). The causes of non-uniform radial gas holdup are: a) gas not well distributed over the entire column cross-section, b) existence of large bubbles, and c) the tendency of a bubble swarm to collect and rise at the centre of a column (Lockett and Kirkpatrick, 1975).

Non-uniform gas holdup and liquid circulation are intimately related, because the density difference produced by non-uniform gas holdup profiles provides the driving force for liquid circulation.

Freedman and Davidson (1969) qualitatively described the steps leading to liquid circulation due to non-uniform gas holdup profiles. Figure 3.1 presents the four stages of liquid circulation generation: (a) Bubbles distributed over an area less than the total cross-sectional area tend to rise in vertical paths above the sparged area, the pressure at

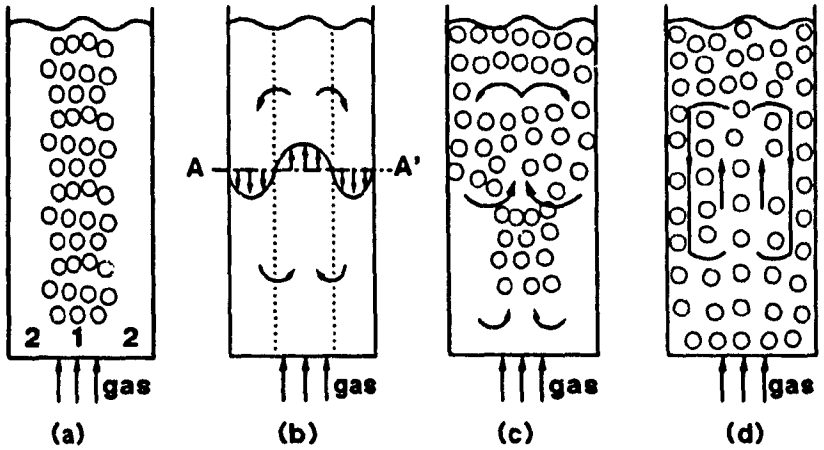

Figure 3.1 The induction of liquid circulation in a column

point 1 is then less than point 2; (b) Liquid begins to circulate within the column in the direction of this pressure difference and a velocity profile is established as indicated at section AA'; (c) Horizontal components of liquid velocity will disperse the bubbles over the cross-section in the upper half of the column, but the inward flow in the lower half will tend to concentrate bubbles at the centre, leaving unaerated regions near the walls; (d) As the gas rate is increased the downward liquid velocity eventually exceeds the rising velocity of the bubbles giving bubble downflow near the walls. Although the outcome is aeration throughout the column, a radial gas holdup variation results. Bubbles in the centre may rise in a stream of concurrent liquid, while bubbles near the walls are held by a liquid downflow in opposition to the buoyancy forces - two entirely different flow situations. One consequence is that the average gas holdup in this case may be quite different from that in a column with no internal circulation.

Liquid circulation patterns are very complex. The most common type of liquid circulation encountered in a column is the 'gulf-stream' circulation (Freedman and Davidson, 1969; Clark et al., 1987). Figure 3.2 presents this type of circulation and the associated radial gas holdup profile. It is noted that liquid moves upwards in the centre, while it moves downwards near the wall. Joshi and Sharma (1979a) proposed the concept of liquid circulation cells, which interact with each other and have a height approximately 0.8 times the column diameter. They applied an energy balance approach to derive an average liquid circulation velocity which is correlated to the liquid axial dispersion coefficient.

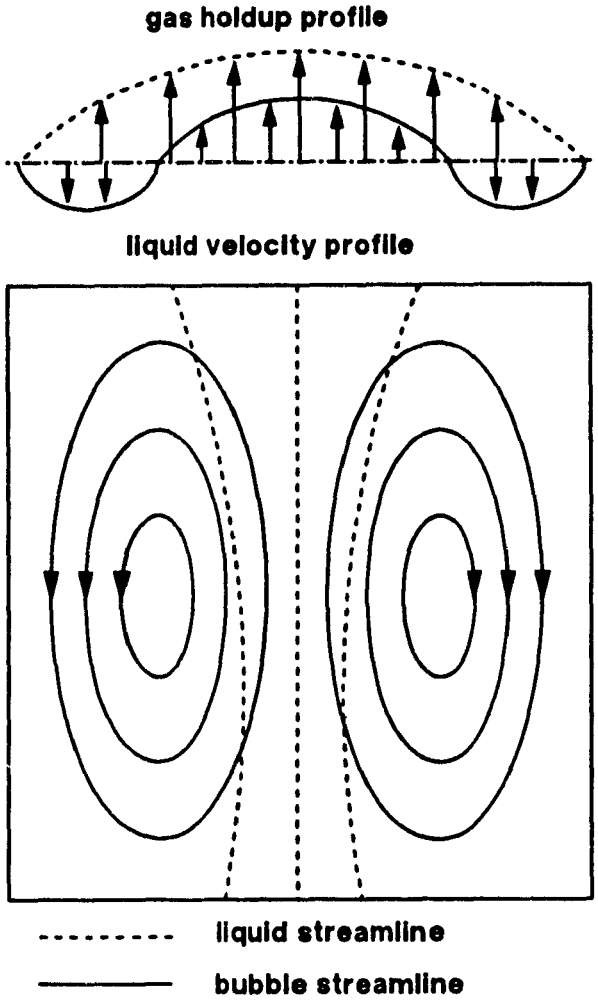

Figure 3.2 Gulf-stream liquid circulation

3.2 Radial Gas Holdup Variation

The shapes of radial gas holdup profiles are complex and dependent on the bubble generation system, gas rate, frother concentration and probably column size. Two general profiles are well-known, the parabolic or radial power law distribution and the saddle-shaped distribution. Both are axisymmetrical in theory but in practice they are usually asymmetrical. The parabolic radial gas holdup profiles can be easily described mathematically, but the saddle-shaped profiles are more difficult.

3.2.1 Parabolic Radial Gas Holdup Profile

The parabolic radial gas holdup profiles can be modelled by,

$$\varepsilon_g(\phi) = (\varepsilon_{gc} - \varepsilon_{gw})(1 - \phi^n) \tag{3.1}$$

where $\phi = r/R$, the dimensionless radial position (r is the radial distance from the centre to a point and R is the radius of the column), ϵ_{gc} and ϵ_{gw} are gas holdup at the centre (maximum) and the wall (minimum) of the column, respectively, n is a constant describing the power law curve. In general, $\epsilon_{gw} = 0$ (assumption) and $n > 1$. Radial gas holdup profiles for ϵ_{gc}=0.2 and various values of n, calculated from Equation (3.1), are presented in Figure 3.3. It is evident that the radial gas holdup becomes flat if n is sufficiently large.

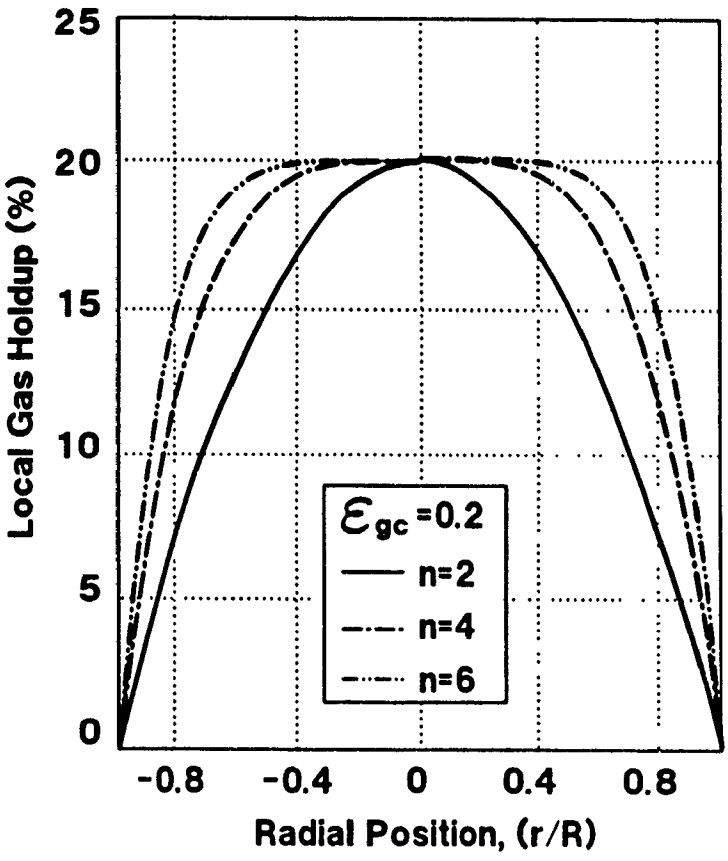

Figure 3.3 Parabolic radial gas holdup profiles calculated using Eq.(3.1) with various n values

In modelling liquid circulation in a bubble column, Ueyama and Miyauchi (1979) used a simplified form (n=2) of Equation (3.1),

$$\varepsilon_g(\phi) = 2\overline{\varepsilon_g}(1-\phi^2) \tag{3.2}$$

The average gas holdup over the column cross-sectional area, $\overline{\varepsilon_g}$, is given by integrating Equation (3.1),

$$\overline{\varepsilon_g} = \frac{1}{\pi R^2}\int_0^{2\pi}\int_0^R \varepsilon_{gc}[1-(\frac{r}{R})^n]r\,dr\,d\theta = \frac{n}{n+2}\varepsilon_{gc} \tag{3.3}$$

3.2.2 Saddle-Shaped Radial Gas Holdup Profile

Herringe and Davis (1976, 1978), Drew and Lahey (1981, 1982) and Beyerlein et al. (1985) have presented a series of mathematical descriptions of the saddle-shaped radial gas holdup profiles. The derived equations involve a number of parameters which need to be specified for the prediction of the saddle-shaped radial gas holdup profiles.

Serizawa et al. (1975) conducted a series of studies on the turbulence structure of air-water two/phase flow and noted that the saddle-shaped radial gas holdup profiles were usually present.

Figure 3.4 presents some typical radial gas holdup profiles measured by Serizawa et al. (1976) and model fitted by Drew and Lahey (1981). At low gas rates, gas holdup is relatively uniform in the central area but sharply increases near the wall. As the gas rates increase, gas holdup in the central area is no long uniform and there is also a sharp increase near the wall.

Beyerlein et al. (1985) noticed that radial gas holdup profiles changed as bubbles rose. They developed the following equation for the prediction of radial gas holdup profile downstream,

$$\frac{\partial \varepsilon_g(\phi)}{\partial x} = \frac{1}{r V_t(\phi)+U_T}\frac{\partial}{\partial r}[r(\varepsilon_g(\phi)V_r-\omega_b\frac{\partial \varepsilon_g(\phi)}{\partial r})] \tag{3.4}$$

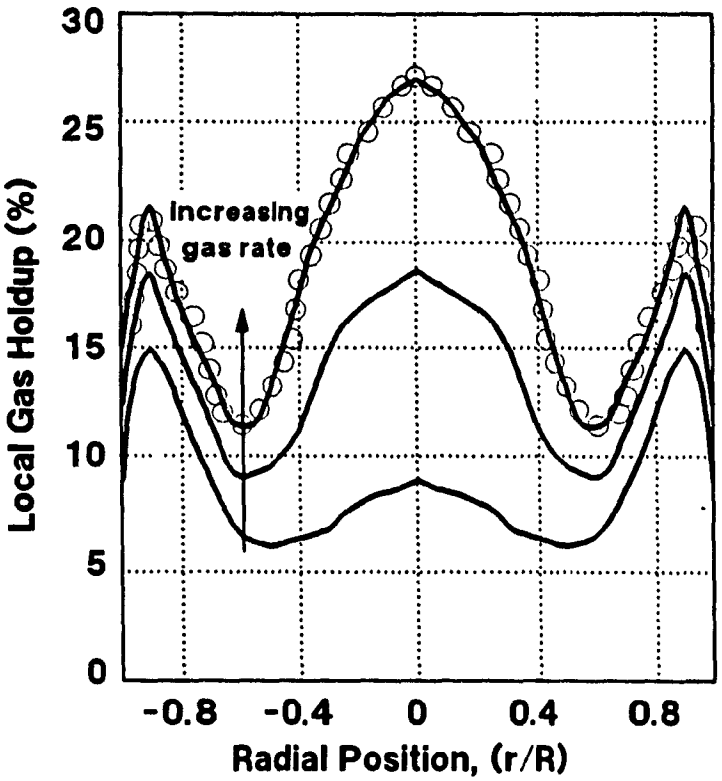

Figure 3.4 Saddle-shaped radial gas holdup profiles from Drew and Lahey (1981) and data from Serizawa et al. (1976)

where x is the axial distance from the initial profile, and r is the radial distance from the centre. V_r is the bubble radial or lateral velocity, and ω_b is the bubble eddy diffusivity. The calculation of radial gas holdup profile from the above equation requires the knowledge of the liquid circulation velocity profile $V_\ell(\phi)$. One expression for $V_\ell(\phi)$ given by Schlichting (1979) can be used,

$$V_\ell(\phi) = \frac{J_\ell}{1-\bar{\varepsilon}_g}(1+n)^2(1-\phi)^n \qquad (3.5)$$

Figure 3.5, taken from Beyerlein et al. (1985), shows the radial gas holdup profiles at various levels for a given initial profile. It can be seen from the plot that the shape of the radial gas holdup profile changes progressively from the bottom to the top; in particular, gas holdup in the central area becomes uniform towards the top with a value relatively close to the average gas holdup at that level.

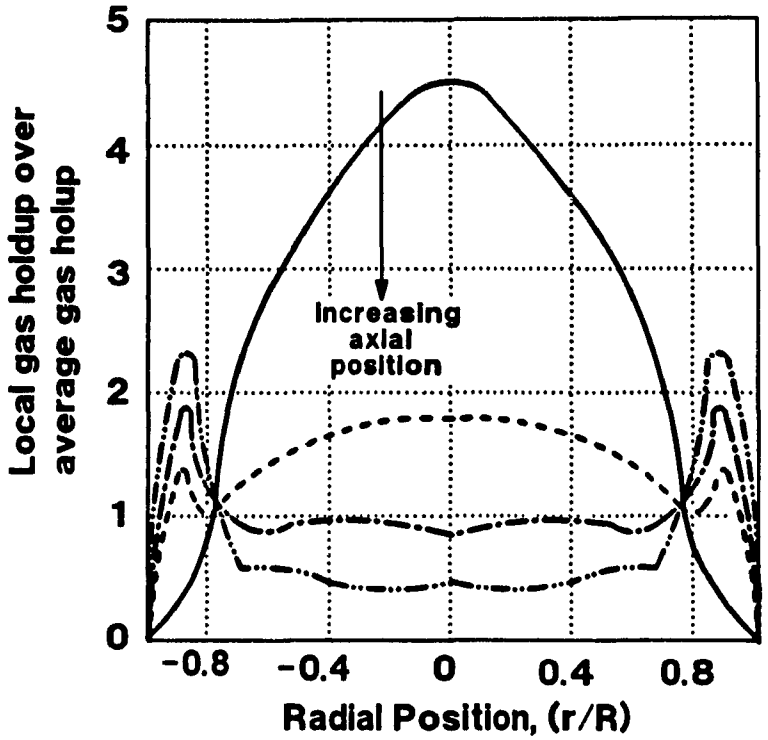

Figure 3.5 Radial gas holdup development as a function of axial distance from the initial profile (after Beyerlein et al., 1985)

3.3 Liquid Circulation Models

Various circulation models are available. Figure 3.6 presents the circulation velocity profile usually associated with the gulf-stream flow pattern. The following equation can be used to describe this type of profile,

$$\frac{V_\ell(\phi) + |V_{\ell w}|}{V_{\ell c} + |V_{\ell w}|} = (1-\phi^2)^2 \qquad (3.6)$$

where $V_{\ell c}$ and $V_{\ell w}$ are the maximum velocities at the centre and near the wall, respectively. It is noted that at the wall liquid circulation velocity is assumed zero, while the circulation velocity decreases linearly from $V_{\ell w}$ to the wall as shown in Figure 3.6.

Hills (1974) used Pavlov tubes to measure liquid circulation velocity profiles and Ueyama and Miyauchi (1979) and Morooka et al. (1986) used a tracer technique. Franz et al. (1984) used a laser-doppler anemometer to determine the velocity profile and found

that the profile is not necessarily axisymmetrical. Usually in bubble columns non-axisymmetric distributions can be discovered due either to imperfect alignment of the column or imperfect horizontal positioning of the gas distributors.

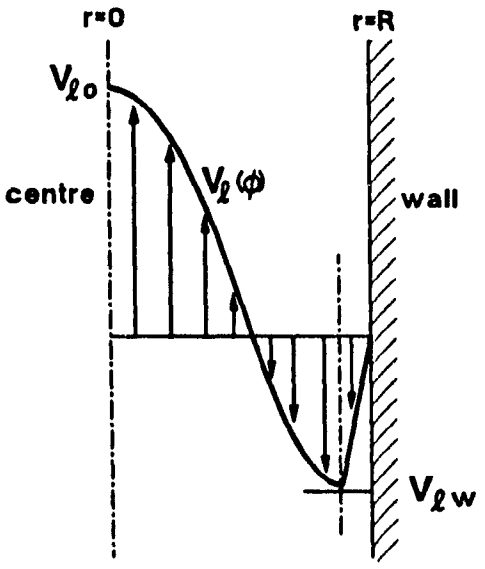

Figure 3.6 Recirculation flow velocity profiles

3.3.1 Model 1: Shear Stress Model

Clark and Flemmer (1987; 1989) proposed a model to describe the gulf-stream liquid circulation. Consider a column with bubbles distributed evenly throughout its volume. The axial hydrostatic head is identical at any radius from the column centre to the wall if the wall effect is neglected. Let one bubble at a given level, due to some reason (e.g. mixing or overall turbulence), move inward from the wall to near the column centre. Since the gas holdup in the column centre is now slightly greater than near the wall, the axial hydrostatic head is now greater near the wall than in the centre, which must lead to an inward radial pressure gradient at that level. The existence of this radial pressure gradient then produces the movement of liquid, carrying even more bubbles, from the wall to the centre so that a circulation loop (gulf-stream) is developed.

It is indeed possible that bubbles moving from the centre toward the wall can initiate a reverse pattern. Such patterns have been observed in fluidized beds (Lin et al., 1985; Surma, 1985) and perhaps are related to the saddle-shaped radial gas holdup profiles observed at low gas rates (Galaup, 1975; Serizawa et al., 1975). However, the gulf-stream circulation pattern observed by Freedman and Davidson (1969) and Hills (1974) usually prevails at high gas rates. Modelling and prediction of liquid circulation are important since it has a profound effect on gas holdup and liquid mixing (Shah et al., 1982). The circulation velocity, however, is usually difficult to measure. In contrast, the radial local gas holdup distribution is readily measured using optical or resistance probes. From measured radial gas holdup profiles, liquid circulation velocity profiles can be calculated.

The following is a brief description of the calculation approach used by Clark and

Flemmer (1987, 1989).

The axial shear stress, $T_t(\phi)$, at some radius r from the centre, is a function the axial stress T_{tw} at the wall and the mixture density of liquid and gas (Clark et al., 1987; Levy, 1963) and given by,

$$T_t(\phi) = T_{tw}[1 + \frac{Rg(\overline{\rho_{gt}} - \rho_i(\phi)}{2T_{tw}}\phi] \tag{3.7}$$

where g is acceleration due to gravity, $\overline{\rho_{gt}}$ is the average density over the cross-section and ρ_i is the average density within a radius r.

The local density, $\rho(\phi)$, of the mixture of gas and liquid at some radius r is given by,

$$\rho(\phi) = \rho_t[1-\varepsilon_g(\phi)] + \rho_g\varepsilon_g(\phi) \tag{3.8}$$

where ρ_t and ρ_g are the liquid and gas densities, respectively, and $\epsilon_g(\phi)$ is the local gas holdup at some radius and can be given by Equation (3.1). Then the average density over the entire column cross-section is calculated by,

$$\overline{\rho_{gt}} = \frac{1}{\pi R^2}\int_0^{2\pi}\int_0^R \rho(\phi) r\,dr\,d\theta = \rho_t(1-\varepsilon_{gc}) + \frac{2\rho_t\varepsilon_{gc}}{2+n} \tag{3.9}$$

The average density $\rho_i(\phi)$ within a radius r is given by,

$$\rho_i(\phi) = \frac{1}{\pi r^2}\int_0^{2\pi}\int_0^r \rho(\phi) r\,dr\,d\theta = \rho_t(1-\varepsilon_{gc}) + \frac{2\rho_t\varepsilon_{gc}}{2+n}\phi^n \tag{3.10}$$

The axial shear stress $T_t(\phi)$ can also be expressed as a function of liquid circulation velocity gradient,

$$T_t(\phi) = F(\frac{dV_t}{dr}) \tag{2.11}$$

The above equation can be inverted to yield dV_t/dr as a function of $T_t(\phi)$, then it can be used in conjunction with Equation (3.6) to calculate dV_t/dr. The boundary

conditions for integrating dV_ℓ/dr to yield the liquid circulation velocity $V_\ell(\phi)$ are,

1. $V_\ell(0)$ is maximum, at the column centre, $r=0$
2. $V_\ell(1)$ is zero, at the wall, $r=R$

Integrating $V_\ell(\phi)$ over the column cross-section yields the net liquid flowrate, Q_ℓ,

$$Q_\ell = \int_0^{2\pi}\int_0^R V_\ell(\phi) r\,dr\,d\theta \tag{3.12}$$

The correct $T_{\ell w}$ will correspond to the known net up or down flow in the column. The correct $T_{\ell w}$ must be found by trial and error.

Analytical Solution: Newtonian Fluid

For a viscous Newtonian fluid, an analytical solution can obtained for the above circulation model. In this particular case,

$$T_\ell(\phi) = \mu_\ell \frac{dV_\ell}{dr} \tag{2.13}$$

so that,

$$\frac{dV_\ell}{dr} = \frac{T_{\ell w}}{\mu_\ell}\left[1+\frac{Rg(\overline{\rho_{g\ell}}-\rho_i(\phi))}{2T_{\ell w}}\right]\phi \tag{3.14}$$

Rearranging the above equation gives,

$$\frac{dV_\ell}{dr} = AR\phi + B(R\phi)^{n+1} \tag{3.15}$$

with

$$A = \frac{T_{\ell w}}{R\mu_\ell} + \frac{g\rho_\ell \varepsilon_{gc}}{\mu_\ell(n+2)} \tag{3.16}$$

and

$$B = -\frac{g\rho_l \varepsilon_{gc}}{\mu_l (2+n) R^n} \tag{3.17}$$

This gives the following velocity profile,

$$V_l(\phi) = \frac{A(R\phi)^2}{2} + \frac{B(R\phi)^{n+2}}{n+2} + C \tag{3.18}$$

where C is given by the boundary conditions,

$$C = -\frac{AR^2}{2} - \frac{BR^{n+2}}{n+2} \tag{3.19}$$

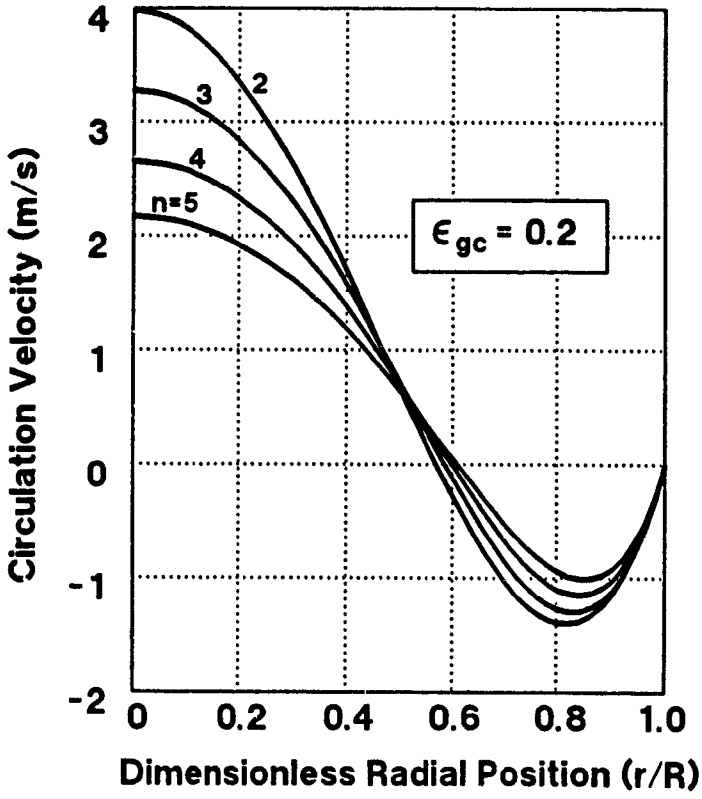

Figure 3.7 Circulation velocity profiles calculated from shear stress model for Newtonian fluid

Figure 3.7 presents the circulation velocity profiles calculated from the above equations. Gas holdup at the column centre is assumed constant (ϵ_{gc}=0.2) with various values of n. For a given n value, the effect of changing ϵ_{gc} is shown in Figure 3.8. Net water flowrate is assumed zero (Q_l=0) in both cases. A computer program written in FORTRAN for the calculations is included in Appendix 4. It is clear that increasing n (i.e. the radial gas holdup profile becomes flat) decreases the circulation velocity while for a given value of n, increasing ϵ_{gc} increases the circulation velocity. Note that circulation velocities can reach values 100 times the net gas and liquid rates (typically 1.0cm/s).

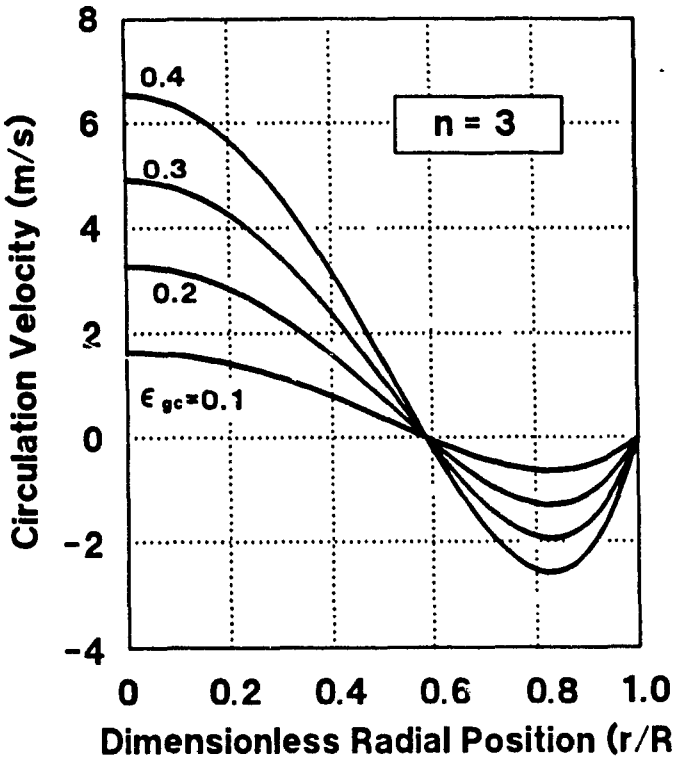

Figure 3.8 Circulation velocity profiles calculated from shear stress model: effect of gas holdup

Numerical Solution: Non-Newtonian Fluid

For a non-Newtonian fluid, the analytical solution is cumbersome or impossible to derive so that a numerical solution is used. Two cases are considered. The first case is the circulation of a power law fluid, where,

$$T_t(\phi) = K\left(\frac{dV_t}{dr}\right)^p \tag{3.20}$$

The second case is to consider both viscous and turbulent effects. Mixing length theory is used and the shear stress is accordingly taken as,

$$T_t(\phi) = K\left(\frac{dV_t}{dr}\right)^p + \ell^2 \rho(\phi)\left|\frac{dV_t}{dr}\right|\left(\frac{dV_t}{dr}\right) \tag{3.21}$$

where ℓ^2 is the mixing length used by Clark and Flemmer (1987) and Levy (1963),

$$\frac{\ell}{R} = 0.14 - 0.08\left(\frac{r}{R}\right)^2 - 0.06\left(\frac{r}{R}\right)^4 \tag{3.22}$$

Due to the complexity of the above equations, a computer program written in FORTRAN was developed (Appendix 5). The computation scheme is shown in Figure 3.9. Assuming a shear stress at the wall, T_{tw}, a radial shear stress profile can be calculated, which is solved for circulation velocity gradient dV_t/dr. The integration of dV_t/dr gives the liquid circulation velocity profile. According to Equation (3.12), the integration of $V_t(\phi)$ over the column cross-section should give the known net liquid flowrate. Otherwise, a new T_{tw} is taken and the calculation process is repeated. The calculations show that the circulation velocity profile is very sensitive to the value of T_{tw} and the selection of constants K and p in Equation (3.21). Figure 3.10 is an example of the calculated profiles using the model concerning the effect of turbulence proposed by Clark and Flemmer (1989). $p=1$ is the simplest case while in principle other values can be applied. Due to the nature of Equation (3.21), it seems that the solution is not unique for other values of p.

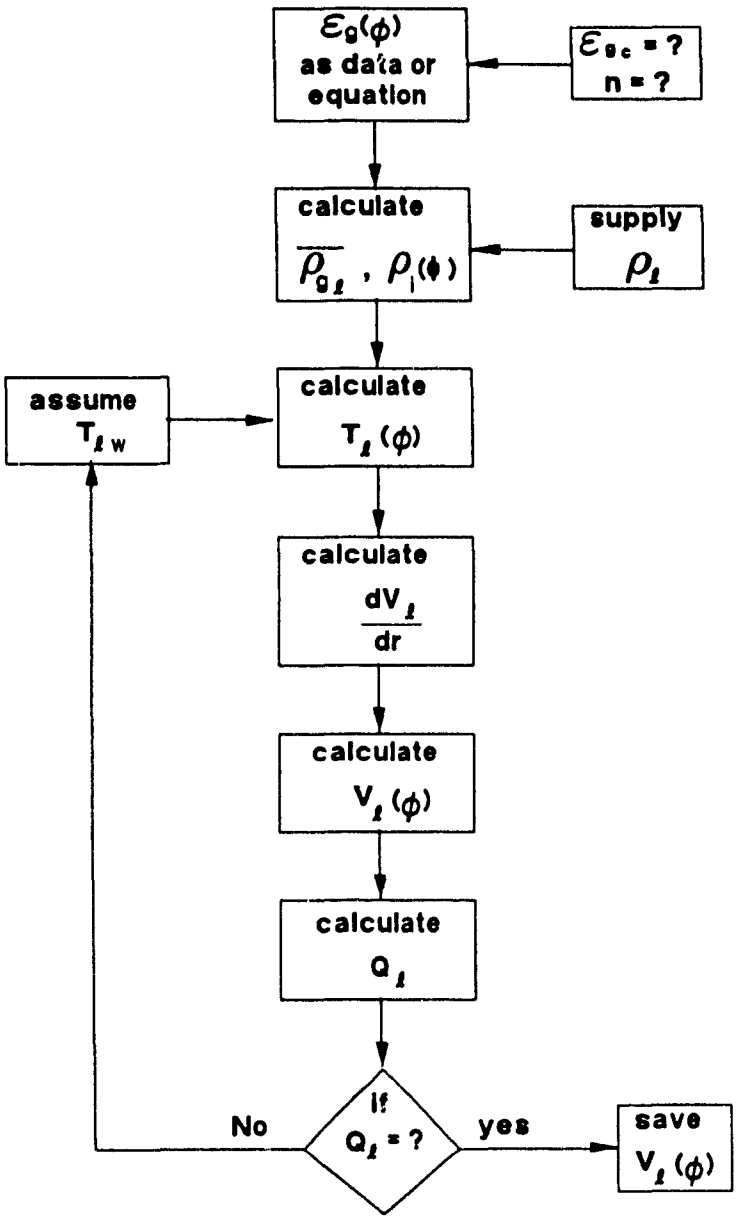

Figure 3.9 Scheme for calculating circulation velocity profile using the circulation model concerning both viscosity and turbulence effect

3.3.2 Model 2: Momentum Balance

The following model was developed by Ueyama and Miyauchi (1979) for a bubble column and was extended to a three-phase fluidized bed (Morooka et al., 1982). The steady state equation of motion for a liquid is given by,

$$-\frac{d(r\,T_{tw}(\phi))}{dr} = \frac{dp}{dz} + (1-\varepsilon_g)\,\rho_l g \tag{3.23}$$

where dP/dz is the axial pressure drop. The shear stress is given by,

$$T_l(\phi) = -(\nu_l + \nu_T)\,\rho_l \frac{dV_l}{dr} \tag{3.24}$$

where ν_l and ν_T are the liquid kinematic viscosity and the turbulent kinematic viscosity, respectively. Several assumptions are made to solve the above equations, namely: $(\nu_l + \nu_T)$ is constant in the turbulent region, and the radial distribution of gas holdup can be approximated by Equation (3.2). The solution to the above equations with these assumptions is,

$$V_l(\phi) = V_{tw} + \frac{1}{32}\frac{g d_c^2 \overline{\varepsilon_g}}{\nu_l + \nu_T}(1-\phi^2)^2 \tag{3.25}$$

and with

$$V_{tw} = -\frac{1}{192}\frac{g d_c \overline{\varepsilon_g}}{\nu_l + \nu_T}\frac{2-3\overline{\varepsilon_g}}{1-\overline{\varepsilon_g}} + \frac{J_l}{\overline{\varepsilon_g}} \tag{3.26}$$

The shear stress is evaluated solely through the turbulent kinematic viscosity since the liquid kinematic viscosity can be neglected. Miyauchi and Shyu (1970) found that the turbulent kinematic viscosity is almost independent of gas rate and is affected mainly by the column diameter as given by,

$$\nu_T = 0.0322\,d_c^{1.7} \tag{3.27}$$

Circulation velocity profiles are calculated using the above equations and shown

in Figure 3.11. Essentially the shape of the profile is similar to that obtained by shear stress model, except at the wall.

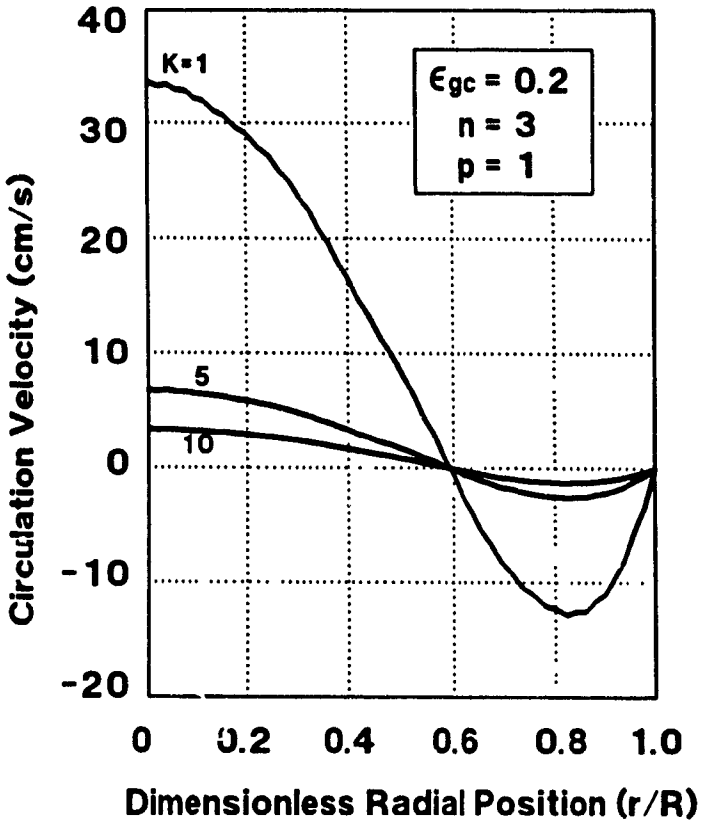

Figure 3.10 Circulation velocity profiles for non-Newtonian fluid calculated from shear stress model

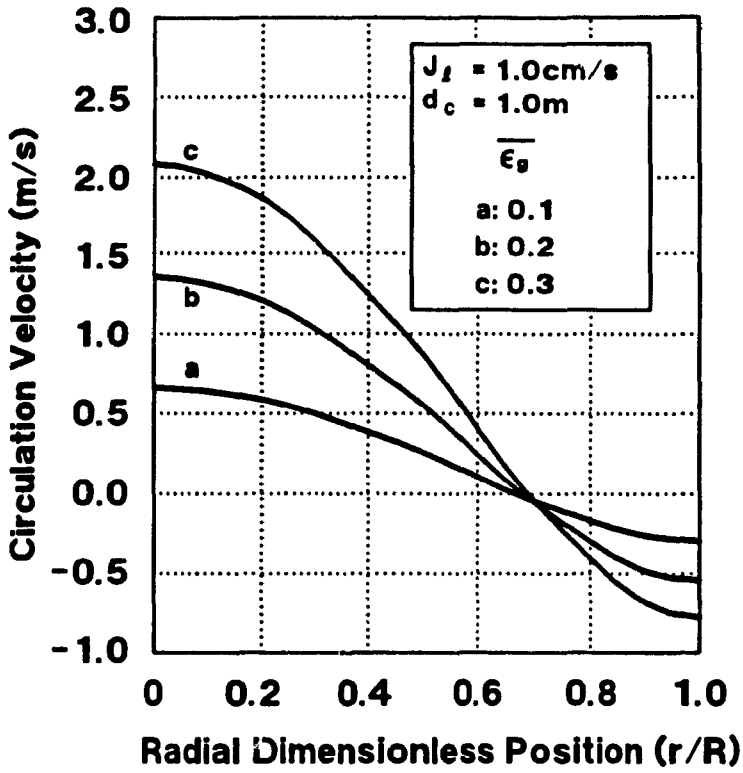

Figure 3.11 Circulation velocity profiles calculated from moment balance model

3.3.3 Model 3: Energy Balance

For the liquid circulation in a bubble column, Whalley and Davidson (1969) adopted the vorticity and stream function relationship in inviscid fluids for steady vortex motion. Substantially, the stream function is correlated to the energy dissipation in the system. As pointed out by Whalley and Davidson (1974), the energy dissipation is due to: (1) wakes behind bubbles, E_1; (2) the bubble breakup, E_2; (3) hydraulic jump at the liquid surface, E_3; (4) the turbulence near the nozzles, E_4; (5) the viscous drag at the wall, E_5; and (6) the kinetic energy loss during the downward flow of the liquid, E_6. They showed that only E_1 and E_3 are important.

Joshi and Sharma (1979a) and Joshi (1980) modified their single circulation cell model into a multiple circulation cell model. Each cell has approximately the same height as the column diameter. Further, they noted that E_6 is more important than E_3. Following this concept, a circulation velocity profile and an average circulation upward velocity are developed.

CHAPTER 4

MIXING

Phase mixing theories (liquid, gas and solids) are reviewed, with the focus on the determination of liquid phase mixing parameters. The one-dimensional plug flow axial dispersion model is described in detail. There are five solutions to the axial dispersion model for five different experimental procedures of column operation and tracer injection and detection. For a pulse tracer with closed-closed boundaries, a numerical solution is developed. Compartment models, such as the backflow compartment model, are also examined. The methods of estimating mixing parameters by fitting experimental residence time distribution (RTD) to the mixing models are presented. Previous correlations for the axial dispersion coefficient of liquid, gas and solid phase in bubble columns are reviewed and examined in this chapter.

4.1 Significance of Mixing in Column Flotation

Prior to the presentation of phase mixing theories, it is important to understand how mixing or transport affects recovery of minerals. Consider, for illustration purposes, the particle collection process in a column is a first-order reaction relative to the solids concentration with a flotation rate constant k_c. The recovery of a mineral is dependent on three variables: this rate constant k_c, the mean residence time τ, and the measure of mixing (for example, N_d, vessel dispersion number). There are two extreme cases of mixing within the collection zone of a flotation column. One extreme is plug flow where the residence time of all components is the same. Plug flow in a column means there is a concentration gradient of floatable mineral along the axis of the column. For a first-order rate reaction, exhibiting plug flow transport and having a retention time t, the recovery R_c is given by,

$$R_c = 1 - \exp(-k_c t) \tag{4.1}$$

while for a system exhibiting perfect mixing, R_c is given by,

$$R_c = 1-(1+k_c\tau)^{-1} \tag{4.2}$$

Mixing has a detrimental effect upon recovery. For example, when $t=\tau=5$min. and $k_c = 0.4$ minute^{-1}, recovery in plug flow is 92% while recovery in perfectly mixed flow is only about 71%.

Mixing conditions in practice are between plug flow and perfectly mixed flow. Axial mixing occurs as well as radial mixing. Radial mixing is usually not considered. The objective of measuring the mixing parameters is to quantify the effect of mixing upon recovery. A relationship between recovery and the vessel dispersion number N_d for a first-order reaction is given by (Levenspiel, 1972),

$$R_c = 1-\frac{4a\exp(\frac{1}{2N_d})}{(1+a)^2\exp(\frac{a}{2N_d})-(1-a)^2\exp(\frac{-a}{2N_d})} \tag{4.3}$$

where

$$a = (1+4k_c\tau N_d)^{1/2}$$

Equation (4.3) reduces to Equation (4.1) for plug flow transport (N_d=0) and reduces to Equation (4.2) for perfectly mixed flow (N_d=∞). Equation (4.3) can be expressed graphically reflecting the dependence of recovery upon k_c, τ and N_d (Finch and Dobby, 1990a).

The emphasis here is the solid and liquid phase mixing in the collection zone of flotation columns. The mixing of the gas phase may also be important, as may be mixing in the froth zone.

4.2 Phase Mixing Theories

The extent of mixing of both liquid and solid phases is heavily dependent on the motion of rising gas bubbles, while mixing in the gas phase is usually not considered

(Fan, 1989). The ultimate objective of studying mixing in a flotation column is to determine the mixing condition of the solid phase and its impact upon recovery.

4.2.1 Liquid Phase Axial Mixing

A large number of correlations are available for predicting liquid phase axial dispersion coefficient in gas-liquid systems. Table 4.1 summarizes some of the correlations which have some applicability in flotation columns (Fan, 1989). Fan (1989) noticed that at relatively high gas rates, the liquid axial dispersion coefficients predicted by these correlations agree fairly well.

In general, the liquid phase dispersion coefficient in a bubble column is proportional to the 0.3-0.5 power of the superficial gas rate, and proportional to the 1-1.5 power of column diameter. It is noted that most experimental work has been done for batch-liquid systems or at relatively low liquid rate and thus, few correlations consider the effect of liquid velocity. Recently, Ityokumbul (1986) carried out a review of reported liquid axial dispersion data. It was found that most of the work was conducted under steady state liquid-backmixing. The liquid backmixing coefficient may not be necessarily the same as the axial dispersion coefficient. Ityokumbul (1986) reported that the liquid axial dispersion coefficient is independent of gas rate in bubbly flow regime and is proportional to the 1-2 power of gas rate in churn-turbulent flow regime.

Rietema (1982) reviewed the mixing mechanisms of bubble columns. If molecular diffusion is neglected, there are three major contributions to the liquid axial mixing,

1. turbulence eddies of both overall and small-scale
2. entrainment of the liquid in the wakes of bubbles and the mass exchange between the wakes and remaining part of liquid
3. overall circulation of the liquid phase

The overall dispersion coefficient of liquid should be the sum of the three contributions, although it is difficult to distinguish between the three mixing mechanisms. So far, no general mixing theory has emerged accounting for these mechanisms.

Specifically related to flotation column studies, Dobby and Finch (1985b) proposed the following equation,

Table 4.1 Correlations for Liquid Phase Axial Dispersion Coefficient (after Fan, 1989)

investigators	correlations (in SI units)	range of variables	systems
Kato and Nishuiwaki (1972)	$Pe = \frac{13Fr_g^{0.5}}{1+6.5Fr_g^{0.4}}$	$0 \le Fr_g \le 0.16$ $d_c \ge 0.122$m	gas-liquid
Kato et al. (1972)	$Pe = \frac{13Fr_g^{0.5}}{1+8Fr_g^{0.425}}$	$2 \le J_g \le 30$ cm/s $0 \le J_l \le 2.2$ cm/s $6.6 \le d_c \le 21.4$ cm	gas-liquid-solid
Towell and Ackerman (1972)	$E_l = 1.225 d_c^{1.5} J_g^{0.5}$	$0.9 \le J_g \le 9$ cm/s $0.4 \le J_l \le 1.6$ cm/s	gas-liquid
Deckwer et al. (1974)	$E_l = 0.678 d_c^{1.4} J_g^{0.3}$		gas-liquid
Baird and Rice (1974)	$E_l = 0.35 d_c^{4/3} (g J_g)^{1/3}$	$0.3 \le J_g \le 45$ cm/s $8.2 \le d_c \le 153$ cm	gas-liquid
Joshi (1980)	$E_l = 0.35 d_c (J_l + U_c)$ $U_c = 1.31 g d_c (J_g - \frac{\varepsilon_g}{1-\varepsilon_g} J_l - \varepsilon_g U_T)]^{1/3}$	$1.0 \le J_g \le 39$ cm/s $0 \le J_l \le 12$ cm/s $0.10 \le d_c \le 1.067$m	gas-liquid and gas-liquid-solid
Riquarts (1981)	$pe = 14.7 (Fr_g^3 / Re_g)^{1/8}$		gas-liquid
Kelkar et al. (1983)	$E_l(1-\varepsilon_g) = 1.42 d_c^{1.33} [J_g - \frac{\varepsilon_g J_l}{1-\varepsilon_g}]^{0.73}$	$d_c = 0.154, 0.3$ m $1.0 \le J_g \le 30$ cm/s $0 \le J_l \le 15$ cm/s	gas-liquid
Kawase and Moo-Young (1986)	$Pe = 2.92 n^{4/3} Fr_g^{1/3}$	$0.625 \le n \le 1.0$ $2 \times 10^{-3} \le Fr_g \le 0.5$	gas-liquid

dimensionless parameters:

$Pe = J_g d_c / E_l$

$Fr_g = J_g^2 / (g d_c)$ and $Re_g = J_g d_c \rho_l / \mu_l$

n = power-law index of liquid viscosity

$$E_l = 0.063 d_c \left(\frac{J_g}{1.6}\right)^{0.3} \tag{4.4}$$

where E_l is in m^2/s, d_c in m and J_g in cm/s. Laplante et al. (1988) re-examined the data and considered the effect of solids on the axial dispersion coefficient by the relation,

$$E_l = 2.98 d_c^{1.31} J_g^{0.33} \exp(-0.025S) \tag{4.5}$$

where E_l is in cm^2/s, d_c in cm, J_g in cm/s and S is the feed solids percentage by weight.

Recently, Luttrell and Yoon (1990) used the following relation to estimate the vessel dispersion number in their computer-aided package for column flotation scale-up,

$$N_d = K\left(\frac{d_c}{H_c} \cdot \frac{J_g}{J_l}\right)^p \tag{4.6}$$

where K, p are constants (which were not given).

Liquid axial dispersion coefficient as a function of gas rate at d_c=50cm and J_l=0.5cm/s is presented at Figure 4.1 estimated from various relationships. Joshi's correlation (1980) is not plotted because it requires both the gas holdup and bubble terminal velocity. The correlation developed by Kelkar et al. (1983) is plotted assuming gas holdup is linearly dependent on gas rate ($\epsilon_g = 0.1 J_g$). This correlation has the largest slope. It is further noted that the correlations of Towell and Ackerman (1972), Deckwer et al. (1974) and Baird and Rice (1975) agree very well. The two correlations proposed specifically for flotation columns have a very similar trend to the others but with smaller values of E_l. The difference between various correlations may be due to: (a) the method of RTD measurement, (b) the models used for estimating E_l, and (c) the RTD fitting routines.

4.2.2 Gas Phase Mixing

Data published on gas phase mixing is mostly limited to the studies of bubble columns without solids. Gas phase axial dispersion coefficients have been measured using pulse, step or frequency response techniques with a low solubility gas as the tracer which is injected into the main gas stream. Molerus and Kurtin (1986) measured the residence

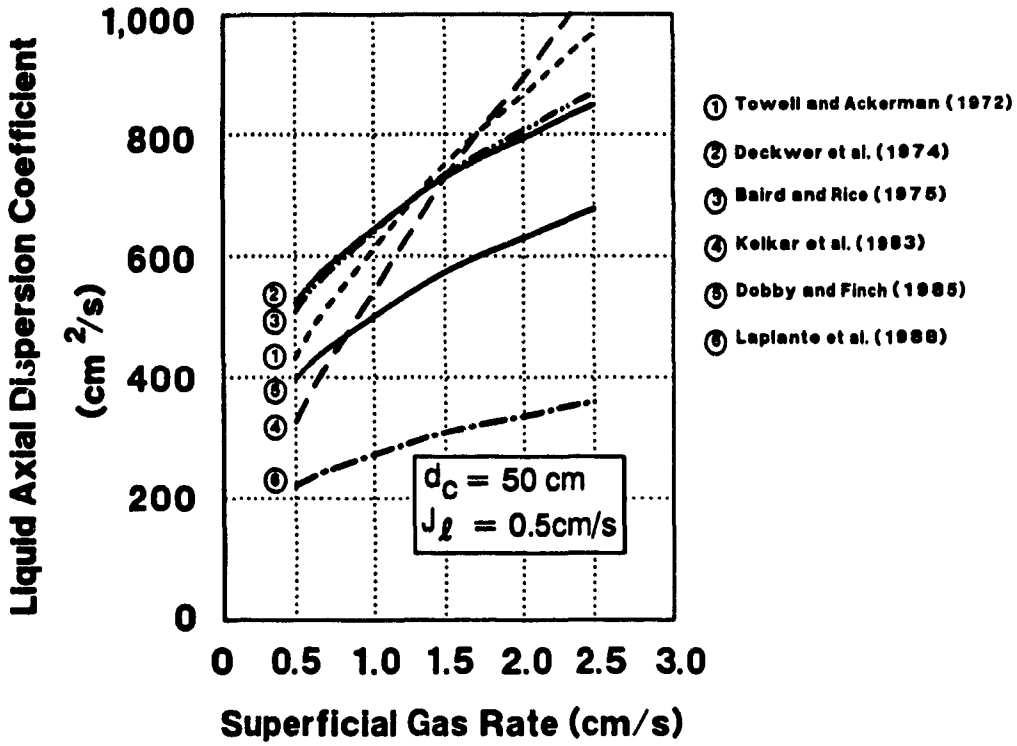

Figure 4.1 Comparison of liquid dispersion coefficient estimated from various correlations

time distribution of gas phase in a bubble column, and a three-parameter model was developed to model the RTD of gas phase. Among the gases used as a tracer are H_2, freon and O_2. Some correlations are summarized in Table 4.2. In general, the gas phase axial dispersion coefficient increases with increasing superficial gas rate to the power of 1-3.56 (see Table 4.2) and with column diameter to the power of 1.33-2, and are roughly 2-10 times greater than the liquid axial dispersion coefficient.

Correlations listed in Table 4.2 show significant deviations in the estimated values of gas phase dispersion coefficient, E_g. The correlation proposed by Joshi (1982) covers a wide range of operating conditions and is the most widely applicable of all the correlations (Fan, 1989).

Magiera (1984) found that the axial gas phase dispersion coefficient in a slurry column with continuous slurry flow is strongly dependent on the superficial slurry rate and solids concentration. The dispersion coefficient increased significantly with

increasing solids concentration and superficial gas rate.

Table 4.2 Correlations for Gas Phase Axial Dispersion Coefficient
(After Fan, 1989)

investigators	correlations (in SI units)	range of variables	system
Towell and Ackerman (1972)	$E_{zg} = 19.7\, d_c^2 J_g$	$d_c = 0.405, 1.07$m $0.85 \le J_g \le 13$ cm/s $0.72 \le J_l \le 1.35$ cm/s	air-water
Field and Davidson (1980)	$E_{zg} = 56.4 d_c^{1.33} (\frac{J_g}{\varepsilon_g})^{2.56}$	$0.076 \le d_c \le 3.2$m $0.85 \le J_g \le 13$ cm/s $0.72 \le J_l \le 1.35$ cm/s	air-water
Mangartz and Pilhofer (1980)	$E_{zg} = 50 d_c^{1.5} (\frac{J_g}{\varepsilon_g})^3$	$0.092 \le d_c \le 1.07$m $1.5 \le J_g \le 13$ cm/s $0.72 \le J_l \le 1.35$ cm/s	gas-liquid
Joshi (1982)	$E_{zg} = 110 d_c^2 (\frac{J_g^2}{\varepsilon_g})$	$0.092 \le d_c \le 1.07$m $0.76 \le J_g \le 13$ cm/s $0 \le J_l \le 6$ cm/s	

4.2.3 Solid Phase Mixing

Solids mixing behaviour in a slurry bubble column is complex. The flow regime has a strong effect on the profile of axial solids concentration. Liquid properties such as density, viscosity and surface tension affect the axial solids dispersion in slurry bubble column systems. The effect is especially obvious in the presence of surfactant due to their strong effects on the bubble properties. In addition, solids properties such as density and size are important in solids mixing.

Quantitative analysis of the axial solids concentration profile in continuous solids flow or solids-batch slurry bubble column systems has been generally based on the sedimentation-dispersion model (Fan, 1989; Jean et al., 1988). The model is characterized by two parameters, namely the axial solid phase dispersion coefficient and the solids settling velocity. There are a number of empirical correlations proposed in the literature to account for these two parameters. However, the application of the correlations is limited due to the inconsistent physical interpretation of the parameters.

Several investigators (Rice et al., 1974; Imafuku et al., 1968; Argo and Cova, 1965) have found that the axial dispersion of fine solids in a bubble column is the same as that of the liquid. Specific to flotation columns, Dobby and Finch (1985b) and Kho and Sohn (1989) also found that fine solid particle mixing was similar to that of the liquid phase. The particle mean residence time τ_p for the case of a descending slurry not contacted with gas bubbles is given by,

$$\tau_p = \tau_l\left(\frac{U_{sl}}{U_{sl}+U_{sp}}\right) \tag{4.7}$$

where U_{sl} is the slurry interstitial velocity ($J_{sl}/(1-\epsilon_g)$) and U_{sp} is the particle slip velocity and can be estimated by the general equation proposed by Masliyah (1979),

$$U_{sp} = \frac{g d_p^2(\rho_p-\rho_{sl})(1-\varepsilon_g)^{2.7}}{18\mu_{sl}(1+0.15Re_b^{0.687})} \tag{4.8}$$

where Re_p is the particle Reynolds number given by,

$$Re_p = \frac{d_p U_{sp}\rho_{sl}(1-\varepsilon_g)}{\mu_{sl}} \tag{4.9}$$

4.3 Mixing Models

To evaluate the axial dispersion coefficient, tracer techniques are used to measure residence time distributions (RTDs). Fitting an appropriate model to experimental RTDs gives the axial dispersion coefficient. Several mixing models are available. The one dimensional plug flow axial dispersion model is still the most frequently used. In this section, the axial dispersion model is investigated in detail. The tanks-in-series model and backflow compartment model are also presented.

4.3.1 Axial Dispersion Model

For the axial dispersion model to be applied to the transport of a tracer in a flotation column, several assumptions must be fulfilled. The most important are:

1. Flow is not disturbed by the injection of the tracer.
2. There is a uniform holdup of the material of interest along the column axis so that the axial convective velocity of the tracer is constant for fixed operating conditions.
3. Tracer concentration is a function only of axial position and time (i.e. tracer concentration is uniform across each section of the column).
4. Tracer behaviour is similar to the bulk phase with which it is flowing (i.e. no segregation).
5. The axial dispersion coefficient, which characterizes the axial transport of the tracer, is constant for given operating conditions.

Based on the assumptions that the velocities and holdups of individual phases are uniform in the radial and axial directions, and the axial and radial dispersion coefficients, E_t and E_{rt}, are constant throughout the column, the two-dimensional unsteady-state dispersion model is,

$$E_t \frac{\partial^2 C(t)}{\partial Z^2} + \frac{E_{rt}}{r} \frac{\partial}{\partial r}\left(r \frac{\partial C(t)}{\partial r}\right) - u_i \frac{\partial C(t)}{\partial Z} - \frac{\partial C(t)}{\partial t} = 0 \qquad (4.10)$$

Equation (4.10) can be reduced to the one-dimensional axial dispersion model when the radial dispersion is negligible (Alexander et al., 1979) in comparison with the axial dispersion, i.e.,

$$E_t \frac{\partial^2 C(Z,t)}{\partial Z^2} - u_i \frac{\partial C(Z,t)}{\partial Z} - \frac{\partial C(Z,t)}{\partial t} = 0 \qquad (4.11)$$

where u_i is the interstitial liquid velocity. u_i is constant, independent of Z and t, and it presents the average interstitial velocity of liquid (or solids, Finch and Dobby, 1990) downwards in a flotation column of constant cross-sectional area. The term $\partial C/\partial t$ represents time dependency. The second term, $u_i \partial C/\partial Z$, corresponds to the convective flow in the axial or Z direction. The first term in Equation (4.11) adds a diffusive mechanism which augments the convective flow (Nauman and Buffham, 1983).

Prior to any solution to the one-dimensional axial dispersion model, it is important to have the partial differential equation in dimensionless form. It is easy to transfer

Equation (4.11) into dimensionless form using the following dimensionless groups,

$$E = \frac{C}{C_0}; \quad x = \frac{Z}{L}; \quad \theta = \frac{t}{\tau}$$

where C_0 is the initial equilibrium concentration, L column collection zone height, τ mean residence time (L/u_i).

Equation(4.11) becomes dimensionless as,

$$\frac{\partial E}{\partial \theta} = N_d \frac{\partial^2 E}{\partial x^2} - \frac{\partial E}{\partial x} \tag{4.12}$$

where N_d, called the vessel dispersion number (a dimensionless group), is the parameter which measures the extent of mixing,

$$N_d = \frac{E_t}{u_i L} \left(= \frac{1}{Pe}\right) \tag{4.13}$$

where Pe is the Peclet number.

The two extreme cases of mixing are determined by,

1. $N_d \to 0$, negligible dispersion, hence plug flow
2. $N_d \to \infty$, large dispersion, hence perfectly mixed flow

The axial dispersion model has frequently been used in the residence time distribution (RTD) studies on flotation columns (Rice, et al., 1974, 1981; Dobby and Finch, 1985b; Ityokumbul, et al., 1988; Kho and Sohn, 1989). The application of the model requires a combination of three choices: first, boundary conditions (e.g. open or closed vessel), column operation and tracer type; second, type of solution (analytical or numerical); and third, the parameter estimation routine (direct search 'least squares' or moments matching).

For a given distance between the tracer injection point and measuring point of response, the amount of spread of tracer depends on the intensity of the dispersion in the system. Levenspiel (1972) showed that the moments reflecting the spread of distribution

can be conveniently related to the vessel dispersion number (or Peclet number).

A closed end vessel, shown in Figure 4.2, is a finite vessel of length L, with tracer input at the vessel entrance and output response measured at the vessel outlet. If the entrance and exit effects are negligible ($E_t = 0$ outside of the two ends, E_t constant throughout the vessel). The variance about the mean residence time, τ, is given by,

$$\sigma_\theta^2 = 2N_d - 2N_d^2(1 - e^{-\frac{1}{N_d}}) \qquad (4.14)$$

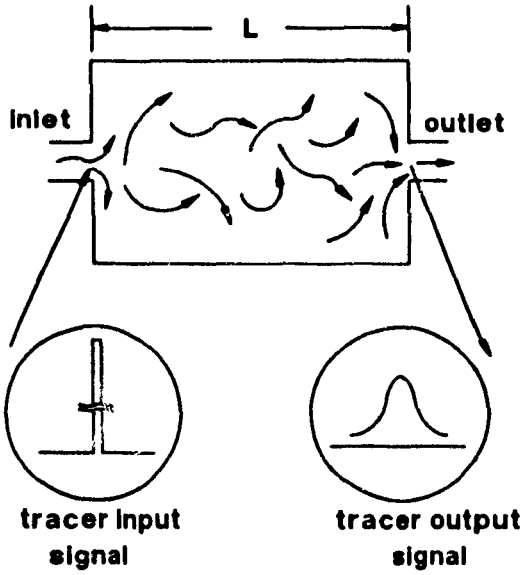

Figure 4.2 Closed-closed boundaries

An open vessel, shown in Figure 4.3, is essentially a vessel with no discontinuity in type of flow at the point of tracer injection or at the point of tracer measurement. The experimental section is simply a section of length L. The variance about the mean is given by,

$$\sigma_\theta^2 = 2N_d + 8N_d^2 \qquad (4.15)$$

The third case considered is shown in Figure 4.4. It is the combination of the first two in which no dispersion occurs at either the tracer injection or detection point but not both. The variance is related to the vessel dispersion number by,

$$\sigma_\theta^2 = 2N_d + 3N_d^2 \qquad (4.16)$$

The choice of inlet and outlet boundary conditions depends on the experimental technique. In RTD studies on the collection zone in flotation columns, particularly in full-size industrial devices, tracer is usually conveniently injected in the feed pipe or by some arrangement directly below the froth/slurry interface, and detected in the underflow line. Since some feed material moves up into the froth from which some may return, this inlet condition has some aspects of an open boundary. The exit is a good approximation of a closed boundary. While in the laboratory other inlet and outlet arrangements are feasible, experimental conditions which fully meet the mathematical definition

of open or closed boundaries are never fully realized. The common approximation is either to consider open-open or closed-closed boundaries.

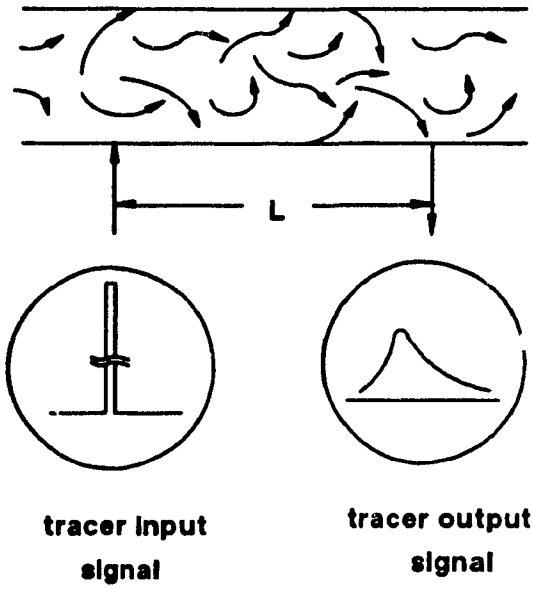

Figure 4.3 Open-open boundaries

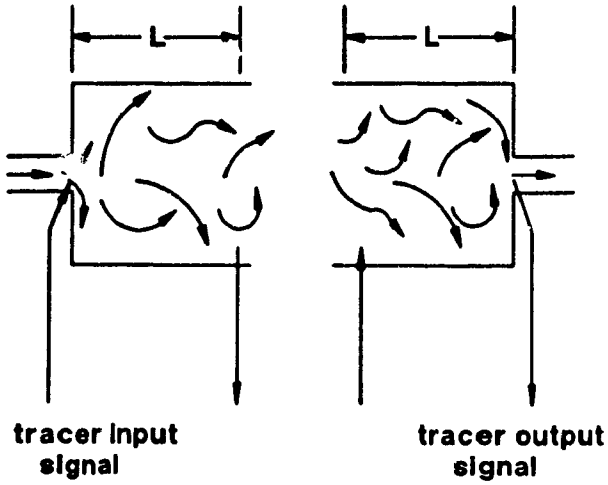

Figure 4.4 Closed-open boundaries

One reason for choosing open-open boundaries is that a relatively simple analytical solution exists (Ityokumbul et al., 1988). An analytical closed vessel solution is also available but is more complex, and as will be shown it is best to substitute a numerical solution.

The solution to the axial dispersion model is determined by the operating mode of the system (batch or continuous), the tracer injection (e.g. pulse or step) and detection method, and the boundary conditions. Figure 4.5 illustrates five commonly employed experimental procedures for studying liquid dispersion in bubble columns: (a) unsteady-state batch liquid and pulse tracer; (b) open-open boundaries and pulse tracer; (c) closed-closed boundaries and pulse tracer; (d) steady-state flow and step tracer; (e) steady-state flow backmixing and step tracer.

In presenting the solutions of the axial dispersion model to the above five cases, the boundary conditions and tracer injection and detection are clarified for each case.

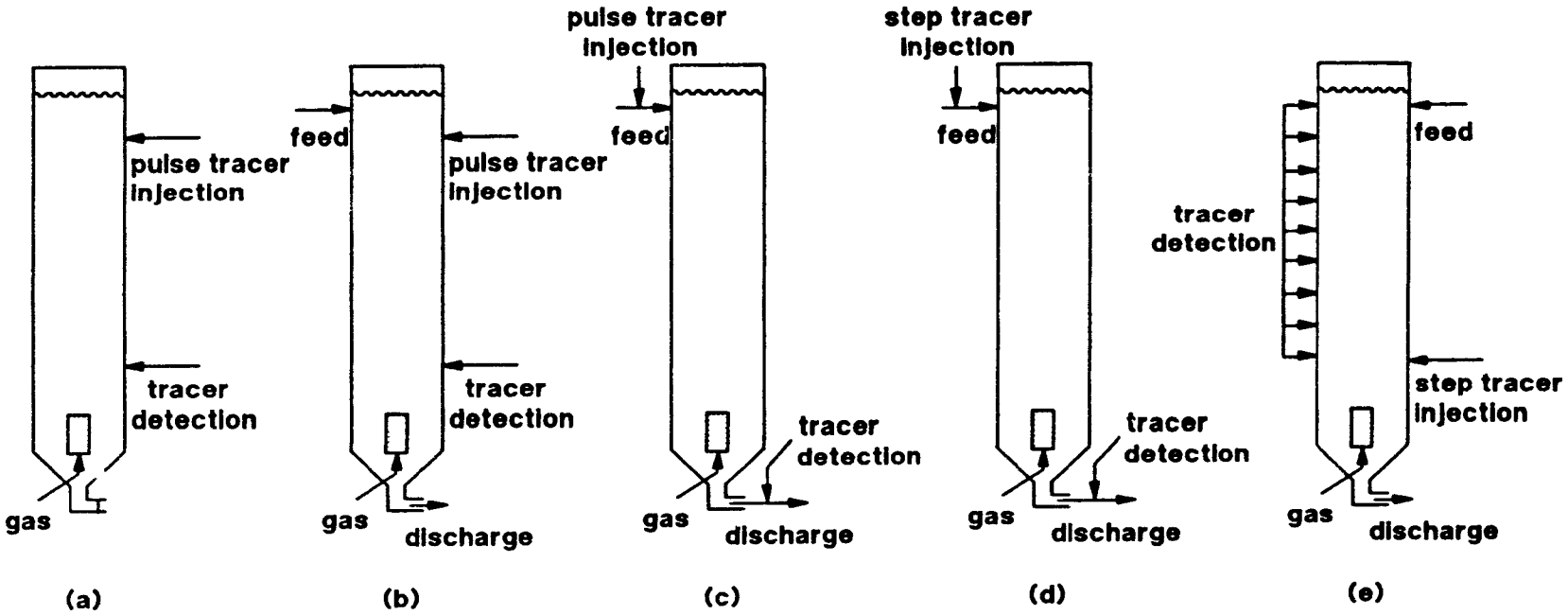

Figure 4.5 Schematic illustration of commonly employed experimental techniques for studying liquid dispersion in bubble columns

(a) unsteady-state batch liquid
(b) open-open boundary conditions
(c) closed-closed boundary conditions
(d) steady-state and step tracer
(e) steady-state liquid backmixing

Solution 1: A Batch System

Shah et al. (1978) suggested that the method for evaluating axial dispersion coefficient from concentration-time response data developed by Ohki and Inoue (1970) can be readily applied to a batch system (i.e. no net liquid flowrate, Figure 4.5(a)) when the distance between the injection point of tracer and the measuring point is sufficiently large in comparison to the total length of the vessel. The axial dispersion model in this case ($u_l=0$) is Equation (4.9) without the second term on the left-hand side, i.e.,

$$E_l \frac{\partial C(t)}{\partial Z^2} - \frac{\partial C(t)}{\partial t} = 0 \tag{4.17}$$

The initial and boundary conditions are,

$$\begin{aligned} C(Z,0) &= 0 \quad for \quad 0<Z<L \quad and \quad t=0 \\ \frac{\partial C}{\partial Z} &= 0 \quad at \quad Z=0 \quad and \quad Z=L \end{aligned} \tag{4.18}$$

and the solution to the axial dispersion model in this case is,

$$\frac{C(t)}{C_0} = 1+2\sum_{n=1}^{\infty}\left[\cos\frac{n\pi Z}{L}\exp\left\{-\left(\frac{n\pi}{L}\right)^2 E_l t\right\}\right] \tag{4.19}$$

where C_0 is the equilibrium concentration of the tracer in terms of the total volume of the vessel (any units); t is time (seconds); L, vessel height (cm); Z, the distance between tracer injection and detection point (cm); and E_l, the dispersion coefficient (cm^2/s). It is noted that E_l is directly determined and that N_d is indeterminable since u_l is zero.

Figure 4.6 presents a computed family of concentration-time response curves (also called RTD in this case). Increasing the E_l value decreases the time required for the system to reach uniform concentration. This time is also known as the mixing time (Guy et al., 1986). When the mixing time is large, the degree of mixing in a system is small.

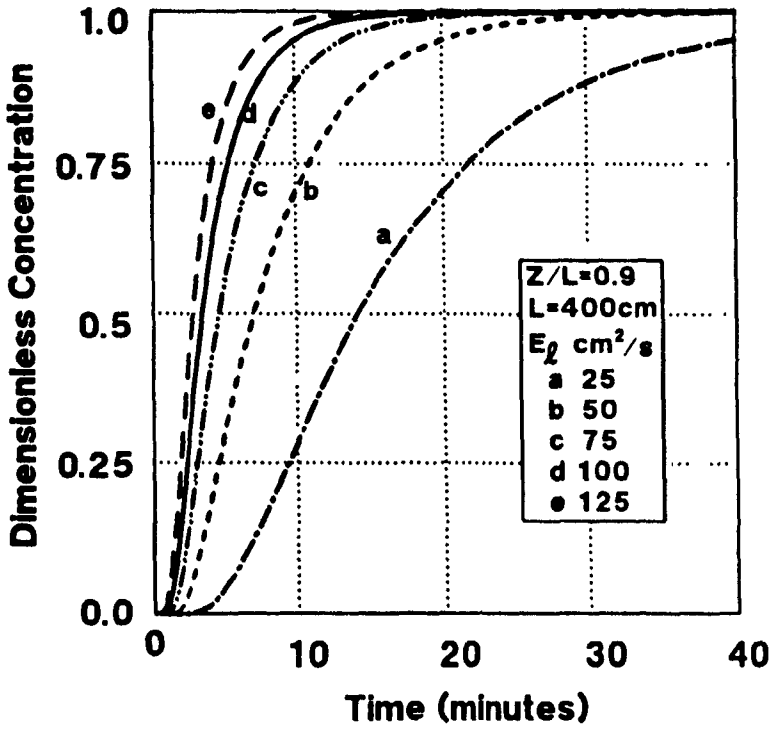

Figure 4.6 Tracer response curves calculated from the solution to the axial dispersion model for a batch system with a pulse tracer injection

Solution 2: An Open Vessel

The physical meaning of open-open boundaries is denoted by the fact that the there exists continuity in flow at the positions of tracer injection and detection as opposed to closed-closed boundaries. More specifically, some of the tracer in the injection position may move away, then return to the same position and eventually pass upstream from that position. Similarly, some of tracer reaching the detection position may move backwards (see Figures 4.3 and 4.5(b)). Levenspiel and Smith (1957) and Gibilaro (1978) discussed this point in detail. The major conclusion by Gibilaro (1978) is that the mean residence time in steady flow through a continuous system is equal to the ratio of the system effective volume to the flow rate regardless of whether the boundaries are open or closed.

The analytical solution to the axial dispersion model in this case (RTD) is given

by (Carslaw, 1945; Levenspiel and Smith, 1957; Rice et al., 1974; Gibilaro, 1978),

$$C(t) = \left(\frac{\tau}{4\pi N_{doo} t^3}\right)^{1/2} \exp\left[\frac{1}{4N_{doo}}\left(2 - \frac{t}{\tau} - \frac{\tau}{t}\right)\right] \qquad (4.20)$$

where $C(t)$ is the normalized concentration and has the unit of reciprocal (mean residence) time. N_{doo} is the vessel dispersion number in the open-open boundary case. The above equation multiplied by the mean residence time τ gives dimensionless RTD,

$$E(\theta) = \left(\frac{1}{4\pi\theta^3 N_{doo}}\right)^{1/2} \exp\left[\frac{1}{4N_{doo}}\left(2 - \theta - \frac{1}{\theta}\right)\right] \qquad (4.21)$$

Figure 4.7 is a family of RTD curves calculated from this solution for various vessel dispersion numbers. The dashed curve is the case of the perfectly mixed flow where $N_d = \infty$ given by $E(\theta) = exp(-\theta)$. It is interesting to note that above $N_{doo} = 0.5$, the peak value again exceeds 1 which does not occur for the case of closed-closed boundaries.

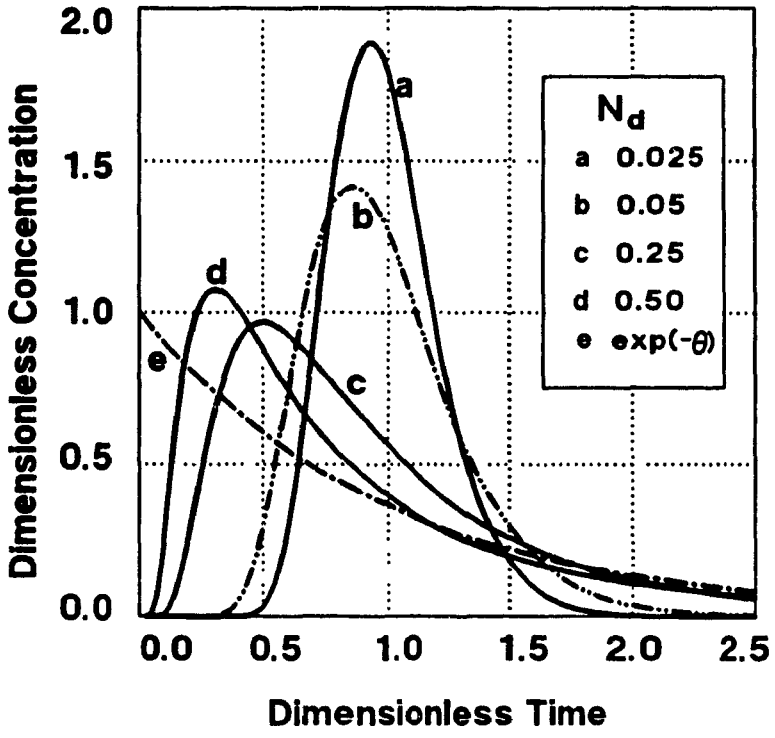

Figure 4.7 RTD curves calculated from the solution of axial dispersion model for a open vessel

Solution 3: A Closed Vessel

The implication of closed boundary conditions is easy to understand and to express in mathematical forms; there is discontinuity in flow at tracer injection and detection positions. The tracer after injection never returns, and once it reaches the detection position, it never returns. For pulse tracer, the corresponding initial and boundary conditions are given as follows (Danckwerts, 1953; Pearson, 1959; Brenner, 1962; Nagata, 1975),

$$\theta = 0,\ E(x,\theta) = 0 \ \textit{for all}\ x,\ 0<x<1$$
$$x = 0,\ N_d \frac{\partial E(0,\theta)}{\partial x} = E(0,\theta) - \delta(\theta)$$
$$x = 1,\ \frac{\partial E(1,\theta)}{\partial x} = 0$$

Two slightly different forms of the analytical solutions in this case have been given. One form is (Miyauchi, 1953; Nagata, 1975; Carslaw and Jaeger, 1959; Froment and Bischoff, 1979),

$$E(\theta) = 4N_{dcc}\exp\left(\frac{1}{2N_{dcc}}\right)\cdot\sum_{n=1}^{\infty}\frac{2(-1)^{N+1}\lambda_n^2 N_{dcc}^2}{4\lambda_n^2 N_{dcc}^2 + 4N_{dcc} + 1}\cdot \cdot\exp\left[-\frac{1+4\lambda_n^2 N_{dcc}^2}{4N_{dcc}}\right] \tag{4.22}$$

where λ_n is the *nth* positive root of the transcendental equation, in the order of increasing magnitude (ignoring $\lambda_0=0$),

$$\tan\lambda_n = \frac{4\lambda_n N_{dcc}}{4\lambda_n^2 N_{dcc}^2 - 1} \tag{4.23}$$

and N_{dcc} represents the N_d for closed-closed boundaries. The other form is (Field and Davidson, 1980; Westerterp et al. 1984; Ityokumbul et al. 1988),

$$E(\theta) = 4N_{dcc}\exp(\frac{1}{2N_{dcc}})\cdot\sum_{n=1}^{\infty}\frac{\lambda_n(2\lambda_n N_{dcc}^2\cos\lambda_n + N_{dcc}\sin\lambda_n)}{4\lambda_n^2 N_{dcc}^2 + 4N_{dcc} + 1}\cdot \cdot\exp[-\frac{1+4\lambda_n^2 N_{dcc}^2}{4N_{dcc}}] \tag{4.24}$$

where λ_n is again given by Equation (4.23).

It has been found that these solutions (eqs.4.22 and 4.24) have poor convergence properties. To avoid this problem, an approximation was developed (Abouzeid et al., 1980; Abouzeid, 1989). However, detailed examination of the approximation equation shows that poor convergence still exists. Alternatively, a numerical solution to the axial dispersion model with closed-closed boundary conditions can be developed (Xu et al., 1990c). The procedure for the numerical solution using finite difference method is described next.

Figure 4.8 presents the initial and boundary conditions in the integration domain for the dimensionless axial dispersion model (eq.4.12).

Partial derivatives can be approximated by finite differences in many ways. All the approximations introduce truncation errors. Equation (4.12) can be reduced to 'equivalent' discrete equations using uniform space increment Δx in x direction and uniform time increment $\Delta\theta$ in the θ direction. The development of the Taylor series for $E(x+\Delta x,\theta)$ about (x,θ) gives,

$$E(x+\Delta x,\theta) = E(x,\theta) + \Delta x\frac{\partial E(x,\theta)}{\partial x} + \frac{(\Delta x)^2}{2!}\frac{\partial^2 E(x,\theta)}{\partial x^2} + + \frac{(\Delta x)^3}{3!}\frac{\partial^3 E(x,\theta)}{\partial x^3} + \cdots + R_n + \cdots \tag{4.25}$$

which, upon division by Δx, and suppression of the truncation error R_n, results in the following forward equation,

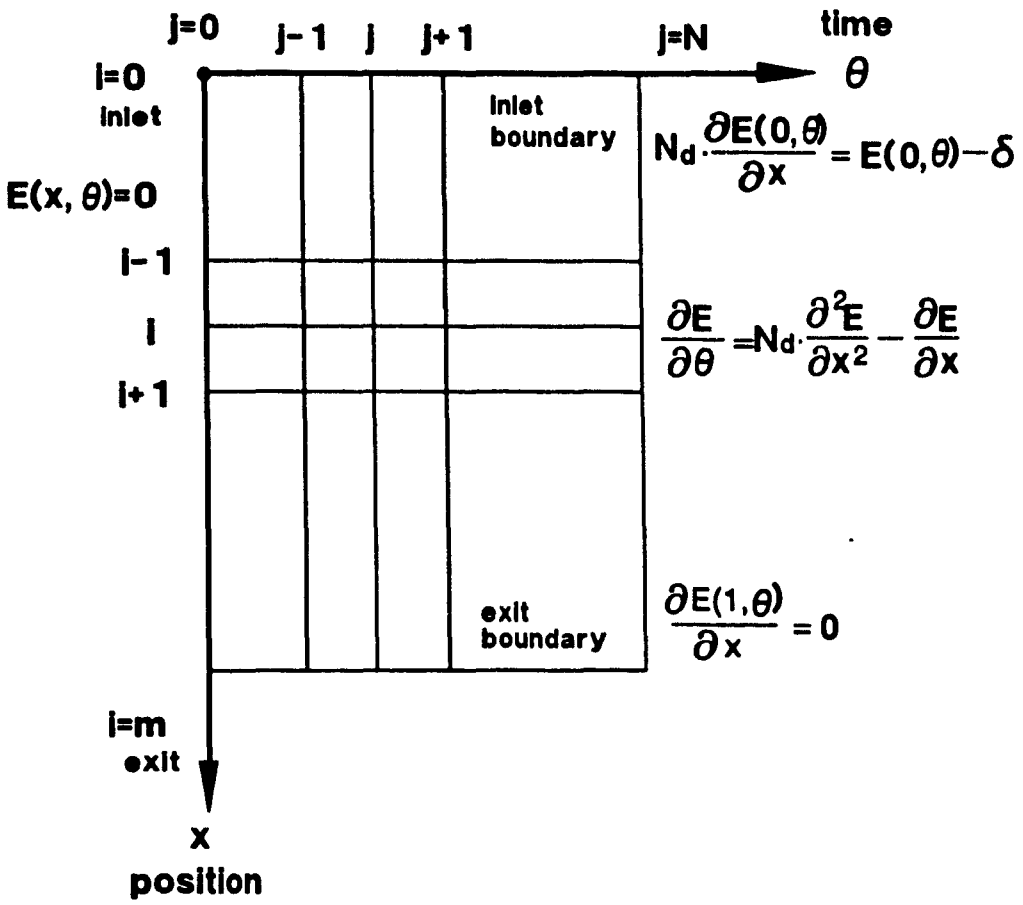

Figure 4.8 Integration domain for the numerical solution to the dimensionless axial dispersion model

$$\frac{\partial E(x,\theta)}{\partial x} = \frac{E(x+\Delta x,\theta) - E(x,\theta)}{\Delta x} = \frac{E_{i+1,j} - E_{i,j}}{\Delta x} \tag{4.26}$$

As an alternative to the forward difference approximation of Equation (4.26), a backward difference approximation is obtained in a similar manner. The Taylor series for $E(x-\Delta x,\theta)$ about (x,θ) is,

$$E(x-\Delta x,\theta) = E(x,\theta) - \Delta x \frac{\partial E(x,\theta)}{\partial x} + \frac{(\Delta x)^2}{2!} \frac{\partial^2 E(x,\theta)}{\partial x^2} - \frac{(\Delta x)^3}{3!} \frac{\partial^3 E(x,\theta)}{\partial x^3} + \cdots + R_n + \cdots \tag{4.27}$$

which, upon division by Δx and suppression of the truncation error, yields a backward difference approximation,

$$\frac{\partial E(x,\theta)}{\partial x} = \frac{E(x,\theta)-E(x-\Delta x,\theta)}{\Delta x} = \frac{E_{i,j}-E_{i-1,j}}{\Delta x} \qquad (4.28)$$

A more accurate second-order approximation can be obtained by combining Equations (4.26) and (4.28),

$$\frac{\partial E(x,\theta)}{\partial x} = \frac{E(x+\Delta x,\theta)-E(x-\Delta x,\theta)}{2\Delta x} = \frac{E_{i+1,j}-E_{i-1,j}}{2\Delta x} \qquad (4.29)$$

In a similar way, the partial derivative for θ and the second derivative for x are obtained,

$$\frac{\partial E(x,\theta)}{\partial \theta} = \frac{E(x,\theta+\Delta\theta)-E(x,\theta)}{\Delta\theta} = \frac{E_{i,j+1}-E_{i,j}}{\Delta\theta} \qquad (4.30)$$

$$\frac{\partial^2 E(x,\theta)}{\partial x^2} = \frac{E(x+\Delta x,\theta)+E(x-\Delta x,\theta)-2E(x,\theta)}{\Delta x^2} = \frac{E_{i+1,j}+E_{i-1,j}-2E_{i,j}}{2\Delta x} \qquad (4.31)$$

The development of the finite difference equation for θ (eq.4.30) requires the introduction of a net whose mesh points are denoted by $x_i = i\cdot\Delta x$, $\theta_j = j\cdot\Delta\theta$ where $i = 0, 1, 2, \cdots, M$; $j = 0, 1, 2, \cdots, N$ with $\Delta x = 1/M$ and $\Delta\theta = T/N$ (T is the total sampling time, dimensionless). The boundaries are specified by $i=0$ and $i=M$. The initial line is denoted by $j=0$ (Figure 4.9). If an approximate solution is assumed to be known at all mesh points up to time θ_j, a method must be specified to advance the solution to time θ_{j+1}.

The advancement is to substitute eqs.(4.29, 4.30 and 4.31) into Equation (4.12),

$$\frac{E_{i,j+1}-E_{i,j}}{\Delta\theta} = N_d\frac{E_{i+1,j}+E_{i-1,j}-2E_{i,j}}{\Delta x} - \frac{E_{i+1,j}-E_{i-1,j}}{2\Delta x} \qquad (4.32)$$

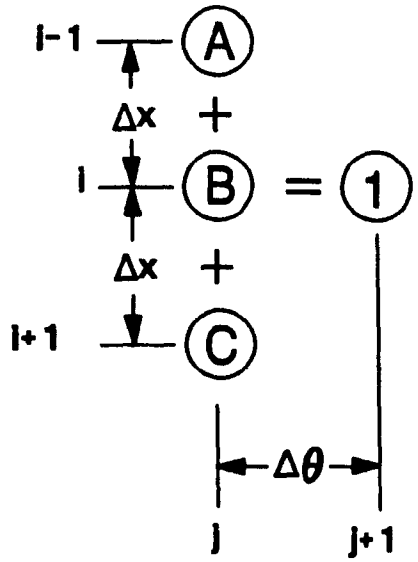

Figure 4.9 Computational molecule for explicit approximation of 'marching' ahead in time

Upon solving the above equation, the following explicit equation for 'marching' ahead in time (that is from $E_{i,j}$ to $E_{i,j+1}$) is obtained,

$$E_{i,j+1} = AE_{i-1,j} + BE_{i,j} + CE_{i+1,j} \tag{4.33}$$

where

$$A = \frac{N_d \Delta\theta}{\Delta x^2} + \frac{\Delta\theta}{2\Delta x} \tag{4.34}$$

$$B = 1 - \frac{2N_d \Delta\theta}{\Delta x^2} \tag{4.35}$$

$$C = \frac{N_d \Delta\theta}{\Delta x^2} - \frac{\Delta\theta}{2\Delta x} \tag{4.36}$$

The computational molecule of 'marching' ahead in time is illustrated in Figure 4.9 for Equation (4.33).

The value of $E_{i,j+1}$ at $i=0$ (or $x=0$) and $i=M$ (or $x=1$) should be selected according to the initial and boundary conditions, which are transformed into the finite

difference equations as follows,

$$J = 0,\ E_{i,0} = 0 \text{ for all } i,\ 0<i<M \tag{4.37}$$

$$i = 0,\ E_{0,j+1} = \frac{N_d}{\Delta x + N_d}(E_{1,j} + \delta) \tag{4.38}$$

$$i = M,\ E_{M,j+1} = E_{M-1,j} \tag{4.39}$$

where δ is the Dirac delta function (pulse tracer input):

$$\delta = M, \text{ at } i=0, j=0$$
$$\delta = 0, \text{ elsewhere}$$

The approximate solution using the finite difference equations is computed as follows. At $\theta=0$, the solution is prescribed by the initial conditions in Equation (4.37). Advance to time $\Delta\theta$ is carried out by employing Equations (4.33), (4.38) and (4.39), whereupon the steps are repeated to advance time $\theta=\Delta\theta$, and so forth. The final results give E_{Mj} (where $j=0,1,2,\cdots, N$) as a function of time θ (or $E(1,\theta)$, $\theta = 0, \cdots, T$). Samples can also be obtained for other locations, for example, a location half-way down the column, as a function of time (i.e. $E(0.5,\theta)$).

The results computed by Equation (4.33) must be examined for stability and accuracy. It is easy to demonstrate that the three coefficients on the right-hand side of Equation (4.33) sum to one ($A+B+C=1$, mass balance) for all values of N_d, Δx and $\Delta\theta$. By inspection, it was found that the numerical solution is not convergent if one of the coefficients (either A, B, or C) is negative; and all of them are nonnegative if,

$$\frac{N_d \Delta\theta}{\Delta x^2} \le \frac{1}{2} \tag{4.40}$$

$$\frac{N_d}{\Delta x} \ge \frac{1}{2} \tag{4.41}$$

The truncation error tends to zero as Δx and $\Delta\theta$ tend to zero. This implies that the solution of the finite difference equation converges to the exact solution of the partial differential equation as Δx and $\Delta\theta$ tend to zero. With the stability criteria satisfied, the explicit finite difference equation can give a very good approximation to the dispersion model. It is also noted that the requirement of convergence places a severe restriction on

the interval size in the θ direction and hence results in long computing time.

Based on the finite difference approximation (eq.4.33) and the initial and boundary conditions (eqs.4.37-39), a FORTRAN program was written (Appendix 6). For an intermediate level of mixing, Figure 4.10 presents the predicted residence time distribution for various number of sections (M). It is clear that increasing the number of sections above 20 does not change the prediction any further. For more extensive mixing ($N_d > 0.75$), a smaller number of sections ($M < 15$) is satisfactory. For relatively low mixing ($N_d < 0.02$), more than 20 sections are required, but this level of mixing is not of interest in most column studies. It is noted from the stability criteria that, for small N_d, Δx must be selected to make $N_d/\Delta x \geq 0.5$. Once this is satisfied, any further increase in the number of sections (or decrease in Δx) does not change the prediction. At the same time, it is clear that further decreasing Δx results in a substantial increase in computing time.

Sampling of the tracer concentration at locations along a flotation column gives age distributions (the age distribution at the exit being the RTD). Figure 4.11 is a simulation of tracer concentrations at four locations as a function of the time for intermediate mixing. At the inlet, the concentration of the tracer deceases continuously until zero concentration is reached, although even after 2 mean residence times there is still some tracer present. The maximum value of tracer concentration decreases and the age distribution curve becomes more spread as the tracer passes from the inlet to the exit. As an alternative, sampling of the tracer concentration along the axis at a specific time can also be performed. Both are combined in the 3-dimensional plot as shown in Figure 4.12; it illustrates the whole process of tracer dispersion from the inlet to the discharge with time.

Figure 4.13 shows the RTD curves for various extent of mixing as predicted from the axial dispersion model using the finite difference method. The prediction is essentially the same as that of Levenspiel (1972). For perfect mixing ($N_d = \infty$), the tracer dispersion is an exponential decay which can only be obtained using $E(\theta) = exp(-\theta)$, although approximation may be obtained using relatively large N_d and small number of sections.

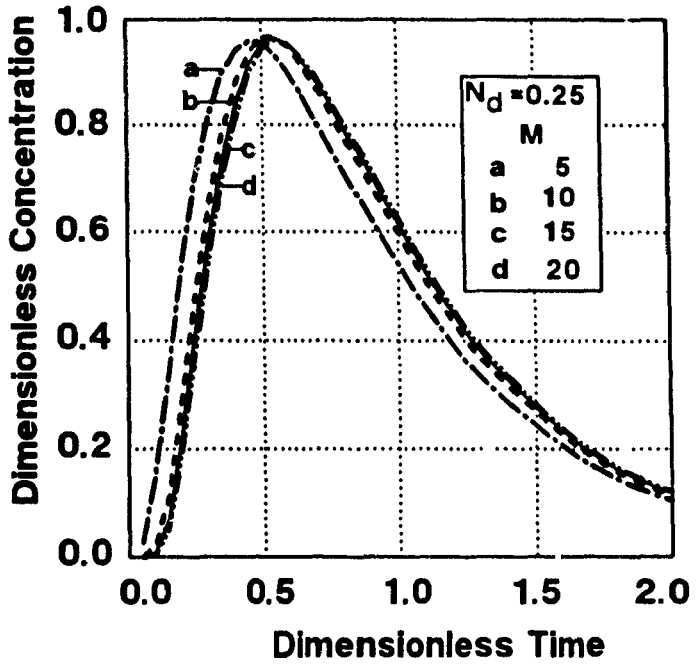

Figure 4.10 Effect of increasing the number of sections (M) on the accuracy of the computation for intermediate mixing

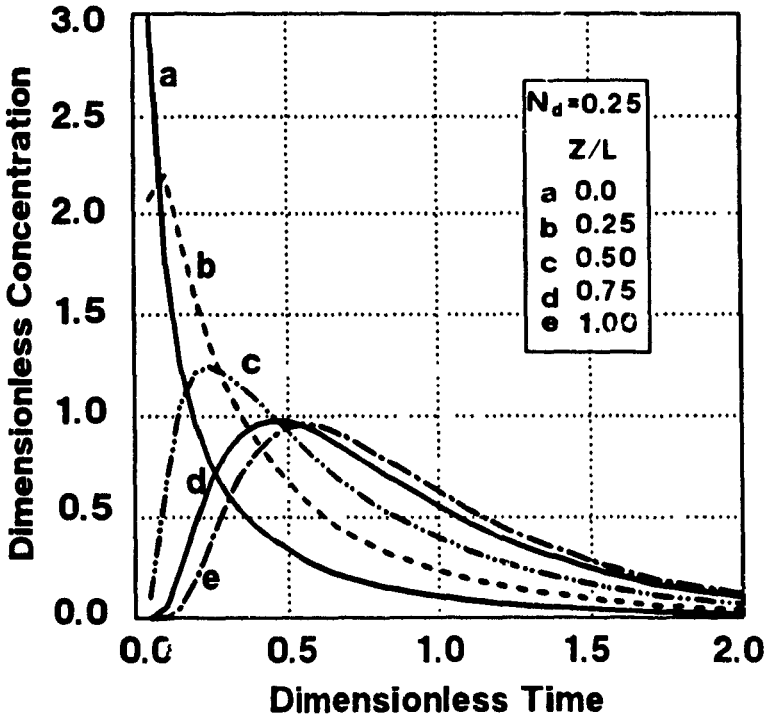

Figure 4.11 A pulse tracer dispersion at different dimensionless locations (Z/L) for intermediate mixing

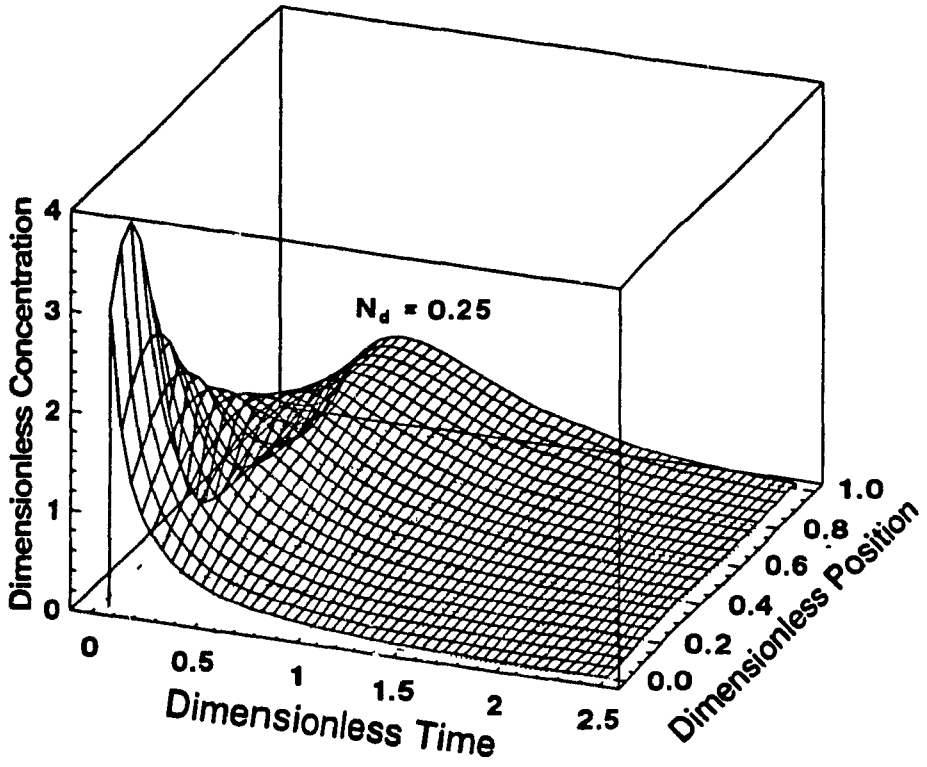

Figure 4.12 A pulse tracer dispersion in a three dimension plot for intermediate mixing

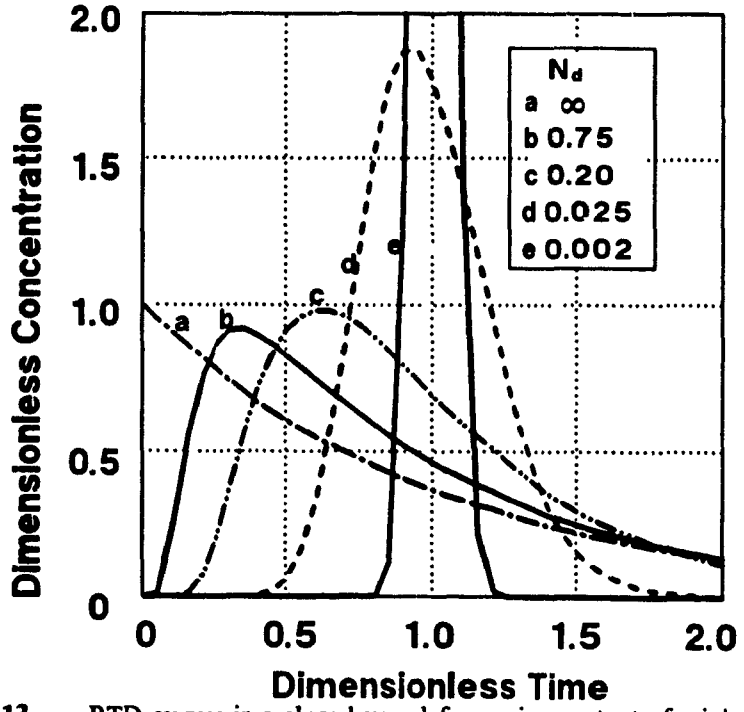

Figure 4.13 RTD curves in a closed vessel for various extent of mixing as predicted from the axial dispersion model using the finite difference method

Solution 4: Step Tracer under Steady-State

RTD measurements can also be carried out under steady-state conditions with step tracer (continuous) injection to the feed stream. This configuration is schematically shown in Figure 4.5(d). Often, an inverse step tracer test is used in place of the normal step tracer test. In this case, the initial concentration of liquid in the column is C_0 (assumed constant throughout the system and feed reservoir). The concentration of new incoming liquid is C_f (usually C_f=0). The dynamic response measurement $C(t)$ at the exit represents the so-called F curve which can be transformed into the E curve by differentiation (Levenspiel, 1972). The mean residence time in this case has to be determined independently by L/u_i, since the F curve does not give information about mean residence time. Solution to the axial dispersion model in this case is given by Brenner (1962). Methods for estimating E_t and u_i have been given by Westerterp et al. (1984).

The boundary conditions are the same as that in configuration (c) in Figure 4.5,

$$N_d \frac{\partial E(0,\theta)}{\partial x} = 0, \text{ at } x=0, \text{ for } \theta>0 \tag{4.42}$$

$$\frac{\partial E(1,\theta)}{\partial x} = 0, \text{ at } x=1, \text{ for } \theta>0 \tag{4.43}$$

while the initial condition is,

$$E(x,0) = 1, \text{ at } \theta = 0, \text{ for } 0<x\leq 1 \tag{4.44}$$

The exit concentration is given by (Brenner, 1962),

$$E(\theta) = \exp\left(\frac{2-\theta}{4N_d}\right)\sum_{k=1}^{\infty} \frac{8N_d^2\lambda_k \sin\lambda_k}{4N_d^2\lambda_k^2 + 4N_d + 1} \cdot \exp(-N_d\lambda_k^2\theta) \tag{4.45}$$

where λ_k (k = 1, 2, 3, $\cdots$), taken in order of increasing magnitude, of the transcendental equation,

$$\tan\lambda_k = \frac{4N_d\lambda_k}{4N_d^2\lambda_k^2-1} \tag{4.46}$$

Equation (4.45) can be simplified using the complementary error function defined by,

$$erfc(z) = 1-erf(z) = \frac{2}{\sqrt{\pi}}\int_z^{\infty}\exp(-y^2)\,dy$$

where *erf*(z) is the error function. The simplified form of Equation (4.45) is,

$$\begin{aligned} E(\theta) = 1-\frac{1}{2}erfc\left[\left(\frac{1}{4N_d\theta}\right)^{1/2}(1-\theta)\right] - \left(\frac{\theta}{N_d\pi}\right)^{1/2}\frac{6N_d+1+\theta}{2N_d}\cdot \\ \cdot\exp\left[-\frac{(1-\theta)^2}{4N_d\theta}\right] + \left[\frac{1}{2}+\frac{3+4\theta}{2N_d}+\frac{(1+\theta)^2}{4N_d^2}\right]\cdot \\ \cdot\exp\left(\frac{1}{N_d}\right)erfc\left[\left(\frac{\theta}{4N_d}\right)^{1/2}(1+\theta)\right] \end{aligned} \tag{4.47}$$

Figure 4.14 presents a family of F curves calculated using the above solution for various values of N_d (see Appendix 7 for the computation procedure).

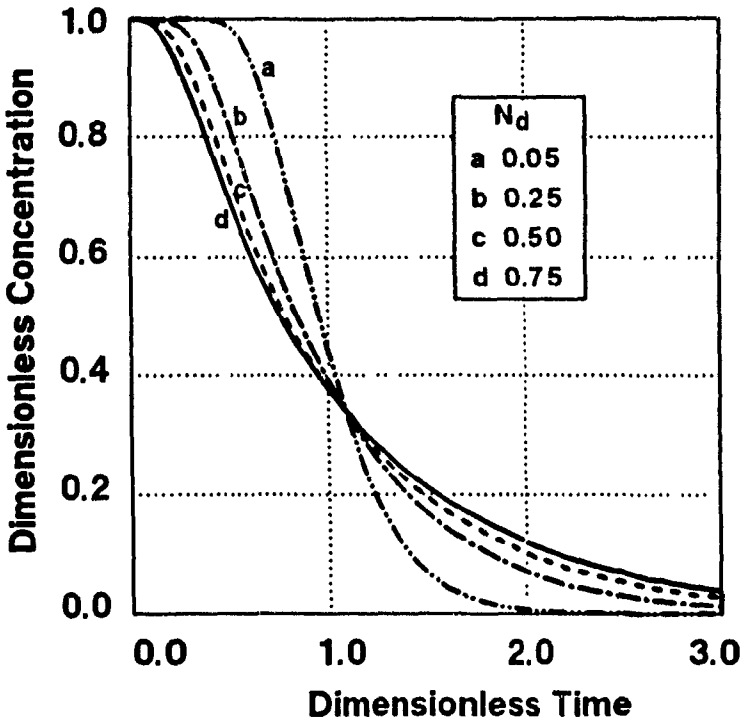

Figure 4.14 RTD curves calculated from the solution to the axial dispersion model (inverse step tracer input, see Appendix 7)

Solution 5: Steady-State Liquid Backmixing

The procedure shown in Figure 4.5(d) is quite popular (e.g., Argo and Cova, 1965; Aoyama et al., 1968; Deckwe et al., 1973; Holcombe et al., 1982; Devine et al., 1985). In this method, the axial concentration profile along the column is determined under steady-state conditions with continuous tracer injection far below the feed level. The axial dispersion model in this case is reduced into a second-order ordinary differential equation, independent of time,

$$E_l \frac{d^2C(Z)}{dZ^2} + u_i \frac{dC(z)}{dZ} = 0 \qquad (4.48)$$

On integration, the following solution is obtained,

$$C(Z) - C_0 \exp(-\frac{u_i}{E_l} Z) \qquad (4.49)$$

where $C(Z)$ and C_0 are the tracer concentration at Z and $Z=0$ (position where step tracer is injected), respectively. In fact, a plot of $ln(C/C_0)$ vs. Z is a straight line with a slope of $-(u_l/E_l)$. With this method, the independent determination of u_l and E_l is not possible. Thus, u_l must be measured from $J_l/(1-\epsilon_g)$. Figure 4.15 presents the concentration profile calculated from the equation for various degrees of mixing.

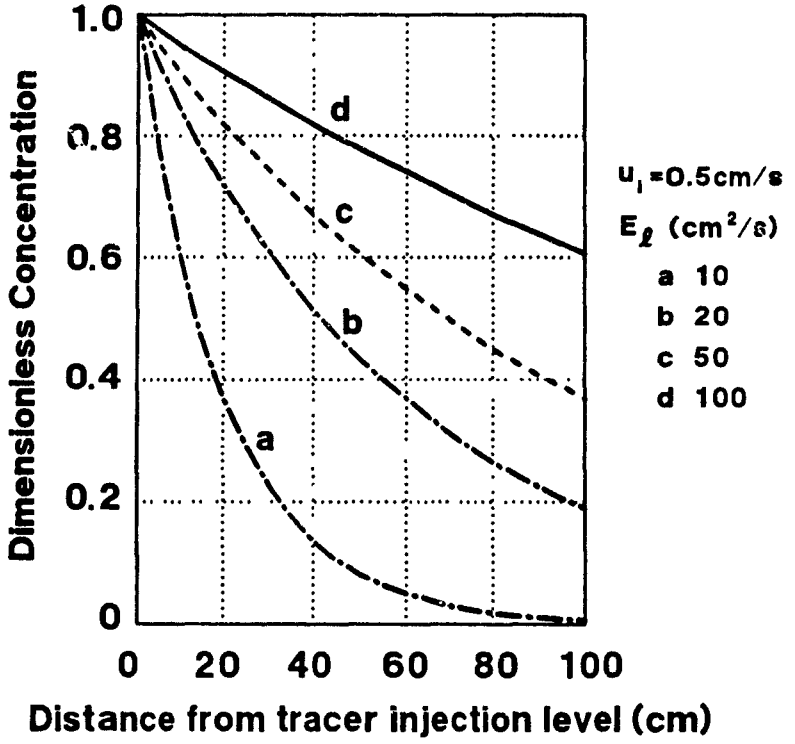

Figure 4.15 Concentration profiles indicating liquid backmixing calculated by the axial dispersion model (eq.4.49)

Specific to flotation column studies, Laplante et al. (1988) suggest that the backmixing characteristics of the zone between feed level and froth/collection zone interface in a flotation column can be investigated using this method. In this case, the step tracer is continuously added in the feed stream having a concentration of tracer C_f and measurement of tracer concentration is conducted along the column from the feed level to the interface level. The tracer concentration below the feed level should be

constant given by,

$$C_0 = C_f \frac{J_f}{J_b + J_f} \tag{4.50}$$

where J_f and J_b are the superficial feed and bias rates, respectively. The solution to the axial dispersion model of Equation (4.48) is,

$$C(Z) = C_0 \exp(-\frac{J_b}{E_l} Z) \tag{4.51}$$

Using this method, Laplante et al. (1988) and Finch and Dobby (1990a) determined the role of the zone between the feed level and interface. It is found that a concentration gradient may exist in a small laboratory column, but not in an industrial flotation column because of the large degree of backmixing. One conclusion is that it is preferable to define the column collection zone height from interface level to sparger level for industrial columns.

4.3.2 Tanks-in-Series Model

Considering the complexity of the flow features in the collection zone of a flotation column, Mavros et al. (1989) and Goodall and O'Connor (1990) suggested using compartment models, rather than the axial dispersion model. The simplest compartment model is the tanks-in-series model. With this model, the flow characteristics are described by a number of perfectly mixed tanks arranged in a sequential chain. To incorporate backmixing due to rising air bubbles, the more sophisticated backflow compartment model has been used in bubble columns. Recently, Mavros et al (1989) utilized this model to describe the liquid mixing in a flotation column.

In the tanks-in-series model, it is assumed that the system can be represented by n perfectly mixed tanks with equal volume (where n can take real or fractional values, Buffham and Gibilaro, 1968); the model is,

$$E(\theta) = \frac{n^n \theta^{n-1}}{\Gamma(n)} e^{-n\theta} \tag{4.52}$$

where $\Gamma(n)$ is the gamma function given by,

$$\Gamma(n) = \int_0^\infty x^{n-1} e^{-x} dx$$

The value of n is the indication of the intensity of mixing. Small values of n denote high extent of mixing and large values of n denote less mixing. n is related to the dimensionless vessel dispersion number with closed-closed boundary conditions by,

$$\frac{1}{n} = 2N_{dt} - 2N_{dt}^2(1 - e^{-1/N_{dt}}) \tag{4.53}$$

where N_{dt} denotes the vessel dispersion number derived from the tanks-in-series model. Figure 4.16 presents a family of curves calculated from tanks-in-series model for various values of n (see Appendix 8).

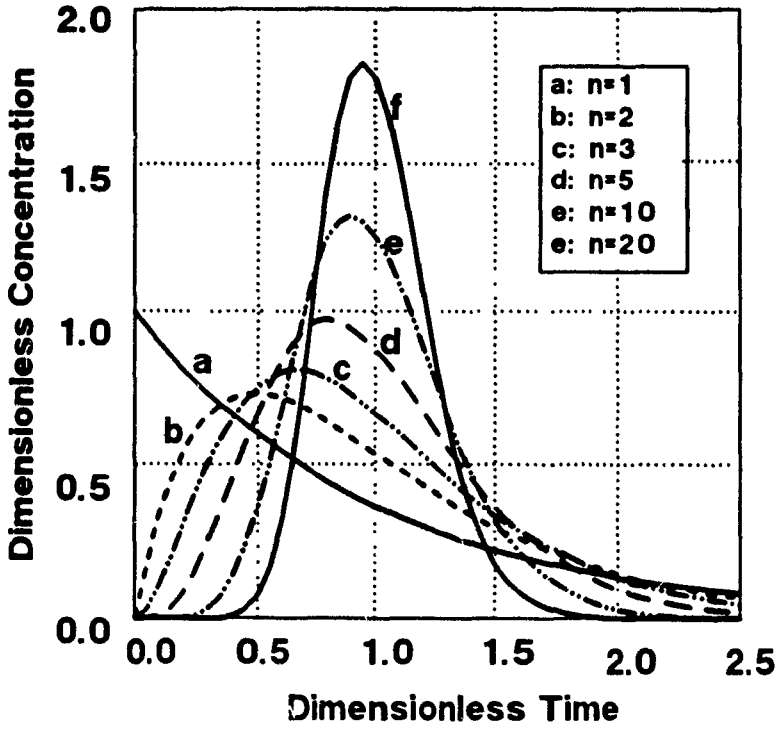

Figure 4.16 RTD curves predicted by the tanks-in-series model

4.3.3 Backflow Compartment Model

A flotation column can be visualized as a combination of several well-mixed zones with a backflow from one zone to the preceding zone (Figure 4.17). This backflow may represent the flow carried upwards in the wake of rising bubbles. With zero backflow, this model reduces to the simple tanks-in-series model and with an infinite backflow, the model approaches a single well-mixed tank. For a given backflow, the model is closer to completely mixed flow for small values of n and closer to plug flow for large values of n.

The backflow compartment model has been used for stirred vessels (Mann et al., 1981) and bubble columns (Todt et al., 1977). More recently, Mavros et al. (1989) used this model in flotation column studies. As shown in Figure 4.17, the column is divided into n perfectly-mixed cells (n is an integer) in series and flow is allowed from the i*th* to both the (i+1)*th* and the (i-1)*th* cells. The material mass balance for the tracer in the i*th* zone is.

$$V_i \frac{dC_i}{dt} = Q_{i-1,i} C_{i-1} + Q_{i+1,i} C_{i+1} - (Q_{i,i-1} + Q_{i,i+1}) C_i \qquad (4.54)$$

where the 'i, $i+1$' denotes the flow from the i*th* cell to the (i+1)*th* cell and V_i is the cell volume. A backflow ratio, λ, is defined as the ratio of backflow, $Q_{i,i-1}$, to the net liquid flow into the column, Q_ℓ,

$$\lambda = \frac{Q_{i,i-1}}{Q_\ell} \qquad (4.55)$$

where the 'i, i-1' denotes flow from the i*th* cell to the (i-1)*th* cell. Then the material mass balance for the tracer in the i*th* cell can be given in dimensionless form,

$$\frac{1}{n} \frac{dE_i}{d\theta} = (1+\lambda) E_{i-1} + \lambda E_{i+1} - (1+2\lambda) E_i \qquad (4.56)$$

for i=2, ···, n-1, whereas for the first and last cells it becomes; respectively,

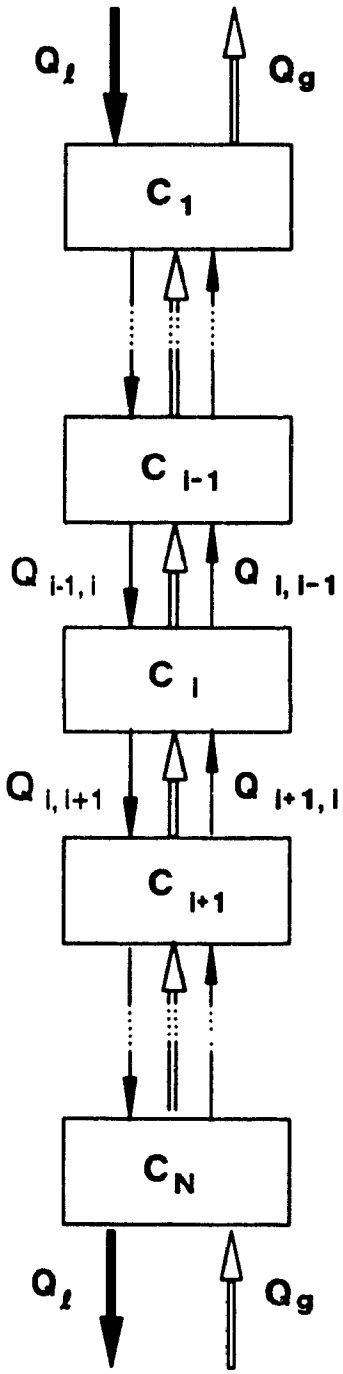

Figure 4.17 Backflow compartment model for the representation of a flotation column

$$\frac{1}{n}\frac{dE_1}{d\theta} = \lambda E_2 - (1+\lambda)E_1 \tag{4.57}$$

$$\frac{1}{n}\frac{dE_n}{d\theta} = (1+\lambda)E_{n-1} - (1+\lambda)E_n \tag{4.58}$$

The tracer concentration of incoming liquid is zero and for a pulse tracer, the initial condition is at time $\theta=0$,

$$E_1(0) = n \text{ and } E_i(0) = 0,\ i=2,\cdots,n$$

The curve, $E_n(\theta)$, which is obtained by solving Equations (4.56), (4.57) and (4.58), is the theoretical RTD of the column. This set of ordinary differential equations is solved numerically using the finite difference method, similar to the approach used for solving the axial dispersion model. The computer program written in FORTRAN is included in Appendix 9.

The backflow compartment model has two parameters: the number of zones n and the backflow ratio λ. The backflow ratio parameter is an indication of the degree of mixing in the column for a given number of cells: low values of λ denote relatively little mixing, whereas large values of λ mean that there is extensive mixing as shown in Figure 4.18. Figure 4.18 presents the calculated theoretical RTD curves for various values of λ at $n=20$. For a given value of λ, small values of n denote high extend of mixing while large values of n mean little mixing (Figure 4.19).

One of the parameters may be set in advance and the other one computed by matching the theoretical RTD curve to the experimental one. Joshi and Sharma (1979) and Joshi (1980) observed that in bubble columns the circulating liquid establishes a pattern of loops, each loop having a height approximately 0.8 times the column diameter($n=L/(0.8d_c)$). Traditionally n and λ are combined into a single parameter, the dimensionless vessel dispersion number N_{dbc}, to describe the degree of mixing (Roemer and Durbin, 1967 and Todt et al., 1977), where (using subscript bc to denote backflow compartment model),

$$N_{dbc} = \frac{1+2\lambda}{2n} \tag{4.59}$$

Klinkenberg (1966, 1968, 1971) mathematically derived the moments of the backflow compartment model, which can be used to match the experimental moments obtained from the RTD data.

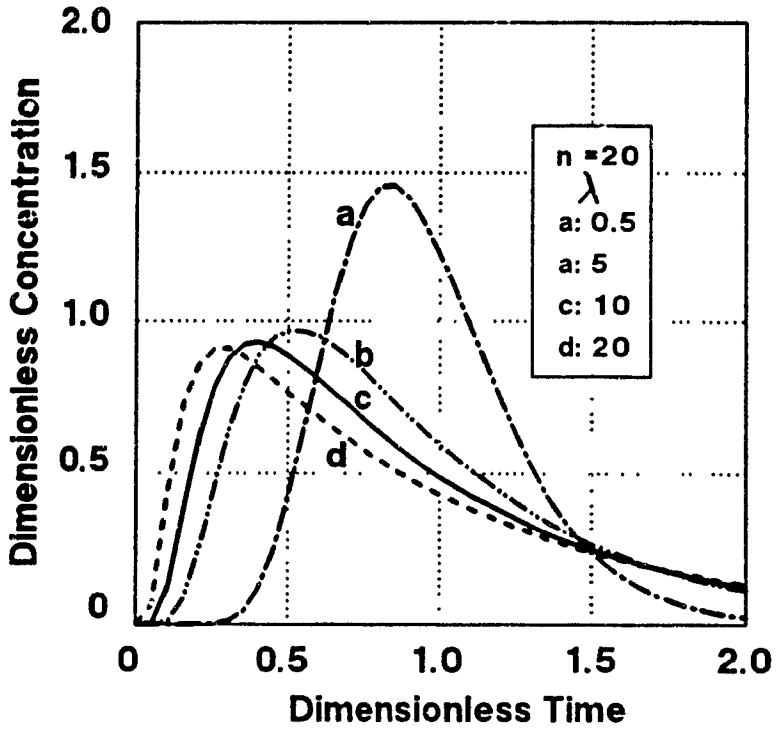

Figure 4.18 RTD curves calculated from the backflow compartment model: effect of the backflow ratio

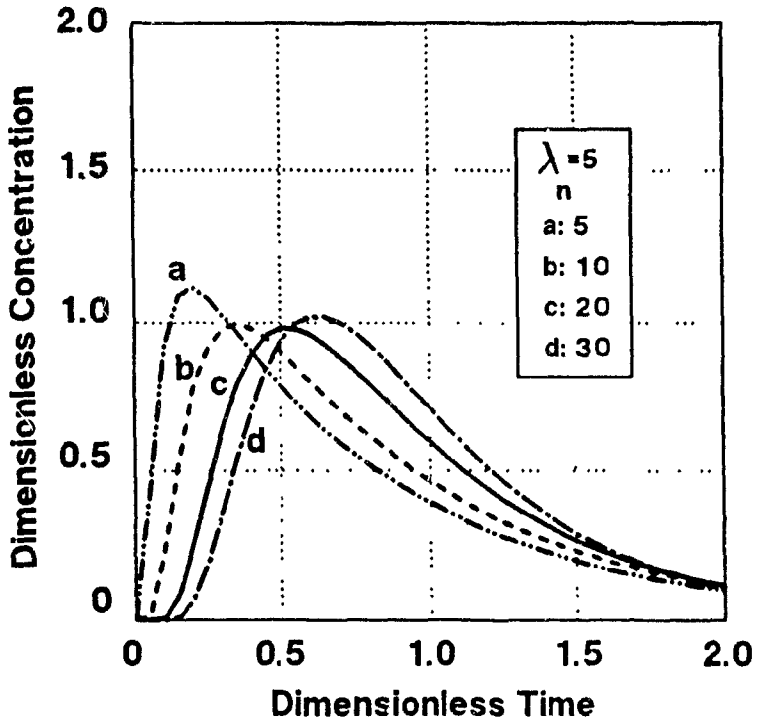

Figure 4.19 RTD curves calculated from the backflow compartment model: effect of number of compartments

4.4 Comparison Between Axial Dispersion Model and Compartment Models

Many types of models can be used to characterized non-ideal flow within vessels. Some draw on the analogy between mixing in the actual flow and a diffusional process. These are called dispersion models. Others build on a chain or network of ideal mixers, while still visualizing various flow regions connected in series or parallel. These are known as compartment models.

The dimensionless RTD curves are uniquely characterized by the magnitude of the dimensionless vessel dispersion number, N_d. As indicated, n (in tanks-in-series model) or n and λ (in backflow compartment model) is related to N_d. Hence, for a given N_d, the RTD curves calculated from the axial dispersion model and compartment models can be

used to compare whether these models are similar. Figure 4.20 presents the RTD curves calculated for a relatively small N_d (0.2). It is quite evident that the backflow compartment model (assuming n=20, λ=3.5) gives more or less the same RTD curve as the axial dispersion model (both the open analytical and closed numerical solutions). There is a clear deviation in the tanks-in-series model. Increasing to N_d=0.5, the continued close agreement (Figure 4.21) between the closed vessel axial dispersion model and backflow compartment model (n=20, λ=9.5) is evident. The tanks-in-series model still deviates and now so does the open solution to the axial dispersion model. It should be noted that, for a given N_d, different n values could be used in the backflow compartment model. For example, n=30 will give λ=5.5 at N_d=0.2. It is found that the larger the n value, the better is the match between the axial dispersion model (closed boundaries) and the backflow compartment model.

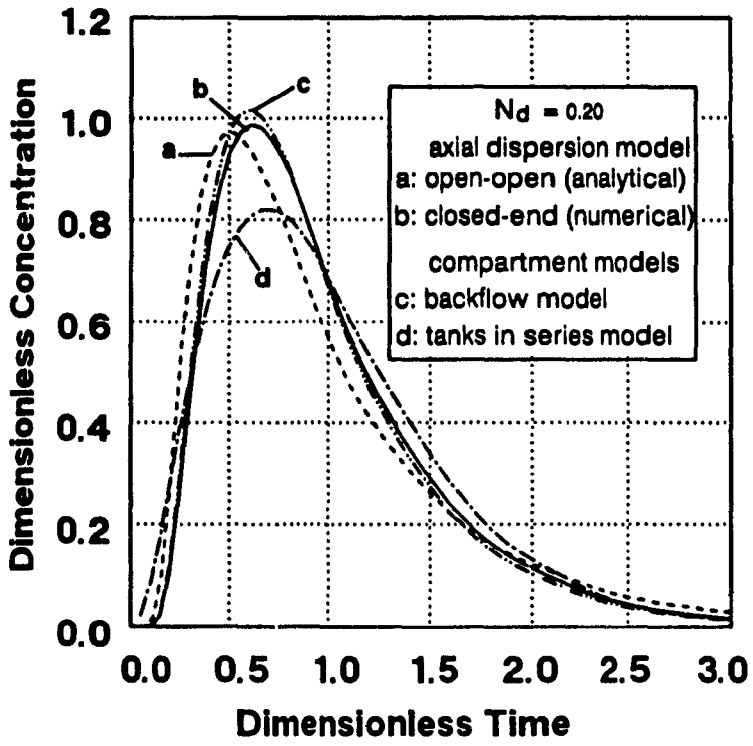

Figure 4.20 Comparison of the axial dispersion to compartment models for a relatively low extent of mixing

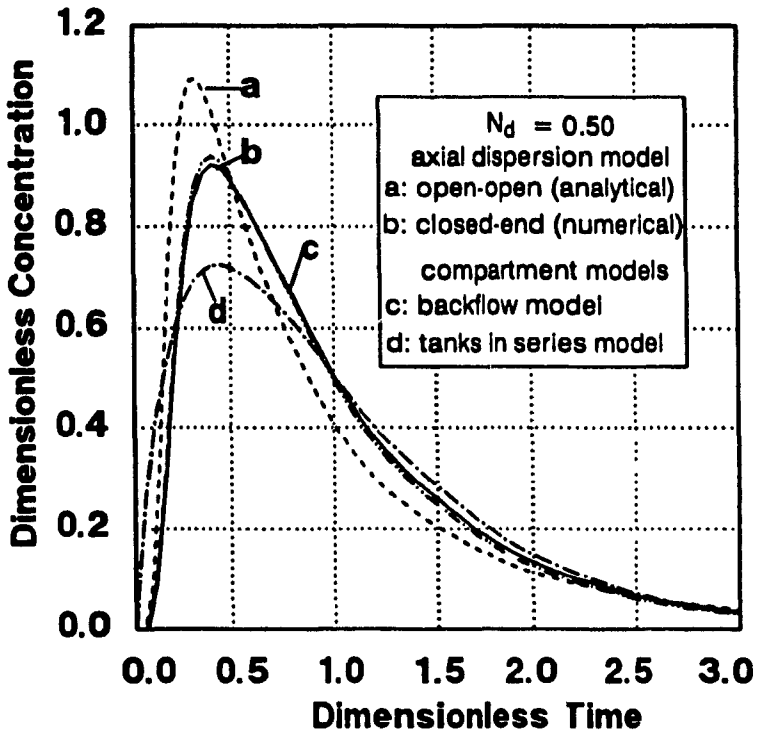

Figure 4.21 Comparison of the axial dispersion model to compartment models for a relatively high extent of mixing

4.5 Fitting RTD to Mixing Models

In general, there are two methods available to fit experimental RTD data to the mixing models for estimating the mixing parameter, the vessel dispersion number N_d (in this work, τ is always estimated directly from the RTD data not by model fitting): moment matching and direct search. Rice et al (1974) applied so-called weighted moments matching. This involves calculating the experimental values for the weighted moments, with an optimum weighting factor, and equating these to the theoretical moments. The weighted moments matching technique is not considered here.

4.5.1 Moments Matching

The moments matching method has been shown to be less reliable than the least squares technique (Butt, 1962; Wakao and Kaguei, 1982 and Ityokumbul, et al., 1988). However, this method is still in use due to its simplicity (e.g. Finch and Dobby, 1990a). Table 4.3 presents the moments for three boundary conditions (the methods of calculating moments for a distribution is given in Appendix 11). It is clear that the means of the RTD curves for the three boundary conditions are identical. Hence, any error in the estimation of the mean residence time, τ, is due to the mathematical treatment of the original data, or the failure of experimental measurements. In contrast, the expressions for the variance of the data are different. These expressions for variance are numerically identical at small values of N_d.

Table 4.3 Moments for three boundary conditions

moments	boundary conditions		
	closed-closed	open-open	open-closed
mean	L/u_i	L/u_i	L/u_i
variance	$2N_d-2N_d^2(1-\exp(-1/N_d))$	$2N_d+8N_d^2$	$2N_d+3N_d^2$

4.5.2 Direct Search (Least Squares) Method

Fitting the numerical results to the experimental results is conducted using the least square method. The objective of this method is to minimize the sum of the squares of the deviation between the experimental and theoretical RTD curves. Mathematically, this is expressed,

$$\Phi = \sum_{k=1}^{n} [F_m(\theta_k) - F_e(\theta_k)] \tag{4.60}$$

where $F_m(\theta_k)$ is the model predicted RTD and $F_e(\theta_k)$ is the experimental one. To minimize the objective function Φ for the given search parameter, the vessel dispersion number N_d, derivative-free methods have to be used since the calculation and evaluation of numerical derivatives takes substantial computing time. Moreover, near the minimum of Φ, the error in the derivatives increases, hence, the termination of the iterative procedure leads to oscillation (Raman, 1985). Thus, the solution to this type of function must be obtained using direct search methods. In present study, the Fibonacci search is used which is briefly described in Appendix 11.

Xu and Finch (1990d) recently conducted a comparison study between moments matching and least squares fitting . It was clearly demonstrated that the least squares fitting is generally superior than moments matching. For example, the least squares fitting is less subject to the cut-off point of the RTD tail than the moments matching.

CHAPTER 5

EXPERIMENTAL SET-UP AND TECHNIQUES

In this chapter, the experimental set-up of the flotation columns and techniques of measuring local gas holdup and liquid residence time distribution are described. The sparger design and gas distribution particularly for the large-scale laboratory flotation column are presented. Theory and application of the conductivity measurement are examined. The experiments mainly consist of two types: local radial gas holdup profiles and liquid residence time distribution (RTD).

5.1 Experimental Columns

Three flotation columns of different sizes were used in the present study. Measurement of liquid RTD was mainly conducted in a flotation column with a diameter of 10.16cm. Local gas holdup measurement was carried out in a 50cm laboratory flotation column and a pilot flotation column with a diameter of 91cm.

The first flotation column used in this work was made of Plexiglas and was 400cm in height and 10.16 cm in diameter as shown in Figure 5.1. This column consists of three sections: a stainless steel sparger was installed in the bottom section; two water manometers were installed in the middle section; 12 pair of electrodes were installed vertically in the top section, with the feed entrance also located in the same section. Wash water was added 5cm below the overflow lip, when it was used. The wash water distributor was built of copper tubing perforated with a number of small orifices (about 5mm in diameter). Two water manometers located at 50cm below the interface and 50cm above the sparger were used to measure the mean gas holdup in the collection zone.

The column was operated continuously: three Masterflex pumps were used, one each for feed, wash water and underflow discharge. Air was introduced into the bottom

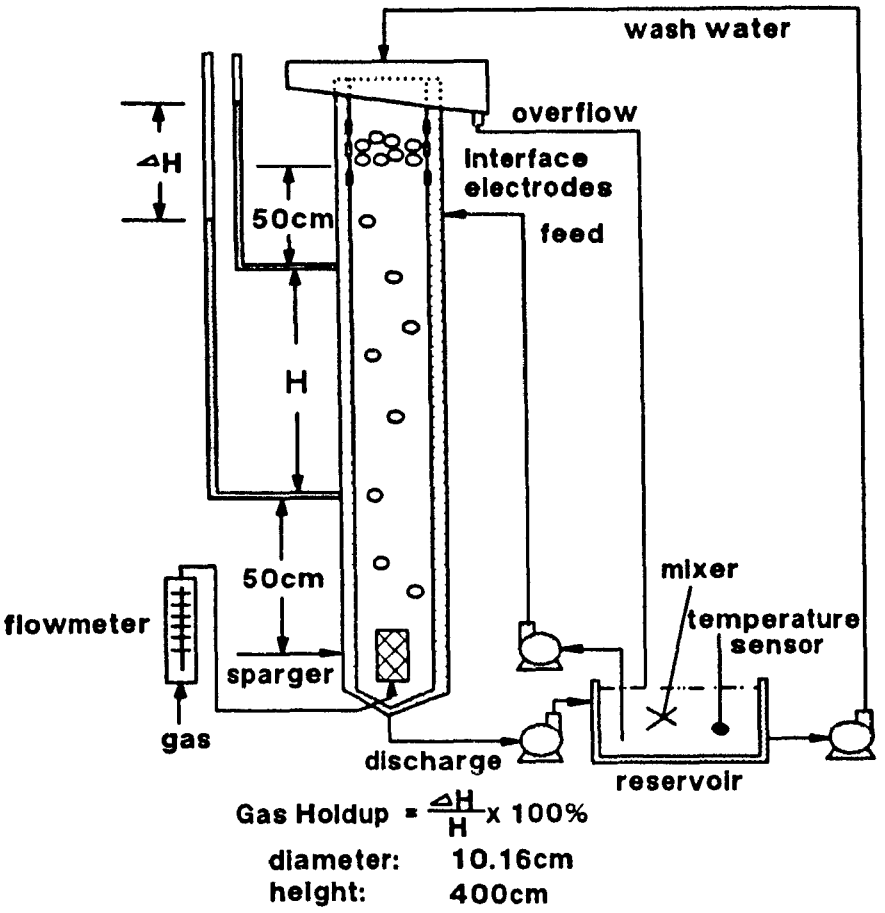

Figure 5.1 Small laboratory flotation column set-up

of the column through the stainless steel sparger, and the air flowrate was monitored using a calibrated gas flowmeter. The stainless steel sparger was cylindrical, 3.8cm in diameter and 7cm in length. This gives a ratio of column cross-sectional area to sparger surface area of about 1:1, which is in the range promoting bubbly flow (Xu and Finch, 1989a). The average orifice diameter is about 50μm and hole density was about 10 holes/cm^2. Dowfroth 250C was used to control the bubble size at different concentrations.

For the study of the radial local gas holdup distribution and liquid circulation, a large-scale laboratory column was constructed (Figure 5.2). It was made in three sections of PVC, and was 50cm in diameter and 400cm in height. The bottom section was specifically designed to permit different sparger configurations (this will be further discussed in section 5.2). Transparent widows were built on each section which enabled

visual observations. Water manometers were used to measure average gas holdup for a specific section. A conductivity probe containing 7 pair of electrodes was used to determine the radial gas holdup profiles (this will be further described in section 5.4.4). The large column was operated batch. Its gas sparger design and gas distribution is described in the next section.

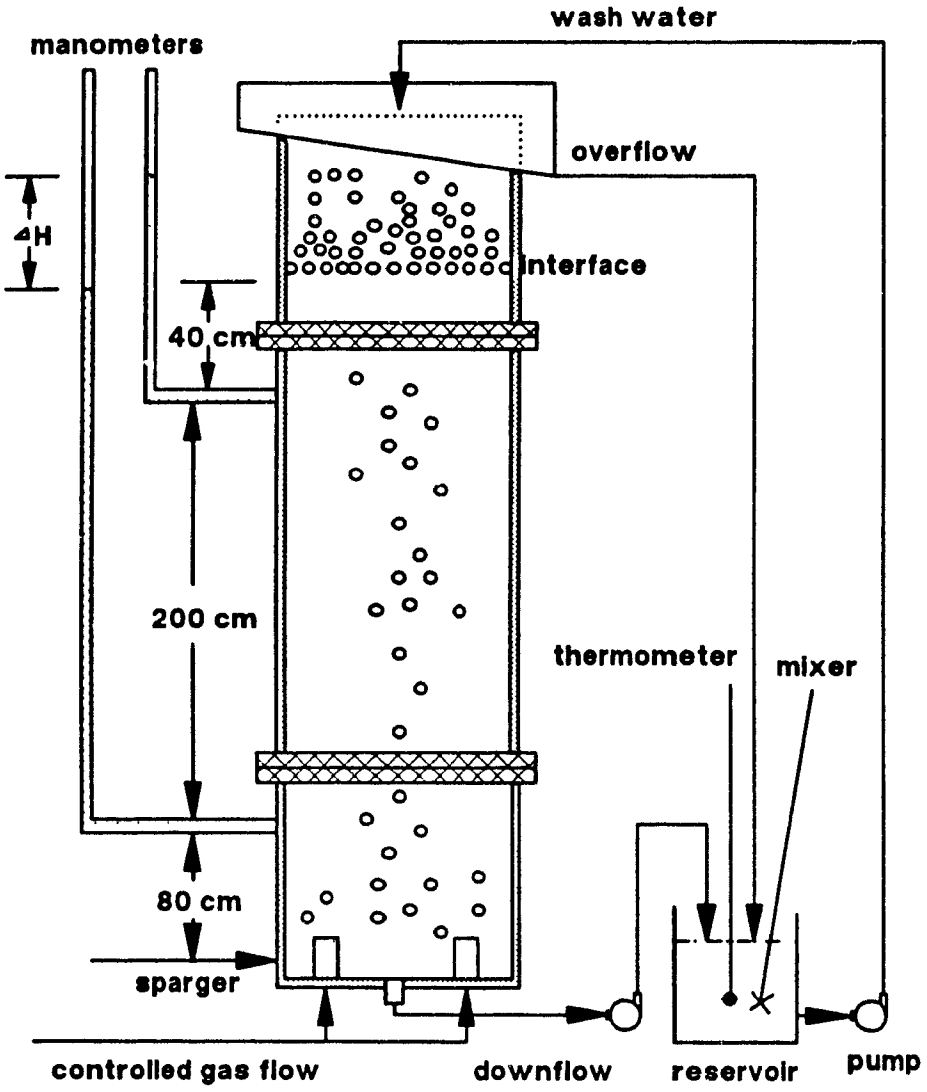

Figure 5.2 Large-scale laboratory flotation column set-up

Radial gas holdup profiles and liquid residence time distributions were also measured in the pilot flotation column at Strathcona Mill, Falconbridge Limited. The flotation column is 12.5m in height and 91cm in diameter. Three Cominco spargers were installed in parallel at the bottom. The electrical conductivity probe specifically built for measuring the radial gas holdup profiles is described in section 5.4.4.

5.2 Sparger System Design and Gas Distribution

For the 50cm laboratory flotation column (A_c=1963cm^2), a multiple-sparger system was used to provide sufficient sparger surface. Filter cloth covered spargers were used. Since a number of spargers had to be used, even gas distribution among the spargers was important to promote uniform bubbling.

5.2.1 Sparger System Design

Figure 5.3 shows a single sparger. The diameter of the sparger is 10cm and the height is 12cm (A_s=942.5cm^2). The supporting frame was made of PVC, and was

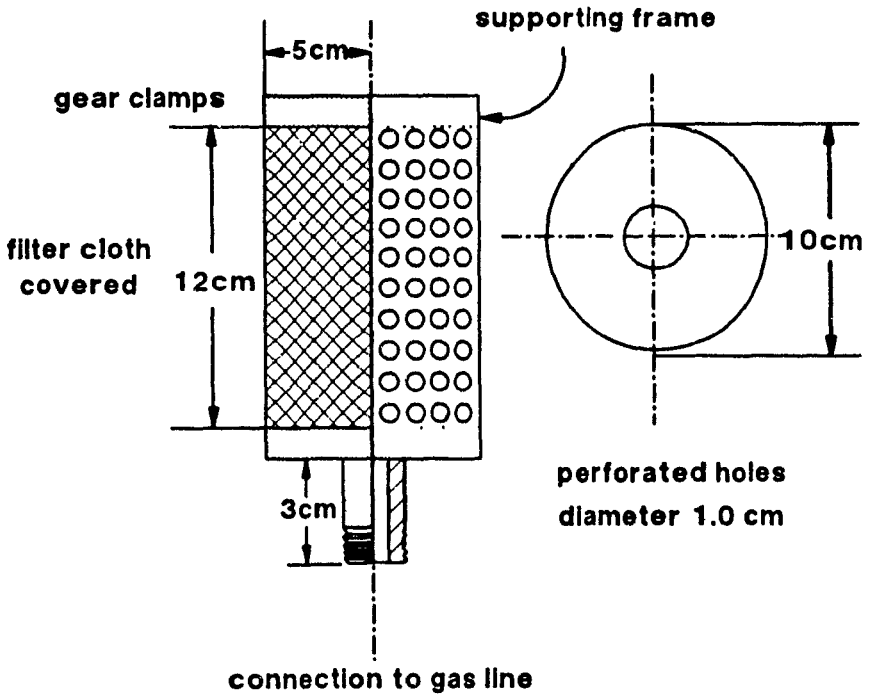

Figure 5.3 Filter cloth sparger design

cylindrical with a large number of perforated orifices (approximately 1.0cm in diameter) uniformly distributed on the whole surface of the cylindrical frame (there were no holes in the two ends). The frame was covered with filter cloth . The texture of the filter cloth was investigated using scanning electron microscopy (Xu and Finch, 1989). Up to eight identical spargers were used give a total possible surface area of spargers of 3770cm^2. The arrangement of these spargers in the bottom section of the column is illustrated in Figure 5.4.

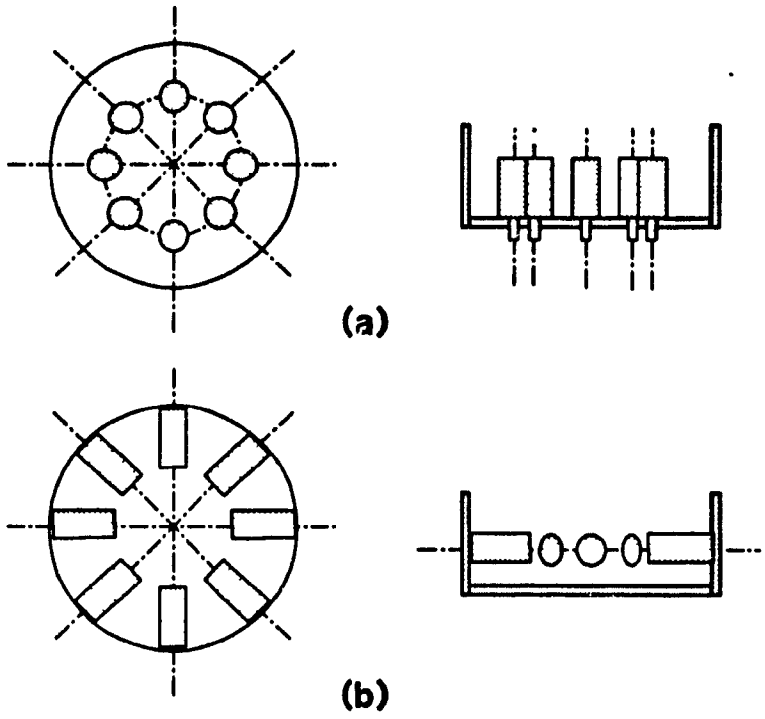

Figure 5.4 Arrangement of multiple-sparger system

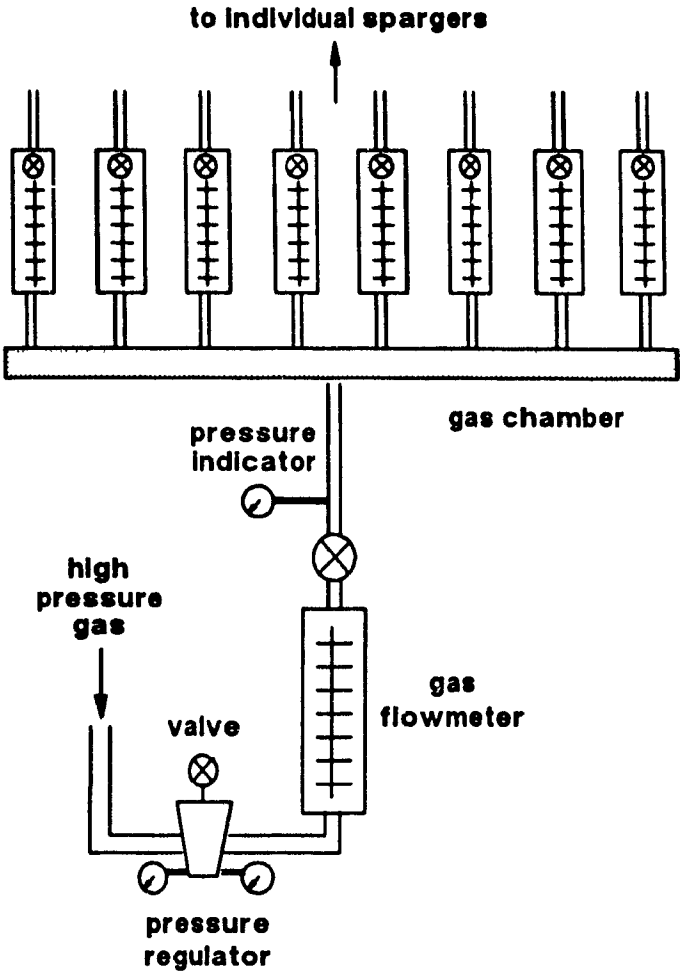

Figure 5.5 Gas regulation system for the large-scale flotation column

5.2.2 Gas Distribution

Even gas distribution among the spargers was achieved using the gas regulation system (Figure 5.5). The main high-pressure gas stream is first regulated to the desired pressure by a pressure regulator. Then the total gas flowrate is measured using a large flowmeter (which is completely open). The gas to each individual sparger was then controlled by identical gas flowmeters, one for each sparger. In this manner, equal gas flowrate to each sparger could be maintained.

This method of gas distribution also allows a simulation of gas maldistribution or

malfunctioning of the sparger system. For example, one or more spargers can be switched off to simulate spargers not working. The effect of malfunctioning of the sparger system on radial local gas holdup distribution and mean gas holdup can then be ascertained.

5.3 Theory and Application of Electrical Conductance Measurement

Electrical conductance techniques were extensively used in this study for two measurements: local gas holdup and liquid residence time distribution. It is important to understand the principles involved in measuring electrical conductance.

5.3.1 Background Principle

Electrical conductivity (from now on, reference to 'electrical' is dropped) is defined as the ability of a substance to conduct electric current. It is the reciprocal of resistivity. All substances possess conductivity to some degree, but the amount varies widely, ranging from extremely low (insulators such as glass and air) to very high (silver and metals in general). The interest here is in measuring the conductivity of water usually with dissolved ionic compounds. These solutions have conductivities between insulators and metallic conductors. The conductivity can be measured quite easily by electronic means and a broad line of conductivity equipment is available for liquids from pure water (low conductivity) to concentrated chemical streams (high conductivity). The special need here is to measure the conductivity of water containing small dispersed air bubbles.

The basic unit of resistance is the *ohm*. Conductance is the reciprocal of resistance, and its basic unit is the *siemens*. It is usually convenient to use specific conductance, or conductivity. This is the conductance as measured between the opposite faces of $1cm^3$ of the material. This measurement (conductivity) has units of *siemens/cm*.

A conductivity cell can be constructed of an insulating material with metallic pieces (usually stainless steel) on opposite faces; therefore, the current lines between the two electrodes are parallel to each other and no extra volume conducts current. Figure 5.6 shows an ideal conductivity cell. If the cell is filled with a solution of conductivity

k_c, the conductance as measured between the two opposite electrodes is,

$$K = k_c \frac{A}{L} \qquad (5.1)$$

where K is conductance in *siemens*; k_c, conductivity of the solution in *siemens/cm*; A, area normal to current flow in cm^2; L, distance in *cm* between the two opposite faces.

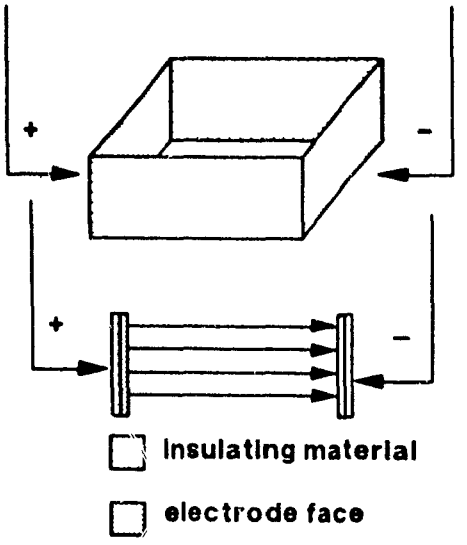

Figure 5.6 An ideal conductivity cell

The term A/L is defined as the cell constant and has dimensions of cm. As the dimensions of the cell changes, the cell constant varies. A useful theoretical concept is a cell consisting of a cube of 1.0cm on a side, which has a cell constant of 1.0cm. As a result, the conductance reading is numerically equal to the solution conductivity.

The terms 'cell', 'probe' and 'sensor' are sometimes used interchangeably, but it is useful to maintain the distinction. In the present context, in a cell the electrodes contact the solution directly with the sample contained between the electrodes, while a 'sensor' or 'probe' is a cell, or series of cells, developed for a specific application.

5.3.2 Conductivity of Liquid with Dispersed Gas Bubbles

The conductivity of a mixture of liquid and dispersed gas bubbles in a liquid phase will clearly be determined by the conductivities of the two phases and their relative volumes.

Maxwell (1873) considered a large sphere (continuous phase) which contains many small spheres (dispersed phase) with a different conductivity (Figure 5.7). Assuming the distance between small spheres is large enough so that their effect in disturbing the path of the current may be taken as independent of each other, the apparent conductivity of this large sphere is given by (Maxwell, 1873; Turner, 1976),

$$k_m = k_1 \frac{1+2\beta f}{1-\beta f} \qquad (5.2)$$

where k_1 is the conductivity of the continuous phase, f is the volumetric fraction of the dispersed phase of conductivity k_2, and β is given by,

$$\beta = \frac{k_2 - k_1}{k_2 + 2k_1} \qquad (5.3)$$

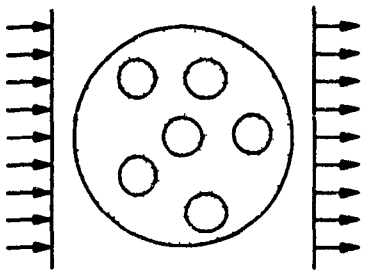

Figure 5.7 Physical presentation of Maxwell model (1873)

Directly adapting this principle to a flotation column where the mixture consists of water and dispersed gas bubbles, then,

$k_m = k_t$, apparent conductivity of the mixture for any ϵ_g
$k_1 = k_c$, conductivity of the continuous phase ($\epsilon_g = 0$)
$k_2 = 0$, conductivity of air
$f = \epsilon_g$, fractional gas holdup

Thus, gas holdup can be expressed in terms of apparent relative conductivity γ,

$$\varepsilon_g = \frac{1-\gamma}{1+0.5\gamma} \qquad (5.4)$$

where γ is,

$$\gamma = \frac{k_e}{k_c} \qquad (5.5)$$

Using the Maxwell model to estimate gas holdup, the apparent relative conductivity has to be measured, which means the cell constant must be known. Assuming the conductivity of the mixture was still the one of the continuous phase, independent of gas holdup, Yianatos et al. (1985) simplified this problem by the cell constant as a function of gas holdup. They derived a geometrical model to relate the cell constant with gas fraction.

The conductance of a liquid system at a fixed temperature is proportional to the

cross-section area of conducting material and inversely proportional to the distance of the path between electrodes (ϵ_g=0, Eq.5.1),

$$K_c = k_c \frac{A}{L} \tag{5.6}$$

For a homogeneous dispersion of gas bubbles in the liquid system, the conductance of the system can be expressed, for any gas holdup ϵ_g, by,

$$K_\epsilon = k_c \frac{A_\epsilon}{L_\epsilon} \tag{5.7}$$

where

$$A_\epsilon = A(1-\varepsilon_g) \tag{5.8}$$

It is noted here that conductivity of the mixture is still that of the continuous phase, but the cell constant changes. In contrast, Maxwell assumed the cell constant does not change but the conductivity of the mixture does. From the geometrical model of Yianatos et al. (1985) for the bubbling zone in a flotation column, the effective length between electrodes is given,

$$L_\epsilon = L(1+0.55\,\varepsilon_g) \tag{5.9}$$

Combining Equations (5.6-5.9), the following expression for gas holdup in the bubbling zone is obtained,

$$\varepsilon_g = \frac{1-\gamma^*}{1+0.55\gamma^*} \tag{5.10}$$

where γ^* is the apparent relative conductance given by,

$$\gamma^* = \frac{K_\epsilon}{K_c} \tag{5.11}$$

It is noted from the geometrical model of Yianatos et al. (1985) that the conductivity (specific conductance, k_c) used for the aqueous solution (ϵ_g=0) and for the dispersion (ϵ_g>0) is the same, but the cell constant changes from A/L to A_ϵ/L_ϵ. This approach eliminates the measurement of relative conductivity of the mixture of liquid/gas.

However, the geometrical model oversimplifies the dependence of cell constant on the gas fraction, and it is not always possible to substitute K_t/K for k_t/k, even in Equation (5.10).

It is noted that Maxwell (1873) did not specify the design of electrode cell to measure the conductivity of the dispersion. Yianatos (1987) described the electrodes used in his work but failed to mention the possible effect of their geometry on the measurements. From the theoretical analysis of Maxwell (1873), Turner (1976) and the work of Yianatos (1987), uniform and parallel current lines between the two opposite faces of a cell are essential for the use of these models. Once this is satisfied, either Equation (5.4) or (5.10) is adequate.

5.3.3 Local Gas Holdup Measurement

From the equations linking gas holdup and the relative conductivity, the local gas holdup can be measured. In the present work, it was found that the geometry of the electrode cell plays an important role in measuring local gas holdup. Maxwell's model assumes that the cell constant of a given electrode cell is independent of the fraction and size of the dispersion phase. However, this can only be obtained for a type of cell, in which the current path is uniform, parallel and definitely constrained to a certain volume. In this case, the current path is not affected by the fraction and size of the dispersed phase. Therefore, the relative conductance (which is the reading actually taken using a conductivity meter and an electrode cell) is the same as the relative conductivity and the cell constant needs not to be known.

Four types of electrode cells were tested in the present study and are shown in Figure 5.8. As a reference, gas holdup measured by water manometers was used. The column used for this purpose was relatively small, 5cm in diameter and 100cm in height. Various frother concentrations, gas rates and liquid rates were used. This particular set-up is shown in Figure 5.9. Figure 5.10 presents the relative conductance vs. the gas holdup measured using water manometers for cell types 1-2. Since the measured section is small, it is assumed that the mean gas holdup measured by the manometers is more or less the same over the entire volume (ABCD) and that the conductivity-based measurement is sensing approximately the same volume (abcd).

Cell type 1 was constructed because the needle inside the O-ring well defines the

single point of interest. After testing this type of cell, no correlation between relative conductance and gas holdup (Figure 5.10) was found possibly due to the path of current flow being a function of gas holdup and bubble size.

Cell type 2 was constructed based on the results from Cell type 1. This cell gives a good correlation between relative conductance and gas holdup (Figure 5.10) probably due to the well restrained current path. Therefore, it is safe to assume relative conductance is the same as the relative conductivity. However, since the length is relatively long (4 cm), it is difficult to maintain its verticality which may have an effect on the measurement.

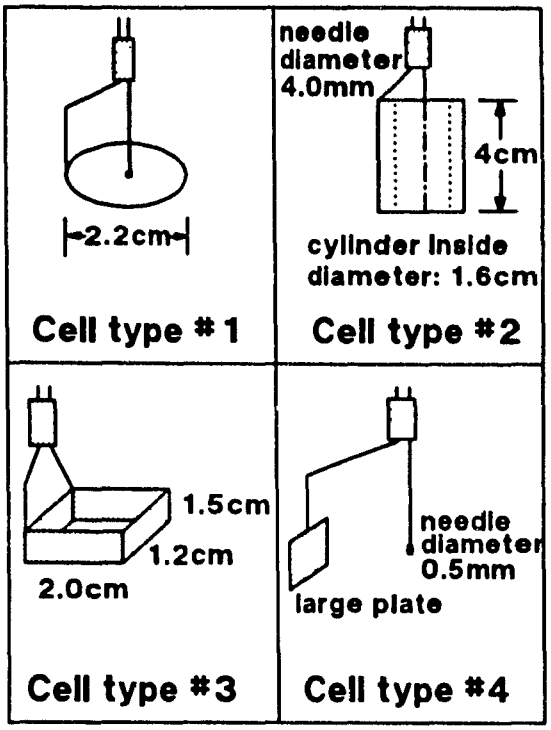

Figure 5.8 Cell designs used in present study

Cell type 3 (the two opposite electrodes are identical) provided a solution to the problem of Cell type 2. Figure 5.10 clearly shows the relation between relative conductance and gas holdup is in good agreement with Maxwell's model. This type of cell was also used by Kaya (1990) for the measurement of local gas holdup in mechanical flotation machines. It is also similar to the cell used by Yianatos (1987). This type of cell takes a volume of sample between the two opposite electrodes. If this cell is used in a relatively large column, the accuracy in the estimation of local gas holdup is satisfactory; relative to the volume of the 50cm diameter laboratory column (Figure 5.2) in which it was used, this cell essentially gives a point gas holdup.

Figure 5.11 presents the comparison of gas holdup between estimated from relative conductance and measured using the water manometers. This data is simply a restatement of Figure 5.10.

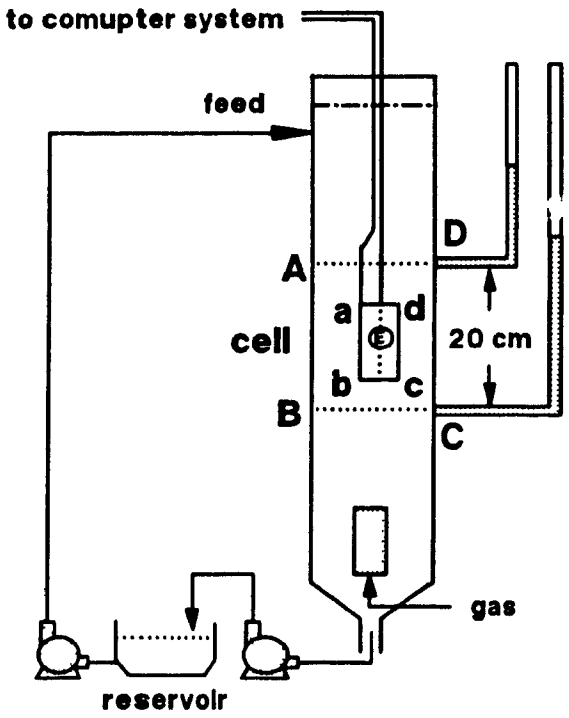

Figure 5.9 Calibrating the electrode cell of local gas holdup measurement

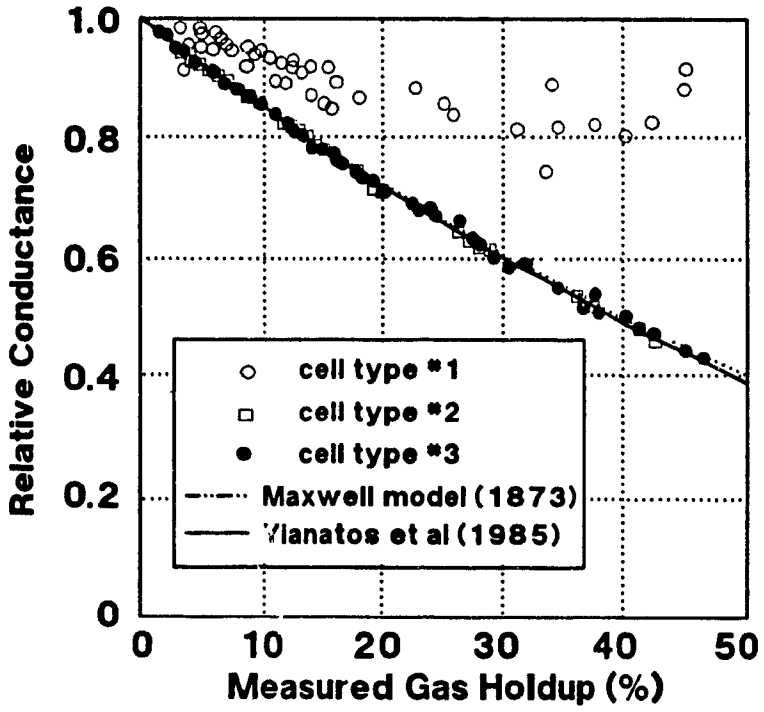

Figure 5.10 Relative conductance vs. gas holdup

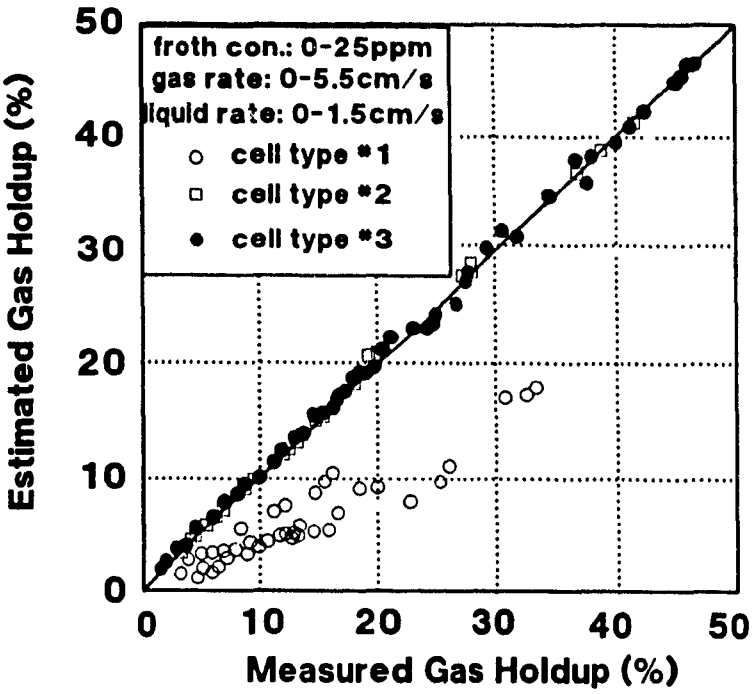

Figure 5.11 Comparison of gas holdup estimated from relative conductance and measured from water manometers

The operating principle of Cell type 4 is quite different from the above three types. The two electrodes of Cell type 4 are different in size and shape. One is a stainless steel plate large enough not to be affected by individual bubbles, the other being a tiny stainless steel needle (about 0.5 mm in diameter), with only the tip not insulated. Because of the small size of the needle tip, almost all the resistance of the cell is concentrated within a very small distance around the tip, and the presence of bubbles other than those very near to the tip has no effect on the resistance between the needle and the plate. This needle comes closest to truly defining a point where point gas holdup is being measured. Ideally, there would only be two possible values of the current flowing through the cell: zero if the needle tip were in contact with a bubble and a value related to the conductivity of the gas-free liquid if the needle tip were in the liquid. The graph of conductivity against time would then be a square wave as shown in Figure 5.12. In practice, the finite size and the finite time required for the liquid film covering it to drain away when the needle penetrates a bubble causes the curve to become rounded as shown by the dashed line in Figure 5.12. Corresponding to the two values of the current flow are two possible values of gas holdup at the needle tip: zero if the point is in the liquid phase, and unity if in the gas phase. This gives the time average gas holdup (Hills, 1974),

$$\varepsilon_g = \lim_{\tau \to \infty} \frac{t}{\tau} \int_0^{\tau} \varepsilon_g(t)\,dt \qquad (5.12)$$

The time average gas holdup is equal to the total area under the peaks in Figure 5.12 divided by the elapsed time. When the peaks are near square waves, the area under them is proportional the sum of the peak widths, or,

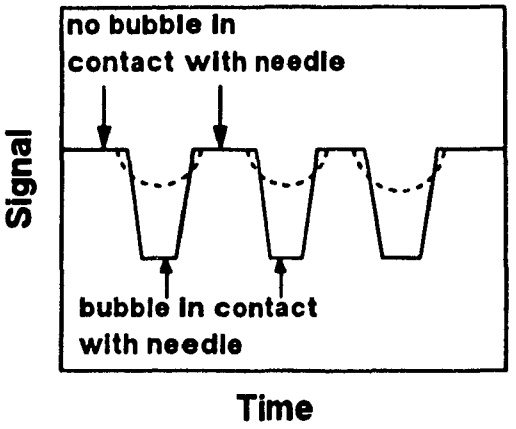

Figure 5.12 Ideal signal of cell type #4

$$\varepsilon_g = \frac{\sum_{i-1}^{n} t_i}{\tau_s} \qquad (5.13)$$

where t_i is the time of the needle tip in the gas phase and τ_s is the total time of sampling. An example of the actual signal-time response obtained using this type of cell is shown in Figure 5.13: it is much more complex than the proposed ideal response curve. It is impossible to obtain the information required for estimating gas holdup from this response curve due to the irregular shape. As pointed out by Hewitt (1978), this type of electrode cell can only be used for relatively large bubbles with relatively low frequency; the current observation confirms this view. A finer needle tip (e.g. $< 10\ \mu$m) may be worth exploring (Serizawa, 1975).

From this study, it can be concluded that Cell type 3 can be used to estimate local gas holdup and Maxwell's model offers a good correlation of gas holdup to the relative conductance. For an electrode cell of types 2 and 3, the relative conductance is the same as the relative conductivity, and cell constant does not change with gas holdup and bubble size at least over the range encountered in this work (Uribe-Salas, 1990). It may be questioned that Cell type 3 is only able to detect the bubbles rising vertically upwards. Since liquid circulation exits in a large-scale flotation column, bubbles at some points may move non-vertically. No attempt was made to study this possible effect systematically since the cell design is best suited to vertical orientation.

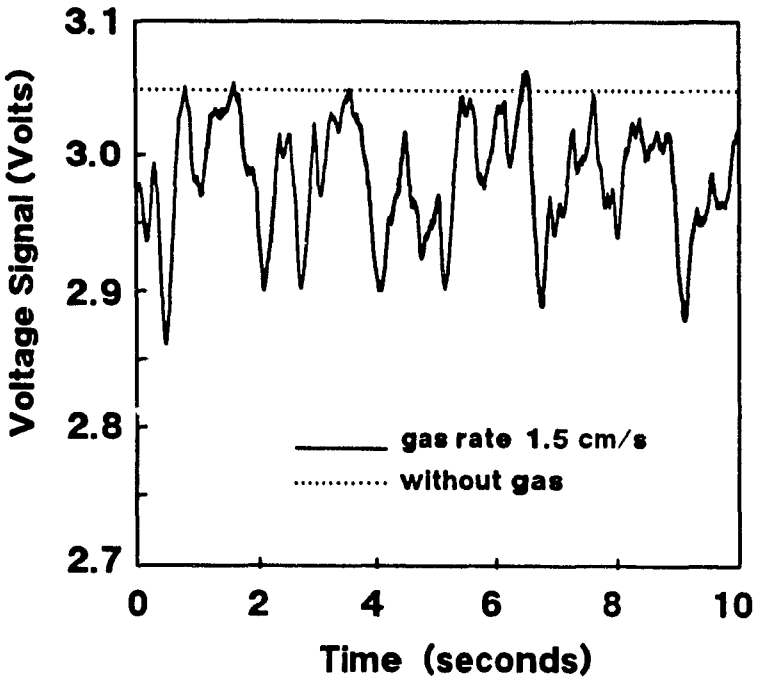

Figure 5.13 Example of response curve for cell type #4 in this work

5.3.4 Local Gas Holdup Measuring Probes

Based on the above principal, two probes for multiple, simultaneous local gas holdup measurements were constructed: one for the large laboratory column and the other for the pilot flotation column at Strathcona Mill, Falconbridge Limited.

The first probe contains seven identical pairs of electrodes (Figure 5.14); the cell dimension is the same as cell type 3 illustrated in Figure 5.8. The cells are equally spaced along a small horizontal tube. There is a supporting tube in the centre; the location and adjustment in the column is performed using this supporting tube.

The second probe consists of two parts, each part has 10 identical electrode cells. The cells were not equally spaced and the distance between cells is shown in Figure 5.15. The cells were numbered 1, 2, ..., 10 and 11, 12, ..., 20. The supporting frame is presented in Figure 5.16. Two crosses were built: one was placed on the top lip of the column, the other was slid into the flotation column. Because the feed pipe to the column extended to the column centre, the bottom cross was designed in such a way that it could

pass the feed pipe. The consequence of this design was that the local gas holdup near the central area below the feed position could not be measured. All the measurements were obtained in batch operation and at 15 ppm frother concentration. Work performed in continuous operation was not successful due to a changing conductivity of the feed water.

Three probe arrangements were used to cover the whole column diameter. Probe arrangement (a) was the case where there were fewer cells near the wall, while arrangement (b) was the case where there were more cells near the wall. Probe arrangement (c) was for the column central area: this arrangement was only used at the location above the feed pipe. Measurements were made at three locations: 1.0m, 6.0m and 10.0m above the sparger level.

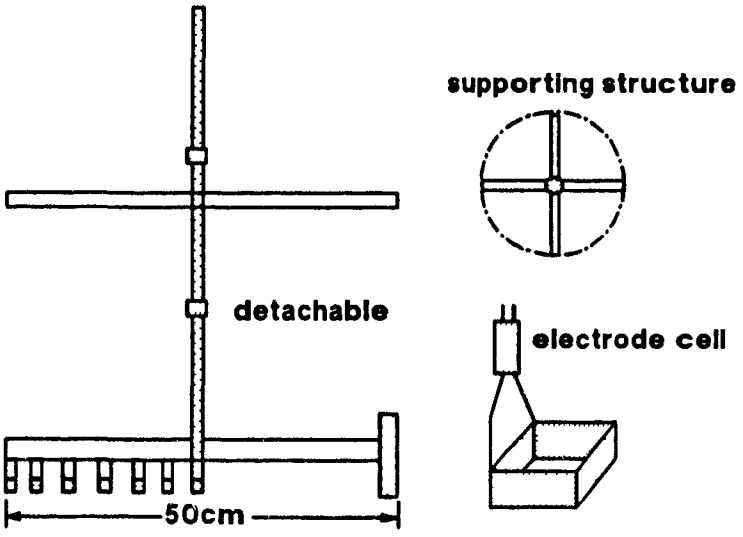

Figure 5.14 Conductivity probe for measuring radial gas holdup profiles in the 50cm laboratory flotation column

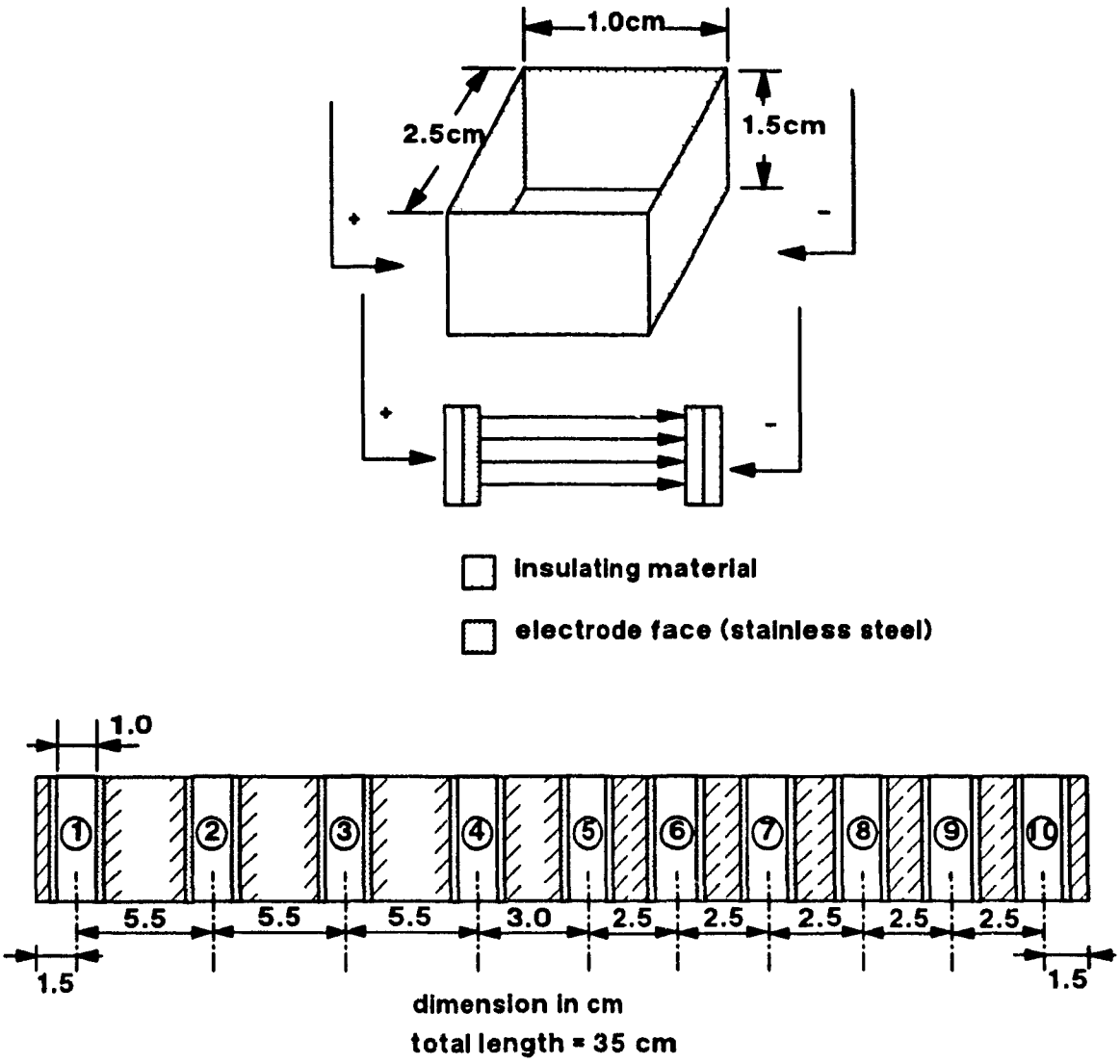

Figure 5.15 Probe structure and electrodes arrangement for the pilot flotation column

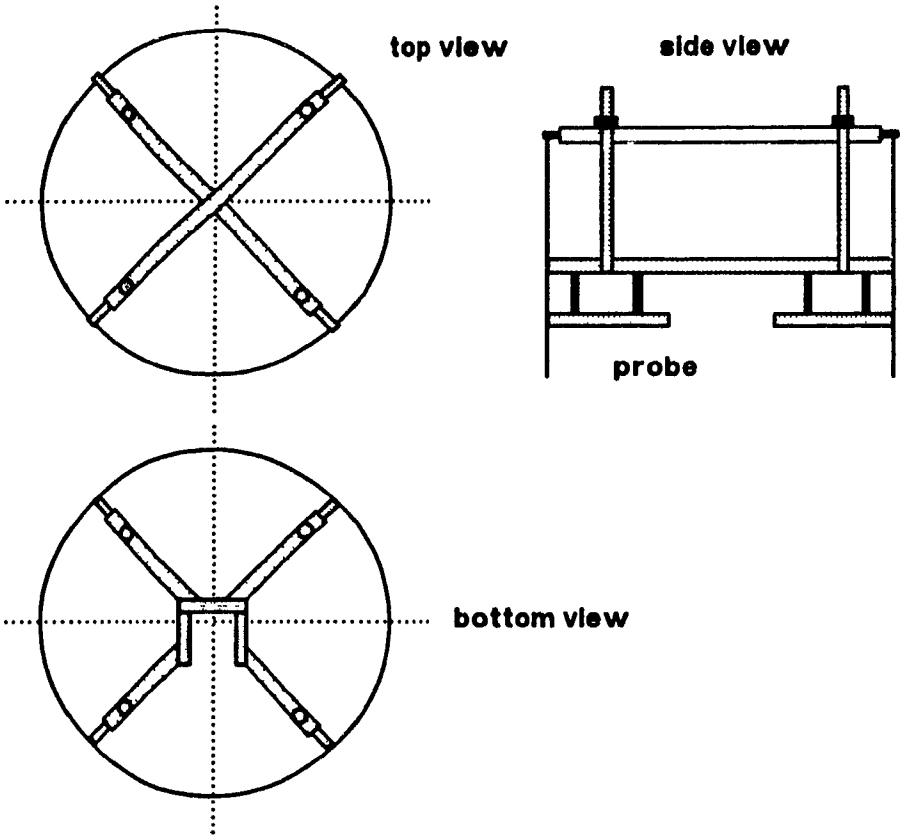

Figure 5.16 Supporting frames of the Probe for measuring local gas holdup in the pilot flotation column

5.4 Axial Gas Holdup Measurement

The axial gas holdup profiles were measured using a pressure transducer (Omega, model PDCR86X). The measurement procedure is shown in Figure 5.17. At $J_g=0$ (or $\epsilon_g=0$), the pressure difference between any two positions is given by,

$$\Delta P = \rho_l \Delta H \tag{5.14}$$

where ρ_l is the water density. At $J_g \neq 0$, the pressure difference between these two positions is given by,

$$\Delta P_c = [\rho_l(1-\epsilon_g) + \rho_g \epsilon_g] \Delta H \tag{5.15}$$

Combining and rearranging Equations (5.14) and (5.15) gives the gas holdup between the two locations (assuming $\rho_g=0$),

$$\varepsilon_g = 1 - \frac{\Delta P_e}{\rho_l \Delta H} = 1 - \frac{dP_e}{dH} \qquad (5.16)$$

Plotting the gas holdup measured using above approach as a function of the position is the axial or vertical gas holdup profile.

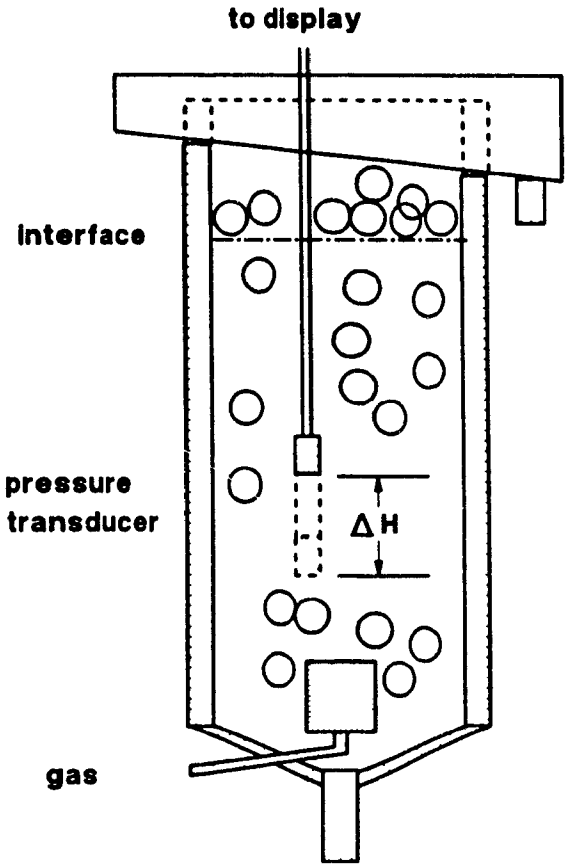

Figure 5.17 Axial gas holdup measurement using pressure transducer

PAGINATION ERROR.

TEXT COMPLETE.

NATIONAL LIBRARY OF CANADA.

CANADIAN THESES SERVICE.

ERREUR DE PAGINATION.

LE TEXTE EST COMPLET.

BIBLIOTHEQUE NATIONALE DU CANADA.

SERVICE DES THESES CANADIENNES.

is the same throughout the system). Fresh water containing no tracer was then used to replace the feed; meanwhile, the computer system recorded the tracer concentration with time at the underflow discharge. After a sufficient time, there was no more tracer in the system and the test was thus terminated.

Although all three of the above techniques were used, most experiments were conducted using configuration (c) to preserve the similarity with most industrial column test work. In general, RTD measurement in industrial flotation columns can only be conveniently conducted using configuration (c).

Liquid RTD in the pilot flotation column was measured using configuration (c) with the cup-sampling method, i.e., samples were taken using beakers and then off-line analyzed for tracer concentration.

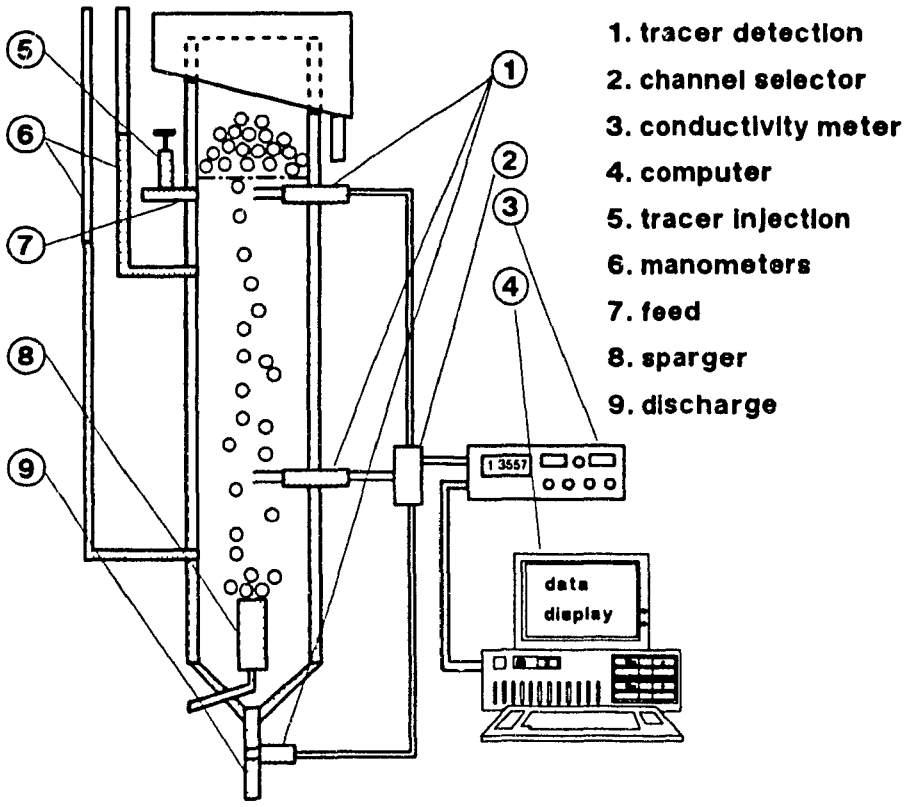

Figure 5.18 RTD measurement set-up

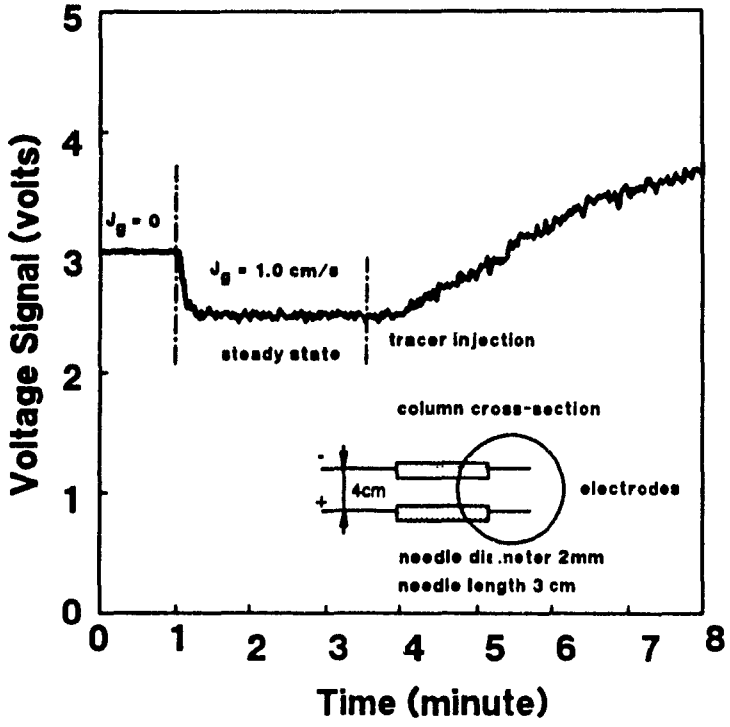

Figure 5.19 Voltage-time response for the electrode cell inside the column

5.5.2 Tracer Selection

Tracer tests usually involve the injection of a tracer at one location in the system and detection of its concentration as a function of time at one or more downstream locations. The selection of a proper tracer for a given system is important so that the RTD is characteristic of the phase of interest and is not influenced by the tracer. Shah et al (1978) present the following basic requirements for a satisfactory test,

1. The tracer should be miscible in and have physical properties similar to the fluid phase of interest, and it should not be transferable to the other phase or phases in the system.

2. The tracer should be accurately detectable in small concentrations so that only a small quantity need be injected into the system, thus minimizing disturbances in the established flow patterns. Also, a

concentration range which yields a linear response on the detection system is highly desirable.

3. Normally, the tracer should be non-reacting so that the analysis of RTD is kept simple.

4. The tracer detection system should cause the least amount of disturbance in the flow patterns as possible.

5. Good sensitivity and quick response time of the detection system are needed.

In the present work, KCl solutions were chosen as the tracer. For the tests performed in the 10.16cm dia. column, 20 ml 20% wt. KCl solution was used (total column volume being around 30800 cm^3). The KCl concentration was detected using conductivity. The correlation between KCl concentration and conductance for the electrodes was established. Figure 5.20 presents a typical calibration curve. It is noted that at high KCl concentration, the relation is no longer linear. In order to avoid the non-linearity, the KCl solution was kept at low concentration (20 wt.%). Tests showed that maximum value of concentration at exit never exceeded 0.1% wt.. Calibration was repeated regularly. For the tests carried out in the pilot column, 3500ml 20% wt. KCl solution was used.

One example of calculating dimensionless RTD, mean residence time, mass balance and variance from the voltage response-time data is given in Appendix 10.

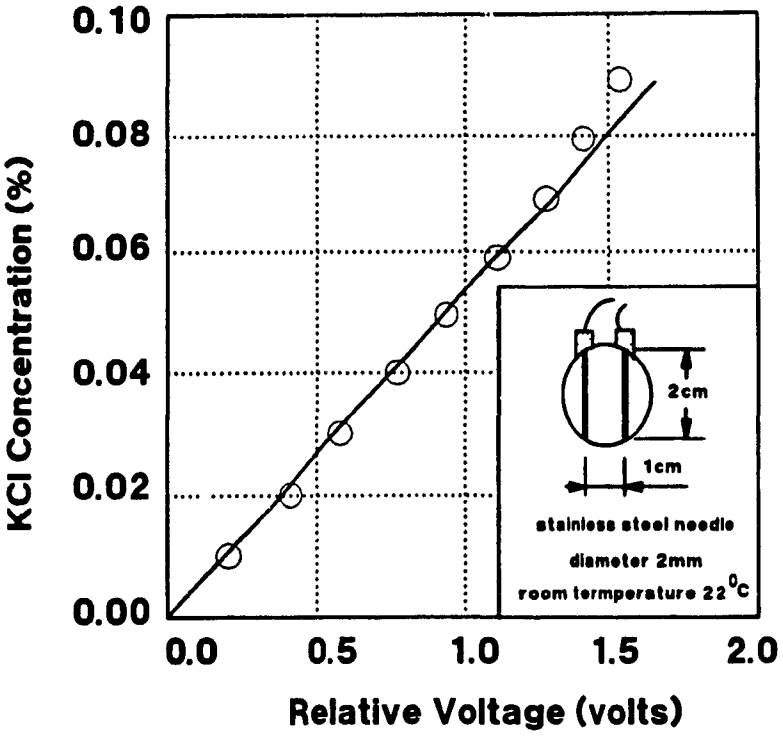

Figure 5.20 A typical calibration curve of KCl concentration (wt. %) vs. relative voltage (voltage of solution - voltage of water alone)

5.6 Data Acquisition and Processing

A computer data acquisition system (Figure 5.21) was used extensively in the present study for measuring local gas holdup and determining RTD. The data acquisition system consists of a microcomputer (micro 2001, IBM compatible, 640K of memory), a 24-channel relay board (Metrabyte, model ERB-24), an I/O interface board to control the relay board (Metrabyte, model PIO-12), an A/D converter interface board (DT2801 or Metrabyte, model DAS-8PGA), and a conductivity meter (Tacussel, model CD-180). Several programs (in QuickBASIC) were developed for different purposes. The flowchart of the data-acquisition program is given in Figure 5.22 (see data acquisition program in Appendix 12).

If more than one channel is used, the time between one channel to the next is important and was decided based on the response time of the whole system (usually about

3 seconds). If only one channel is activated, the time can be as short as desired. The raw data file for RTD measurement has about 600 data points and was processed and reduced to about 100 data points. The data processing includes transfer of voltage signal into KCl concentration and calculation of mass balance. The mean residence time and variance about the mean were also computed during the data processing and reduction (See the data processing and reduction program in Appendix 13).

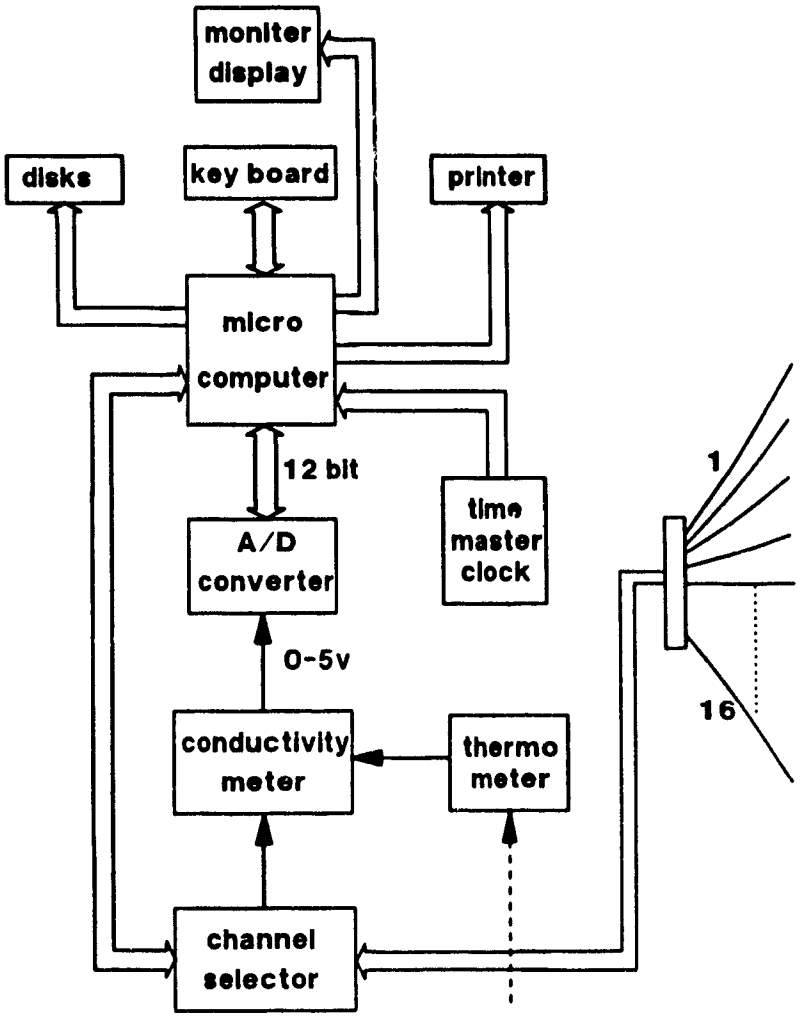

Figure 5.21 Computer data acquisition system

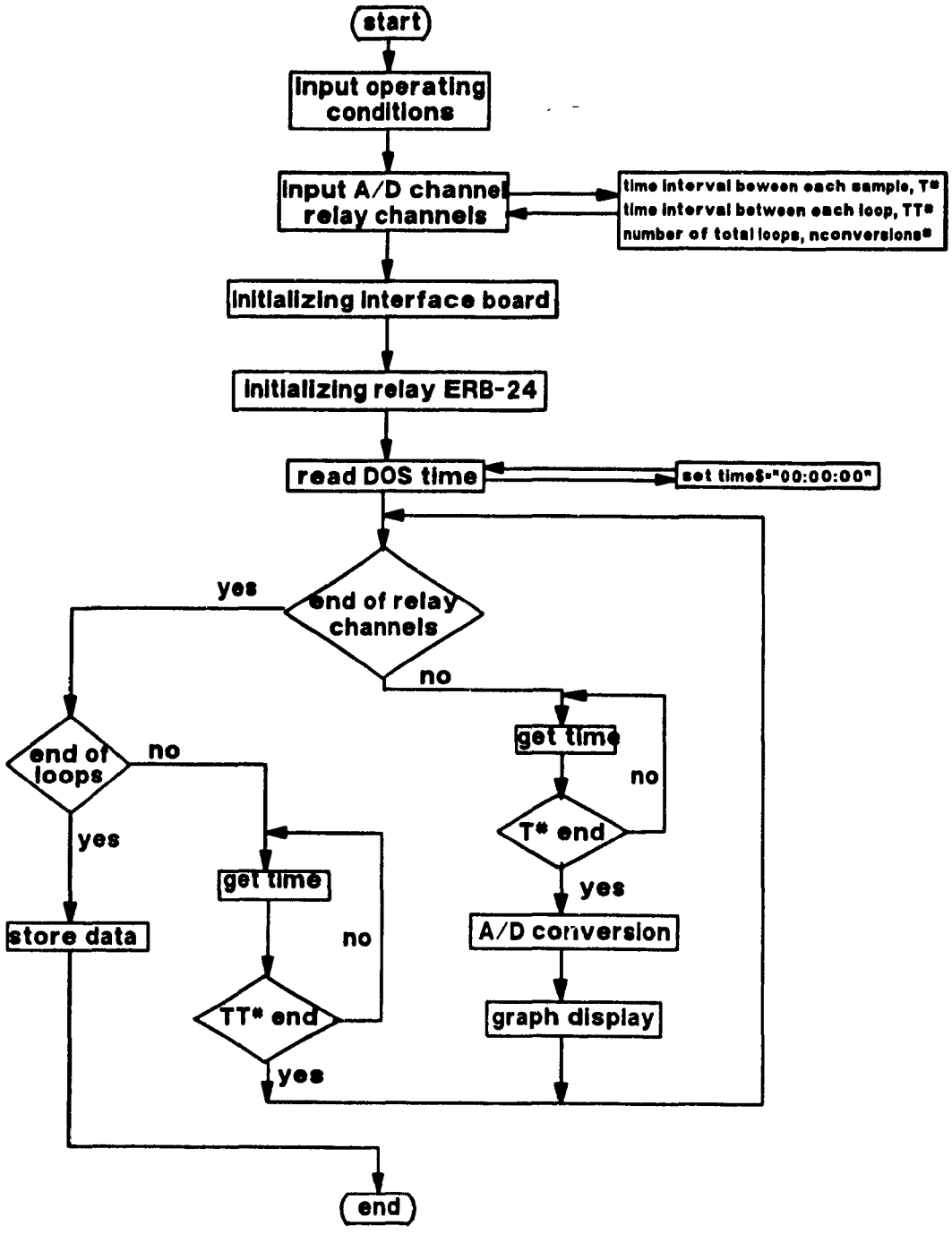

Figure 5.22 Flowchart of computer data acquisition program

CHAPTER 6

RESULTS: GAS HOLDUP DISTRIBUTION

Axial gas holdup profiles were determined using the pressure transducer. It was found that in the large-scale laboratory column, gas holdup increased by about 3-8% (absolute), depending on gas rate. The increase in gas holdup from the bottom to the top is related to the hydrostatic pressure change. Two methods have been used to account for the hydrostatic change: pressure change only or pressure change with bubbly flow model. It was shown that the experimental change in gas holdup was larger than the prediction of both methods. Radial gas holdup distribution was measured using the conductivity technique in the 50cm diameter laboratory flotation column under various conditions. It was found that the gas holdup distribution profiles were either parabolic, 'W' or saddle shape depending on the gas rate and sparger system, and changed only slightly from the bottom to the top. Effect of gas maldistribution on these holdup distribution profiles was also investigated. Approximate parabolic profiles were obtained at relatively large gas rates. In these cases, the liquid circulation velocity was calculated using the shear stress model developed by Clark and Flemmer (1987; 1989). Work conducted in the pilot flotation column showed that the radial gas holdup profiles were a 'W' shape at low gas rates, while at high gas rates, it was a saddle shape.

6.1 Axial Gas Holdup Profiles

Figure 6.1 presents the voltage signal from the pressure transducer for a period of 200 seconds for 4 different depths of the transducer location. It is clear from the signal that the pressure at all the levels is relatively consistent, although there is a high frequency variation. These measurements were conducted for various gas rates. The voltage signal vs. distance from the interface level (no froth) is presented in Figure 6.2 for three different gas rates and for the case of zero gas rate (calibration).

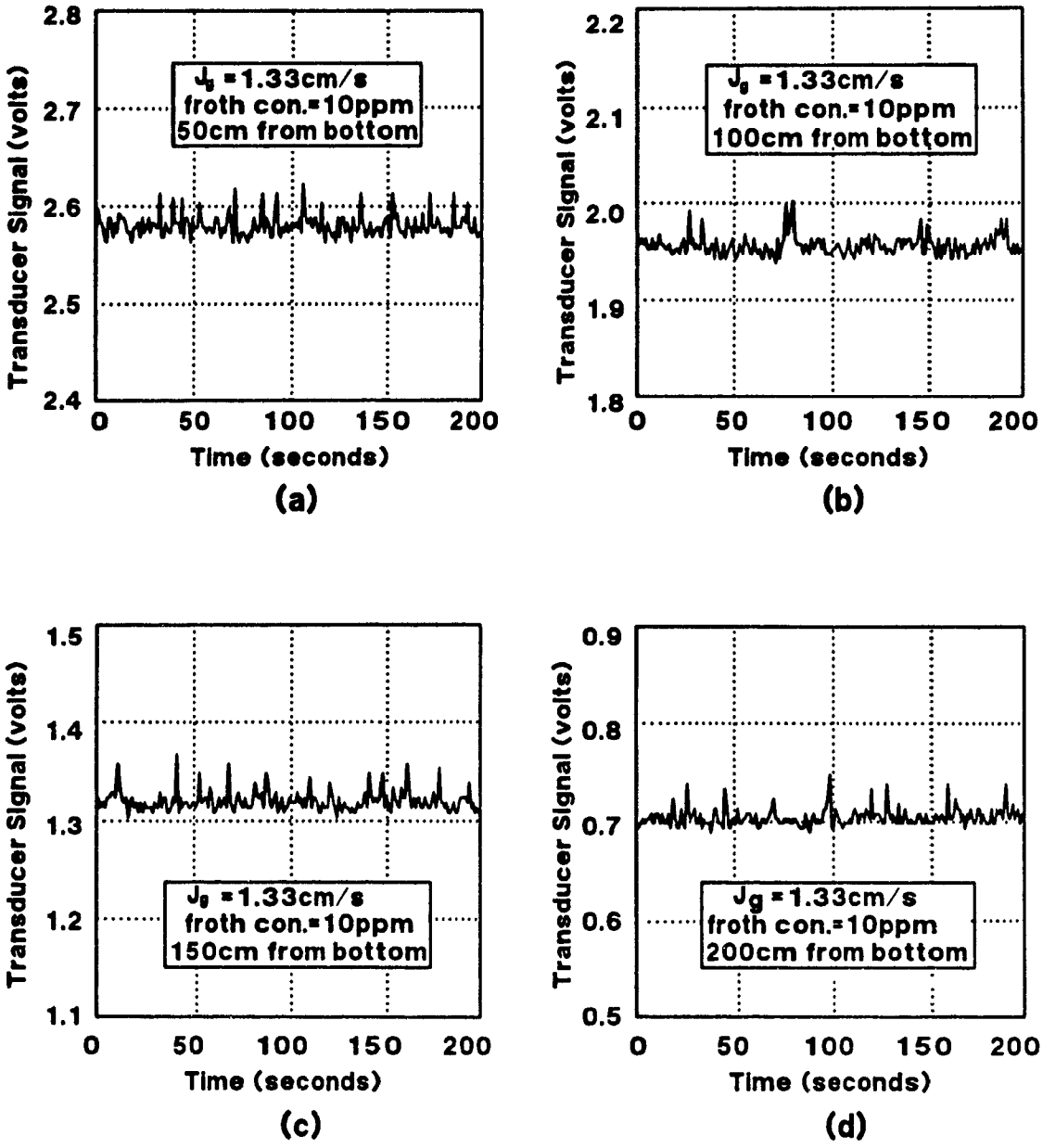

Figure 6.1 Voltage signal from the pressure transducer at different levels over a period of 200 seconds (8 spargers in equal operation)

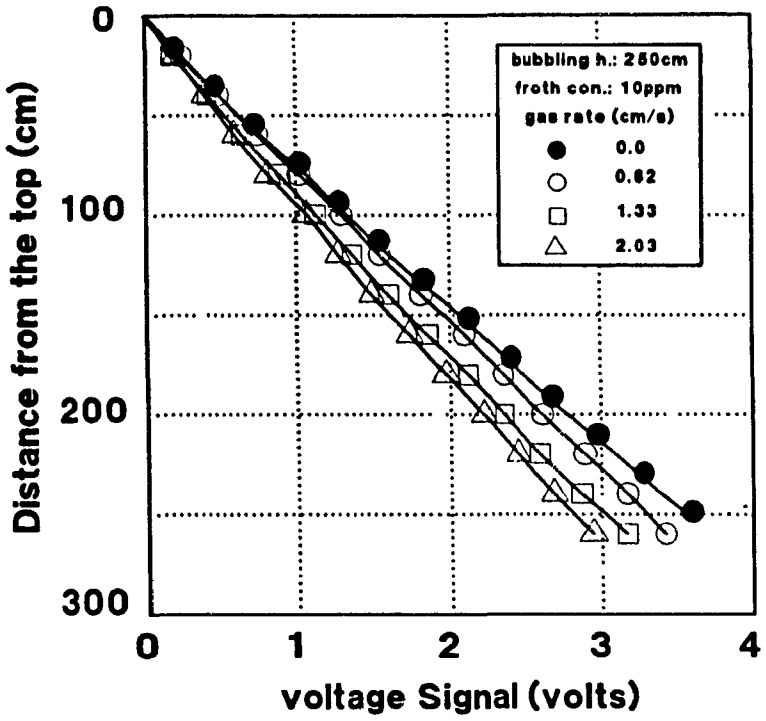

Figure 6.2 Voltage signal from pressure transducer vs. distance from the top of the column collection zone (no froth) for various gas rates

The voltage signal can be transferred into gas holdup. Table 6.1 shows an example of calculating gas holdup from the pressure measurements. It shows that the distance taken between two positions is very important, for instance, gas holdup can be calculated between every 20cm, 40cm or 60cm. Large differences in gas holdup are found using different distances, reflecting the sensitivity of the pressure measurements. Large fluctuation is evident if the distance between two measuring levels is very short. Plotting the gas holdup calculated based on different distances as a function of the axial distance (from top) is shown in Figure 6.3. Increasing the distance in the calculation can smooth the fluctuation and a general trend is clear.

Gas holdup measured using water manometers is also indicated in Figure 6.3. Though only two points are available, it shows a good agreement between the two types of measurements.

Table 6.1 Gas holdup calculation from pressure measurements

distance (cm)	voltage (volts)	water height (cm)*	20cm		40cm		60cm	
			depth (cm)	ϵ_g (%)	depth (cm)	ϵ_g (%)	depth (cm)	ϵ_g (%)
0	0.000	0.00	10	14.72	20	12.43	30	9.67
20	0.238	17.06	30	10.14	40	7.14	50	6.88
40	0.490	35.03	50	4.14	60	5.24	70	3.92
60	0.758	54.20	70	6.35	80	3.81	90	4.12
80	1.019	72.93	90	1.27	100	3.01	110	3.41
100	1.300	92.67	110	4.74	120	4.47	130	4.46
120	1.562	111.73	130	4.24	140	4.31	150	4.47
140	1.830	130.88	150	4.42	160	4.60	170	4.22
160	20.97	150.00	170	4.78	180	4.12	190	4.10
180	2.363	169.04	190	3.46	200	3.76	210	3.42
200	2.633	188.35	210	4.06	220	3.40	230	3.61
220	2.901	207.54	230	2.74	240	3.38		
240	3.173	226.99	250	4.03				
260	3.441	246.19						

* In terms of water height, a conversion factor applies (volts = 0.013978*depth (cm)) from the calibration curve.

Two methods are available to consider the effect of hydrostatic head change. First method is just to take into account for the pressure by assuming a single large bubble with a volumetric fraction as ϵ_{g1} at one position. At the next position, its volumetric fraction ϵ_{g2} is given by, for ideal gas at constant temperature,

$$\varepsilon_{g2} = \varepsilon_{g1} \frac{P_1}{P_2} \tag{6.1}$$

where P_1 and P_2 are the pressures at two different levels.

The other way is that, for a given bubble with size d_{b1} (and volume V_1, pressure P_1) at one level, the bubble size d_{b2} (and volume V_2, pressure P_2) at a second level, is given by,

$$d_{b2} = d_{b1}(\frac{P_1}{P_2})^{1/3} \tag{6.2}$$

Similarly, the superficial gas rate at the second level is related to that at the first level by,

$$J_{g2} = J_{g1}\frac{P_1}{P_2} \tag{6.3}$$

With a known bubble size and gas rate (zero liquid rate) at a given level, gas holdup at that level can be calculated using the bubbly flow model.

Included in Figure 6.3 are the predicted axial gas holdup profiles using the above two methods. The results suggest that gas holdup calculated based on pressure change or the bubbly flow model does not change as much as is observed. Application of the bubbly flow theory is questionable since it does not consider liquid circulation, which may result in an increase in gas holdup due to increased bubble retention time.

All the above results were obtained under the following conditions: frother concentration (Dowfroth 250C), 10ppm; batch operation; 8 filter cloth spargers in equal operation.

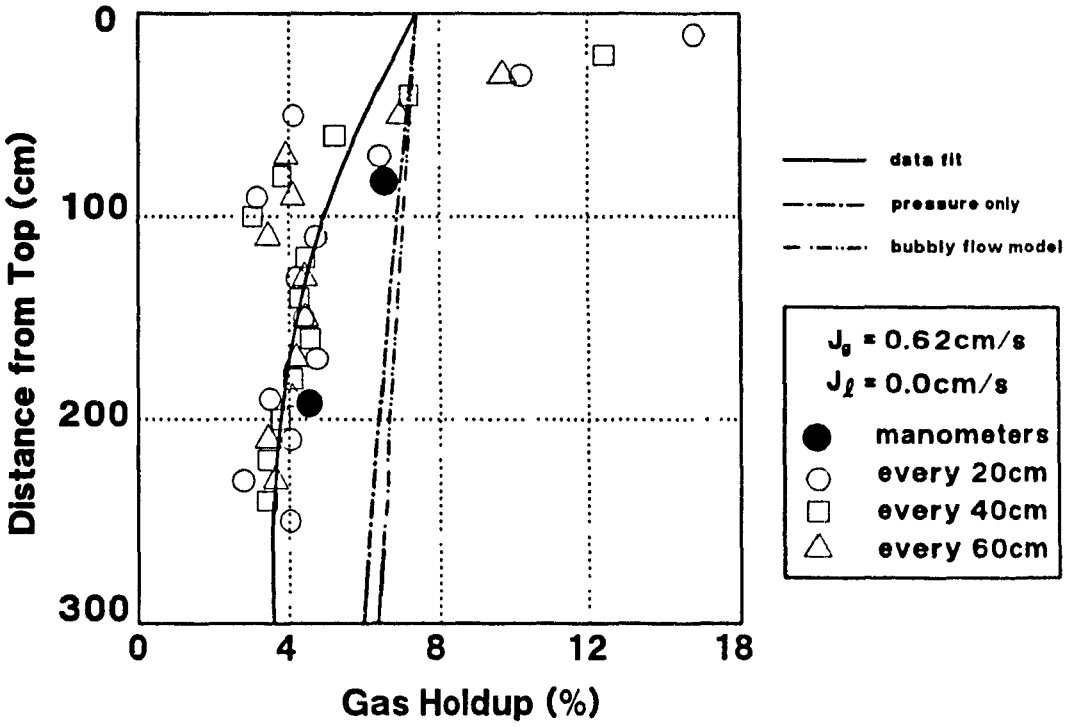

Figure 6.3a Axial gas holdup profile at J_t=0.62cm/s (8 spargers in equal operation)

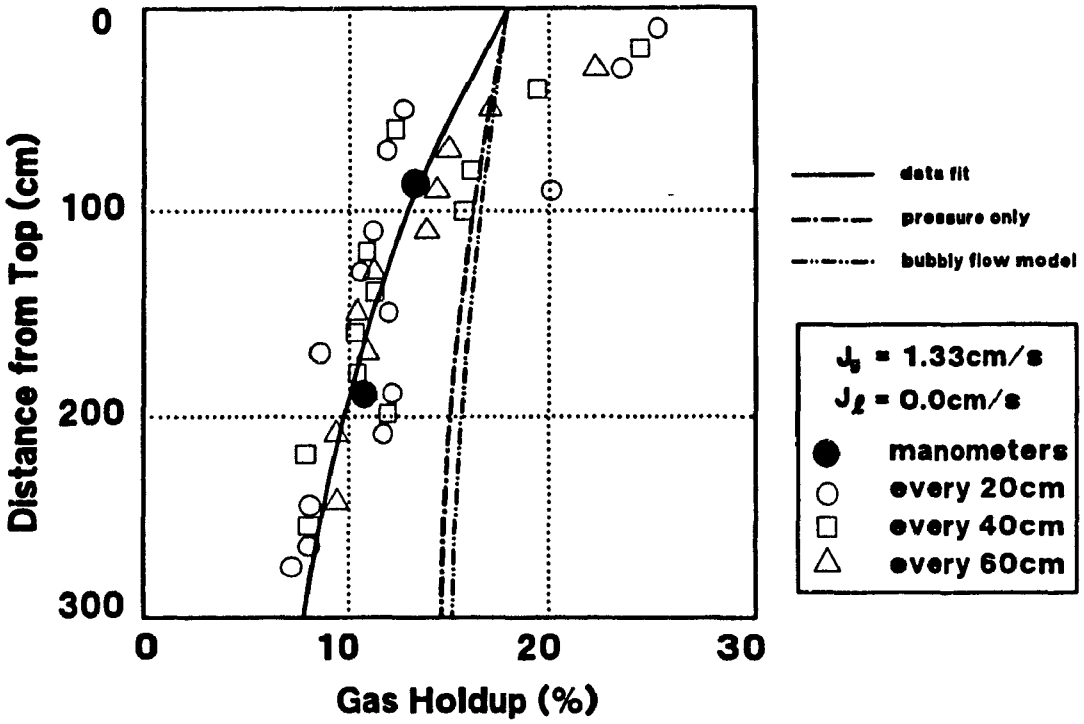

Figure 6.3b Axial gas holdup profile at $J_g = 1.33$cm/s (8 spargers in equal operation)

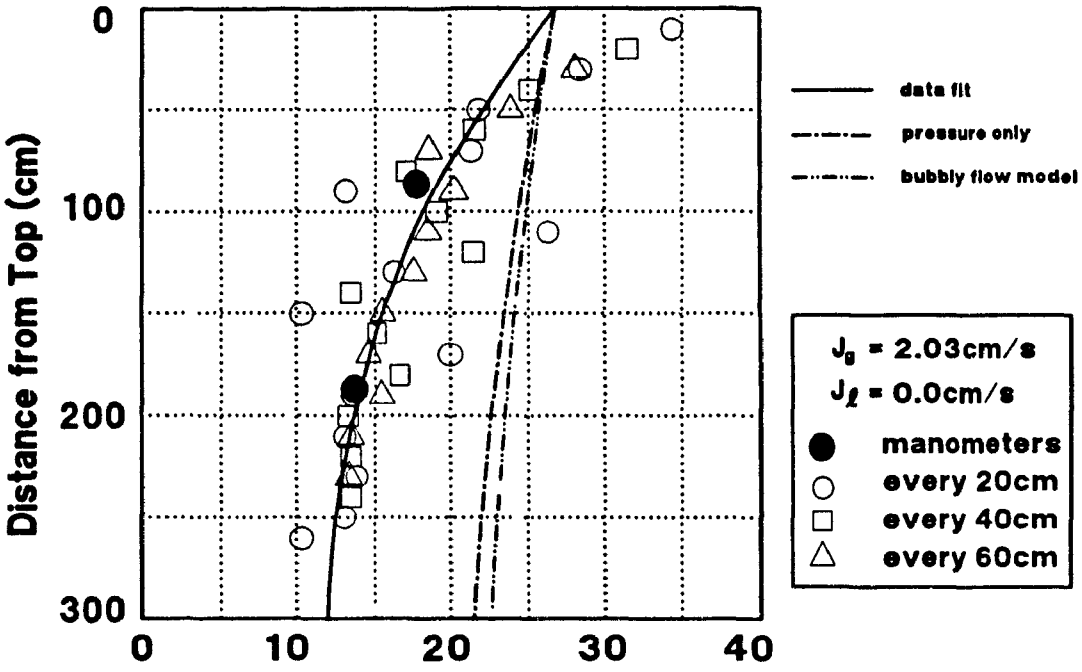

Figure 6.3c Axial gas holdup profile at $J_g = 2.03$cm/s (8 spargers in equal operation)

6.2 Radial Gas Holdup Profiles

Radial gas holdup distributions were measured under various operating conditions, and in particular the effect of frother addition, gas rate and gas maldistribution was investigated.

Before presenting the holdup distribution, measurement of gas holdup at a single point is first examined in Figure 6.4. Figure 6.4 shows gas holdup over a period of 200 seconds at different radial positions at a distance of 200 cm from the bottom of the column. At the column centre (Figure 6.4a), $r/R=0$, a large variation in gas holdup over the given period was observed, from a minimum around 5% to a maximum around 22% giving an average of 15.3%. Slightly away from the centre, $r/R=0.32$, and near the wall, $r/R=0.96$, the variation in gas holdup with time was less. The larger variation in gas holdup at the column centre is possibly due to the tendency of large bubbles to accumulate and rise at the column centre (Lockett and Kirkpatrick, 1975).

Due to the gas holdup variation with time, the results reported are time-average (3 repeated tests over 30 minutes). Figure 6.5 presents repeated holdup profiles as a function of the radial position (r/R) for three depths. It shows that the time-average reproducibility is relatively good.

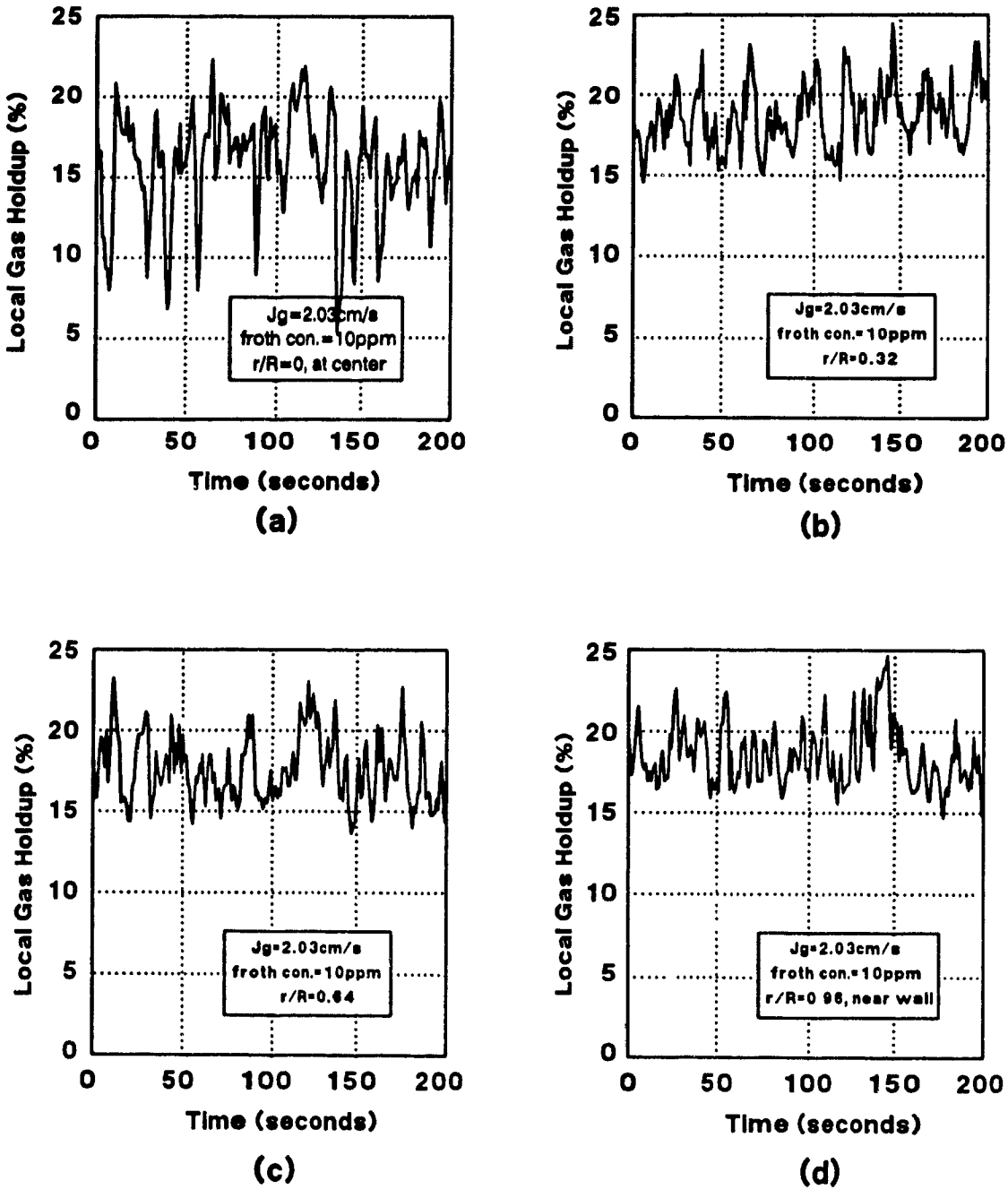

Figure 6.4 Local gas holdup as a function of time at the location 2.0m above the bottom (8 spargers in equal operation, 10ppm frother concentration)

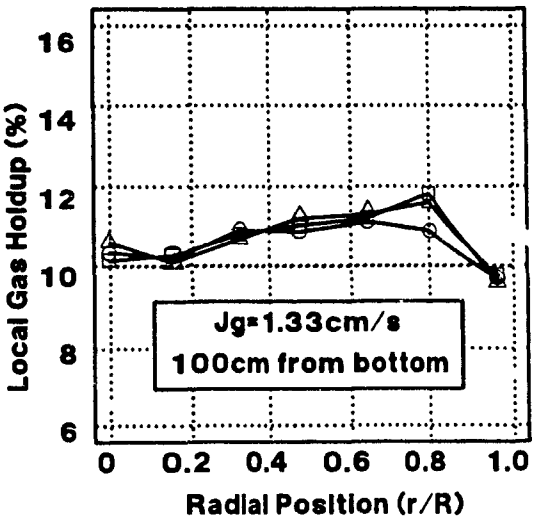

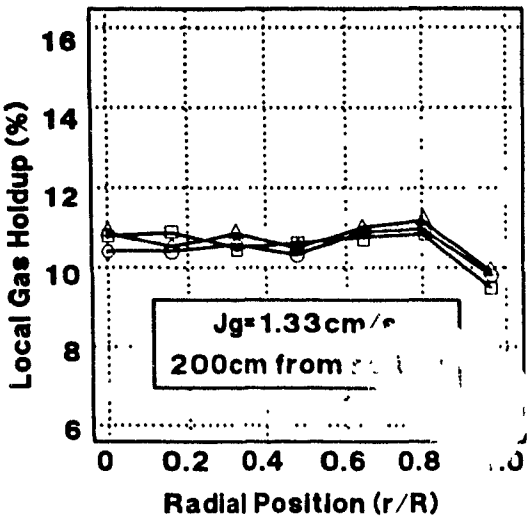

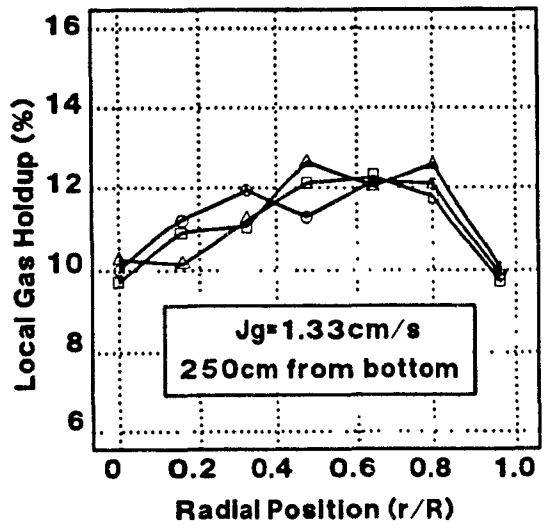

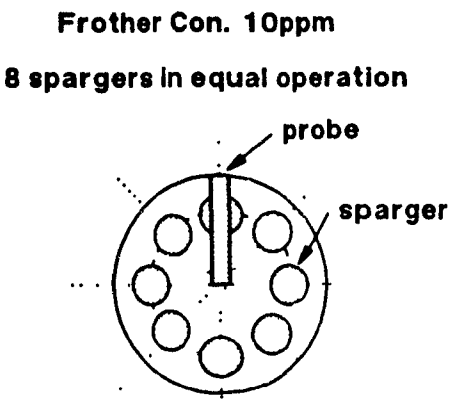

Figure 6.5 Radial gas holdup profiles at three different levels and the reproducibility

6.2.1 No Frother Condition

Under the conditions of no frother addition (similar to many bubble column operations in Chemical Engineering), a series of tests were conducted.

Figures 6.6, 6.7, 6.8 and 6.9 present the radial gas holdup distribution for various gas rates at 4 different levels, when 8 spargers are operated equally. The dashed curves are the equation fit (eq.3.1, gas holdup at the column centre ϵ_{gc} and power constant n being the fitting parameters). In general, large values of n imply that the radial gas holdup distribution is flat. Several important points can be obtained from these figures: (a) At relatively low gas rates, gas holdup distribution is relatively flat (the change from the wall to the centre is small), and these distributions are not parabolic or saddle-shaped, (b) At high gas rates, the change in local gas holdup from the wall to centre is relatively large and the distribution is near parabolic, (c) For a given level at low gas rates, the highest gas holdup is above the location of spargers, and the maximum shifts to the centre as gas rate increases.

When only 4 spargers were used, similar observation to the case of 8 spargers in equal operation are apparent (Figures 6.10 and 6.11). It is worth noting that when the number of spargers is reduced, average gas holdup is decreased at the same gas rate. This reflects the effects of sparger surface area on the gas holdup (Xu and Finch, 1989).

When only one sparger (off-centre) is used (Figures 6.12 and 6.13), local gas holdup above where the sparger is located is much higher than elsewhere. It seems that local gas holdup consistently decreases from the location of the sparger to the wall (both directions). The significance of these figures is in helping to interpret effect of mal-functioning of gas spargers on the column performance. Strong circulation was observed in column in this case, which would result in poor performance of the flotation columns.

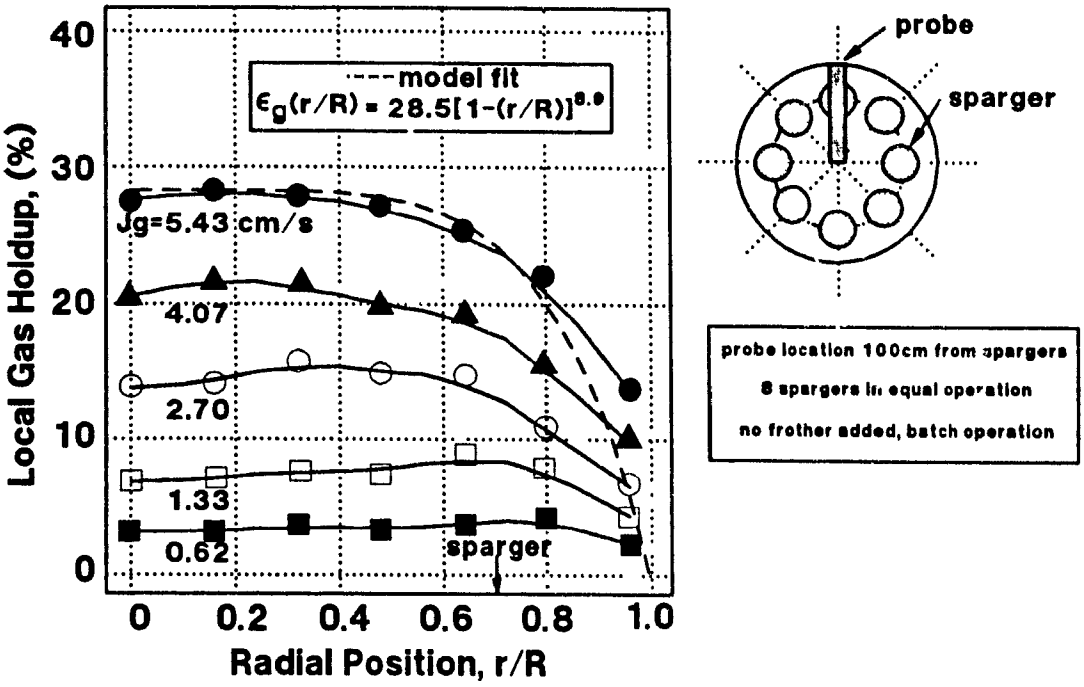

Figure 6.6 Radial gas holdup profiles at various gas rates near the bottom level

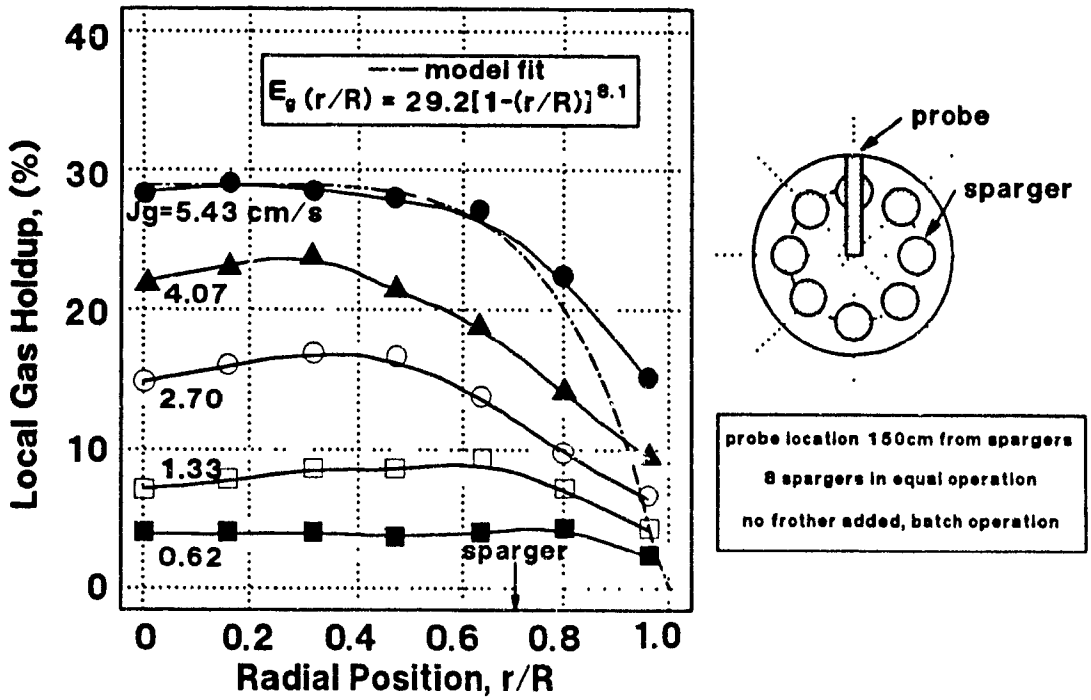

Figure 6.7 Gas holdup profiles at various gas rates at 150cm above the sparger level

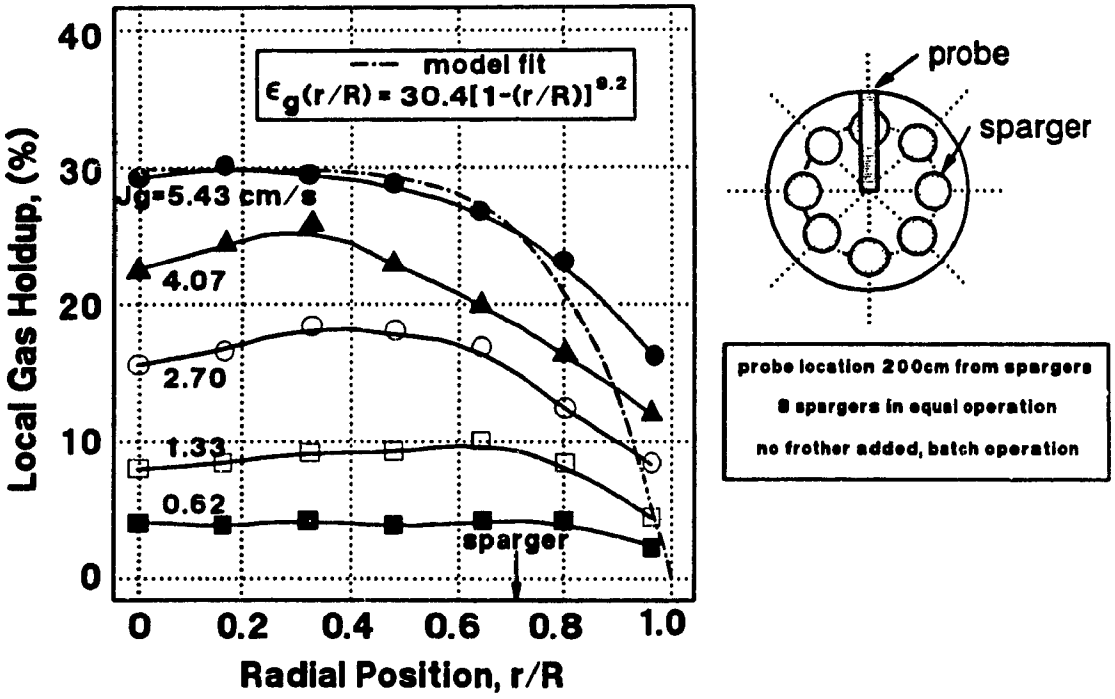

Figure 6.8 Gas holdup profiles at various gas rates at 200cm above the sparger level

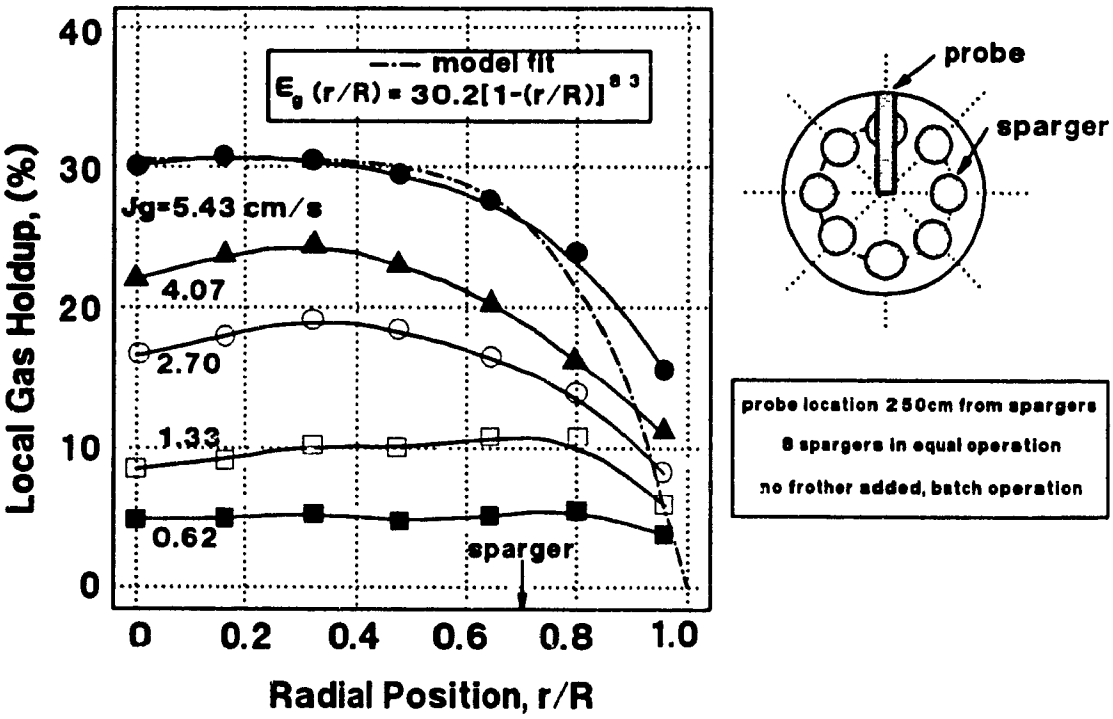

Figure 6.9 Gas holdup profiles at various gas rates near the interface level

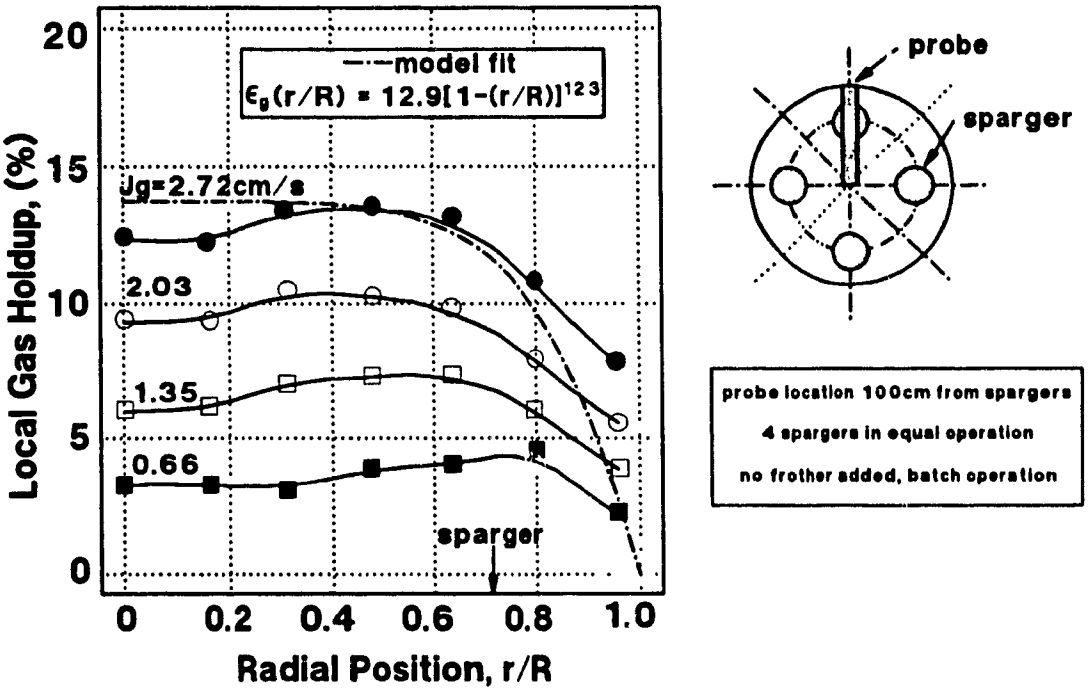

Figure 6.10 Gas holdup distribution at various gas rates near the bottom level

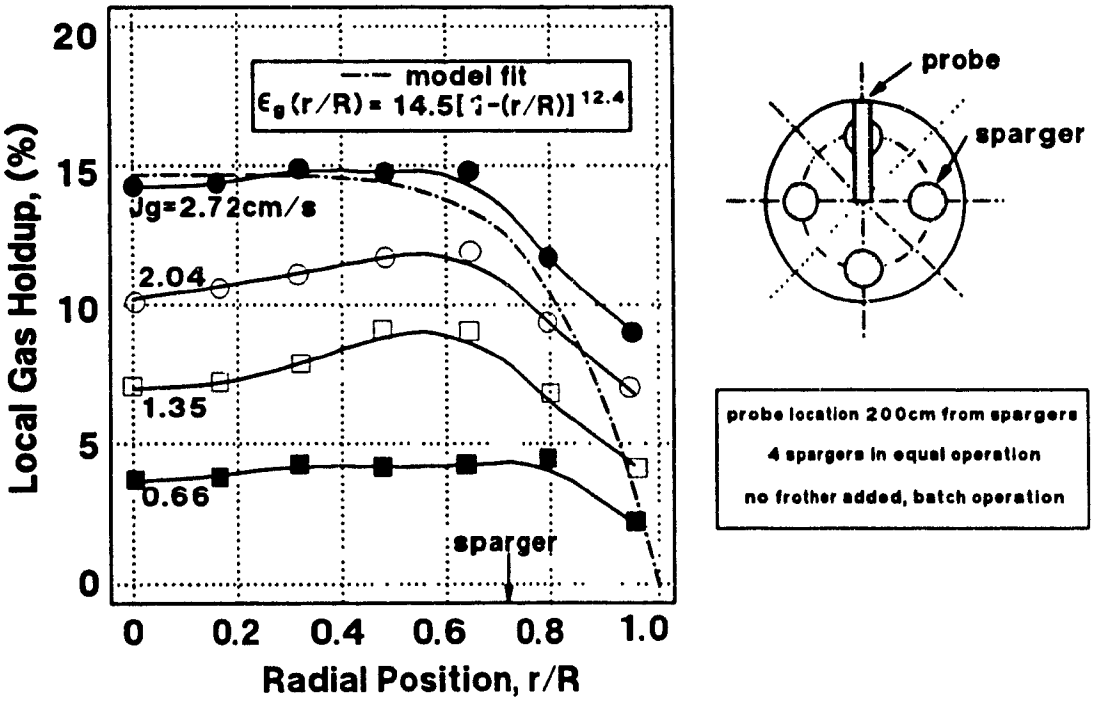

Figure 6.11 Gas holdup profiles at various gas rates at 200cm above the sparger level

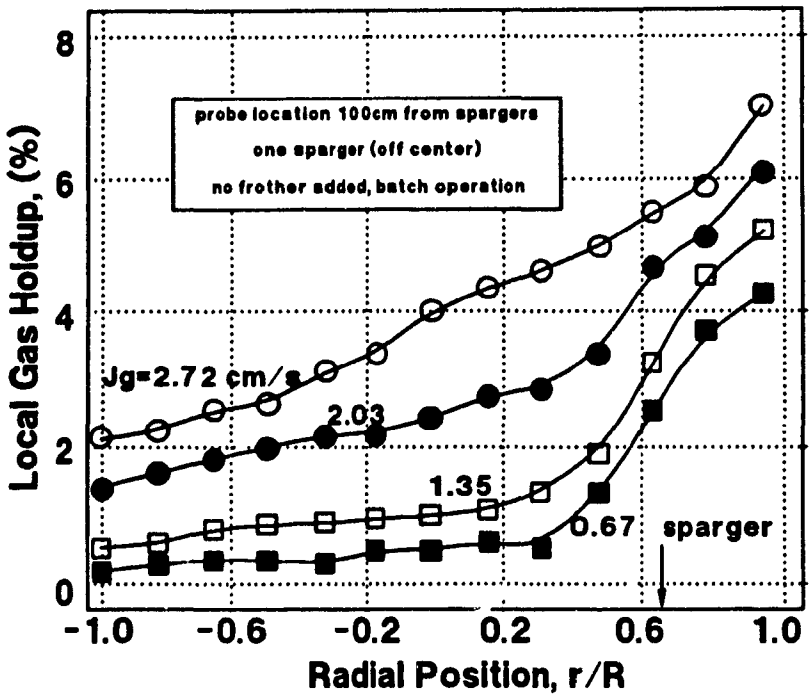

Figure 6.12 Radial gas holdup profiles at various gas rates near the bottom level when only one sparger in operation (off-centre, no frother addition)

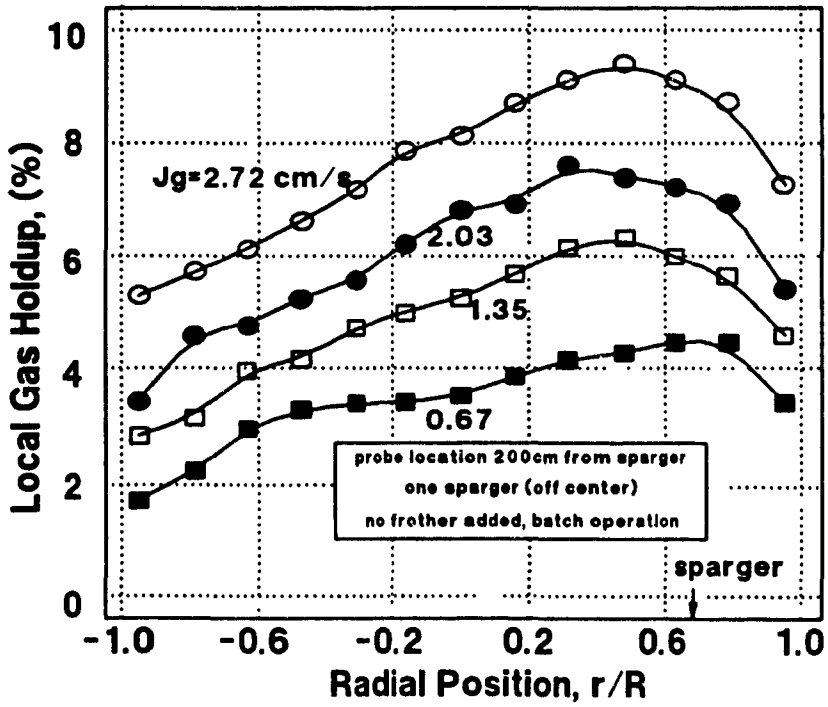

Figure 6.13 Radial gas holdup profiles at various gas rates near the interface level when only one sparger in operation (off-centre,no frother addition)

6.2.2 10ppm Frother Concentration

When frother is added, bubble size is reduced and bubbles are more uniform in size. Figures 6.14, 6.15 and 6.16 were obtained with 10 ppm frother concentration and 8 spargers in equal operation. Each of the figures is for a single gas rate and 3 different levels. From these figures, the following observations can be made: (a) Local gas holdup above the sparger location is higher than for any other location; (b) Gas holdup increases from the bottom to the interface level and the increase is larger than that in the case of no frother addition; (c) The shape of the radial gas holdup distribution is very similar to that in the case of no frother addition.

Essentially similar observations are clear when the number of spargers in operation was reduced (Figures 6.17 and 6.18).

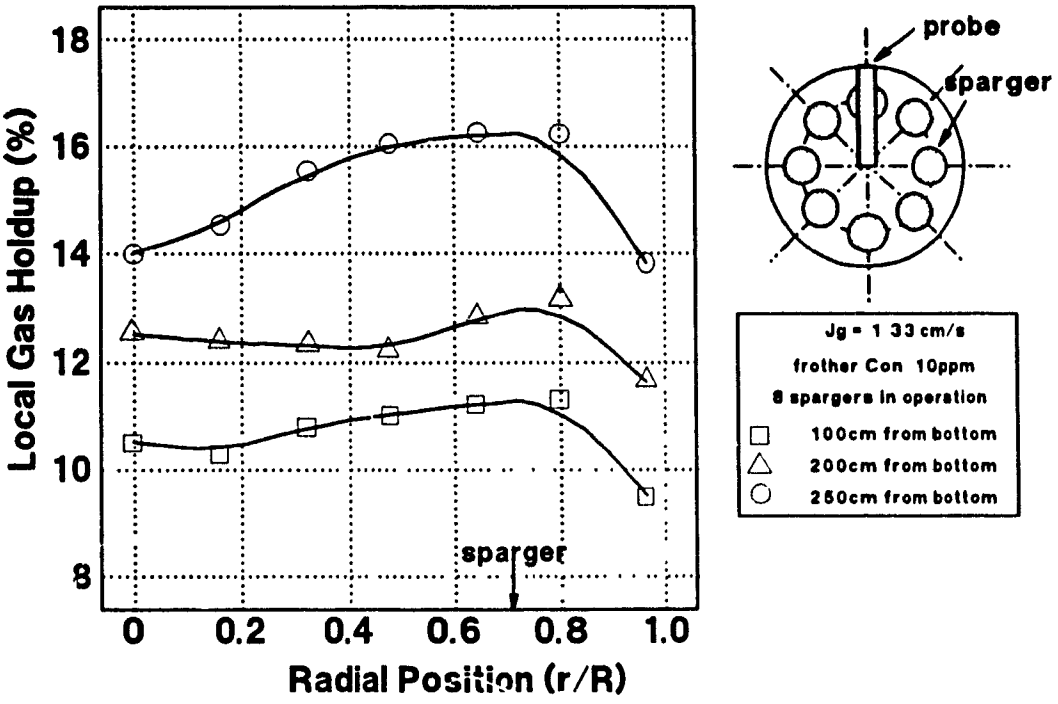

Figure 6.14 Gas holdup profiles at three different levels at J_g=1.33cm/s

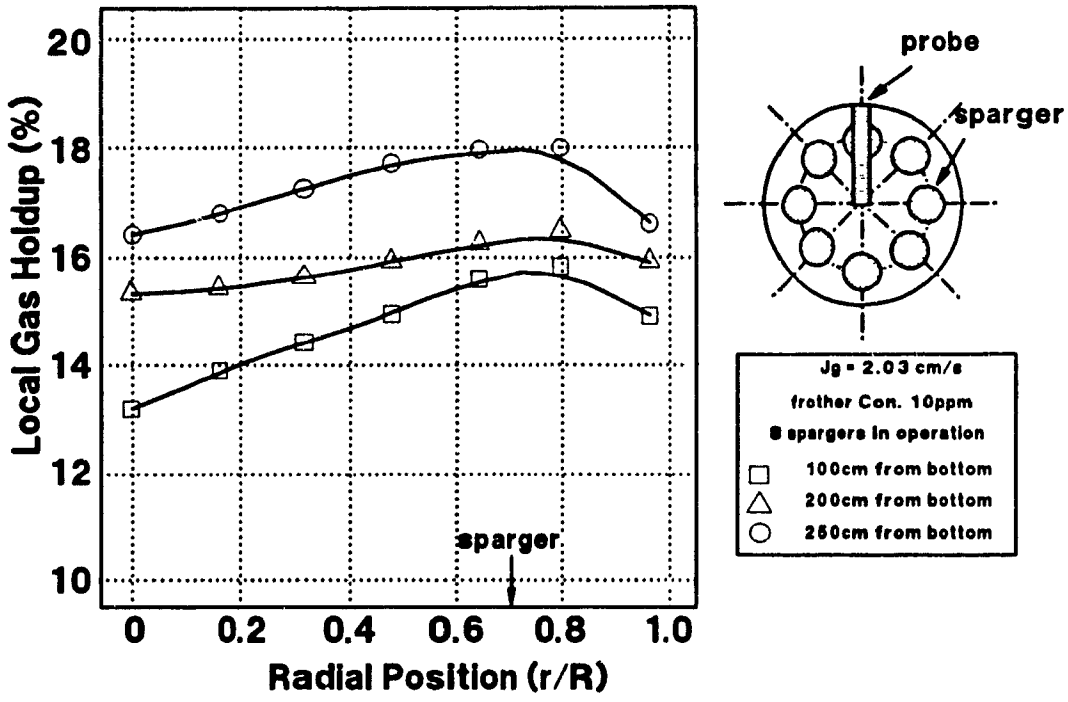

Figure 6.15 Gas holdup distribution at three different levels at J_g=2.03cm/s

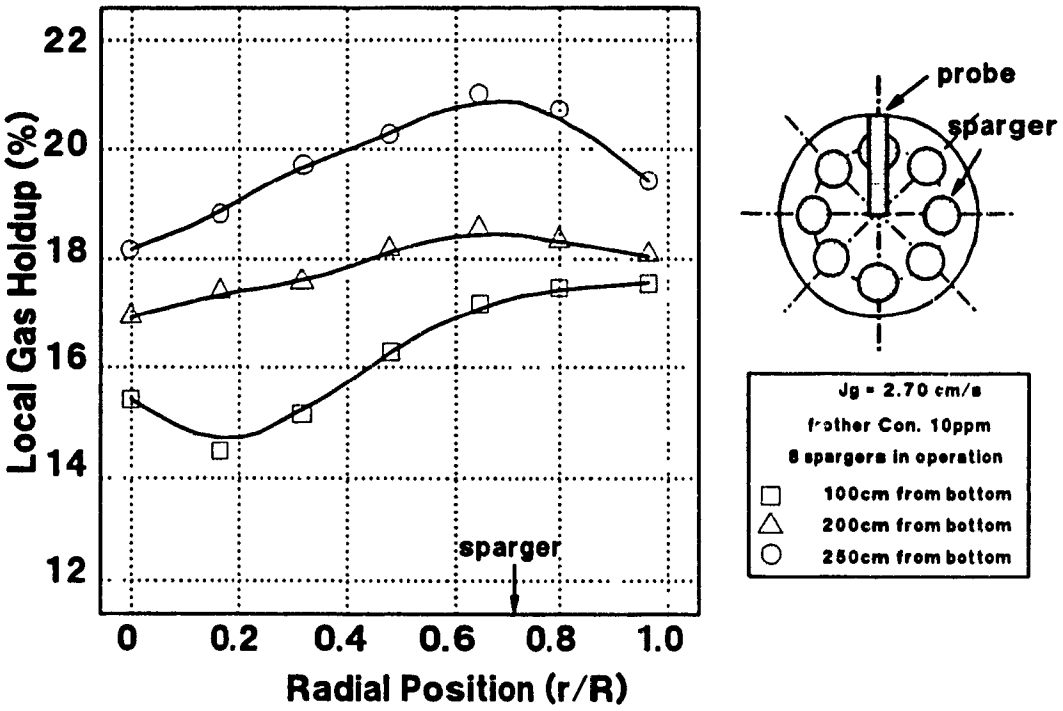

Figure 6.16 Gas holdup profiles at three different levels at J_g=2.70cm/s

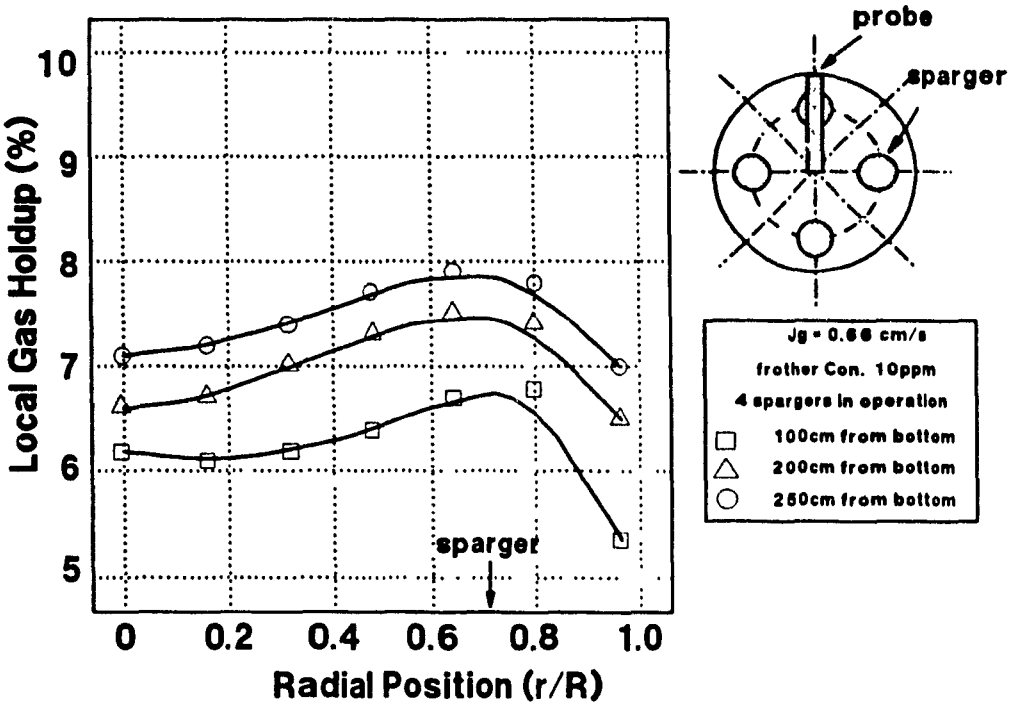

Figure 6.17 Gas holdup profiles at three different levels at J_g=0.66cm/s

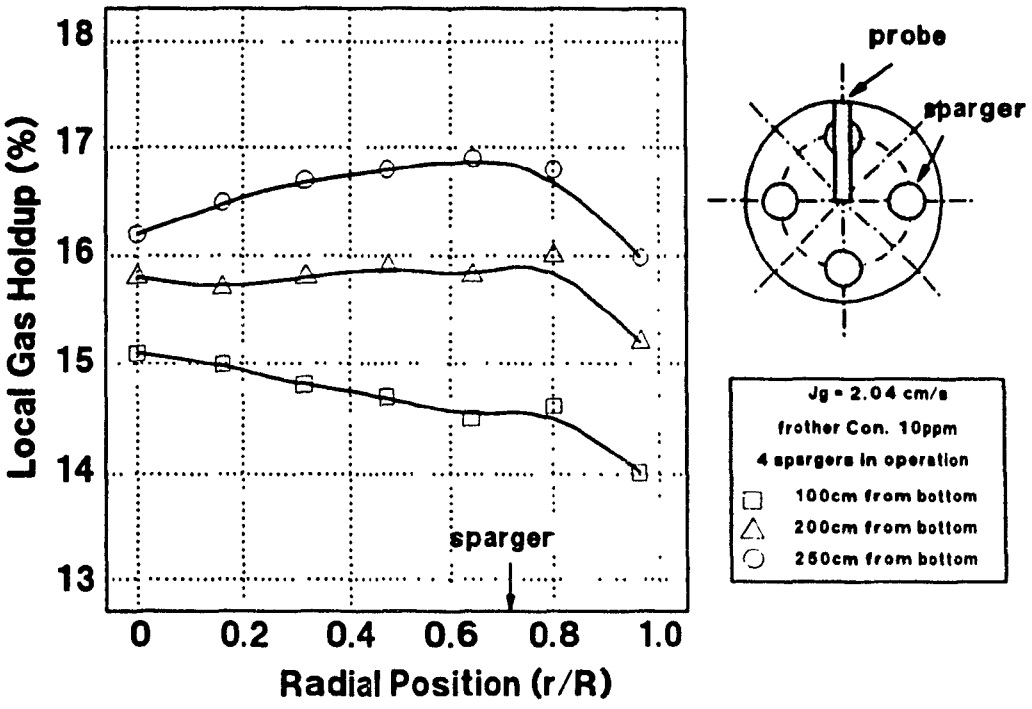

Figure 6.18 Gas holdup profiles at three different levels at J_g=2.04cm/s

6.2.3 In the Pilot Flotation Column

Figures 6.19, 6.20 and 6.21 presents local gas holdup as a function of the radial position (r/R) at three different vertical locations for superficial gas rates, J_g=0.6, 0.9 and 2.15 cm/s, respectively. (Sparger locations are indicated on the figures). These radial gas holdup profiles are more or less similar in shape to those obtained in the 50cm flotation column. They have a 'W' shape. At low gas rates, the highest gas holdup was observed near the wall. From the wall to the centre, local gas holdup first decreases and then increases (see the measurement 10m above sparger level). The lowest gas holdup was found at location where r/R=0.3 ~ 0.5. All the profiles are more or less axisymmetrical. At a relatively high gas rate (Figure 6.17), the shape of the profiles is a saddle. This is particularly evident at location 10m above the sparger level.

Radial gas holdup profile was also measured when only one sparger was used. When the sparger was located at the column centre, the radial gas holdup profiles had a saddle shape (Figure 6.22), similar to the case where three spargers were used at a high gas rate (Figure 6.21). When the sparger was located at r/R=0.5, the radial gas holdup profiles changed significantly (Figure 6.23). The profiles also changed from the bottom to the top of the column. The gas holdup on the side where the sparger was located was higher than the gas holdup on the other side.

It is important to note here that the gas rate cited in each figure may subject to 50% error due to the operating conditions in the mill. This may partly explain the reason for small gas holdup in Figure 6.19 (there spargers) in comparison with Figure 6.22 (one sparger).

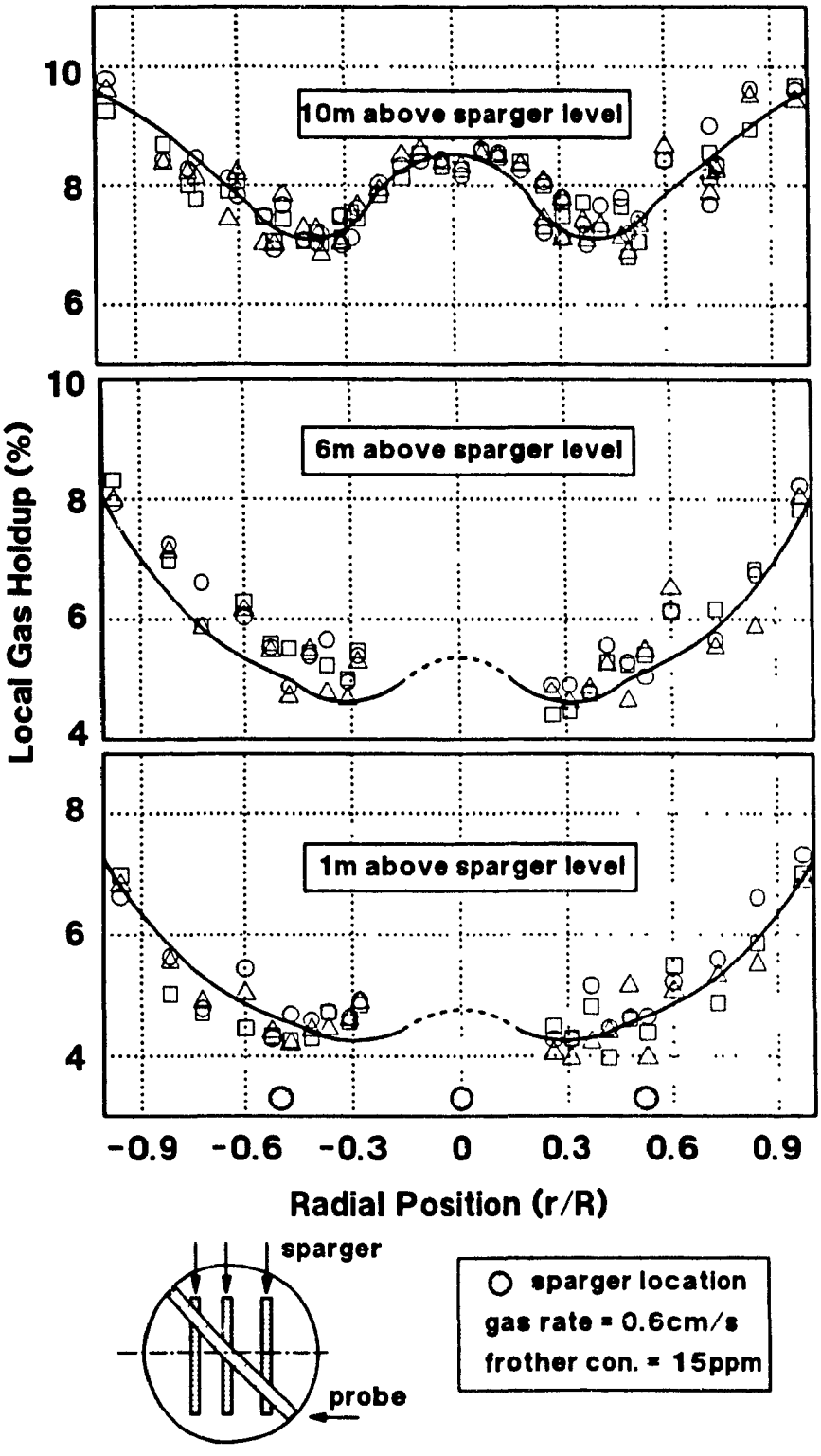

Figure 6.19 Radial gas holdup profiles at three different levels in the pilot flotation column (J_g=0.6cm/s, 15ppm frother concentration)

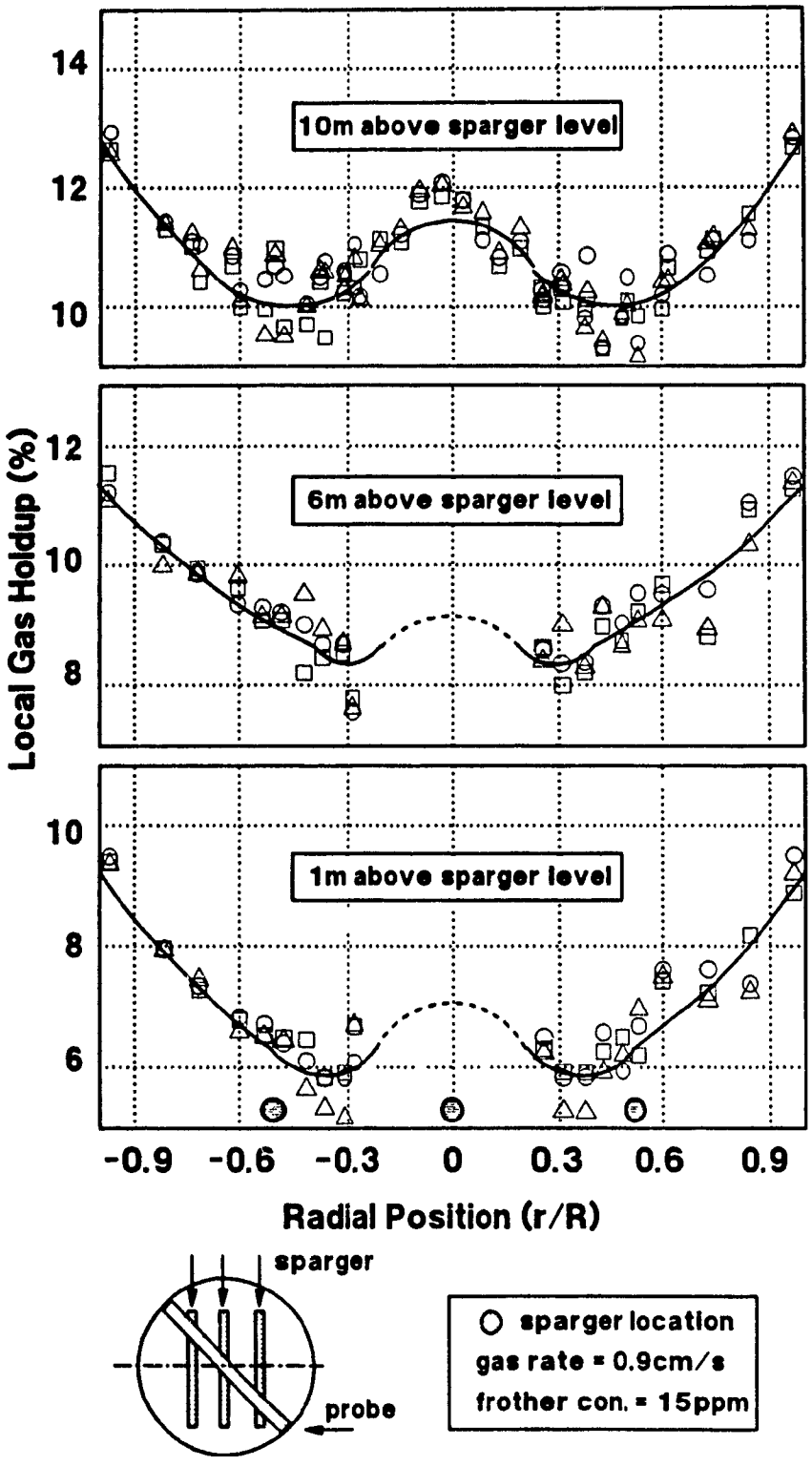

Figure 6.20 Radial gas holdup profiles at three different levels in the pilot flotation column (J_g=0.9cm/s, 15ppm frother concentration)

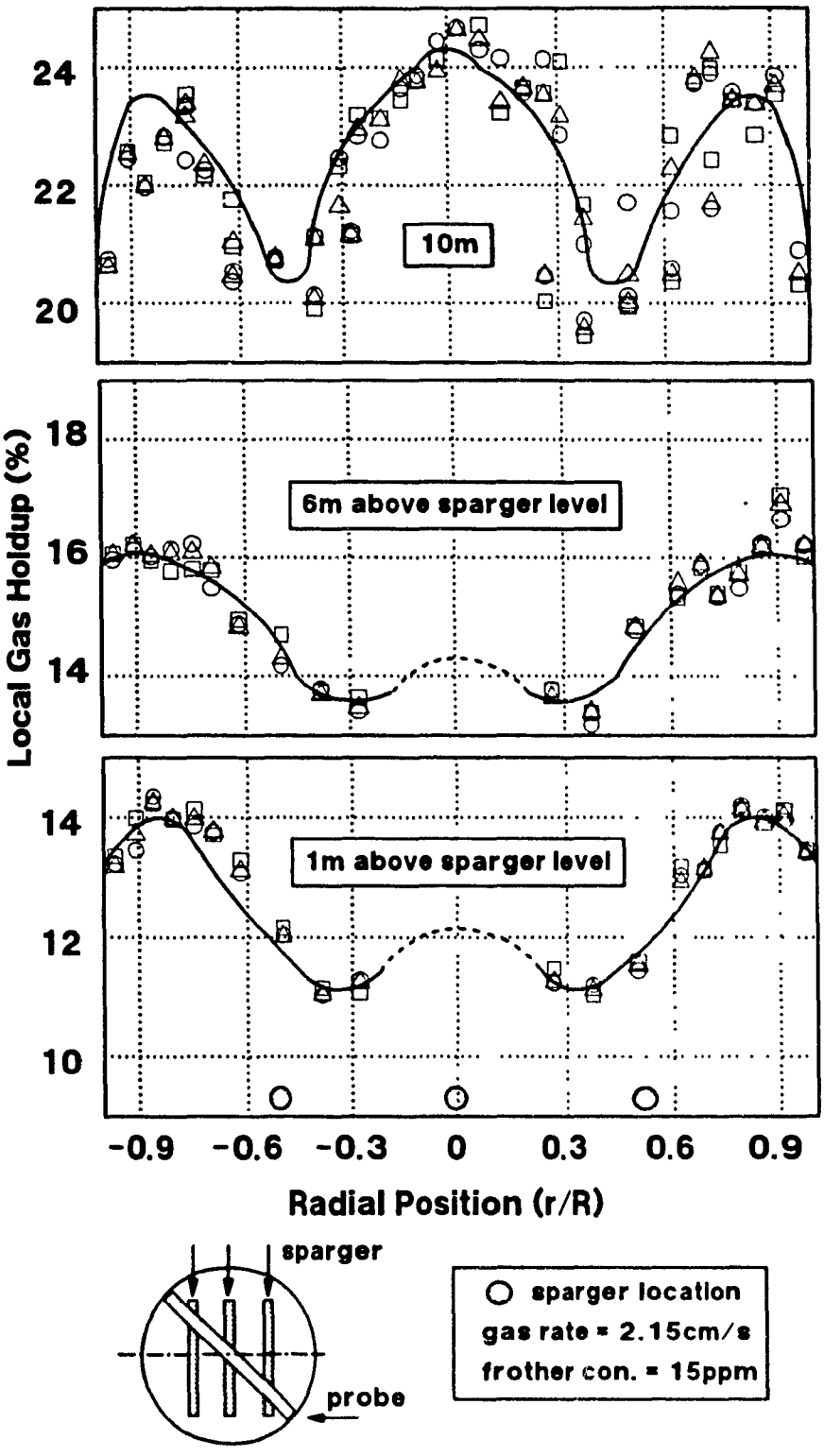

Figure 6.21 Radial gas holdup profiles at three different levels in the pilot flotation column (J_g=2.15cm/s, 15ppm frother concentration)

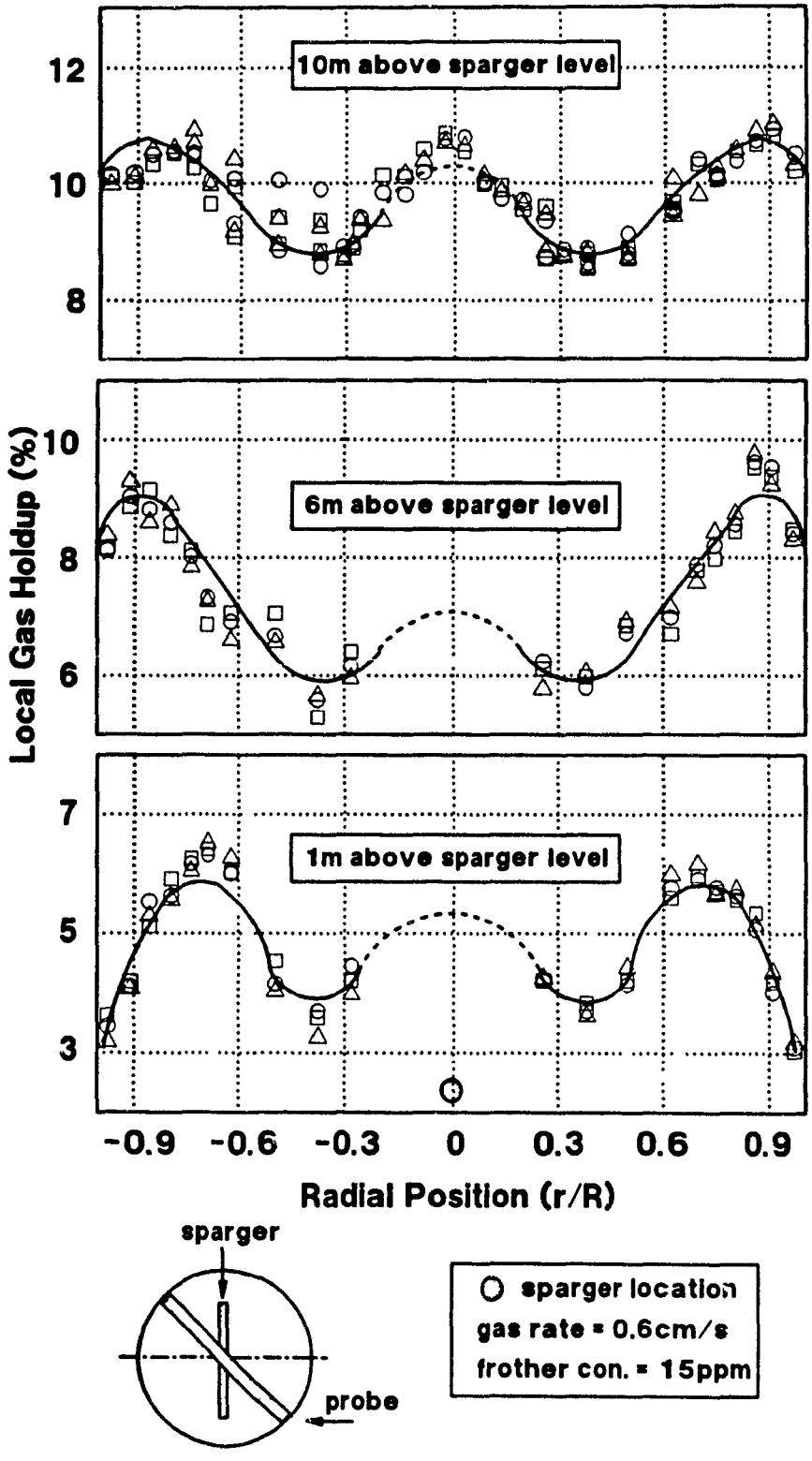

Figure 6.22 Radial gas holdup profiles at three different levels in the pilot flotation column (J_g=0.6cm/s, 15ppm, one sparger at centre)

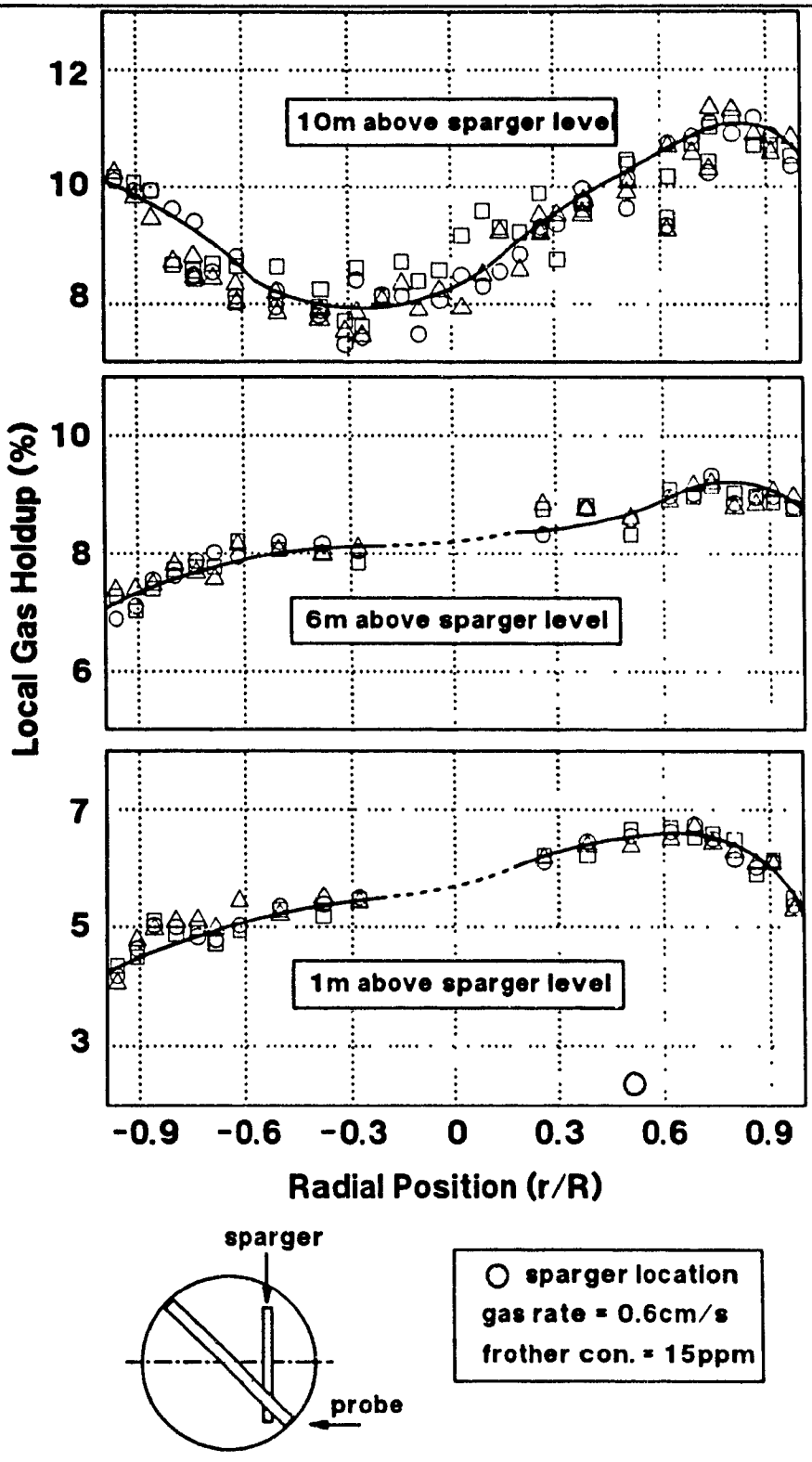

Figure 6.23 Radial gas holdup profiles at three different levels in the pilot flotation column (J_g=0.6cm/s, 15ppm, one sparger off-centre)

6.3 Liquid Circulation Velocity Profiles

Liquid circulation velocity profiles in the case where radial local gas distributions are near parabolic are calculated using the shear stress model (Section 3.3.1). Two case are considered: Newtonian fluid and non-Newtonian fluid.

Figure 6.24 is calculated based on the radial gas holdup distribution (Figure 6.6) obtained at J_g=5.43cm/s and 100cm above the bottom level. The liquid circulation velocity calculated in the case of Newtonian fluid is less than in the case of non-Newtonian fluid. In the case of non-Newtonian fluid, two parameter (p and K) must be preset. As a result, various circulation velocity profiles may be computed if different values of p and K are selected.

Based on the radial local gas holdup distribution obtained at the same gas rate and 200cm above the bottom level (Figure 6.8), the circulation velocity profile is presented in Figure 6.25. In this case, the gas holdup ϵ_{gc} in the column centre and the constant n are slightly increased, as compared to Figure 6.6 at 100cm above the sparger level. As discussed in Section 3.3.1, an increase in central local gas holdup increases the circulation velocity for a given value of n. On the other hand, an increase in n values for a given centre local gas holdup decreases the circulation velocity. Consequently, the circulation velocity profiles at the different levels are very similar in magnitude.

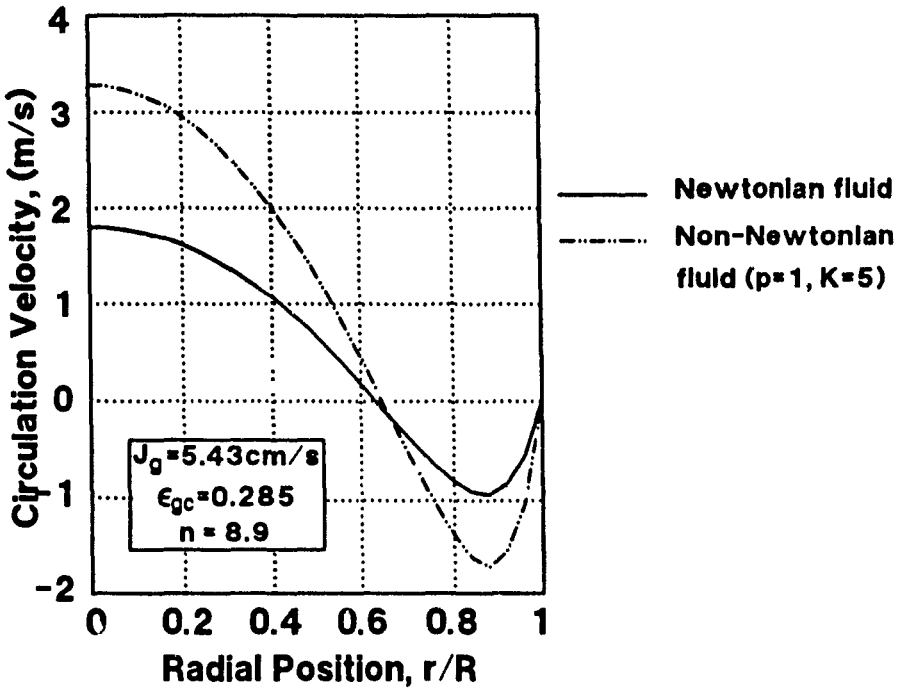

Figure 6.24 Liquid circulation velocity profiles at 100cm above the bottom calculated using the shear stress model (see gas holdup profiles in Figure 6.6)

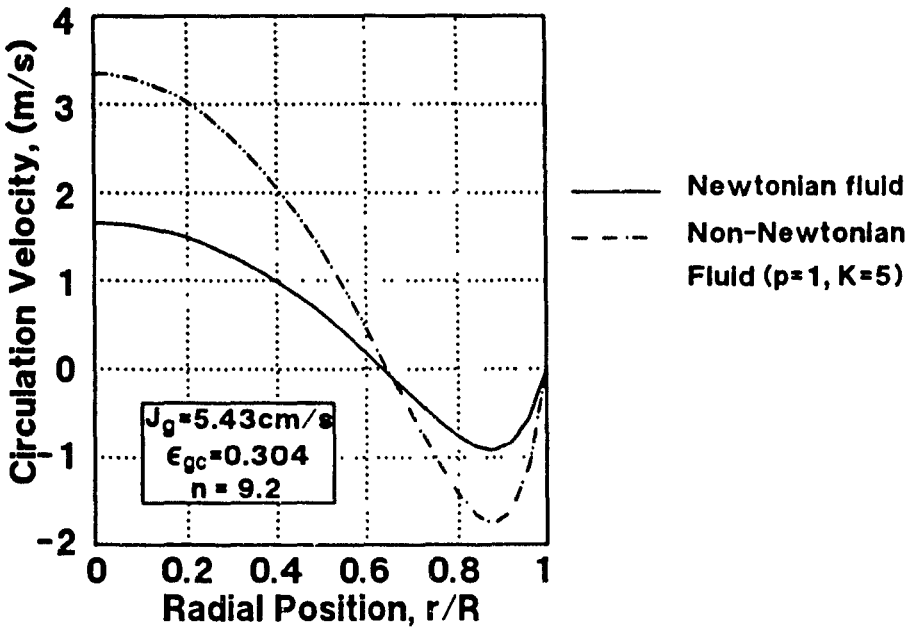

Figure 6.25 Liquid circulation velocity profiles at 200cm above the bottom calculated using the shear stress model (see gas holdup profiles in Figure 6.8)

CHAPTER 7

RESULTS: MIXING

Fitting of experimental residence time distributions and predicting age distributions obtained in laboratory and industrial flotation columns using the axial dispersion model are presented. Comparison between the closed vessel numerical solution and the open vessel analytical solution to the axial dispersion model is investigated based on experimental data. Comparison between the axial dispersion model (the closed vessel numerical solution) and the compartment models is also described. Then, the numerical solution to the axial dispersion model with closed boundary conditions is selected to fit all the experimental residence time distributions (to estimate the liquid vessel dispersion number). The effect of gas and liquid rates, column length to diameter ratio, column verticality and feed solid percentage on the vessel dispersion number is presented. Based on both present work and previously published data, a new correlation is proposed to estimate the liquid vessel dispersion number in the collection zone of flotation columns. The new correlation includes the effect of gas and liquid rates, column length to diameter ratio and feed solid percentage, and it is considered adequate for the purpose of flotation column scale-up.

7.1 Testing Model Fit

7.1.1 Closed Vessel Numerical Solution with Open Vessel Analytical Solution

The application of the axial dispersion model in flotation columns requires a combination of three choices: first, boundary conditions (e.g. open or closed vessel); second, type of solution (analytical or numerical); and third, the fitting (or parameter estimation) routine (direct search or moments matching).

To identify N_d values estimated from the different combinations, the subscripts, *cc* and *oo*, are used for closed vessel and open vessel, and the superscripts, *M* and *L*, are used to denote fitting by moments matching and direct search, respectively.

One set of experiments performed for various gas rates (at liquid rate J_l=0.5cm/s and frother concentration 10ppm) is used to illustrate the fits to the RTD of the various solutions to the axial dispersion model. Figure 7.1 represents the closed vessel case, comparing fits using moments matching with those using direct search (Figure 7.1a for a low gas rate, Figure 7.1b for a high gas rate). It is evident that direct search method gives an improved fit, and also a smaller vessel dispersion number (see also Table 7.1). This last point is emphasized in Table 7.2 where $N_{dcc}{}^{M}$ is consistently greater than $N_{dcc}{}^{L}$ over a range in N_d.

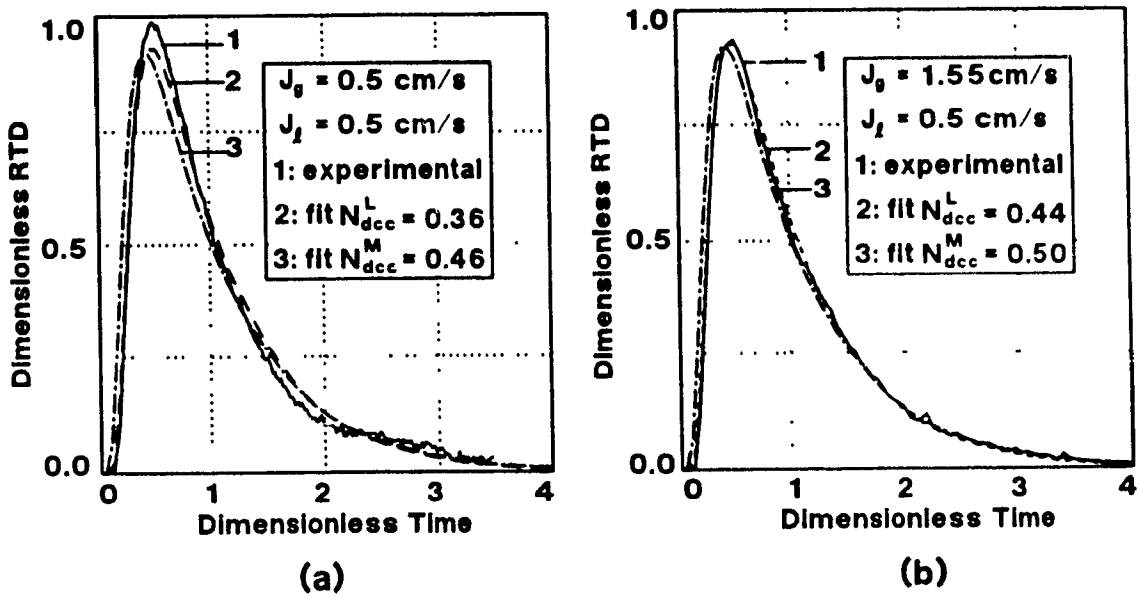

Figure 7.1 Closed vessel case: comparison of model fitting between moments matching and least squares (a) at a low gas rate, (b) at a high gas rate

To illustrate one difficulty with moments matching - that of the influence of the tail of the RTD -- Figure 7.2 shows that $N_{dcc}{}^{M}$ is dependent on the maximum t value selected for the cut-off point of the tail in estimating the variance, while $N_{dcc}{}^{L}$ is relatively insensitive to the cut-off time.

Included in Table 7.1 is the gas holdup ϵ_g (measured using water manometers), which was used to estimate the mean residence time, τ' ($=H_c(1-\epsilon_g)/J_l$), the values are in good agreement with τ estimated from the RTD.

Table 7.1 Comparison of N_d values obtained between moments matching and least squares in closed vessel case

J_l = 0.50cm/s
H_c = 320 cm
frother con. = 10ppm

J_g (cm/s)	ϵ_g (%)	τ (min)	τ' (min)	$N_{dcc}{}^{M}$	$N_{dcc}{}^{L}$
0.00	0.0	10.67	10.71	0.080	0.028
0.50	4.3	10.42	10.60	0.387	0.273
1.01	9.2	9.69	9.62	0.455	0.363
1.55	14.2	9.34	9.42	0.503	0.436
1.84	16.5	8.90	8.93	0.552	0.470
2.28	20.8	8.45	8.48	0.581	0.472

The open vessel analytical solution was also fitted to the same set of data. A comparison with the fits given by the closed vessel numerical solution (both were fitted using least squares) shows that the fits are generally good for $N_d < 0.25$ but at larger N_d values the open vessel case becomes less good (e.g. Figure 7.3a). This point is emphasized in the attempt to fit industrial data for large N_d values (Figure 7.3b).

A comparison of the open and closed vessel estimates of N_d for the same set of data as in Table 7.1 is given in Table 7.2. Generally, for $N_d < 0.25$ the two solutions give similar N_d values but for larger N_d values, $N_{doo}{}^{L} < N_{dcc}{}^{L}$.

A summary of the observation on the N_d values from the various combinations of solutions and fitting routine is given in Table 7.3.

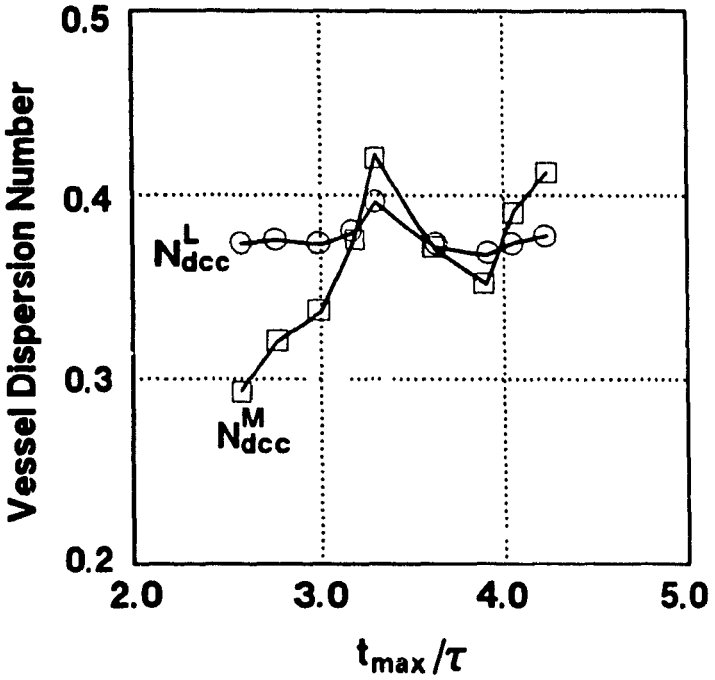

Figure 7.2 Effect of the cut-off t_{max} on RTD tail on calculated vessel dispersion number

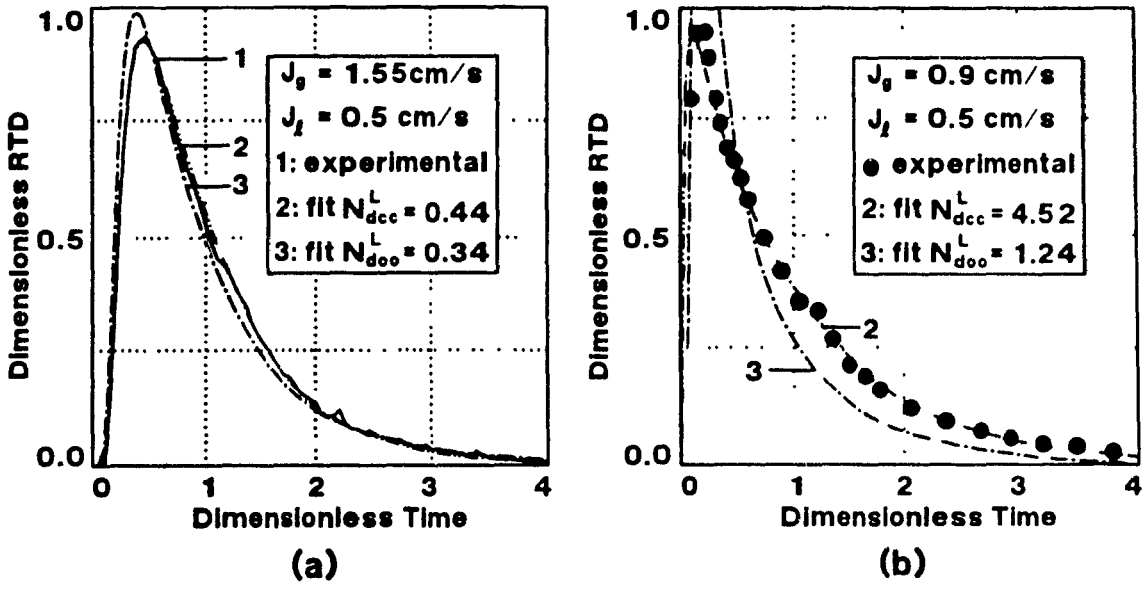

Figure 7.3 Comparison of the fitting to experimental data between open vessel analytical and closed vessel numerical solutions (a) at a laboratory column (d_c = 10.16cm), (b) at an industrial column (d_c = 250cm, raw data supplied by Espinosa et al., 1989)

Table 7.2 Comparison of N_d values between open vs. closed solutions
J_t = 0.50 cm/s
H_c = 320cm
frother con. = 10ppm

J_g (cm/s)	$N_{dcc}{}^{L}$	$N_{doo}{}^{L}$
0.00	0.028	0.027
0.50	0.273	0.253
1.01	0.363	0.293
1.55	0.435	0.341
1.84	0.470	0.353
2.28	0.418	0.365

Table 7.3 Summary of N_d values

N_d	observations
<0.25	$N_{doo}{}^{L} \approx N_{dcc}{}^{L}$
>0.25	$N_{doo}{}^{L} < N_{dcc}{}^{L}$
>0.50	$N_{doo}{}^{L}$ poor fit
all	$N_{doo}{}^{M} < N_{dcc}{}^{M}$
all	$N_{dcc}{}^{M} < N_{dcc}{}^{I}$
all	$N_{doo}{}^{M} < N_{doo}{}^{L}$
all	$N_d{}^{M}$ poorer fit than $N_d{}^{L}$

7.1.2 Age Distributions

One advantage of the numerical solution to the axial dispersion model is that age distributions inside the column can be computed and compared with experimental age distributions. In contrast, the analytical solutions do not have this ability. Figure 7.4 shows the excellent fit of the numerical solution to experimental age distribution. The fits at the feed and middle locations in the column are calculated using the estimated vessel dispersion number from the RTD (age distribution at the exit). It is clear that a single vessel dispersion number is adequate to describe the mixing along the column.

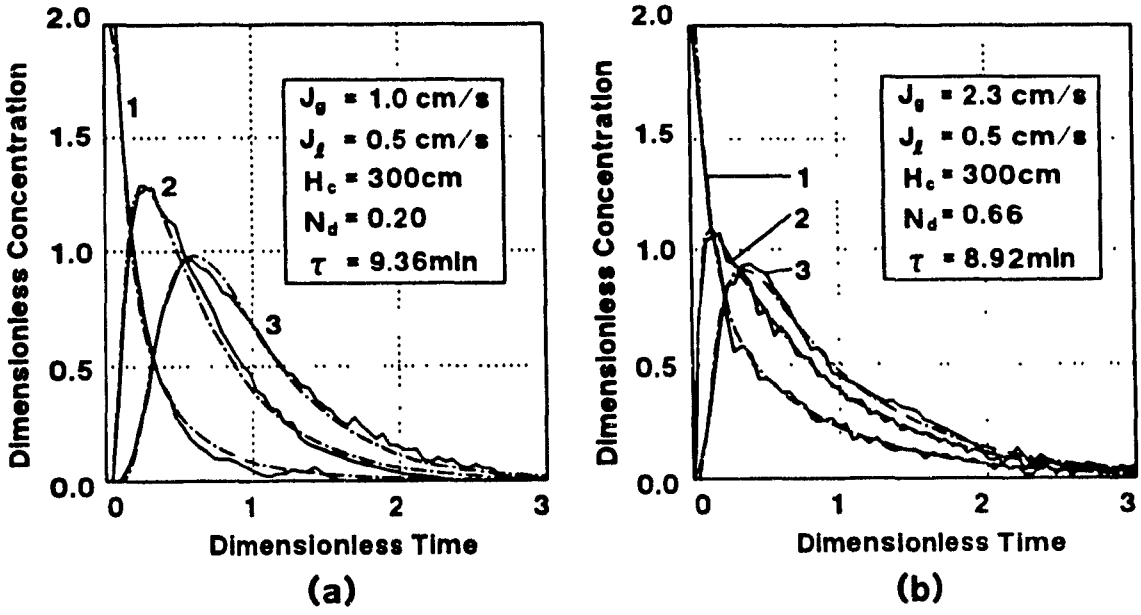

Figure 7.4 Experimental age distributions in a laboratory column and comparison with model fit (1: feed, 2: middle; 3: exit) (a) at a low gas rate, (b) at a high gas rate

Data in Figure 7.5a are taken from the work of Yianatos et al. (1987) on an industrial flotation column at Les Mines Gaspe. In Figure 7.5a, the age distribution at Z/L=0.175 is accurately fitted using the vessel dispersion number obtained from the RTD at the exit. Z and L were measured from the interface level of collection/froth zones, as suggested by Laplante et al. (1988) and Finch and Dobby (1990). Measuring

from the feed location gives Z/L=0.16 which gave a result indistinguishable on the figure.

Experimental age distribution in an industrial flotation column has also been reported by Espinosa et al. (1989) at Mount Isa Mines. Figure 7.5b presents the fit to the experimental RTD and shows, in this case, the mixing in the column is close to perfect mixing (the dashed line is the prediction using $E(\theta)=exp(-\theta)$, i.e. perfect mixing). The best fit gives a vessel dispersion number of 4.52. The successful fit to the age distribution at the feed level is shown on the same figure using the same vessel dispersion number.

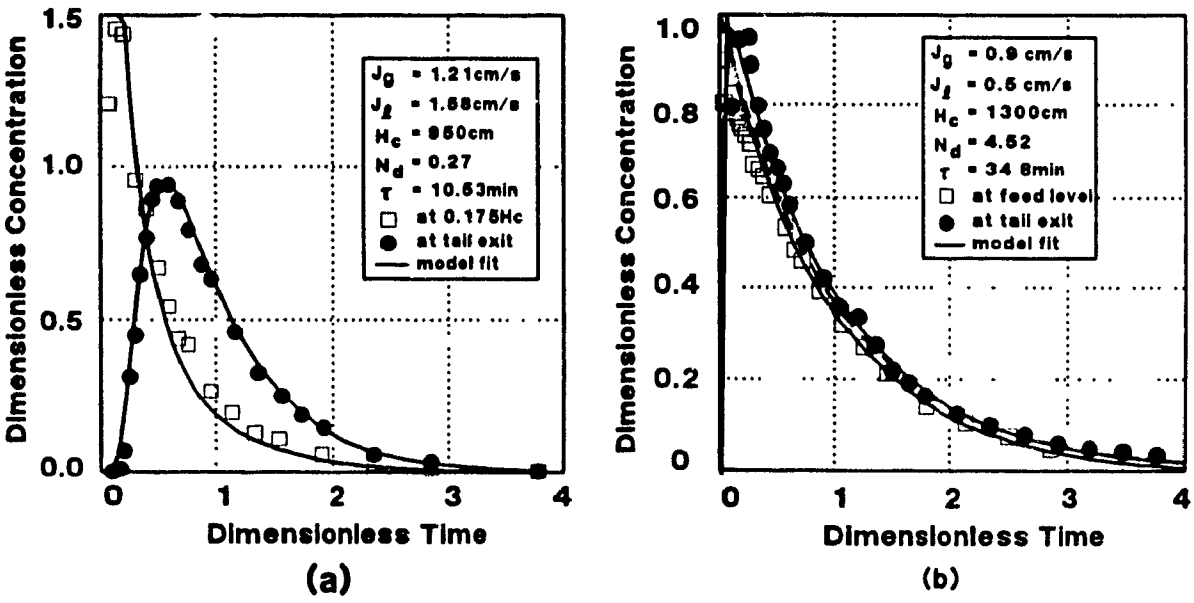

Figure 7.5 Experimental age distributions in industrial flotation columns and comparison with model fit: (a) column size 45X45X9500 cm (data from Yianatos et al., 1988), (b) column size 250X1300 cm (data from Espinosa et al., 1989, also see Figure 7.3b)

7.1.3 Comparison between Axial Dispersion Model and Compartment Models

In this section, a comparison between the axial dispersion model and the compartment models is presented. The similarity between the models is revealed based on fitting experimental data.

As described in Section 4.4, the dimensionless RTD curves are uniquely characterized by the magnitude of the dimensionless vessel dispersion number, N_d, and the similarity between the axial dispersion model and the backflow compartment model was explored theoretically.

The comparison between the models can be illustrated by fitting to experimental RTD data. The fitting was carried out using the least squares technique. Figure 7.6 presents the fitting of the axial dispersion model (the closed vessel numerical solution) and compartment models at two gas rates (J_g=0.5cm/s and 1.55cm/s). The fits are excellent except for the case of the tanks-in-series model. Comparison of fitting was done for various gas rates at a constant liquid rate (J_l=0.5cm/s). Table 7.4 shows the results obtained from the model fitting. For backflow compartment model, n=20 is used, and N_{dbc} represents the N_d values estimated from fitting the backflow compartment model. For the tanks-in-series model, N_{dt} represents the N_d values estimated from fitting the model. It can be found that N_{dbc} is quite close to N_{dcc}, while N_{dt} is consistently smaller.

Table 7.4 N_d values obtained from different model fits

J_l = 0.50 cm/s
H_c = 320cm
frother con. = 10ppm

J_g (cm/s)	$N_{dcc}{}^L$	$N_{dbc}{}^L$	λ	$N_{dt}{}^L$
0.00	0.028	0.027	0.048	0.027
0.50	0.273	0.274	4.970	0.255
1.01	0.364	0.362	6.730	0.286
1.55	0.436	0.435	8.192	0.337
1.84	0.470	0 470	8.904	0.346
2.28	0.482	0.488	9.268	0.358

note: N_{dbc} is the N_d estimated from backflow compartment model, and N_{dt} is the N_d estimated from tanks-in-series model

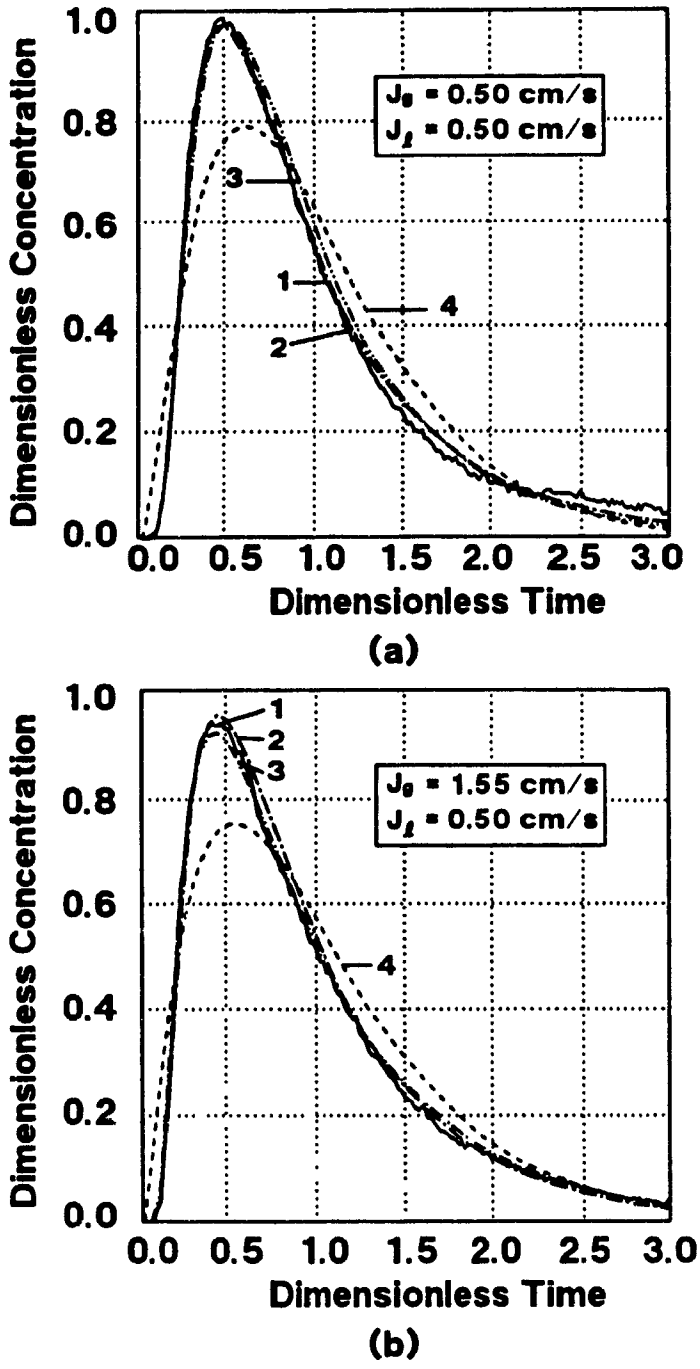

Figure 7.6 Fitting to experimental RTD: comparison between axial dispersion model and compartment models. (a) at a low gas rate, (b) at a high gas rate (also see Table 7.4 for N_d values). 1. experimental data, 2. axial dispersion model (closed vessel), 3. backflow compartment model, 4. tanks-in-series model

7.2 Effect of Variables on N_d

From the above work, it can be concluded that the numerical solution to the axial dispersion model with closed boundary conditions and the least squares fitting routine is quite adequate for fitting experimental RTDs and estimating the vessel dispersion number. With this established, an experimental program to determine how the design and operating parameters affect N_d was executed.

7.2.1 Batch Operation: Effect of Gas Rate

This set of tests was performed in order to investigate the effect of gas rate on the liquid dispersion when $J_l=0$. In this case, E_l is directly determined and N_d is indeterminable since $u_l=0$.

Figure 7.7 presents experimental RTD curves and the model fits. An excellent model fit to the experimental data is evident. Table 7.5 summarizes the E_l values. It can be seen that as gas rate increases, the axial dispersion coefficient increases.

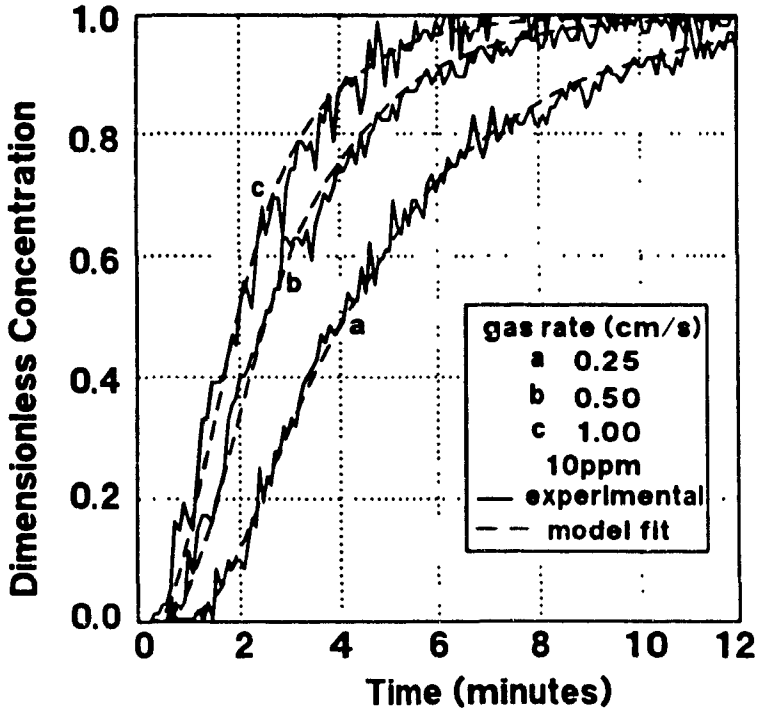

Figure 7.7 Tracer response curves and model fits in batch operation: the effect of gas rate (see also Table 7.5)

Table 7.5 E_ℓ values obtained in batch operation

J_ℓ = 0.0 cm/s
H_c = 320cm
H_c/d_c = 31.50
frother con. = 10ppm

J_g (cm/s)	ϵ_g (%)	N_d	E_ℓ (cm^2/s)
0.25	2.5	N.A.	48.89
0.25	2.6		50.22
0.50	5.0		70.66
1.01	10.0		103.34
1.55	14.8		117.98
1.55	15.0		115.62
1.84	15.8		122.84
2.28	18.5		126.14
2.28	18.5		128.71

7.2.2 Continuous Operation: Effect of Gas and Liquid Rates

Figure 7.8 presents the dimensionless RTD curves obtained at various gas rates and three different liquid rates, respectively. Figure 7.8a is for J_ℓ=0.28cm/s, a relatively low liquid rate. In Figure 7.8b, the RTD curve at J_g=0 is shown in comparison with the RTD curves when $J_g \neq 0$. It is clear that the intensity of mixing is considerably increased once gas is introduced. At J_g=0, the liquid mixing behaviour is close to plug flow. By comparing Figure 7.8a to Figures 7.8b and 7.8c, it is evident that increasing the liquid rate decreases the intensity of liquid mixing.

Table 7.6 summarizes all the N_d values obtained from the experimental work. Some tests were repeated; these are included in the table and show that the reproducibility is good. The mean gas holdup in the collection zone, measured by the water manometers, is also presented in Table 7.6. From the measured gas holdup and liquid rates, the mean residence time, τ', is calculated and compared with the mean residence, τ, determined from the RTD data. It shows that the two mean residence times are in a very good agreement, and this verifies the validity of the experimental procedure. A point which may be of practical significance is that the gas holdup estimated by doing a tracer RTD can be used to confirm any instrumental method of estimating gas holdup

in industrial flotation columns.

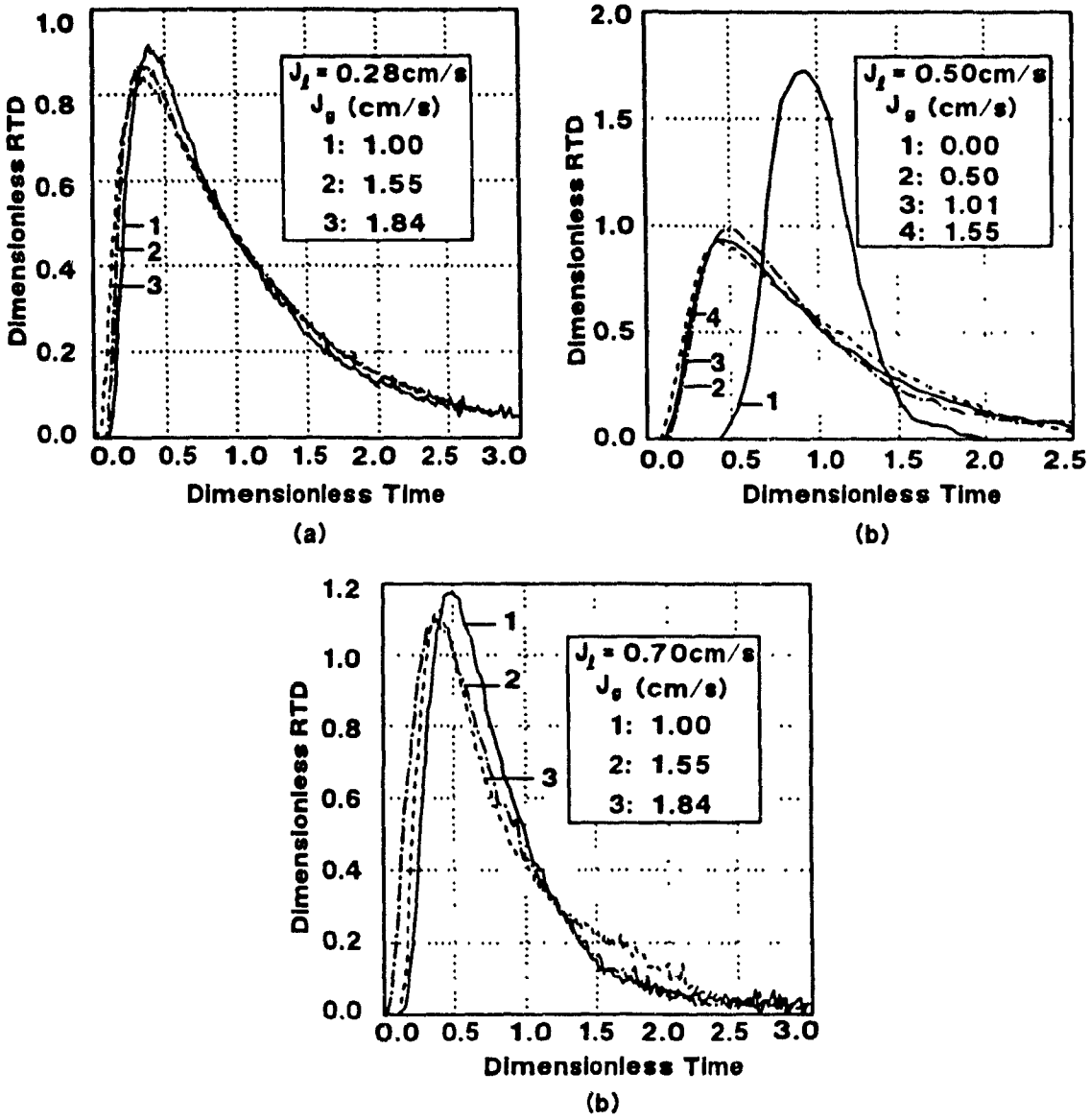

Figure 7.8 Dimensionless RTD curves: the effect of gas and liquid rates (also see Table 7.7 for N_d values)

Table 7.6 Vessel dispersion number obtained at various gas and liquid rates

frother con. = 10ppm
bubbling zone height = 320cm
H_c/d_c = 31.50

J_g (cm/s)	J_l (cm/s)	ϵ_g (%)	τ'* (min)	τ** (min)	N_d	E_l*** (cm^2/s)
0.50	0.28	4.4	18.21	17.88	0.378	36.04
1.01	0.28	8.5	17.43	17.02	0.490	49.17
1.01	0.28	8.6	17.41	17.25	0.494	48.88
1.55	0.28	12.9	16.59	16.65	0.575	58.97
1.55	0.28	12.6	16.65	16.62	0.581	59.61
1.84	0.28	15.4	16.11	16.55	0.597	61.54
1.84	0.28	15.6	16.08	16.25	0.605	63.54
2.28	0.28	20.4	15.16	15.45	0.631	69.70
2.28	0.28	20.5	15.14	15.05	0.622	70.52
0.50	0.50	4.3	10.21	10.60	0.273	43.89
1.01	0.50	9.2	9.69	9.62	0.363	64.36
1.01	0.50	9.3	9.67	9.68	0.374	65.96
1.55	0.50	14.2	9.15	9.42	0.436	79.05
1.84	0.50	16.5	8.91	8.93	0.470	89.90
2.28	0.50	20.8	8.45	8.48	0.472	94.91
2.28	0.50	21.0	8.43	8.35	0.484	98.95
0.50	0.70	4.9	7.25	8.05	0.243	51.50
1.01	0.70	10.4	6.83	6.86	0.319	79.41
1.55	0.70	14.4	6.52	6.32	0.369	99.67
1.84	0.70	17.3	6.30	6.20	0.391	107.49
2.28	0.70	21.8	5.96	6.03	0.422	119.38
0.00	0.28	0.0	19.05	19.16	0.066	5.87
0.00	0.50	0.0	10.67	10.65	0.028	4.42
0.00	0.70	0.0	7.62	7.84	0.023	4.90

* $\tau' = H_c (1-\epsilon_g)/J_l$

** τ from RTD data

*** $E_l = N_d H_c J_l/(1-\epsilon_g)$

Some tests were performed at J_g=0 for different liquid rates. Figure 7.9 shows the comparison of the RTD curves at three liquid rates. In this case, the normalized RTD curves are used to show the location of mean residence time. All are more or less symmetrical distribution curves indicating the mixing is quite small when no gas is introduced. In Table 7.6, N_d values for these situations are included and show that increasing liquid rate reduces the vessel dispersion number.

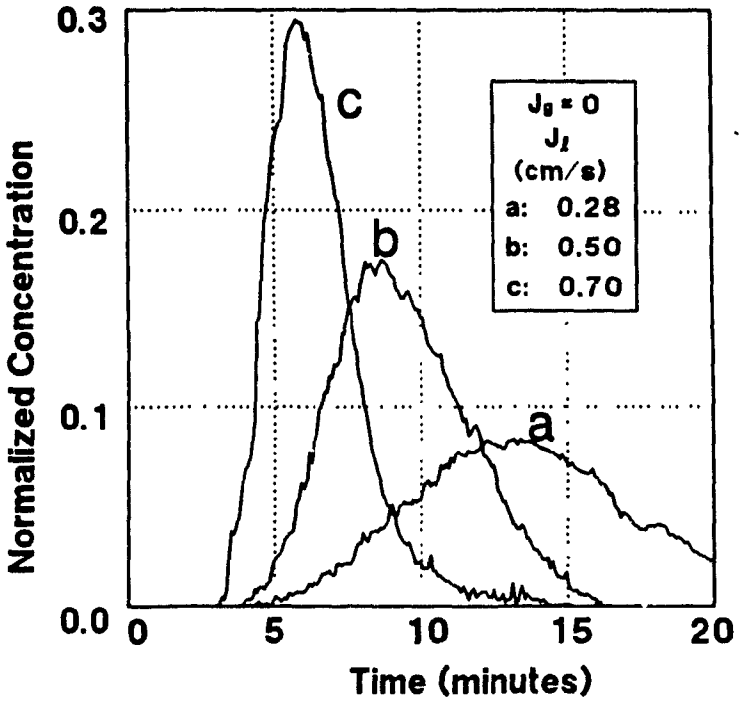

Figure 7.9 RTD curves at zero gas rate: the effect of liquid rate

RTD measurements were also performed at the pilot flotation column. Figure 7.10 presents the RTD curves obtained under various gas and liquid rates. The solid lines are the model fit. The N_d values in this case are shown in Table 7.7. Again, increasing gas rate increases the vessel dispersion number and increasing the liquid rate decreases the vessel dispersion number. This shows the same trend observed in the laboratory flotation column.

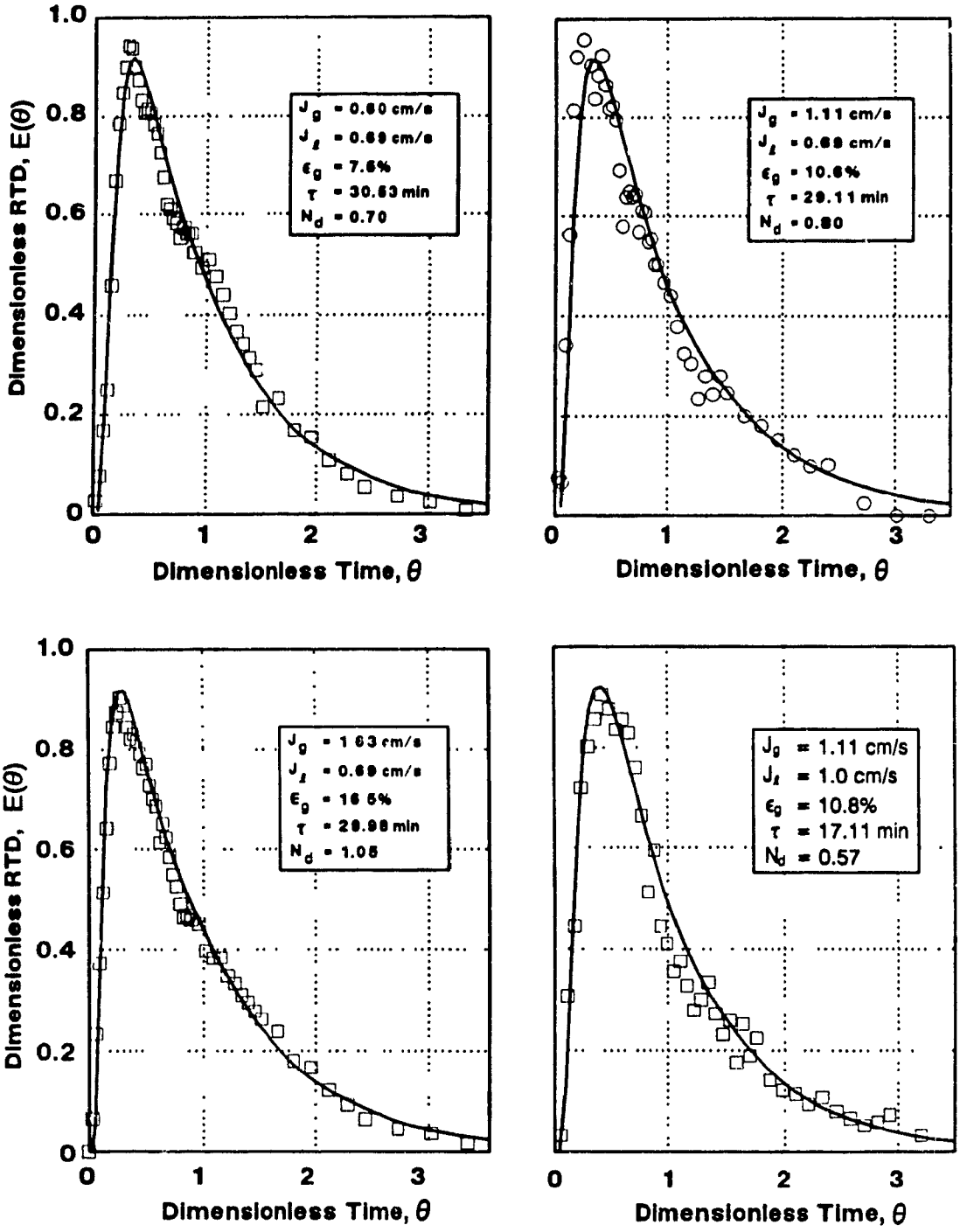

Figure 7.10 RTD and model fit in the pilot flotation column

Table 7.7 Vessel dispersion number obtained in the pilot flotation column
frother con. = 15ppm
column dia. d_c = 90cm
column length H_c = 1000cm

J_g (cm/s)	J_l (cm/s)	ϵ_g (%)	τ' (min)	τ (min)	N_d	E_l (cm²/s)
0.60	0.69	7.5	22.34	30.54	0.70	353.48
1.11	0.69	10.6	21.59	29.19	0.80	409.48
1.63	0.69	16.5	20.17	29.98	1.01	468.84
1.11	1.00	10.8	14.87	17.11	0.57	495.27

note: the values of gas rate and liquid rate were reported by the control room, which can be in 15% error relatively. Gas holdup was obtained using the pressure transducer over 10m in the collection zone

7.2.3 Continuous Operation: Effect of Column Length

The length of the experimental column (the 10.16cm diameter column) was changed to test the effect of column length on the vessel dispersion number, N_d. Three values were used.

For each length, a series of tests was conducted at various gas rates. Table 7.8 summarizes all the N_d values obtained in this case. It is clear that decreasing the column length increases the N_d values but decreases the E_l values. The different behaviour between N_d and E_l is because E_l is a direct function of length and vessel dispersion number.

The family of RTD curves at different lengths are presented in Figure 7.11. Figure 7.11a is at J_g=1.0cm/s and Figure 7.11b at J_g=1.55cm/s. Table 7.8 summarizes the N_d values obtained at different column lengths.

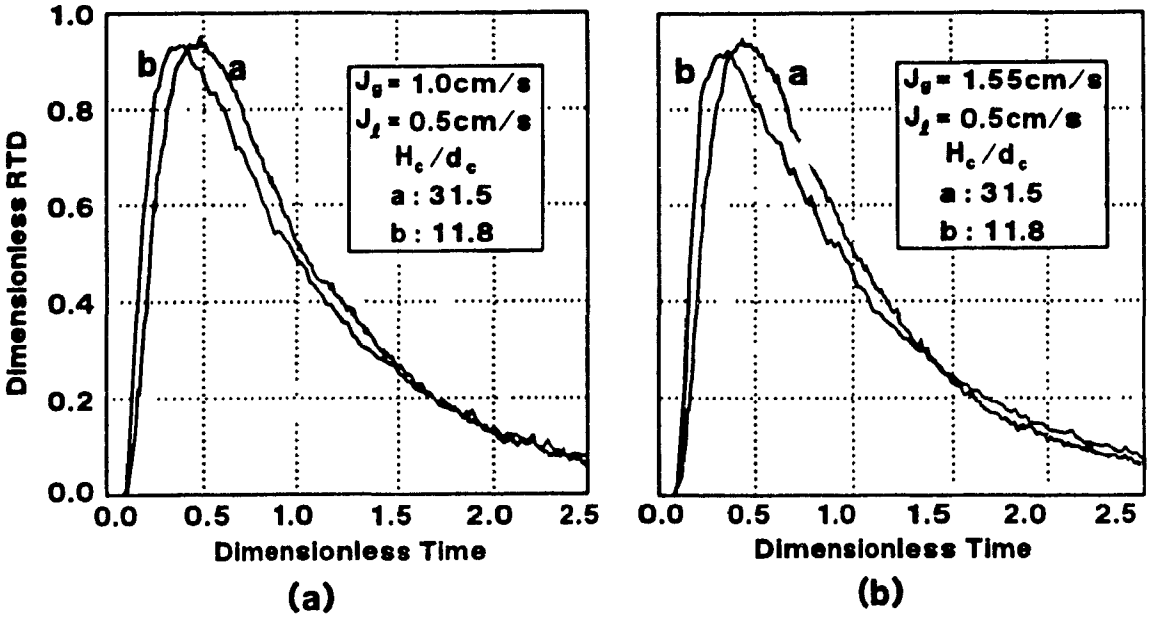

Figure 7.11 RTD curves: the effect of column length

Table 7.8 Vessel dispersion number obtained at different column lengths
frother con. = 10ppm
J_l = 0.50cm/s
d_c=10.17cm

H_c (cm)	H_c/d_c	J_g (cm/s)	ϵ_g (%)	τ' (min)	τ (min)	N_d	E_l (cm^2/s)
220	21.65	0.50	4.5	7.00	6.95	0.332	38.48
		1.01	9.0	6.67	6.86	0.410	48.21
		1.55	12.4	6.42	6.52	0.527	65.16
		1.84	16.3	6.14	6.33	0.611	77.82
120	11.81	0.50	4.5	3.82	4.11	0.420	24.55
		1.01	9.0	3.64	3.92	0.536	32.82
		1.55	12.4	3.50	4.00	0.704	42.32
		1.84	16.5	3.34	3.82	0.868	54.54

7.2.4 Continuous Operation: Effect of Column Verticality

The experimental column was inclined with an angle from the vertical axis. Two tilt angles were used, 1° and 3°.

The RTD curves obtained are presented in Figure 7.12. It shows that with increasing tilt angle the intensity of mixing is increased. The larger the tilt angle, the more is the increase in the extent of mixing.

Table 7.9 summarizes the data obtained at various gas rates with the two tilt angles (For comparison with the case without tilt, refer to Table 7.6). The general trend noted in Figure 7.12 is also shown.

By observation, when the column was tilted, most of the bubbles moved along the upper side of the column while at the lower side, liquid and some bubbles moved downwards. A colour tracer was used to visualize the liquid circulation. In general, for a vertical column, the colour tracer moves downward uniformly (with tracer added at top of column). When there is a tilt, the tracer does not move uniformly and the lower side of the column becomes coloured much faster than the upper side. These observations are offered, since visually the system seems more disturbed upon tilting than the increase in N_d values would imply.

Table 7.9 Vessel dispersion number obtained at different verticality
frother con.= 10ppm
bubbling zone height = 320cm
J_l = 0.50cm/s

degree	J_g (cm/s)	ϵ_g (%)	τ' (min)	τ (min)	N_d	E_l (cm^2/s)
1°	0.50	3.6	10.28	10.42	0.334	54.64
	1.01	7.5	9.87	9.65	0.395	69.77
	1.55	10.2	9.58	9.42	0.504	91.22
	2.84	14.6	9.11	9.15	0.526	98.04
3°	0.50	3.5	10.29	10.35	0.404	66.55
	1.01	7.6	9.86	10.15	0.485	81.47
	1.55	9.8	9.62	9.77	0.551	96.27
	1.84	13.4	9.22	9.20	0.601	111.56

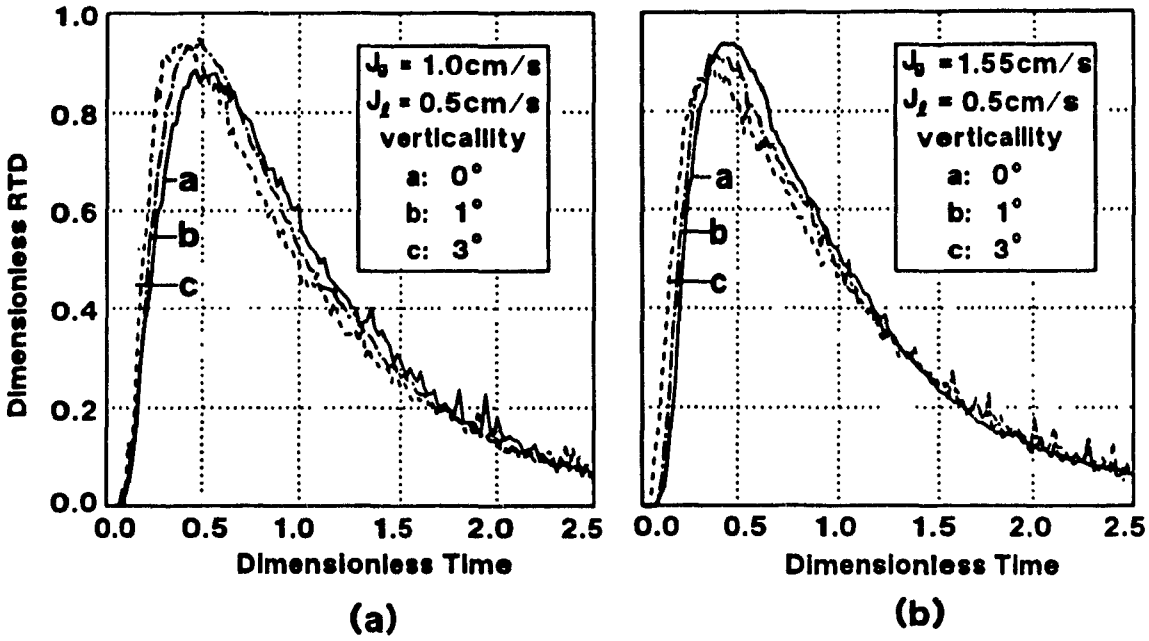

Figure 7.12 RTD curves: the effect of column verticality

7.2.5 Continuous Operation: Effect of Feed Solid Particles

Some tests were conducted with different feed solid percentages. The solid particles used were silica with density 2.65g/cm^3 and size 50% passing 15μm. Two series of experiments were performed at a constant solid percentage with various gas rates, and at a constant gas rate with various solid percentages.

Figure 7.13 presents the RTD curves for the three feed solid percentages. It is noted that increasing the feed solid percentages generally decreases the intensity of mixing but only slightly. The vessel dispersion number, N_d, obtained in this case is summarized in Table 7.10.

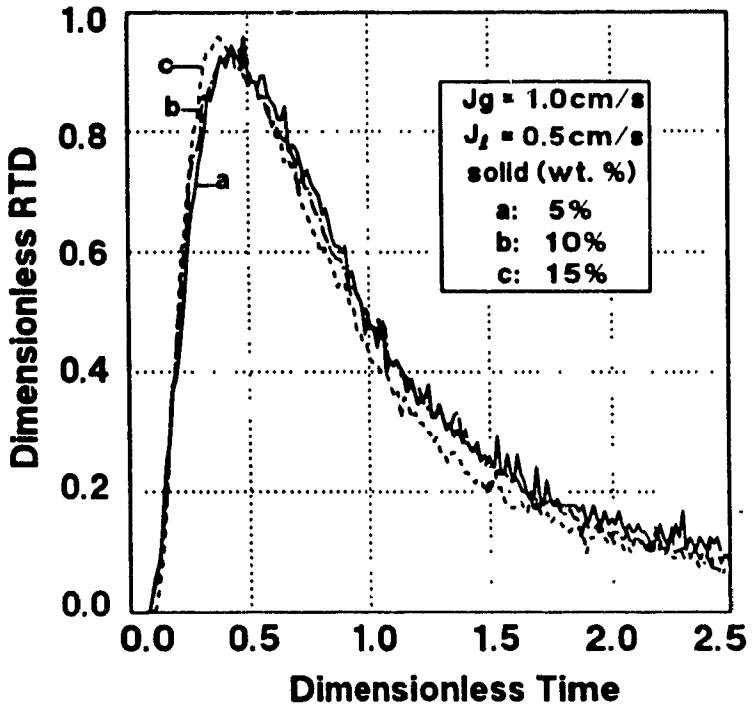

Figure 7.13 RTD curves: the effect of the feed solid percentage

Table 7.10 Vessel dispersion number obtained at different feed solid percentage

frother con. = 10ppm
bubbling zone height = 320cm
H_c/d_c = 31.50
J_l = 0.50cm/s

solids (%)	J_g (cm/s)	ϵ_g (%)	τ' (min)	τ (min)	N_d	E_l (cm^2/s)
5.0	0.50	4.5	10.19	10.82	0.262	41.37
	0.50	4.5	10.19	10.75	0.280	44.47
	1.01	9.5	9.65	9.91	0.365	62.78
	1.01	9.5	9.65	9.23	0.362	66 86
	1.55	12.5	9.33	9.88	0.420	72.50
	1.55	12.5	9.33	10.05	0 406	68.86
	1.84	14.5	9.12	9.96	0.442	75.67
	2.28	20.5	8.48	8 23	0.465	94 47
10.0	1.01	9.5	9.65	9.89	0.353	60.83
15.0		9.5	9.65	9.77	0.358	62.47
20.0		9.5	9.65	9.92	0.341	58.60
25.0		9.5	9.65	9.93	0.355	57.58

7.3 Dispersion of Solid Particles

An attempt to measure the vessel dispersion number of solid particles in this work is shown in Figure 7.14. These data were obtained using the inverse step response tracer technique. The feed slurry was first prepared at a given solid percentage. Once the system was in steady state, the feed was switched to fresh water containing no solids. At the same time, sampling of the discharge was undertaken. The solid concentration in the discharge samples vs. time gives the inverse response curve. This method has a drawback in that the particle concentration in the vessel changes with time. Nevertheless, the model fit (Section 4.3, Eq.4.47) gives N_d=0.25 for the case of no solids and N_d=0.22 for both 10% and 18% solids. This suggests that the vessel dispersion number of solids is slightly comparable to that of the liquid, implying the liquid and solid dispersion coefficients are similar as expected for such fine solids (Finch and Dobby, 1990a)

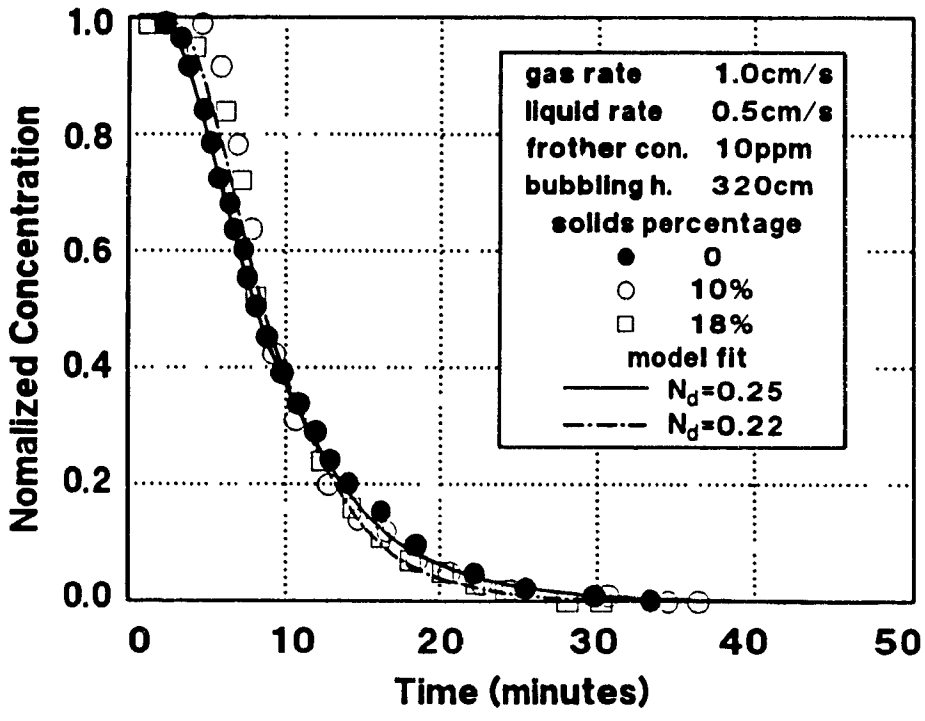

Figure 7.14 Normalized inverse step response curves for solid mixing

7.4 Data Analysis: Predicting Vessel Dispersion Number

The present work has determined the vessel dispersion number of liquid under various conditions. The effect of gas and liquid rates, column length, column verticality and feed solid percentage was investigated. For the effect of increasing either liquid rate or column length, it was noted that the N_d values decreased while E_t increased. This indicates that it is necessary to investigate which one - N_d or E_t - should be used in generating empirical correlations.

7.4.1 Data Analysis

Figure 7.15 presents liquid dispersion coefficient as a function of gas rate for various liquid rates. Included are the prediction from several published correlations (Towell and Ackerman, 1972; Dobby and Finch, 1985a; and Laplante et al., 1988). These correlations are of the right order but non of them include the effect of liquid rate.

The axial dispersion coefficient as a function of gas rate on log-log scale is presented in Figure 7.16. The average slope is about 0.48. Plotting vessel dispersion number as a function of gas rate (Figure 7.17), an average slope of 0.36 is obtained. The change in ϵ_g upon changing J_g and thus changing u_l cause this difference.

To determine the effect of liquid rate on E_t, a log-log scale plot of the axial dispersion coefficient vs. liquid rate is given in Figure 7.18. The average slope is 0.53, or in other words, E_t increases as liquid rate increases. Figure 7.19 plots the vessel dispersion number with liquid rate (log-log scale) and gives an average slope of -0.47. This means that the vessel dispersion number decreases as the liquid rate increases.

Laplante (1990) recently also found that increasing the feed rate to a grinding mill decreased the variance of the RTD (and hence decreased N_d), but the axial dispersion coefficient increased significantly.

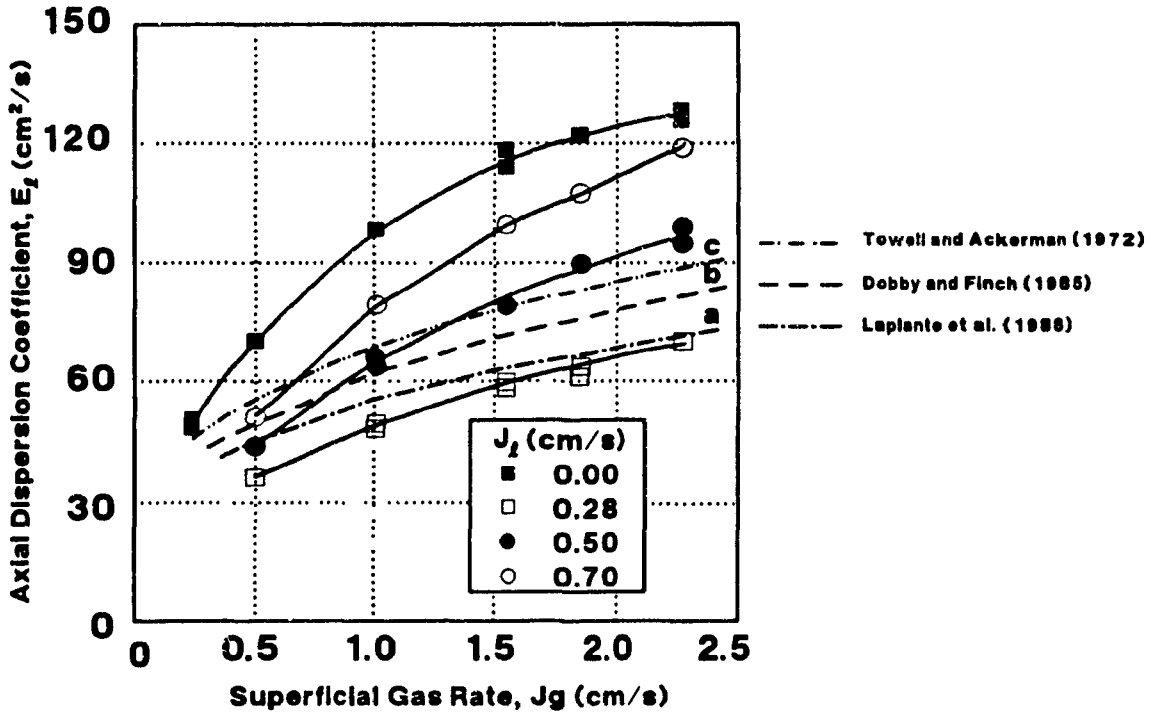

Figure 7.15 Liquid axial dispersion coefficient as a function of gas rate for various liquid rates

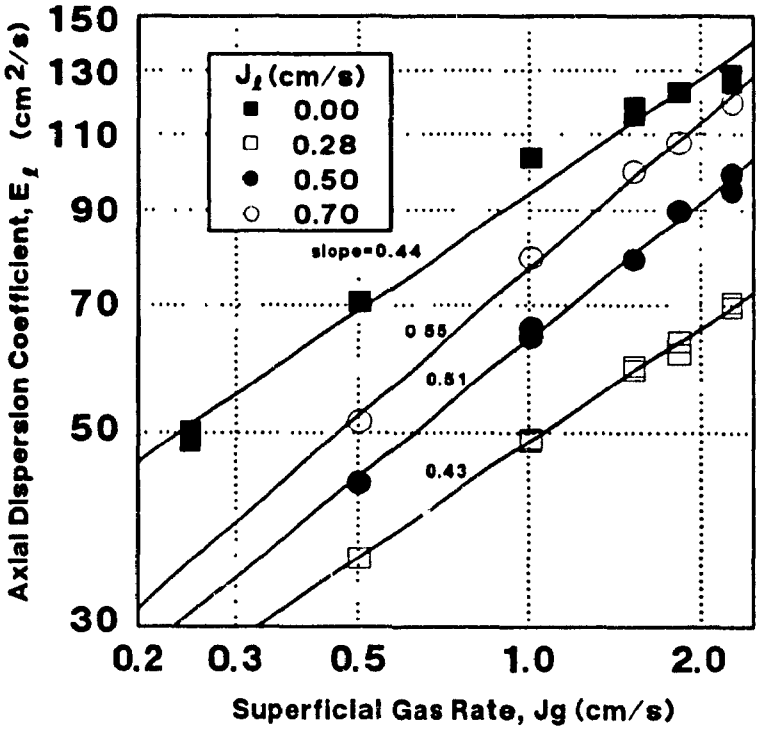

Figure 7.16 Liquid axial dispersion coefficient vs. gas rate (log-log scale)

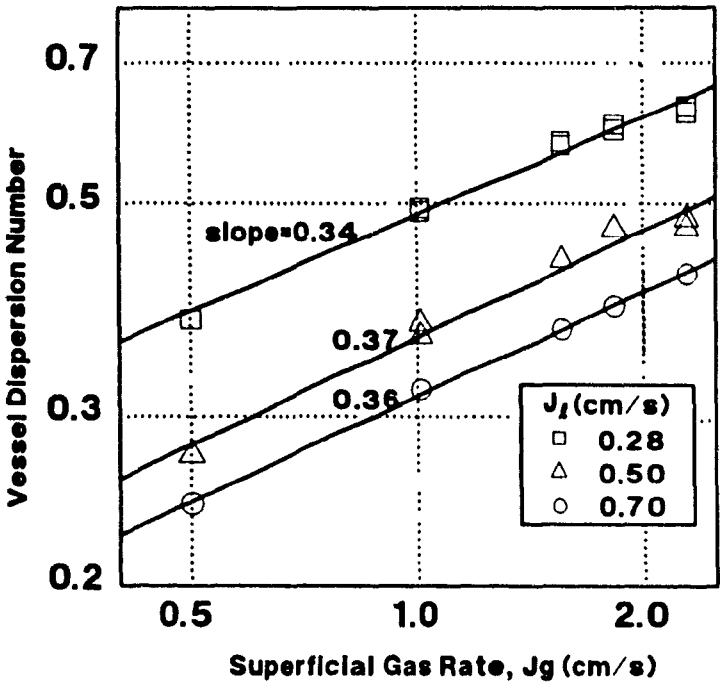

Figure 7.17 Liquid vessel dispersion number vs. gas rate (log-log scale)

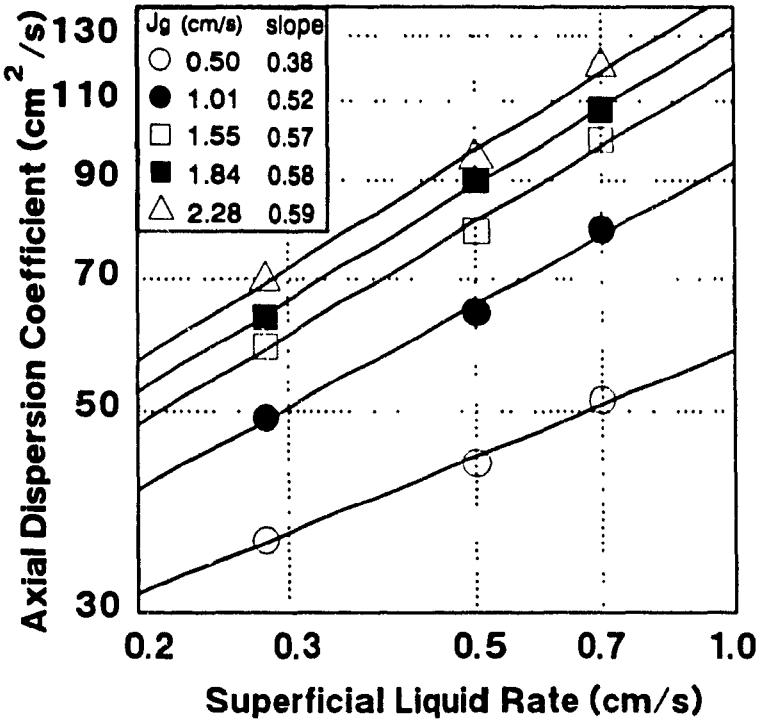

Figure 7.18 Liquid axial dispersion coefficient vs. liquid rate (log-log scale)

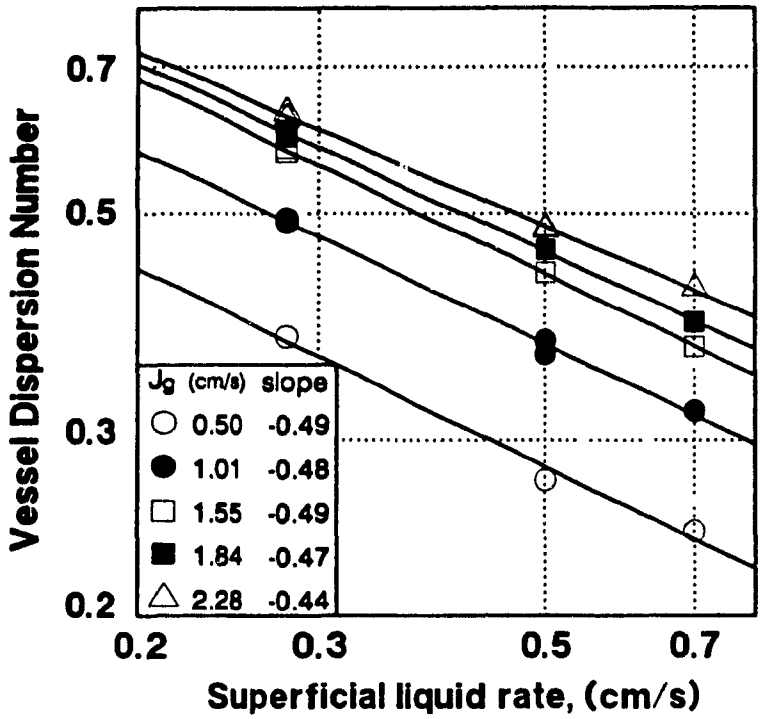

Figure 7.19 Liquid vessel dispersion number vs. liquid rate (log-log scale)

The liquid axial dispersion coefficient as a function of column length for several gas rates is plotted in Figure 7.20. It is clear that increasing the length increases the axial dispersion coefficient. A similar observation was also made by Laplante and Redstone (1984) with regard to increasing length of a grinding mill. A log-log scale plot of vessel dispersion vs. column length to diameter ratio is presented in Figure 7.21. This gives the slope of range from -0.44 to -0.62 (average -0.48). This means increasing the column length to diameter ratio decreases the vessel dispersion number.

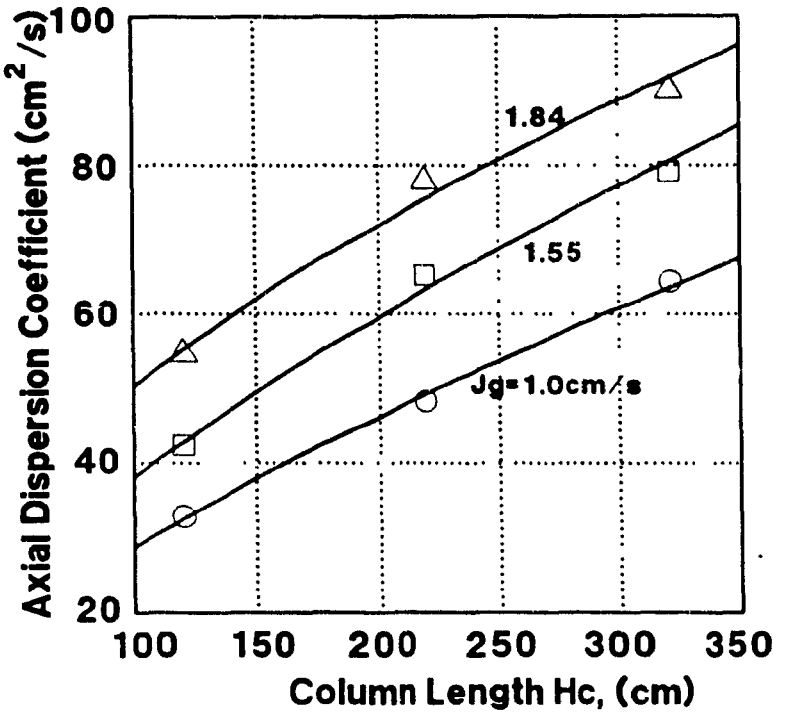

Figure 7.20 Liquid axial dispersion coefficient: the effect of column length

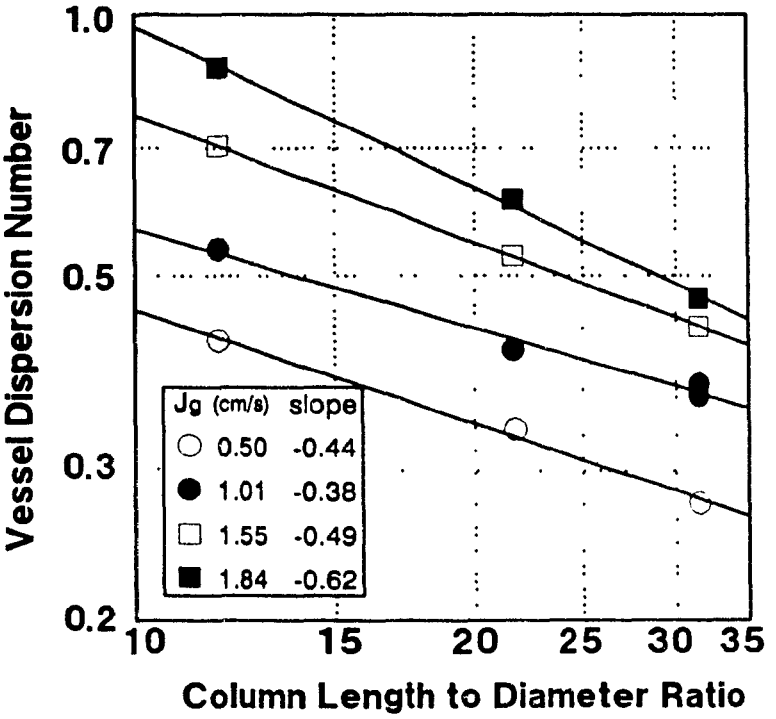

Figure 7.21 Liquid vessel dispersion number vs. column length to diameter ratio (log-log scale)

The effect of column verticality on the liquid vessel dispersion number is presented in Figure 7.22. The effect is not as large as expected, as shown by the trend predicted by the relationship of Tinge and Drinkenburg (1986),

$$E_{l,\alpha} = E_l(1 + C \cdot \alpha \cdot d_c)^2 \qquad (7.1)$$

where $E_{l,\alpha}$ is the liquid axial dispersion coefficient with a tilt; E_l, the axial dispersion coefficient without tilt; α, the inclination (rad.); C, a constant ($rad^{-1} \cdot m^{-1}$); d_c, column diameter in m. Tinge and Drinkenburg (1986) gave a value of 1100 $rad^{-1} \cdot m^{-1}$ for constant C. Applying the similar equation with N_d and fitting to the present experimental data, C=23$rad^{-1} \cdot m^{-1}$ was obtained (dashed line in Figure 7.22), which is very small in comparison to the value obtained by Tinge and Drinkenburg (1986).

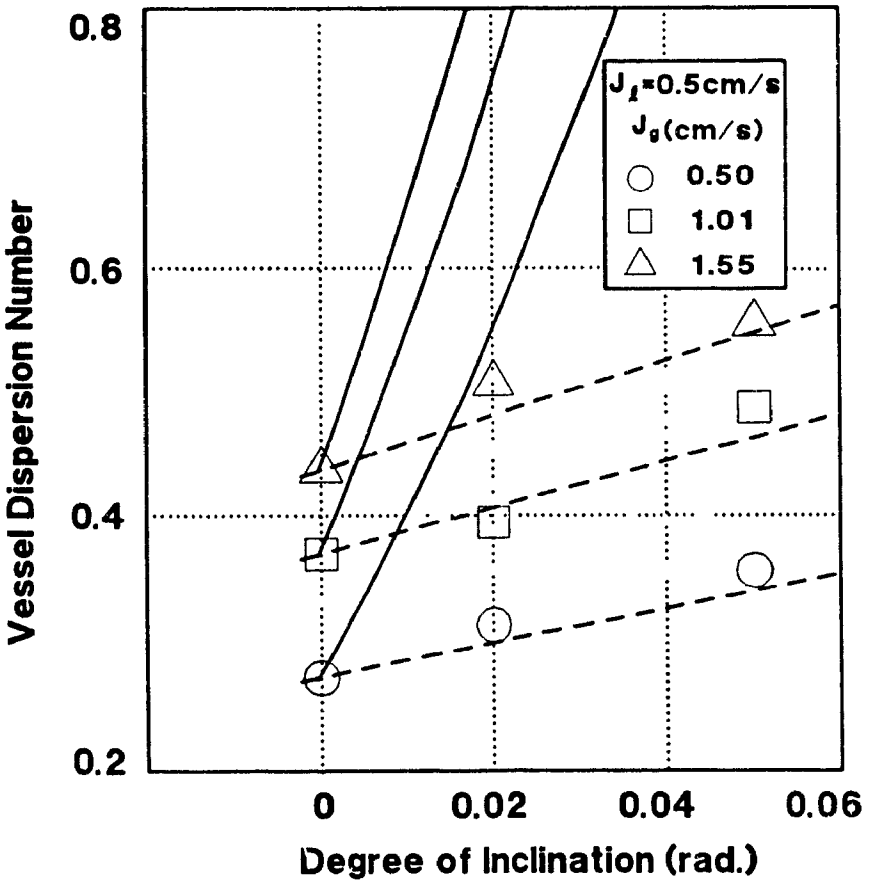

Figure 7.22 Liquid vessel dispersion number: the effect of column verticality (solid lines are the prediction of the correlation of Tinge and Drinkenburg, 1986)

The effect of feed solid percentage on liquid vessel dispersion number is shown in Figure 7.23. The decrease in liquid dispersion number as the feed solid percentage is increased is only slight, being less than that predicted by the correlation of Laplante et al. (1988).

$$E_{tS} = E_t \exp(C \cdot S) \tag{7.2}$$

where $E_{t,S}$ is the liquid axial dispersion coefficient with feed solid percentage S. Laplante et al. (1988) obtained C=-0.025 from the data collected from various sources. The present work shows that C=-0.004 (dashed line in Figure 7.23).

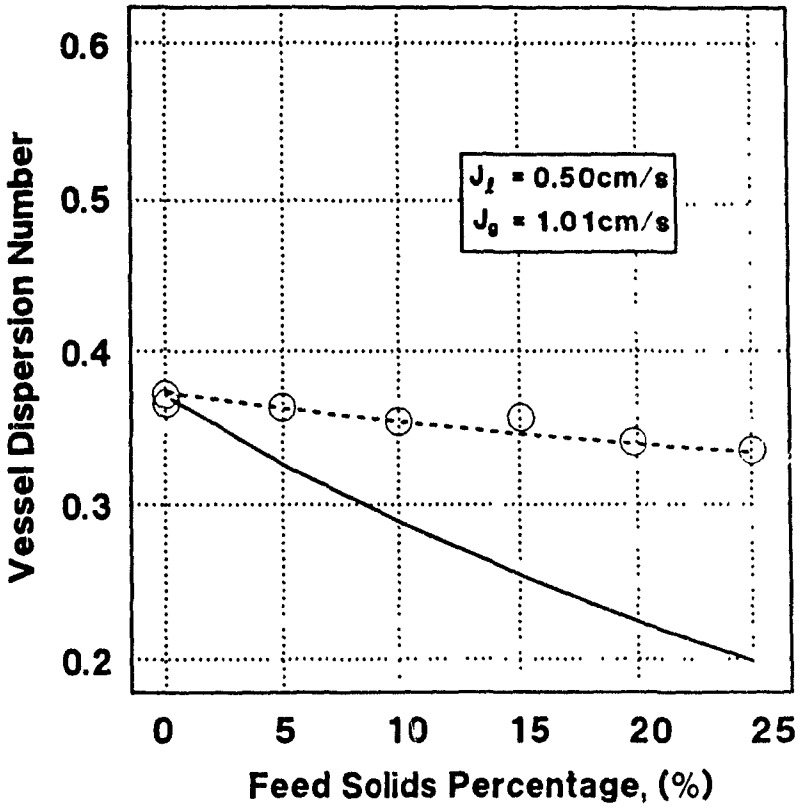

Figure 7.23 Liquid vessel dispersion number: the effect of feed solid percentage (solid line is the prediction of the correlation of Laplante et al., 1988)

7.4.2 Estimating the Vessel Dispersion Number

From the present work and the previous published mixing data on flotation columns (see Table 7.11), an empirical correlation is proposed (correlation coefficient 0.86),

$$N_d = 1.6\left(\frac{d_c}{H_c}\right)^{0.48}\frac{J_g^{0.36}}{J_l^{0.47}}\exp(-0.004S) \qquad (7.3)$$

where S is the feed solid percentage (% wt.). The power constants on each term in Equation (7.3) were obtained based on individual terms (see Figures 7.17, 7.19, 7.21,).

The parameter ranges for Eq.(7.3) are $8.2\text{cm} < d_b < 91\text{cm}$, $300\text{cm} < H_c < 1000\text{cm}$, $0.5\text{cm/s} < J_g < 2.5\text{cm/s}$, $0.5\text{cm/s} < J_l < 2.1\text{cm/s}$ and $0 < S < 30\%$.

Figure 7.24 shows the fit to the present data, and those of Rice et al (1974), Dobby and Finch (1985b) and Laplante et al. (1988). Data from these investigators is presented in Table 7.11. The effect of column verticality is not included in this correlation since it is not a usual design parameter. Data from Espinosa et al (1989) is not used because their N_d is considerably larger than expected; the predicted value of N_d in their case using Eq.(7.3) is about 1.0, rather than 4.5. It should be appreciated that with $N_d \geq 1.0$, the exact values are not critical -- they could all be reasonably considered as approximately perfectly mixed. The vessel dispersion numbers from Mavros et al. (1989) are extraordinarily large under the stated operating conditions, where gas rate and liquid rate were extremely small. Because they fall outside the usual range of column operation, the data of Mavros et al. (1989) were not included.

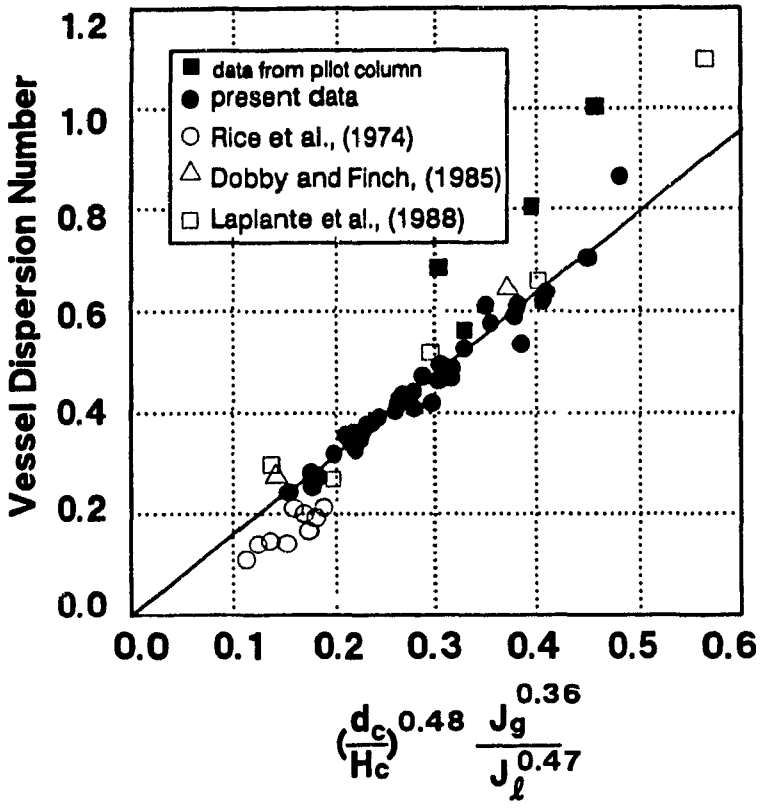

Figure 7.24 A proposed correlation between vessel dispersion number and design and operating variables

Table 7.11 Summary of previous data from other researchers

column size (cm·cm)	J_g (cm/s)	J_l (cm/s)	ϵ_g (%)	N_d	E_l (cm²/s)	reference
8.2×464.2 circular	1.12 0.96 0.80 0.57 1.08 1.35 0.63 0.38 0.73	0 50 0.50 0.50 0.52 0.52 0.52 0.52 0.52 0.52	15.0 11.5 8.5 10.0 20.0 22.0 12.0 9.0 16.0	0.153 0.159 0.169 0.117 0.134 0.169 0.099 0.082 0.113	41.90 41.68 42.77 31.50 40.50 52.17 27.12 21.87 32.60	Rice et al., (1974)
45.7x45.7x950 (square)	1.40	1.20	5.5	0.278	335.34	Dobby and Finch (1985)
91.4x91.4x1000 (square)	1.80	1.06	7.0	0.476 0.644	542 54	rederived
3.4x180 (circular)	1.80	1.47	12.0	0.282	56.51	Kho and Sohn (1989)
250x1300 (circular)	0.90	0.50		4.520	2260.00	Espinosa et al. (1989)
45.7X45.7x950 (circular)	0.68 1.21	2.08 1.58	5.0 10.0	0.300 0.270	624.00 450.03	Yianatos et al., (1989)
91.4x91.4x1000 (square)	2.10 1.50	1 50		0.660 0.520	1450.00 720.00	Laplante et al. (1989)
183x1010 (square)	2.2	0.8	7.0	1.1	580.00	
5.7x890 (square)	1.60	1.0		0.030	26.70	
8x100 (circle)	0.03 0.10 0.03 0.10 0.03 0.03 0.03 0.03 0.10 0.10 0.10	0.13 0.13 0.20 0.20 0.07 0.14 0.20 0.27 0.14 0.20 0.27		1.111 2.350 0.769 1.136 2.000 1.333 0.769 0.555 3.334 1.429 0.741		Mavros et al. (1989)

CHAPTER 8

DISCUSSION

8.1 Gas Holdup Distribution

The homogeneous bubbly flow theory is not applicable to the situations where liquid circulation and large bubbles exist. A major factor that complicates the study of the overall behaviour of two-phase flow is the existence of different flow regimes. In each flow regime, flow structure and development is different. Detailed knowledge of the local properties, such as gas holdup and bubble sizes, are required for understanding the mechanisms involved in determining the two-phase flow. The present work is focused on the determination of the radial local gas holdup distribution in flotation columns. Before considering this, the axial gas holdup distribution is briefly addressed.

8.1.1 Axial Gas Holdup Distribution

There was a gas holdup change from the sparger level to the interface level. This vertical change in gas holdup measured using a pressure transducer in this work was about 3-8% (absolute, Figure 6.3), dependent on gas rate.

The increase in gas holdup with height was also reflected in the radial gas holdup profiles measured at different levels using conductivity technique. For example, Figures 6.19 to 6.23 show the radial gas holdup profiles measured at three levels in the pilot flotation column. The increase in gas holdup with height from radial gas holdup profiles is similar to the one determined using the pressure transducer.

The increase in gas holdup with respect to the height is partly due to the change in hydrostatic head. To model ϵ_g with column height, H_c, the bubble size d_b is estimated

from the known gas holdup and gas rate at the top using the bubbly flow model; at a distance from the top, bubble size and gas rate are corrected for the pressure change using the ideal gas law; then the gas holdup at this level can be estimated using the bubbly flow model. The calculations (Section 6.1) showed that the predicted change in gas holdup was smaller than the measured. If the gas holdup is only corrected for the hydrostatic pressure, the change in gas holdup with height is larger than predicted from the bubbly flow model, but still less than the experimental one. The relatively large change in gas holdup shown by the experimental data is possibly due to gas and liquid circulations, which may lead to an increased change in gas holdup with height, since the column length to diameter ratio in the 50cm column is only about 5.

8.1.2 Radial Gas Holdup Distribution

Local radial gas holdup was measured using the electrical conductivity technique. The comparison between the gas holdup measured using this technique and the one measured using water manometers in a small column (Figure 5.11) showed the conductivity technique is applicable. The choice and design of the electrodes are very important in terms of using Maxwell's model or the equation derived by Yianatos et al. (1985). It is shown that an electrode cell which encloses a certain volume is usually capable of measuring local gas holdup. The conductivity probe which consists of one large plate and one small needle was not applicable due to the high frequency and small size of bubbles in this study, at least using the size of needle (0.5mm) selected.

Local gas holdup measured at a given point over a period of time showed that the considerable variation (Figure 6.4). It seems that the variation in gas holdup with time is largest at the column centre and smallest near the wall. This can be interpreted by the large bubbles tending to accumulate and rise in the centre (Locket and Kirkpatrick, 1975; Shah et al., 1982), and thus the detector periodically senses these large bubbles. Due to the change in local gas holdup with time, a long sampling time is required to obtain the (time-average) local gas holdup. In the present work, three repeated tests over 30 minutes were used. The reproducibility was good (Figure 6.5).

Radial local gas holdup distribution was obtained under several operating conditions. With no frother addition and 8 spargers uniformly arranged at the column bottom, a relatively uniform distribution in local gas holdup was observed at low gas rates, and the distribution is close to a parabolic profile at high gas rates. This

observation is similar to the work of Hills (1972) who measured the radial gas holdup distribution in a bubble column (d_c=13.8cm) with water only. In the present work, radial gas holdup distribution was measured at several depths. It is noted that with no frother addition, the shape of the local gas holdup distribution does not change very much with depth (see Figures 6.6-6.9). Reducing the number of spargers used to inject air reduced the local and average gas holdup but did not change the shape of the profiles (Figures 6.10-6.11). One sparger tested off centre (Figures 6.12-6.13) gave a radial gas holdup profile which varied considerably with the highest gas holdup above the sparger location. The shape of the profiles changed from the bottom to the top, with the maximum towards the column centre. The local gas holdup distribution with frother addition was also determined (Figures 6.14-6.18). There is a change in average gas holdup and local gas holdup with height. It seems that the shape of the radial gas holdup profiles is consistent with respect to the height, with the highest gas holdup observed above the sparger.

Local radial gas holdup profiles were measured in the pilot flotation column (Figure 6.19-6.23). The sparger system used in this column was entirely different from one used in the laboratory flotation column. A 'W' shape of radial gas holdup profiles was found at low gas rates when all three spargers were used. At high gas rates, the radial gas holdup profiles became a saddle shape. A saddle shape of profiles was evident even at low gas rate when only one sparger at centre was used (Figure 6.22). When the single sparger was located off-centre, the radial gas holdup profile changed considerably. Miller and Mitchie (1970) and Nassos (1963), all using resistivity probe measurements, reported that radial gas holdup profile was dependent on the method of gas injection. Koide et al. (1979) also determined the radial gas holdup profiles in a column (d_c=5.5m), and similar observation to these made here about the shape of the profiles was made. The work by Herringe and Davis (1976) demonstrated that the radial gas holdup profile was independent of the gas inlet condition at a sufficient distance (at least 8 times diameter) from the gas inlet. They attributed this to the flow tendency towards a common equilibrium flow structure.

Parabolic radial gas holdup profiles can be easily described mathematically. The 'W' or saddle shape of the profiles are more difficult. As a consequence, the structure and development of 'W' or saddle-shaped radial gas holdup profiles were not mathematically modelled in the present study. In literature, Herringe and Davis (1976, 1978) and Drew and Lahey (1981, 1982) presented a series of studies on this subject.

8.2 Liquid Circulation Velocity Profile

The shear stress model was used to calculate the liquid circulation velocity profile from a known radial gas holdup distribution, which was close to parabolic (Figures 6.24 and 6.25). The calculated liquid circulation velocity profiles showed that the liquid circulation velocity was maximum upwards at the column centre. From $r/R=0.4\sim0.5$ to column wall, the liquid circulation velocity was negative i.e. moved downwards near the wall. This was approximately observed visually in the laboratory flotation column where some bubbles indeed moved downwards near the column wall. The liquid circulation velocity profiles were not calculated for 'W' or saddle-shaped radial gas holdup profiles.

The shear stress model has several limitations in practice. The gas holdup distribution used in the model is assumed to vary from a maximum at the centre to a minimum at the wall (i.e. parabolic shape). An equation was developed to describe this form of radial gas holdup distribution. In reality, radial gas holdup distribution can vary widely from this parabolic pattern, which poses a difficulty in describing the radial gas holdup distribution mathematically. In general, flatter gas holdup profiles will reduce the liquid circulation and the saddle-shaped gas holdup profiles will cause a reverse circulation pattern (Clark et al., 1987). It has been found that the shear stress at the wall is strongly related to the radial gas holdup distribution; for example, a negative shear stress (downwards) corresponds to the parabolic gas holdup profiles while positive shear stress (upwards) corresponds to the saddle-shaped gas holdup profiles (Clark et al., 1987).

The presence of small air bubbles in the liquid affects the liquid rheology. The application of the mixing length theory may partly account for this. Most liquids used in flotation are not Newtonian fluids. To relate the shear stress, $T_w(\phi)$, with the circulation velocity gradient (dV_l/dr), two parameters are used, i.e., K and p. As described in Chapter 3, the selection of the two parameters changes the magnitude of the calculated liquid circulation velocity

Despite the limitations of describing the radial gas holdup distribution and selecting the parameters, this model provides a simple estimate of liquid circulation velocity distribution in a flotation column, since in general the liquid circulation velocity is difficult to measure directly. Hills (1974) measured the liquid circulation velocity using

the Pavlov tube, and found that liquid circulation was a 'gulf streaming' pattern, similar to the one calculated using the shear stress model for the parabolic radial gas holdup profiles.

8.3 Mixing Models

In the present study, mixing models such as the axial dispersion model, the tanks-in-series model and the backflow compartment model were examined to find which is the most suitable model for the RTD studies in flotation columns.

8.3.1 Axial Dispersion Model

In estimating the vessel dispersion number from the residence time distribution, the axial dispersion model was extensively explored. There are many possible combinations in applying this model: boundary conditions (experimental procedure), types of solutions (analytical or numerical) and RTD fitting routines. From the present work, it was found that the most suitable combination in estimating vessel dispersion number (N_d) is the numerical solution with closed-closed boundary conditions and a least squares fitting routine, symbolized as $N_{dcc}{}^{L}$. The reasons for selecting $N_{dcc}{}^{L}$ are discussed below.

Boundary Conditions and Solution Options

Two types of boundary conditions were examined: open-open and closed-closed boundaries. One reason for employing open-open boundary conditions is because a relatively simple analytical solution to the axial dispersion model exists. The most commonly employed experimental procedure, because of its convenience in large columns, is to inject a pulse tracer at the feed inlet and to detect the tracer concentration at the exit. This procedure reasonably approximates closed-closed boundary conditions. The poorer fit to experimental RTD using the open vessel solution compared with closed vessel solution is partly a consequence of the experimental procedure.

Ityokumbul et al. (1988) derived regression equations to convert N_{doo} to N_{dcc} so that the simplicity of the analytical open vessel solution could be preserved but the more appropriate closed vessel N_{dcc} still be used. The conversions are reasonably accurate as shown in Table 8.1 (Finch and Dobby, 1990b).

Table 8.1 Comparison of N_d values

J_g (cm/s)	$N_{doo}{}^{L}$	$N_{doc}{}^{L}$	$N_{doc}{}^{M}$	$N_{doc}{}^{L*}$
0.00	0.027	0.028	0.080	0.030
0.50	0.253	0.273	0.387	0.327
1.00	0.293	0.363	0.457	0.383
1.55	0.341	0.436	0.503	0.451
2.28	0.365	0.472	0.581	0.485

Note: $N_{doc}{}^{L*}$ derived from $Pe_{cc}{}^{*}/Pe_{oo} = 0.70\ Pe_{oo}{}^{0.073}$
where $Pe = 1/N_d$

The closed vessel solution gives a good fit over the full range of N_d, in contrast to $N_{doo}{}^{L}$ which gives a progressively poorer fit for $N_d > 0.5$. This degradation in the fit is characterized by a sharpening of the peak in the model RTD. The results of Ityokumbul et al. (1988) also show this sharpening of the peak with the open vessel solution.

The least squares fit is generally superior to that of moments matching and is less subject to errors; for example, in defining the RTD tail (Figure 7.2). This observation corresponds to that also made by Butt (1962), Wakao and Kaguei (1982) and Ityokumbul et al. (1988). Moments matching remains popular because of its simplicity. Ostergaard and Michelsen (1969) also observed that the vessel dispersion number obtained from moments matching can be in error because the RTD tail, which normally can not be determined with great accuracy, contributes very heavily to the second moment. They presented a modified analysis of moments.

Numerical Solution

The main reason for using the numerical solution to the axial dispersion model is that the analytical solutions with closed-closed boundary conditions are very complex and do not readily converge. It is also confusing that two different forms are in the literature.

The finite difference approximation of the axial dispersion model was shown to be accurate as long as the convergence criteria (Equations 4.40-4.41) were satisfied. The excellent agreement between the experimental and fitted RTD also indicates that the finite difference equations at the two boundaries (the inlet and exit) are accurate for a closed vessel.

An advantage of a numerical solution is the ability to fit experimental age distributions measured inside the column. In contrast, the available analytical solutions do not have this facility. The demonstrated ability to fit the age distribution is seen as a strong endorsement of the use of the axial dispersion model in column flotation studies. There appears to be no need for the added flexibility of the compartment models, as claimed by Mavros et al. (1989) and Goodall and O'Connor (1990) (see below). The dispersion model, however, is difficult to extend to the region between the feed position and the interface. The N_d value in this region is expected to be different from that below the feed position due to the different liquid interstitial velocities. In this situation, the flexibility of a compartment model may be an advantage. However, whether $x=0$ is taken at the feed or interface level did not markedly affect the fit in the industrial flotation column case considered here (Figure 7.5), as expected from the work of Laplante et al. (1988).

The axial dispersion model appears to be adequate, certainly for the present level of sophistication in flotation column studies. It fits over the full range of N_d, although the physical significance of the fit at $N_d > 1.0$, i.e. with such a large deviation from plug flow, may be questioned (Levenspiel, 1979, Goodall and O'Connor 1990). While transport needs to be modeled, the necessary accuracy must be kept in perspective. For example, for scale-up, the estimation of rate constants and froth carrying capacity probably present more of a challenge than modelling transport. At the industrial scale, i.e., a relatively large N_d, the effect of N_d on predicted performance becomes small, which further relaxes the need to model mixing precisely. In fact for scale-up, Luttrell et al. (1988) suggest using a single value of N_d (0.25) and Newall et al. (1989) applied the fully mixed approximation in design calculations. In terms of gaining insight into the fundamentals of the process, detailed transport models are needed but they do not appear to be necessary for scale-up.

8.3.2 Compartment Models

Considering the complexity of the flow in a flotation column, Mavros et al. (1989) and Goodall and O'Connor (1990) suggested that compartment models were more appropriate than the axial dispersion model. However, in neither case was experimental evidence presented to support this contention.

The compartment models examined in the present study were the tanks-in-series and the backflow compartment models. The tanks-in-series model, as used by Goodall and O'Connor (1990) did not successfully fit the experimental data in this work. The backflow compartment (or cell) model gives an equally good fit (and similar N_d values), as the axial dispersion model (numerical solution with closed-closed boundaries). Roemer and Durbin (1967) and Shinnar and Naor (1967) reached a similar conclusion, the latter noting that with an increasing number of compartments, the backflow compartment model progressively better approximated the axial dispersion model. An examination of the partial derivatives as a form of finite difference equations suggests that the backflow compartment model is more or less the same as the axial dispersion model: this provides an additional reason for them to give similar N_d values.

The axial dispersion model can characterize the degree of mixing but provides no information on the mixing mechanism. The backflow cell model has two parameters, one of which, the backflow ratio λ, may represent the backmixing of the liquid in the wake of air bubbles. However, as noted, increasing the number of compartments increases λ (also see Mavros et al., 1989). This implies that the higher column length to diameter ratio, the larger is the backflow ratio (since n is approximately the column length to diameter ratio). This is debatable. It is not obvious why more liquid should be backmixed as column length to ratio increases.

Of all the models considered, the backflow model has the greatest flexibility. Consider the situation of a flotation column, with the tracer injected in the feed. In the backflow compartment model, tracer addition can be arranged in the $4th$ or $5th$ cell depending on the distance between the interface and the feed position. The detailed liquid mixing mechanism may be described by treating the water carried by the bubbles as dead-water, where there is an exchange between dead-water and bulk water. This model requires a number of parameters to be determined, such as the volume of dead-water and the exchange coefficient.

8.4 Liquid Dispersion

With the method of determining N_d established, the effect of operating and design variables on the liquid vessel dispersion number was extensively investigated. A general correlation between the vessel dispersion number and the operating and design variables was proposed based on previous and the present data.

8.4.1 Experimental Results

The effect of gas and liquid rates on the mixing were determined. The dependence of N_d and E_t on J_g is in agreement with other investigators (Fan, 1990). The effect of J_t on N_d and E_t has apparently not been investigated until this work (although a parallel study appears to have been done by Luttrell et al., 1990), partly because the relation between N_d and E_t already includes J_t and partly because of work being done in batch system. The present work shows that increasing J_t decreased the vessel dispersion number N_d but increased the axial dispersion coefficient E_t.

The effect of column length on the mixing was also determined and appears to be a new finding (with the possible exception of the work by Luttrell et al., 1990). Previous work always emphasized the dependency of N_d on the column diameter. Once again, the column (collection zone) length is also included in the relation between N_d and E_t, and this may partly explain why previous investigators did not test the effect of column length. Another possible reason is that usually all columns are 10 to 15m high and the height was not considered as a prime design parameter.

Recently, Mankosa et al. (1990) and Luttrell et al. (1990) present a series of modelling and scale-up studies in flotation columns. In the calculation, they suggest the following equation for estimating the vessel dispersion number,

$$N_d = K\left(\frac{d_c}{H_c}\cdot\frac{J_g}{J_t}\right)^p \qquad (8.1)$$

but K and p were not specified. They also did not give the experimental data to support this. From the present study, it appears that the form of the equation (Eq.8.1) is acceptable.

The effect of column verticality on the vessel dispersion number was determined to be not as large as expected based on the model of Tinge and Drinkenburg (1986), who conducted the work in bubble columns. They noted that the effect of column verticality on mixing is far more severe for large-scale columns with short height. In comparison, the diameter of column used in present work was relatively small but with large height, therefore, the effect of vertical misalignment is small. This does not imply that the verticality of a flotation column is not important. Visual observations showed that there is significant liquid circulation when the column is tilted. Further work may want to consider the effect of verticality directly on recovery, rather than on mixing

A slight decrease in the vessel dispersion number as the feed solid percentage increased was found in the present study. The effect of the feed solid percentage on the liquid axial dispersion coefficient is expected to be larger if the volume occupied by the solids is taken into account (interstitial rate of liquid is reduced). This corresponds to the work of Laplante et al. (1988).

8.4.2 Predicting Vessel Dispersion Number

From the present work, several points are significant in predicting the mixing parameters. First, the intensity of a mixing process is uniquely indicated by the value of N_d rather than E_t. Second, the operating and design variables should be directly correlated to N_d rather than to E_t (then from which N_d is then calculated using the relation between E_t and N_d). Third, in correlating N_d to the operating and design variables, the method of generating N_d values should be consistent. As demonstrated in the present work, different combinations of model selection, boundary conditions and model fitting routines give different N_d values.

The following correlation (correlation coefficient 0.86) from the present work and previous data from other investigators was obtained,

$$N_d = 1.6\left(\frac{d_c}{H_c}\right)^{0.48}\left(\frac{J_g^{0.36}}{J_t^{0.47}}\right)\exp(-0.004S) \qquad (8.2)$$

This equation covers the mixing data both in laboratory and industrial flotation columns, and provides a good estimation of the liquid vessel dispersion number for

column scale-up (also see Figure 7.24).

Retaining the form of the equation proposed by Mankosa et al. (1990) and Luttrell et al. (1990), then

$$N_d = 1.85 \left(\frac{d_c}{H_c} \cdot \frac{J_g}{J_l}\right)^{0.63} \tag{8.3}$$

is obtained (correlation coefficient 0.77). The fit to the data is shown in Figure 8.1. This correlation is probably acceptable for column scale-up, also.

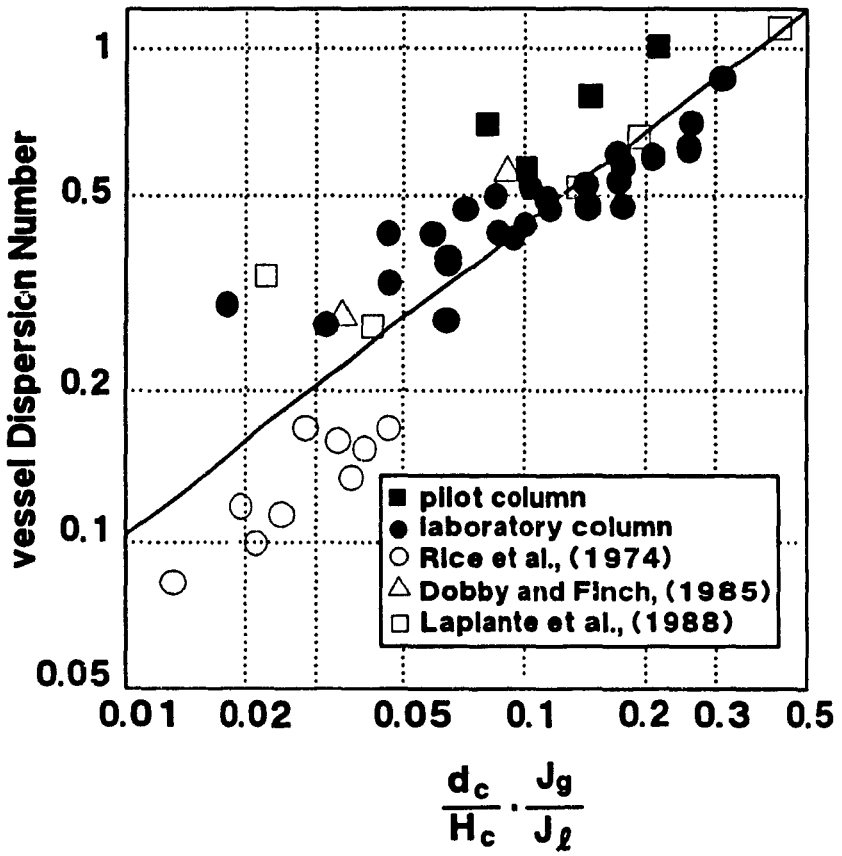

Figure 8.1 Correlation between vessel dispersion number and design and operating variables (Eq.8.3)

Factors not considered in Equations (8.2) and (8.3) which may affect mixing are gas holdup and bubble size. There have been attempts to account for the effect of gas holdup. For example, the models proposed by Joshi (1980) and Kelkar et al. (1983) included gas holdup in their derived correlation (see Section 4.2.1). The term containing gas holdup used in their correlations seems to be a modified form of the bubble slip velocity. Including the bubble slip velocity in Equation (8.1) gives the following correlation (correlation coefficient 0.88),

$$N_d = 0.56\left[\frac{d_c}{H_c}\cdot\frac{J_g}{J_l}\cdot\left(\frac{J_g}{\varepsilon_g}+\frac{J_l}{1-\varepsilon_g}\right)\right]^{0.41} \qquad (8.4)$$

as illustrated in Figure 8.2. It is evident from Figures 7.24, 8.1 and 8.2, Equation (8.4) is better than the other two correlations, since it fits the data better over the range tested (N_d from 0.08 to 1.1).

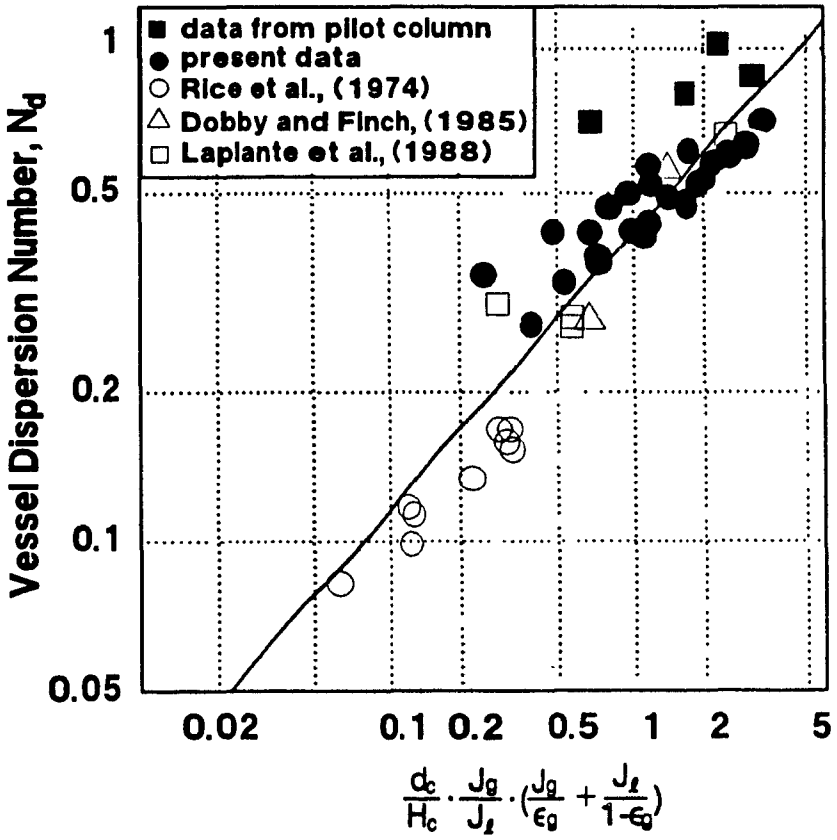

Figure 8.2 Correlation between vessel dispersion number and design and operating variables, considering the effect of gas holdup (Eq.8.4)

It is noted that for column scale-up, Equations (8.2) and (8.3) are preferable to Equation (8.4), since Equation (8.4) needs to first estimate gas holdup, which is a complex function of gas rate, frother/sparger system, and is difficult to predict. For gaining insight in mixing, Equation (8.4) is useful.

8.5 Solids Dispersion

Solid dispersion was not fully investigated in the present work. The work shown in Figure 7.14 was a trial using the inverse step tracer technique. It did show that the solid dispersion is similar to the liquid phase.

Dobby and Finch (1985) studied the axial mixing of solids using the solids residence time distribution, which was well fitted by the axial dispersion model. They found that the axial dispersion coefficient of solids was the same as the liquid phase, which was in agreement with the work of Rice et al. (1974). The other aspect of studying the solid dispersion is to measure the axial solids concentration profile that is fitted using the sedimentation-dispersion model. The model in its general used form is characterized by two parameters, namely the solids dispersion coefficient and the solids setting velocity (Fan, 1990). There are a number of empirical correlations proposed in the literature to account for these two parameters. However, due to the inconsistent physical interpretation of these parameters, the application of these correlations are limited (Fan, 1990).

CHAPTER 9

CONCLUSIONS AND SUGGESTIONS FOR FUTURE WORK

9.1 Conclusions

1 A simplified bubbly flow model was developed in this work. Applications of the model include: correlating gas holdup as a function of gas rate; correlating bias rate as a function of gas rate; estimating bubble size and predicting the effect of solid particles on gas holdup. The model correlation of gas holdup vs. gas rate was in good agreement with experimental data. Bubble size estimated using the bubbly flow model was close to that measured by photography.

2. An electrical conductivity technique was developed to measure local gas holdup. The geometry and size of the electrode cell was shown to play an important role in local gas holdup measurement. An electrode cell which encloses a certain volume was shown to be applicable in measuring local gas holdup. The local gas holdup measured using this technique was in good agreement with that measured using a pressure technique.

3. Radial local gas holdup distribution was measured using the electrical conductivity technique. In the large-scale laboratory flotation column (d_c = 50cm), with no frother addition at low gas rates, the local gas holdup showed an axially symmetric 'W' shape. At high gas rates, the profiles became parabolic. All the profiles were similar regardless of axial position. With frother addition, the radial gas holdup profiles were 'W' shape. When an off-centre sparger was used, non-symmetric gas holdup resulted with visually evident liquid circulation.

4. Radial gas holdup profiles were determined in a pilot flotation column (d_c=90cm). Profiles had a 'W' shape, with the highest gas holdup near the column wall. From the wall to the column centre, the local gas holdup first decreased and then increased, with the lowest gas holdup at r/R=0.3-0.5. At a relatively high gas rate, radial gas holdup profiles had a saddle shape and this was particularly evident at the 10m location above the sparger level.

5. Radial gas holdup profiles, when only one sparger off-centre was used in the pilot flotation column, were non-symmetrical but still revealed good gas distribution.

6. Measurements of radial gas holdup profiles at different heights using the conductivity technique confirmed the existence of vertical or axial change in gas holdup.

7. Liquid circulation velocity profiles for the parabolic radial gas holdup profiles were calculated using the shear stress model, which was the only case for which a solution was found.

8. The axial dispersion model was extensively explored: various combinations of experimental procedure, type of solutions and fitting routines were examined. The numerical solution with closed boundary conditions and least squares fitting was found to be the best.

9. A numerical solution to the axial dispersion model using finite difference method was developed. Liquid residence time and age distribution in laboratory and industrial flotation columns, covering a range in column diameter from 10cm to 250cm, were successfully fitted using this solution.

10. Comparison between the axial dispersion and the compartment models revealed that the backflow compartment model fitted experimental RTD data equally as well as the closed vessel axial dispersion model and gave a similar vessel dispersion number.

11. The effect of gas rate, liquid rate, column length, column verticality and

feed solid percentage on the liquid mixing in flotation columns was determined. The observed dependence of the vessel dispersion number on gas rate was similar to that in the previous work. A new finding in this work was the dependence of the vessel dispersion number on liquid rate and column length.

12. The effect of feed solids percentage and column verticality on the vessel dispersion number was found to be minor.

13. A general empirical correlation to predict the liquid vessel dispersion number was obtained based on the present and previous data,

$$N_d = 1.6\left(\frac{d_c}{H_c}\right)^{0.48}\left(\frac{J_g^{0.36}}{J_l^{0.47}}\right)\exp(-0.004S)$$

where S is the feed solid percentage (% wt.). This correlation provides an estimate of the liquid vessel dispersion number sufficiently accurate for scale-up.

14 Retaining the form of the equation suggested by Luttrell et al. (1990), the following correlation was obtained,

$$N_d = 1.85\left(\frac{d_c}{H_c}\cdot\frac{J_g}{J_l}\right)^{0.63}$$

which is also acceptable for column scale-up.

15. Considering the effect of gas holdup on mixing, the following correlation was proposed,

$$N_d = 0.54\frac{d_c}{H_c}\frac{J_g}{J_l}\left(\frac{J_g}{\varepsilon_g}+\frac{J_l}{1-\varepsilon_g}\right)^{0.40}$$

This equation fits the experimental data tested (N_d from 0.08 to 1.1) better than the other two correlations.

9.2 Claims for Original Research

1. An electrical conductivity technique was developed to measure the local gas holdup in flotation columns. The design of electrode cells was found to be important. A cell which encloses a certain of volume is generally applicable for local gas holdup measurement.

2. New empirical correlations to predict the liquid vessel dispersion number as a function of design and operating variables were developed.

9.3 Suggestions for Future Work

1. The bubble size measurement in large-scale flotation columns needs to be conducted to examine the applicability of the bubbly flow model.

2. The effect of solid particles on the hydrodynamics of flotation columns, for example, the stability of froth phase, gas holdup and bubble behaviours, needs to be investigated theoretically and experimentally.

3. The three phenomena found for maximum gas rate should be thoroughly investigated by changing the bubble size using different sparger sizes instead of frother concentration.

4. Radial local gas holdup distribution should be measured in industrial-scale flotation columns. The liquid circulation due to the non-uniformity of radial gas holdup distribution should be investigated.

5. Axial gas holdup profiles should be investigated and modelled.

6. Solid particle dispersion should be extensively examined.

7. Mixing in the froth zone of a flotation column should be studied.

PAGINATION ERROR.

TEXT COMPLETE.

ERREUR DE PAGINATION.

LE TEXTE EST COMPLET.

NATIONAL LIBRARY OF CANADA.

CANADIAN THESES SERVICE.

BIBLIOTHEQUE NATIONALE DU CANADA.

SERVICE DES THESES CANADIENNES.

REFERENCES

[1] Abouzeid, A.Z.M., Fuerstenau, W.W. and Sastry, K.V.S., 1980; Transport Behaviour of Particulate Solids in Rotary Drums: Scale-up of Residence Time Distribution Using the Axial Dispersion Model; *Power Technology*, vol.27, pp.241-250

[2] Abouzeid, A.Z.M., 1989; Transport of Particulates in Mineral Processing Systems -- Tumbling Units; *Powder Handling and Processing*, vol.1, No.3, pp.255-262

[3] Ahmed, N., and Jameson, G.S., 1985; The Effect of Bubble Size on the Rate of Flotation of Fine Particles; *Int. J. Mineral Process.*, vol.14, pp.195-215

[4] Alexander, B.F., Shah, Y.T. and Wilson, J.H., 1979; Radial Dispersion in Vertically Suspended Packed Baskets inside a Bubble Column; *Trans. IChemE*, vol.57, pp.252-255

[5] Amelunxen, R.L. and Redfearn, M.A., 1985; The Mechanics of Operation of Column Flotation Machines; *17th Annual CMP Meeting*, CIM, Ottawa

[6] Aoyama, Y., Ogushi, K., Koide, K. and Kubota, H., 1968; Liquid Mixing in Concurrent Bubble Columns; *J. Chem. Eng. of Japan*, vol.1, No.2, pp.158-163

[7] Argo, W.B. and Cova, D.R., 1965; Longitudinal Mixing in Gas-sparged Tubular Vessels; *I & EC Process Design and Development*, vol.4, No.4, pp.352-359

[8] Baird, M.H.I. and Rice, R.G., 1975; Axial Dispersion in Large Unbaffled Columns; *Chem. Eng. J.*, vol.9, 171-174

[9] Beyerlein, S.W., Cossmann, R.K. and Richter, H.J., 1985; Prediction of Bubble Concentration Profiles in Vertical Turbulent Two-Phase Flow; *Int. J. Multiphaseflow*, vol.11, No.5, pp.629-641

[10] Boutin, P. and Wheeler, D.A., 1967; Column flotation; *Mining World*, vol.20, No.3, p.47-50

[11] Brenner, H., 1962; The Diffusion Model of Longitudinal Mixing in Beds of Finite Length: Numerical Values; *Chem. Eng. Sci.*, vol.17, pp.229-243

[12] Bridge, A.G., Lapidus, L. and Elgin, J.C., 1964; The Mechanics of Vertical Gas-Liquid Fluidized System 1: Countercurrent Flow; *AIChE J.*, vol.10, pp.819-826

[13] Buffham, B.A. and Gibilaro, L.G., 1986; A Generalization of the Tanks-in-Series Model; *AIChE J.*, vol.14, pp.805

[14] Butt, J.B., 1962; A Note on the Method of Moments; *AIChE J.*, vol.8, No.4, pp.553-556

[15] Carslaw, H.S., 1945; Introduction to the Mathematical Theory of the Conduction of Heat in Solids; 2nd ed., *Dover Publications*

[16] Carslaw, H.S. and Jaeger, J.C., 1959; Conduction of Head in Solids; *Oxford Universities Press*, London

[17] Cienski, T. and Coffin, V.L., 1981; Column Flotation Operation at Mines Gaspe Molybdenum Circuit; *13th Annual CMP Meeting*

[18] Clark, N.N , Atkinson, C.M. and Flemmer, R.L.C., 1987; Turbulent Circulation in Bubble Columns; *AIChE J.*, vol.33, No.3, pp.515-518

[19] Clark. N.N. and Flemmer, L.C., 1989; Non-newtonian Two-phase Circulation in Bubble Colur.ins; paper to be published

[20] Clift, R., Grace, J.R. and Weber, M.E., 1978; Bubbles, Drops and Particles; *Academic Press*, New York, Chpt.12. pp.321-347

[21] Clingan, B.V. and McGregor, A.R., Feb. 1987; Column Flotation Experience at Magma Copper Company with Related Experience of Other Mineral Processors; presented at *the SME Annual Meeting of AIME*, Denver, Colorado

[22] Coffin, V.L. and J. Miszczak, 1982; Column Flotation at Mines Gaspe; presented at *14th International Mineral Processing Congress*, paper IV.21, Toronto

[23] Danckwerts, P.V., 1953; Continuous Flow Systems: Distribution of Residence Times; *Chem. Eng. Sci.*, vol.2, pp.1-13

[24] Davidson, J.F. and Harrison, D., 1966; The Behaviour of a Continuity Bubbling Fluidized Bed; *Chem. Eng. Sci.*, vol.21, pp.273

[25] Deckwer, W.D., Burckhart, R. and Zoll, G., 1974; Mixing and Mass Transfer in a Tall Bubble Columns; *Chem. Eng. Sci.*, vol.29, pp.2177-2188

[26] Devine, W.D., Shah, Y.T. and Morsi, B.I., 1985; Liquid Phase Axial Dispersion in a Bubble Column with Viscous Non-Newtonian Liquids; *Canadian J. Chem. Eng* , vol.63, pp.195

[27] Dobby, G.S., 1984; A Fundamental Flotation Model and Flotation Column Scale-up; Ph.D thesis, *McGill University*, Canada

[28] Dobby, G.S., Amelunxen, R.L. and Finch, J.A., 1985a; Column Flotation -- Some Experience and Model Development; presented at *IFAC Symposium on Automation for Mineral Resource Development*; Brisbane, Australia, pp 59-63

[29] Dobby, G.S. and Finch, J.A., 1985b; Mixing Characteristics of Industrial Flotation Columns; *Chem. Eng. Sci.*, vol.40, No.7, pp.1061-1068

[30] Dobby, G.S. and Finch, J.A., 1986a; Flotation Column Scale-up and Modelling; *C.I M Bull.* vol.79, No.889, pp.89-96

[31] Dobby, G.S. and Finch, J.A., 1986b; Particle Collection in Columns -- gas rate and bubble size effects; *Canadian Metall. Q.*, Vol.25, No.1, 9-13

[32] Dobby, G.S. and Finch, J.A., 1987; Particle Size Dependence in Flotation Derived from a Fundamental Model of the Capture Process; *Int. J. Miner. Process.*, vol.21, pp.241-260

[33] Dobby, G.S., Yianatos, J.B. and Finch, J.A., 1988; Estimation of Bubble Diameter in Flotation Columns from Drift Flux Analysis; *Canadian Metall. Q.*, vol.27, No.2, pp.85-90

[34] Drew, D.A. and Lahey, R.T., 1981; Phase Distribution Mechanisms in Turbulent Two-phase Flow in Channels of Arbitrary Cross Section; *J. Fluid Eng.*, vol.103, pp.583-589

[35] Drew, D.A. and Lahey, R.T., 1982; Phase Distribution Mechanisms in Turbulent Low-Quality Two-Phase Flow in a Circular Pipe; *J. Fluid Mech.*, vol.117, pp.91-106

[36] Egan, J.R., Fairweather, M.J. and Meekel, W.A., 1988; Application of Column Flotation to Lead Zinc Benificiation at Cominco; in Column Flotation'88 (ed., Sastry, K.V.S.), *SME Annual Meeting*, pp.19-26

[37] Espinosa-Gomez R. Finch, J.A. and Johnson, N.W., 1988a; Column Flotation of Very Fine Particles; *Minerals Engineering*, vol.1, No.1, pp.3-18

[38] Espinosa-Gomez, R., Finch, J.A., Yianatos, J.B. and Dobby, G.S., 1988b; Flotation Column Carrying Capacity: Particle Size and Density Effects; *Minerals Engineering*, vol.1, No.1, pp.77-79

[39] Espinosa-Gomez, R., Yianatos, J.B. and Finch, J.A., 1988c; Carrying Capacity Limitations in Flotation Columns; *in Column'88* (ed. Sastry K.V.S.)

[40] Espinosa-Gomez, R., Johnson, N.W., Pease, J.D. and Munro, P.D., 1989; The Commissioning of the First Flotation Columns at Mount Isa Mines Limited; In *Processing of Complex Ores* (eds. G.S. Dobby and S.R. Rao); pp.293-302

[41] Fair, J.R., July, 3, 1967; Designing Gas-spargers Reactors; *Trans. Instn. Chem. Eng.*, vol.47, pp.67-74

[42] Fan, L.-S., 1989; Gas-Liquid-Solid Fluidized Engineering; *Butterworths* Boston

[43] Feeley, C.D., Landolt, C.D., Miszczak, J. and Steenburgh, W M., 1987; Column Flotation at INCO's Matte Separation Plant; presented at *the 89th Annual General Meeting of CIM*, Toronto, Canada

[44] Flint, L.R. and Howarth, W. J., 1971; The Collision Efficiency of Small Particles with Spherical Air Bubbles; *Chem. Eng. Sci.*, vol.26, pp.1155-1168

[45] Field, R.W. and Davidson, J.F., 1980; Axial Dispersion in Bubble Columns; *Trans. Icheme*, vol.58, pp.228-235

[46] Finch, J.A. and Dobby, G.S., 1990a; Column Flotation; *Pergamon Press*, New York

[47] Finch, J.A. and Dobby, G.S., 1990b; Column Flotation: A Selected Review; in *Workshop on Sulphide Flotation*, Lulea, Sweden, pp.149-160

[48] Franz, K., Borner, T., Kantorek, H.J. and Buchholz, R., 1984; *Ger. Chem. Eng.*, vol.7, pp.365

[49] Freedman, W. and Davidson, J.B., 1969; Holdup and Liquid Circulation in Bubble Columns;

Trans. Instn. Chem. Engrs., vol.47, pp.251-262

[50] Froment, G.E. and Bischoff, K.B., 1979; Chemical Reactor Analysis and Design; *Wiley*, New York, chap.12, pp.592-659

[51] Galaup, J.P., 1975; Contribution of the Study of Methods for Measuring Two Phase Flow; Ph.D thesis, University of Grenoble

[52] Gibilaro, L.G., 1978; On the Residence Time Distribution for Systems with Open Boundaries; *Chem. Eng. Sci.*, vol.33, pp.487-492

[53] Goodall, C.M. and O'Connor, C.T., 1990; Residence Time Distribution of the Solid and Liquid Phases in a Laboratory Column Flotation Cell; *SME Annual Meeting*, Salt Lake City

[54] Guy, C. Carreau, P.J., and Paris, J., 1986; Mixing Characteristics and Gas Holdup of a Bubble Column; *Canadian J. Chem. Eng.*, vol.64, pp.23-32

[55] Harris, C.C., 1976; in Flotation -- A.M. Gaudin Memorial Volume, *AIME*, New York, pp.753-815

[56] Herringe, R.A. and Davis, M.R., 1976; Structure Development of Gas-Liquid Mixture Flows; *J. Fluid Mech.*, vol.73, pp.37-123

[57] Herringe, R.A. and Davis, M.R., 1978; Flow Structure and Distribution Effects in Gas-liquid Mixture Flows; *Int. J. Multiphase flow*, vol.4, pp.461-486

[58] Hewitt, G.G., 1978; Measurement of Two Phase Flow Parameters; *Academic Press*, chpt.XI, pp.120-127

[59] Hills, J.H., 1974; Radial Non-uniformity of Velocity and Voidage in A Bubble Column; *Trans. Instn. Chem. Engrs.*, vol.52, pp.1-9

[60] Hills, J.H., 1976; The Operation of a Bubble Column at High Throughput, I. Gas Holdup Measurements; *Chem. Eng. J.*, vol.12, No.89

[61] Hills, J.H. and Darton, R.C., 1976; The Rising Velocity of A Large Bubble in A Bubble Swarm; *Trans. Instn. Chem. Engrs.*, vol.54, 256-264

[62] Holcombe, N.T., Smith, D.N., Knickle, H.N. and O'Dord, W., 1982, Thermal Dispersion and Head Transfer in Non-Isothermal Bubble Columns; *Chem. Eng. Commu* , vol.21, pp 125

[63] Hu, W. and Liu, G., 1988; Design and operating experiences with flotation columns in China; in *Column Flotation'88* (ed., Sastry, K.V.S.), *SME Annual Meeting*, pp.35-42

[64] Huls, B.J., Lachance, C.D. and Dobby, G.S., 1991; Bubble Generation Assessment for An Industrial Flotation Column; *Minerals Engineering*, vol.4, No 1, pp 37-42

[65] Imafuku, K, Wang, T., Koide, K. and Kubota, H., 1968; The Behaviour of Suspended Solid Particles in the Bubble Column; *J. Chem. Eng. of Japan*, vol.1, No 2, pp.153-163

[66] Iordache, O. and Jinescu, G., 1986; The Stability of Flow in Bubble Columns; *Chem. Eng. Sci.*, vol.41, No.10, pp.2585-2588

[67] Ityokumbul, M.T., 1986; A Hydrodynamics Study of Bubble Column Flotation; Ph.D. thesis, University of Western Ontario, Canada

[68] Ityokumbul, M.T., Kosaric, N. and Bulani, W., 1988; Parameter Estimation with Simplified Boundary Conditions; *Chem. Eng. Sci.*, vol.43, No.9, pp.2457-2462

[69] Jameson, G.J. and Allup, 1984; A Survey of Bubble Size in Industrial Flotation Cells; *Australian Minerals Industry Research Association*, Melbourne, Australia

[70] Jameson, G.J., 1986; Private communication

[71] Jameson, G.J , 1988; A New Concept in Flotation Column Design; in *Column Flotation'88* (ed. K.V.S., Sastry), *SME Annual Meeting*, pp.281-285

[72] Jean, R.H., Tang, W.T. and Fan, L.S., 1988; The Sedimentation-Dispersion Model for Slurry Bubble Columns; *AIChE J.* vol.35, No.4, pp.662-665

[73] Johnson, N.W., 1988; Private communication

[74] Joshi, J.B. and Sharma, M.M., 1978; Liquid Phase Backmixing in Sparged Contactors; *Canadian J. Chem. Eng.*, vol.56, pp.116-119

[75] Joshi, J.B. and Sharma, M.M., 1979; A Circulation Cell Model for Bubble Columns; *Trans. Instn. Chem. Engrs.*, vol.57, pp.244-251

[76] Joshi, J.B., 1980; Axial Mixing in Multiphase Contactors -- A Unified Correlation; *Trans. Instn. Chem. Engrs.*, vol.58, pp.155-165

[77] Joshi, J.B., 1982; Gas Phase Dispersion in Bubble Columns; *Chem. Eng. J.*, vol.24, pp.213-216

[78] Kasireday, V.K. and Al Taweel, A.M., 1989; Hydrodynamics of Unagitated Flotation Columns: 1. Gas Holdup and Maximum Throughputs; paper to be published

[79] Kato, Y. and Nishiwaki, A., 1972; Longitudinal Dispersion Coefficient of a Liquid in a Bubble Column; *Int. Chem. Eng.*, vol.12, No.1, pp.182-187

[80] Kato, Y., Nishiwaki, A., Fukuda, T. and Tanaka, T., 1972; The Behaviour of Suspended Solid Particles and Liquid in Bubble Columns; *J. Chem. Eng. of Japan*, vol.5, pp.112-118

[81] Kawase, Y. and Moo-Young, M., 1986; Liquid Phase Mixing in Bubble Columns with Newtonian and Non-Newtonian Fluids; *Chem. Eng. Sci.*, vol.41, pp.1969-1977

[82] Kaya, M., 1989; Froth Washing in Mechanical Flotation Cells; Ph.D thesis, McGill University, Canada

[83] Kelkar, B.G., Godbole, S.P., Honath, M.F., Shah, Y.T., Carr, N.L., and Deckwer, W.D., 1983; Effect of Addition of Alcohols on Gas Holdup and Backmixing in Bubble Columns; *AIChE*

J., vol.29, pp.361-369

[84] Kho, C-J. and Sohn, H-J., 1989; Column Flotation of Talc; *Int. J. Miner. Process.*, vol.27, pp.157-167

[85] Klinkenberg, A., 1966; Distribution of Residence Time Distributions in a Cascades of Mixed Vessels with Backmixing; *I & EC Fundamentals*, vol.5, No.2, pp.283-285

[86] Klinkenberg, A., 1968; Moments of Residence Time Distributions for Cascades of Stirred Vessels with Backmixing; *Chem. Eng. Sci.*, vol.23, pp.175-181

[87] Klinkenberg, A., 1971; Moments of Residence Time Distributions for Cascades of Stirred Vessels with Backmixing; *Chem. Eng. Sci.*, vol.26, pp.1133-1134

[88] Koide, K., Morooka, S., Ueyama, K., Matsuura, A., Yamashita, F., Iwamoto, S., Kato, Y., Inoue, H., Shigeta, M., Suzuki, S. and Akehata, T., 1979; Behaviour of Bubbles in Large Scale Bubble Column; *J. Chem. Eng. of Japan*, vol.12, No.2, pp.98-104

[89] Kulkarni, A., Shah, Y.T. and Kelkar, B.G., 1987; Gas Holdup in Bubble Column with Surface-Active Agents: A Theoretical Model; *AIChE J.*, vol.33, No.4, pp.690-693

[90] Kosick, G.A., Freberg, M. and Kuehn, L.A., 1988; Column Flotation of Galena at the Polaris Concentrator, *CIM Bulletin*, vol.81, No.920, pp.54-60

[91] Laplante, A.R. and Redstone, J., 1984; Modelling of Grinding Kinetics at the Sidebec-Normines Port-Cartier Palletizing Plant; *Mineral and Metallurgical Processing*, (August) pp.143-149

[92] Laplante, A.R., Yianatos, J.B. and Finch, J.A., 1988; On the mixing Characteristics of the Collection Zone in Flotation Columns; in *Column Flotation'88*, (ed., Sastry, K.V.S.), chpt.9, pp.69-79

[93] Laplante, A.R., 1990; Modelling Residence Time Distribution in Mineral Processing Units Using Tanks-in-Series Models; paper to be published

[94] Lapidus, L. and Elgin, J.C., 1957; Mechanics of Vertical Moving Fluidized system; *AIChE J.*, vol.3, pp.163

[95] Levenspiel, O. and Smith, W.K., 1957; Notes on the Diffusion-Type Model for the Longitudinal Mixing of Fluids in Flow; *Chem. Eng. Sci.*, vol.6, pp.227-233

[96] Levenspiel, O., 1972; Chemical Reaction Engineering; Second Edition, *John Wiley & Sons*, Chpt.9, pp.253-315

[97] Levenspiel, O., 1979; The Chemical Reactor Ominbook; *OSU Book Stores*, Corvallis, Or. pp.61-64

[98] Levy, S., May, 1963; Prediction of Two Phase Pressure Drop and Density Distribution from Mixing Length Theory; *J. Head Transfer (ASME)*, pp.137-152

[99] Lin, J.S., Chen, M.M. and Chao, B.T., 1985; A Novel Radioactive Particle Tracking Facility

for Measurement of Solids Motion in Gas Fluidized Bed; *AIChE J.*, vol.31, pp.465-473

[100] Lockett, M.J. and Kirkpatrick, R.D., 1975; Ideal Bubbly Flow and Actual Flow in Bubble Columns; *Trans. Instn. Chem. Engrs.*, vol.53, 267-273

[101] Luttrell, G.H, Weber, A.T. Adel, G.T. and Yoon, R.H., 1988; Microbubble Flotation of fine coal; in *Column Flotation'88*, (ed., Sastry, K.V.S.), *SME Annual Meeting*, pp.205-211

[102] Luttrell, G.H. and R.H., Yoon, 1990; A flotation Column Simulator Based on Hydrodynamic Principles; to be published

[103] Magiera, J., 1984; Longitudinal Dispersion of Gas in Two- and Three-Phase Flow; *Chem. Eng. Commu.*, vol.30, pp.119-130

[104] Mangartz, K.H. and Pilhofer, T., 1980, *Verfahreustechnik*, vol.14, pp.40

[105] Mankosa, M.J., Adel, G.T., Luttrell, G.H. and Yoon, R.H., 1990; Modelling of Column Flotation with a View toward Scale-up and Control; *Proceedings of Control'90*, Mineral and Metallurgical Processing (SME Annual Meeting, Salt Lake City, Ed. K. Rajamani)

[106] Mann, R., Mavros, P. and Middleton, J.C., 1981; A Structured Stochastic Flow Model for Interpreting Flow-Follower Data from a Stirred Vessel; *Trns. IChmE*, vol.59, pp.271

[107] Masliyah, J.H., 1979; Hindered Settling in A Multi-species System; *Chem. Eng. Sci.*, vol.34, pp.1166-1168

[108] Marruchi, G., 1985; Rising Velocity of a Swarm of Spherical Bubbles; *Ind. Eng. Chem. Fund.*, vol.4, pp.224

[109] Mavros, P., Lazaridis, N.K. and Matis, K.A., 1989; A Study and Modelling of Liquid--Phase Mixing in a Flotation Column; *Int. J. Miner. Process.*, vol.26, pp.1-16

[110] Maxwell, J.C., 1873; A Treatise on Electricity and Magnetism; *Clarendon Press*, Oxford, Vol.1, Chpt.IX, pp.360-366

[111] Mersmann, A., 1978; Design and Scale-up of Bubble and Spray Columns; *German Chem. Eng.*, vol.1, pp.1-11

[112] Miller, D.N., 1980; Gas Holdup and Pressure Drop in Bubble Column Reactors; *Ind. Eng. Chem. Process Des. Dev.*, vol.19, pp.371-376

[113] Miller, D.N. and Mitchie, R.E., 1970; *J. British Nucl. Eng. Sco.*, vol.9, pp.94-100

[114] Mills, P.J.T. and O'Connor, C.T., 1990; The Modelling of Liquid and Solids Mixing in a Flotation Column; *Minerals Engineering*; vol.3, No.6, pp.567-576

[115] Miyauchi, T., 1953; Kagaku Kogaku (Japanese), vol.17, pp.387

[116] Miyauchi, T. and Shyu, C.N., 1970; *Kagaku Kogaku*, vol.34, pp.958

[117] Molerus, O. and Kurtin. M., 1986; Modelling of Residence Time Distribution of the Gas Phase in Bubble Columns in the Liquid Circulation Regime; *Chem. Eng. Sci.*, vol.41, No.10, pp.2693-2698

[118] Morooka, S., Uchida, K. and Kato, Y., 1982; Recirculating Turbulent Flow of Liquid in Gas-Liquid-Solid Fluidized Bed; *J. Chem. Eng. of Japan*, vol.15, pp.29-33

[119] Nagata, S., 1975; Mixing: Principles and Applications; *Wiley*, New York, chpt.5, pp.215-247 and chpt.8, pp.335-367

[120] Nassos, G.P., 1963; *Argonne National Laboratory Report*, No.6738

[121] Nassos, G.P. and Bankoff, S.G., 1967; Slip Velocity Ratios in An Air-Water System under Steady-State and Transient Conditions; *Chem. Eng. Sci.*, Vol.22, pp.661-665

[122] Nauman, E.B. and Buffham, B.A., 1983; Mixing in continuous Flow Systems; *John Wiley & Sons*

[123] Newall, A., Gray, D. and Alfrd, R., 1989; The Application of Flotations to Gold Recovery to at Paddington Gold Mine, W.A., pres. Precious Metals Symp., Montreal

[124] Ohki, Y. and Inoue, H., 1970; Longitudinal Mixing of the Liquid Phase in Bubble Columns; *Chem. Eng. Sci.*, vol.25, pp.1-16

[125] Ostergaard, K. and Michelsen, M.L., 1969; On the Use of the Imperfect Tracer Pulse Method for Determination of Holdup and Axial Mixing; *Canadian J. Chem. Eng.*, vol.47, pp.107-112

[126] Pal, R. and Masliyah, J.H., 1990; Flow in Froth Zone of A Flotation Column; *Canadian Met. Q.*, vol.29, No.2, pp.97-102

[127] Pearson, J.R.A., 1959; A Note on the 'Danckwerts' Boundary Conditions for Continuous Flow Reactors; *Chem. Eng. Sci.*, vol.10, pp.281-284

[128] Raman, R., 1985; Chemical Process Computations; *Elsevier*, New York

[129] Rice, R.G., Oliver, A.D., Newman, J.P. and Wiles, R.J., 1974; Reduced Dispersion Using Baffles in Column Flotation; *Powder Techn.*, vol.10, pp.201-210

[130] Rice, R.G., Tupperainen, M.T. and Hedge, R.M., 1981; Dispersion and Holdup in Bubble Columns, Comparison of Rigid and Flexible Spargers; *Canadian J. of Chem. Eng.*, vol.59, pp.677-687

[131] Richardson, J.F. and Zaki, W.N., 1954; Sedimentation and Fluidization: part I; *Trans. Inst. Chem. Engrs.*, vol.32, pp.32-35

[132] Rietema, K., 1982; Science and Technology of Dispersed Two-phase Systems; *Chem. Eng. Sci.*, vol.37, No.8, pp.1123-1150

[133] Riquarts, H.P., 1981; *Ger. Chem. Eng.*, vol.4, pp.18

[134] Roemer, M.H. and Durbin, L.D., 1967; Transient Response and Moments Analysis of Backflow

Cell Model for Flow systems with Longitudinal Mixing}; *I & EC Fundamentals*, vol.6, No.1, 1967

[135] Sastry, K.V.S. and Fuerstenau, D.W., 1970; Theoretical Analysis of a Countercurrent Flotation Column; *Trans. SME/AIME*, vol.247, pp.46-52

[136] Schlichting, H., 1979; Boundary Layer Theory, *McGraw-Hill*, New York

[137] Schiller, L. and Naumann, A., 1933; *Z. Ver. dt Ing.*, vol.77, pp.318

[138] Schneider, J.C. and van Weert, G., 1988; Design and Operation of the Hydrochem Flotation Column; in *Column Flotation'88*, (ed., Sastry, K.V.S.), SME Annual Meeting, pp.287-292

[139] Serizawa, A., Kataoka, I., and Michyoshi, I., 1975; Turbulence Structure of Air-water Bubbly Flow -- 1. Measuring Techniques; *Int. J. Multiphase Flow*, vol.2, pp.221-233

[140] Serizawa, A., Kataoka, I., and Michyoshi, I., 1975; Turbulence Structure of Air-water Bubbly Flow -- 2. Local Properties; *Int. J. Multiphase Flow*, vol.2, pp.235-246

[141] Serizawa, A., Kataoka, I., and Michyoshi, I., 1975; Turbulence Structure of Air-water Bubbly Flow -- 3. Transport Properties; *Int. J. Multiphase Flow*, vol.2, pp.247-259

[142] Serizawa, A., Kataoka, I. and Michyoshi, I., 1976; Turbulence Structure of Air-Water Bubbly Flow; *Int. J. Multiphase Flow*, vol.2,

[143] Shah, Y.T., Stiegel, G,J. and Sharma, M.M., 1978; Backmixing in Gas-Liquid Reactors; *AIChE J.*, vol.24, pp.369-375

[144] Shah, Y.T. and Deckwer, W.D., 1981; Scale-up Aspects of Fluid-Fluid Reaction; *Scale-up in Chemical Process Industries* (ed. Kabel, R. and Bisio, A.), John Wiley

[145] Shah, Y.T., Kelkar, B.G. and Godbole, S.P., 1982; Design Parameters Estimation for Bubble Column Reactors; *AIChE Journal*, vol.28, No.3, 353-379

[146] Shinnar, R. and Naor, P., 1967; Residence Time Distribution with Internal Reflux; *Chem. Eng. Sci.*, vol.22, pp.1369-1381

[147] Surma, J.E., 1985; The Determination of Bubble Velocity of Fluidized Beds, M.S. thesis, Monata State University

[148] Szatkowski, M. and Freyberger, W.L., 1985; Kinetics of Flotation with Fine Bubbles; *Trans. Instn. Min. Metall.* (section C), vol.84, pp.C61-C70

[149] Szatkowski, M., 1987; Factors Influencing Behaviour of Flotation Froth; *Trans. Instn., Min. Metall.* (sect. C), vol.96, pp.C115-C122

[150] Tinge, J.T. and Drinkenburg, A.A. H., 1986; The Influence of Slight Departure from Vertical Alignment on Liquid Dispersion and Gas Holdup in a Bubble Column; *Chem. Eng. Sci.*, vol.41, No.1, pp.165-169

[151] Todt, J., Lucke, J., Schugerl, K. and Renken, A., 1977; Gas Holdup and Longitudinal Dispersion in Different Types of Multiphase Reactors and Their Application for Microbial Processes; *Chem. Eng. Sci.*, vol.32 , pp.369-375

[152] Towell, D.D. and Ackerman, G.H., 1972; Axial Mixing of Liquid and Gas in Large Bubble Reactors; *Proceedings of the Fifth European/Second International Symposium on Chemical Reaction Engineering*, Amsterdam

[153] Turner, J.C.R., 1966; On Bubble Flow in Liquids and Fluidized Beds; *Chem. Eng. Sci.*, vol.21, pp.971

[154] Turner, J.C.R., 1976; Two-Phase Conductivity: The Electrical Conductance of Liquid Fluidized Beds of Spheres; *Chem. Eng. Sci.*, vol.31, pp.487-492

[155] Ueyama, K. and Miyauchi, T., 1979; Properties of Recirculating Turbulent Two Phase Flow in Gas Bubble Columns; *AIChE J.*, vol.25, pp.258-266

[156] Ueyama, K., Tsuru and Furusaki, S., 1989; Flow Transition in a Bubble Column; *Int. Chem. Sci.*, vol.29, No.3, pp.523-529

[157] Uribe-Salas, A.; private communication, 1990

[158] Wakao, N. and Kaguei, S., 1982; Head and Mass Transfer in Packed Beds; *Gordon and Breach*, New York

[159] Wallis, G.B., 1962; Proceedings of the Symposium on the Interaction between Fluids and Particles; (ed., Rottenberg, P.A.); London: *Institution of Chemical Engineers*

[160] Wallis, G.B., 1969; One Dimensional Two-Phase Flow; *McGraw-Hill*, N.Y., chpt.9

[161] Westerterp, K.R., Swaaij, W.P. van and Beenackers, A.A.C.M., 1984; Chemical Reactor Design and Operations; 2nd ed., *John Wiley*, Chichester

[162] Whalley, P.B. and Davidson, J.F., 1974; Liquid Circulation in Bubble Columns; *Inst. Chem. Eng. Symp.* Ser. No.38

[163] Wheeler, D.A., 1966; Big Flotation Column Mill Tested; *E & MJ*, vol.167, No.11, pp.98-99

[164] Wheeler, D.A., 1988; Historical View of Column Flotation Development; in *Column Flotation '88* (ed., Sastry, K.V.S.), SME Annual Meeting Phoenix, Arizona, pp.3-4

[165] Xu, M., 1987; Sparger Study in Flotation Columns; Master's Thesis, McGill University, Canada

[166] Xu, M., Finch, J.A. and Yianatos, J.B., 1987; Carrying Capacity in Column Flotation -- Bubble Size and Gas Rate Effects; presented at *the Annual Conference of Metallurgists, CIM*, Winnipeg

[167] Xu, M. and Finch, J.A., 1989a; Effect of Sparger Surface Area on Bubble Diameter in Flotation Columns; *Canadian Metall. Q.*, vol.28, No.1, pp.1-6

[168] Xu, M., Uribe-Salas, A., Finch, J.A. and Gomez, C.O., 1989b; Gas Rate Limitation in Column

Flotation; in *Processing of Complex Ores* (Eds. Dobby, G.S. and Rao, S.R.), pp.387-407

[169] Xu, M., Uribe-Salas, A. and Finch, J.A. , 1990a; Maximum Gas and Bubble Surface Rates in Flotation Columns; Submitted to *Int. J. Min. Process.*

[170] Xu, M. and Finch, J.A., 1990b; Simplification of Bubble Size Estimation in a Bubble Swarm; accepted in *J. Colloid & Interface Sci.*

[171] Xu, , Finch, J.A. and Laplante, A.R., 1990c; Numerical Solution to Axial Dispersion Model in Flotation Column Studies; *Canadian Met. Q.*, in press

[172] Xu, M. and Finch, J.A., 1990d; The Axial Dispersion Model in Flotation Column Studies; *Minerals Engineering*, in press

[173] Yang, D.C., 1988; A New Packed Column Flotation System; in *Column Flotation'88* (ed., Sastry, K.V.S.), *SME Annual Meeting*, pp.257-265

[174] Yianatos, J.B., Laplante, A.R. and Finch, J.A, 1985; Estimation of Local Gas Holdup in the Bubbly and Froth zones; *Chem. Engng. Sci.*, vol.40, No.10, pp.1965-1968

[175] Yianatos, J.B., 1987; Column Flotation Froths; Ph.D. thesis, McGill University, Canada

[176] Yianatos, J.B., Finch, J.A. and Laplante, A.R., 1987; Cleaning Action in Column Flotation Froths; *Trans. I.M.M.*, vol.96, pp.C199-C205

[177] Yianatos, J.B., Finch, J.A., Dobby, G.S. and Xu, M., 1988a; Bubble Size Estimation in a Bubble Swarm; *J. Colloid & Interface Sci.*, vol.126, No.1, pp.37-44

[178] Yianatos, J.B. and Finch, J.A., 1990; Gas Holdup vs. Gas Rate in the Bubbly Regime; *Int. J. Min. Process.*, vol.29, pp.141-146

[179] Yoon, R.H., Adel, G.T. and Lutrell, G.H., 1987; Development of the Microbubble Flotation Process; in *Processing and Utilization of High Surfur Coals II* (ed., Y.P. Chugh and R.D. Caudle)

[180] Young, P., 1982; Flotation Machines; *Mining Magazine*, vol.146, pp.35-59

APPENDIX 1

GAS HOLDUP CALCULATION USING BUBBLY FLOW MODEL

The following program written in FORTRAN is used to calculate gas rate as a function of gas holdup (it is similar to that of gas holdup as a function of gas rate) for a given set of operating conditions, using the bubbly flow model developed in this work (section 2.3). The given parameters (input variables) are,

C = ?; bubble diameter at J_g=1.0cm/s
J_l = ?; liquid down velocity, cm/s
m = ?; constants, two choices

The choices for m values are either m=2.0 (simplified case) or given as a function of *Re* (programmed). To solve the complex equations of bubbly flow model, Secant method (refer to any numerical textbook) is used and outlined here.

For only a particular value of x_i (root), a function $f(x_n)$=0. Let x_1, x_2 be any two values (approximately near the root, x_i), the x_3 which is closer to the real solution than x_1, x_2 is obtained by,

$$x_3 = \frac{x_1 f(x_2) - x_2 f(x1)}{f(x_2) - f(x_1)} \qquad (A.1)$$

By exchanging x_1=x_2, x_2=x_3 and repeatedly using Eq.(A1.1), a new x_n can found. When,

$$f(x_n) = \epsilon(\epsilon - 10^{-8}) \qquad (A.2)$$

x_n is the solution to function $f(x)$=0. The program is listed as follows.

```
C
C       Calculating gas holdup using bubbly flow model
C       PROGRAM: DRIFT4.FOR
C
        IMPLICIT REAL*8(A-Z)
        INTEGER I,K
        DIMENSION EG(40),JG(40),N(40),UT(40),DB(40),RE(40)
        OPEN (2,FILE='B:DATA.PRN')
        JL=0.50D0
        C=0.075D0
        DO 40 I=1,30
              EG(I)=0.025D0*I
              JGJ1=0.5D0
              JGJ2=2.0D0
              K=0
10      CALL SECANT1(JGJ1,UTU1,RER1,DBD1,M1,C)
        CALL SECANT2(F1,JGJ1,UTU1,EG(I),M1)
        CALL SECANT1(JGJ2,UTU2,RER2,DBD2,M2,C)
        CALL SECANT2(F2,JGJ2,UTU2,EG(I),M2)
        JGJ3=(JGJ1*F2-JGJ2*F1)/(F2-F1)
        CALL SECANT1(JGJ3,UTU3,RER3,DBD3,M3,C)
        CALL SECANT2(F3,JGJ3,UTU3,EG(I),M3)
        A=DABS(F3)
        K=K+1
        IF (A.LT.1.0D-7) GOTO 20
        IF (K.GT.100) GOTO 20
        JGJ1=JGJ2
        JGJ2=JGJ3
        GOTO 10
20      JG(I)=JGJ3
        UT(I)=UTU3
        RE(I)=RER3
        N(I)=M3
        DB(I)=DBD3
        WRITE (*,30) EG(I),JG(I),DB(I)
        WRITE (2,30) EG(I),JG(I),DB(I)
30      FORMAT (4X,6(F8.4,4X))
40      CONTINUE
        CLOSE(2)
        STOP
        END
C
        SUBROUTINE SECANT1(JGJ,UT,RE,DBD,M,C)
        IMPLICIT REAL*8(A-Z)
        INTEGER I,K
        DBD=C*JGJ**0.25
        UTU=48.9D0*DBD**0.514-0.309D0/DBD
10      RE=DBD*UTU/0.01D0
        UT=980.0D0*DBD*DBD/(18.0D0*0.01*(1.0D0+0.15*RE**0.687))
        A=DABS(UTU-UT)
        IF (A.LT.0.0001) GOTO 20
```

```
      UTU=UT
      GOTO 10
C20   M=4.45D0*RE**(-0.1)
20    M=2
      RETURN
      END
C
      SUBROUTINE SECANT2(F,JGJ,UT,EG,M)
      IMPLICIT REAL*8(A-Z)
      INTEGER I,K
      JL=0.38D0
      F=JGJ-UT*EG*(1.0D0-EG)**(M-1.0D0)-JL*EG/(1.0D0-EG)
      RETURN
      END
```

The model fit (solid lines) in Figure 2.4 is calculated using this program.

APPENDIX 2

ESTIMATION OF BUBBLE SIZE USING BUBBLY FLOW MODEL

The following program written in QuickBASIC is used to calculate bubble size for a given set of operating conditions, mainly gas holdup, gas rate and liquid rate. The choices for m values are either $m=2.0$ (simplified case) or given as a function of Re (programmed). To solve the complex equations of bubbly flow model, Secant method is used and outlined in Appendix 1.

```
DECLARE SUB SLIP (X!, F!)    'PROGRAM:SIZE.BAS
COMMON SHARED /DATA1/ JG, JL, EG, G, UL, PL, M
LOCATE 12, 25: PRINT "**********************************"
LOCATE 13, 25: PRINT "**        BUBBLE SIZE         **"
LOCATE 14, 25: PRINT "**     ESTIMATION PROGRAM     **"
LOCATE 15, 25: PRINT "**********************************"
CLS
LOCATE 12, 25: INPUT "(1) SUP GAS RATE (cm/s) = "; JG
LOCATE 13, 25: INPUT "(2) SUP LIQ RATE (cm/s) = "; JL
LOCATE 14, 25: INPUT "(3) GAS HOLDUP   (%)   = "; EG
X1 = 2                'assume a bubble size
CLS
EG = EG / 100: X2 = X1 * .5
G = 980: UL = .01: PL = 1!
```

```
        I = 1: X = X1
10      CALL SLIP(X1, F1)       'call subroutine
        CALL SLIP(X2, F2)
        XN = (X1 * F2 - X2 * F1) / (F2 - F1)
        X = XN
        CALL SLIP(XN, F3)
        FD = ABS(F3)
        IF FD < .00001 THEN GOTO 20
        IF I > 60 THEN GOTO 30
        X1 = X2: X2 = XN
        I = I + 1
        GOTO 10
20      CLS : LOCATE 12, 25: PRINT "(1) SUP GAS RATE (cm/s) = "; JG
        LOCATE 13, 25: PRINT "(2) SUP LIQ RATE (cm/s) = "; JL
        LOCATE 14, 25: PRINT "(3) GAS HOLDUP     (%)  = "; EG * 100; "%"
        X = INT(X * 10000 + .5) / 1000
        LOCATE 15, 25: PRINT "(4) BUBBLE SIZE   (mm)  = "; X
        LOCATE 16, 25: PRINT "(5) parameter   m  ="; M
        LOCATE 20, 30: PRINT "The variance = "; FD
        END
30      CLS : LOCATE 15, 30: PRINT "Please check input data": END
        SUB SLIP (X, F)
        VS = JG / EG + JL / (1 - EG)
        REB = VS * X * PL / UL
        'M = 2          'user can define m=2
        M = 4.45 * REB ^ (-.1)
        UT = G * X ^ 2 * PL / (18 * UL * (1 + .15 * REB ^ .687))
        US = UT * (1 - EG) ^ (M - 1)
        F = US - VS
        END
```

The principle of calculation scheme is illustrated in Figure 2.6.

APPENDIX 3

CALCULATION OF SOLIDS EFFECT ON GAS HOLDUP

The following program written in FORTRAN is used to calculate gas holdup under three conditions: (a) no solids; (b) all solids loaded on bubbles; and (c) all solids in suspension, for a given combination of gas rate, liquid rate and solid particles (reflecting on the bubble-particle aggregate density or slurry density).

```
C
C       PROGRAM FOR CALCULATING THE
C       EFFECT OF SOLIDS ON GAS HOLDUP
C       PROGRAM: SOLIDS.FOR
C
C       parameter definitions:
C       JL      : superficial liquid down velocity (cm/s)
C       JG      : superficial gas rate (cm/s)
C       UL      : slurry viscosity (g/cm^2 s)
C       DB      : bubble size (cm)
C       PB      : bubble-particle aggregate density (g/cm^3)
C       PSL     : slurry density (g/cm^3)
C       UT      : bubble terminal velocity (cm/s)
C       RE      : bubble Reynolds number
C       M       : constant
C       EG      : gas holdup being computed
C
        IMPLICIT REAL(A-Z)
        INTEGER I,K
        JL=0.50
        UL=0.01
        JG=1.0
        DB=0.20
        PB=0.0
        PSL=1.20
        UTU=48.9*DB**0.514-0.30 /DB
10      RE=DB*UTU/UL
        UT=980*DB*DB*(PSL-PB)/(18*UL*(1+0.15*RE**0.687))
        A=ABS(UTU-UT)
        IF (A.LT.0.0001) GOTO 20
        UTU=UT
        GOTO 10
C20     M=4.45*RE**(-0.1)
20      M=2.0
        CALL SECANT(JG,UT,EG,M,JL,A)
        WRITE (*,*) JG,A
        WRITE (*,25) JG,EG,DB,UT
25      FORMAT (2X,6(F10.4,2X))
        STOP
        END
C
        SUBROUTINE SECANT(JG,UT,X,M,JL,A)
        IMPLICIT REAL(A-Z)
        INTEGER I,J
        X1=0.02
        X2=0.2
        I=0
10      F1=JG-UT*X1*(1-X1)**(M-1)-JL*X1/(1-X1)
        F2=JG-UT*X2*(1-X2)**(M-1)-JL*X2/(1-X2)
        X3=(X1*F2-X2*F1)/(F2-F1)
        I=I+1
```

```
      F3=JG-UT*X3*(1-X2)**(M-1)-JL*X3/(1-X3)
      A=ABS(F3)
      IF (A.LT.1E-6) GOTO 20
      IF (I.GT.200) GOTO 20
      X1=X2
      X2=X3
      GOTO 10
20    X=X3
      RETURN
      END
```

Figure 2.7 is calculated using this program.

APPENDIX 4

CALCULATION OF CIRCULATION VELOCITY PROFILES FOR NEWTONIAN FLUID

For Newtonian fluids, the shear stress is linearly proportional to the velocity gradient. An analytical solution is obtained for the calculation of liquid circulation velocity profile (Chapter 3, Section 3.3). This program is written in FORTRAN.

```
C
C     PROGRAM  FOR CALCULATING CIRCULATION
C     VELOCITY PROFILE USING Clark's MODEL
C     FOR Newtonian FLUID
C     PROGRAM: newton.for
C
      IMPLICIT REAL(A-Z)
      INTEGER I,N,M,K
      COMMON V(51),PH(51)
      COMMON PL,G,MU,EGC,N,R,PI
      OPEN (2,FILE='B:DATA.PRN')
C
C     parameter definition
C     PL     : liquid density (g/cm^3)
C     G      : gravity acceleration (9.8 m/s^2)
C     MU     : liquid viscosity (0.01 cm/g.s)
C     EGC    : gas holdup at column centre (0.2)
C     N      : power index of the gas holdup profile
C     TW     : shear stress at the wall, to be adjusted
C     QL     : net volumetric liquid flowrate (cm^3/s)
C     V(I)   : circulation velocity at some radius (m/s)
```

```
C       PH(I)   : dimensionless radial position (r/R)
C       R       : radius (R=1.0)
C
        PL=1.0
        G=9.8
        MU=0.01
        EGC=0.40
        R=1.0
        PI=3.1415926
        N=3
        M=0
        TW1=-2.05
        TW2=2.05
10      CALL SECAND(TW1,G1)
        CALL SECAND(TW2,G2)
        TW3=(G1*TW2-G2*TW1)/(G1-G2)
        CALL SECAND(TW2,G3)
        IF (M.GT.100) GOTO 20
        IF (ABS(G3).LT.1E-3) GOTO 20
        TW1=TW2
        TW2=TW3
        M=M+1
        WRITE (*,*) TW3,G3
        GOTO 10
20      WRITE (*,30) TW3,G3
        WRITE (2,30) TW3,G3
30      FORMAT (2X,'TW =',F8.4,4X,'QL =',F8.4)
        DO 40 I=1,51
        WRITE (2,50) I,PH(I),V(I)
40      CONTINUE
50      FORMAT(2X,I3,2X,2(F8.4,2X))
        CLOSE(2)
        STOP
        END
C
        SUBROUTINE SECAND(TW,QL)
        IMPLICIT REAL(A-Z)
        INTEGER I,N,M,K
        COMMON V(51),PH(51)
        COMMON PL,G,MU,EGC,N,R,PI
        DO 10 I=1,51
        PH(I)=(I-1)/50.0
        A=TW/R/MU+G*PL*EGC/MU/(N+2)
        B=-G*PL*EGC/MU/(N+2)/R**N
        C=-A*R*R/2-B*R**(2+N)/(2+N)
        V(I)=A/2*PH(I)**2+B/(N+2)*PH(I)**(N+2)+C
10      CONTINUE
C
C       using Simpson's rule to calculate NET liquid flowrate
C
        QL=0.0
```

```
      DO 20 I=2,50
      QL=QL+2*V(I)*PH(I)
      IF (I.NE.I/2*2) QL=QL+2*V(I)*PH(I)
20    CONTINUE
      QL=1.0/50/3*(V(1)*PH(I)+QL+V(51)*PH(51))*2*PI
      RETURN
      END
```

Figures 3.7 (ϵ_{gc}=0.2 for various values of n) and 3.8 (n=3 for various values of ϵ_{gc}) are calculated using this program.

APPENDIX 5

CALCULATION OF CIRCULATION VELOCITY PROFILES FOR NON-NEWTONIAN FLUID

For non-Newtonian fluids, the shear stress is a complex function of the velocity gradient and the turbulence. Analytical solution can not be obtained and numerical solution is used for the calculation of liquid circulation velocity profile (Chapter 3, Section 3.3.1). This program is written in FORTRAN.

```
C
C     PROGRAM FOR  CALCULATING CIRCULATION
C     VELOCITY PROFILE USING Clark's MODEL
C     FOR NON-Newtonian FLUID
C     PROGRAM: nonnew.for
C
      IMPLICIT REAL*8(A-Z)
      INTEGEk I,J,L
      COMMON XX(51),E(51),P(51),PP(51),T(51),PH(51),V(51)
      COMMON R,EGC,PL,M,PA,N,K,G,PI
      OPEN(2,FILE='B:DATA4.PRN')
C
C     parameter definition
C
C     PL     : liquid density (cm^3/s)
C     G      : gravity acceleration (980 cm/s^2)
C     EGC    : gas holdup at column centre
C     E(I)   : gas holdup at some radius
C     P(I)   : local mean density of gas and liquid mixture
C     PP(I)  : mean density within some radius
C     PA     : average density over column cross-section
```

```
C       N       : power of gas holdup profile
C       TW      : shear stress at the wall, to be adjusted
C       QL      : net volumetric liquid flowrate (cm^3/s)
C       V(I)    : circulation velocity at some radius (m/s)
C       PH(I)   : dimensionless radial position (r/R)
C       R       : radius (R=1.0)
C       XX(I)   : dV/dr at some radius
C       T(I)    : shear stress at some radius
C       K       : coefficient of dV/dr
C       M       : power of dV/dr
C
        R=1.0D0
        EGC=0.2D0
        PL=1.0D0
        N=3.0D0
        G=9.8D0
        PI=3.1415926D0
        K=0.1D0
        M=1.0D0
C
        DO 10 I=1,51
        PH(I)=(I-1)/50.0D0
        E(I)=EGC*(1.0-PH(I)**N)
        P(I)=PL*(1.0-E(I))
        PP(I)=PL*(1.0-EGC)+2.0*PL*EGC/(2.0+N)*PH(I)**N
10      CONTINUE
        PA=PL*(1.0-EGC)+2.0*PL*EGC/(2.0+N)
C
        L=0
        TW1=3.17D0
        TW2=3.12D0
20      CALL ROOT(TW1,G1)
        CALL ROOT(TW2,G2)
        TW3=(G1*TW2-G2*TW1)/(G1-G2)
        CALL ROOT(TW3,G3)
        IF (L.GT.100) GOTO 30
        IF (DABS(G3).LT.1D-4) GOTO 30
        TW1=TW2
        TW2=TW3
        L=L+1
        WRITE (*,*) TW3,G3
        GOTO 20
30      WRITE (*,40) K,N
40      FORMAT (5X,'K  = ',F6.3,5X,'n = ',F6.3)
        WRITE (*,50) TW3, G3
50      FORMAT (8X,'Tw = ',F10.8,8X,'QL = ',F10.8)
        DO 60 I=1,51
        WRITE (2,70) I,PH(I),V(I)*1000
60      CONTINUE
70      FORMAT (6X,I3,5X,2(F8.4,5X))
        CLOSE(2)
```

```
      STOP
      END
C
      SUBROUTINE ROOT(TW,QL)
      IMPLICIT REAL*8(A-Z)
      INTEGER I,J,L
      COMMON XX(51),E(51),P(51),PP(51),T(51),PH(51),V(51)
      COMMON R,EGC,PL,M,PA,N,K,G,PI
      DO 10 I=1,51
      T(I)=TW*(1.0+R*G*(PA-PP(I))/(2.0*TW))*PH(I)
10    CONTINUE
      CALL ROOTT
      CALL FINITE
C
C     using simpson's rule to calculate liquid flowrate
C
      QL=0.0
      DO 20 I=1,51
      QL=QL+2*V(I)*PH(I)
      IF (I.NE.I/2*2) QL=QL+2.0*V(I)*PH(I)
20    CONTINUE
      QL=1.0/50.0/3.0*(V(1)*PH(1)+QL+V(51)*PH(51))*2.0*PI
      RETURN
      END
C
C     using secand method to calculate dV/dr
C
      SUBROUTINE ROOTT
      IMPLICIT REAL*8(A-Z)
      INTEGER I,J,L
      COMMON XX(51),E(51),P(51),PP(51),T(51),PH(51),V(51)
      COMMON R,EGC,PL,M,PA,N,K,G,PI
      DO 30 I=1,51
      AX1=-0.15D0
      AX2=-0.5D0
      L=0
20    AX=(F(AX1,I)*AX2-F(AX2,I)*AX1)/(F(AX1,I)-F(AX2,I))
      L=L+1
      IF (L.GT.100) GOTO 25
      IF (DABS(F(AX,I)).LT.1D-8) GOTO 25
      AX1=AX2
      AX2=AX
      GOTO 20
25    XX(I)=AX
30    CONTINUE
      RETURN
      END
C
      DOUBLE PRECISION FUNCTION F(AX,I)
      IMPLICIT REAL*8(A-Z)
      INTEGER L,I,J
```

```
      COMMON XX(51),E(51),P(51),PP(51),T(51),PH(51),V(51)
      COMMON R,EGC,PL,M,PA,N,K,G,PI
      AL=R*(0.14-0.08*PH(I)**2-0.06*PH(I)**4)
      F=T(I)-K*DABS(AX)**M+AL**2*P(I)*DABS(AX)*AX
      RETURN
      END
C
C     using finite difference method to calculate V(I)
C
      SUBROUTINE FINITE
      IMPLICIT REAL*8(A-Z)
      INTEGER L,I,J
      COMMON XX(51),E(51),P(51),PP(51),T(51),PH(51),V(51)
      COMMON R,EGC,PL,M,PA,N,K,G,PI
      XH=R/50.0D0
      V(51)=0.0D0
      V(50)=-XH*XX(51)
      DO 10 I=50,2,-1
      V(I-1)=V(I+1)-2.0D0*XH*XX(I)
10    CONTINUE
      RETURN
      END
```

Figure 3.10 (ϵ_{gc}=0.2, n=3 and p=1) for various values of K and is calculated using this program.

APPENDIX 6

NUMERICAL SOLUTION TO AXIAL DISPERSION MODEL USING FINITE DIFFERENCE METHOD

Numerical solution to the axial dispersion model (closed-closed boundary conditions) using the finite difference method is described in detail in Section 4.2.1. The computer program written in FORTRAN is listed here.

```
C
C     THIS PROGRAM SOLVES THE AXIAL DISPERSION
C     MODEL USING FINITE DIFFERENCE METHOD
C     PROGRAM: numer2.for
C
      IMPLICIT REAL(A-Z)
      INTEGER I,J,K,M,N,M1
      DIMENSION F(4001),E(41),E0(41)
      OPEN(2,FILE='B:DATA1.PRN')
```

```
C
C     parameter definitions
C     M       : number of the sections for a total length, X=1
C     N       : number of time interval for a total time, T
C     DX      : width of each section, DX=1/M
C     DT      : time increment <0.001
C     DN      : vessel dispersion number
C     A,B,C   : coefficients
C
      M1=21
      M=M1-1
      DX=1.0/FLOAT(M)
      DT=0.001
      N=4000
      DN=0.25
      A=DN*DT/DX/DX+DT/DX/2.0
      B=1-2.0*DN*DT/DX/DX
      C=DN*DT/DX/DX-DT/DX/2.0
      WRITE (*,10) A,B,C
C
10    FORMAT (5X,'A  =',F8.4,5X,'B =',F8.4,5X,'C =',F8.4)
      WRITE (*,20)
20    FORMAT (15X,'constant A, B, C must be POSITIVE')
      WRITE (*,30)
30    FORMAT (15X,'ENTER to continue, or control-break to stop')
      PAUSE
      DO 40 I=1,M1
      E0(I)=0.0
      E(I)=0.0
40    CONTINUE
      DO 60 J=1,N
      IF (J.EQ.1) THEN
      E(1)=DX*M/(DX+DN)
      ELSE
      E(1)=DN*E0(2)/(DX+DN)
      ENDIF
      DO 50 I=2,M
      E(I)=A*E0(I-1)+B*E0(I)+C*E0(I+1)
50    CONTINUE
      E(M1)=E0(M)
      IF (J.EQ.J/100*100) THEN
      WRITE (*,*) J*DT,E(1),E(M1)
      ENDIF
      DO 55 I=1,M1
      E0(I)=E(I)
55    CONTINUE
      F(J)=E(M1)
60    CONTINUE
      SUM1=0.0
      DO 70 J=1,N
      SUM1=SUM1+F(J)*DT
```

```
70      CONTINUE
        DO 80 J=1,N
        IF (J.EQ.J/50*50) THEN
        F(J)=F(J)/SUM1
        WRITE (2,90) J*DT,F(J)
        ENDIF
80      CONTINUE
90      FORMAT(2X,F4.2,2X,F7.4,2X)
        CLOSE(2)
        STOP
        END
```

Figures 4.10, 4.11, 4.12 and 4.13 are calculated using this program. In calculating Figure 4.12, the 3-dimensional plot, output of the program is modified. Or, sampling at any time and at any position can be obtained just by slightly modifying the output routine of the program.

APPENDIX 7

CALCULATION OF RTD CURVES USING THE SOLUTION TO STEP TRACER INJECTION UNDER STEADY STATE

The difficulty in calculating RTD curves from this solution (eq.4.42) is to compute the complimentary error function *erfc(z)*, which has the form,

$$erfc(z) = 1 - erf(z) = \frac{1}{\sqrt{\pi}} \int_z^{\infty} \exp(-y^2)\, dy \qquad (A.3)$$

This integration is computed using Simpson's Rule, which belongs to the group of the Newton-Cotes formulas. Since this method is extensively used in the thesis for the integration of complex function, it is outlined here for easy reference. For an integration as,

$$I = \int_a^b f(x)\, dx \qquad (A.4)$$

Using Simpson's Rule, the following equation can be obtained,

$$\int_a^b f(x)\,dx = \frac{h}{3}[f(a)+4f(a+h)+2f(a+2h)+4f(a+3h)+\cdots + \cdots +2f(a+\{2n-2\}h)+4f(a+\{2n-1\}+f(b)] \quad \text{(A.5)}$$

The above equation can be easily program as follows,

```
      F=0.0
      N=?
      H=(A-B)/N
      DO 10 I=1, N
      X=A+I*H
      TERM=F(X)
      F=F+2*TERM
      IF (I.NE.2/2*2) F=F+2*TERM
      IF (ABS(TERM).LT.1E-8) GOTO 20
10    CONTINUE
20    F=H/3.0*(F(A)+F+F(B))
```

The program is listed as follows.

```
      IMPLICIT REAL(A-Z)
      INTEGER I,J,K,M,N
      DIMENSION E(100),T(100)
      OPEN (2,FILE='B:DATA1.PRN')
      VESS=0.05
      DO 10 I=1,100
      T(I)=0.05*(I-1)
10    CONTINUE
      T(1)=0.01
      DO 20 I=1,100
      X1=(0.25/T(I)/VESS)**0.5*(1-T(I))
      CALL SIMPS(X1,Y1)
      X2=(1+T(I))/(4.0*VESS*T(I))**0.5
      CALL SIMPS(X2,Y2)
      A1=(T(I)/3.1415926/VESS)**0.5*(3.0+(1+T(I))/(2.0*VESS))
      A2=EXP(-(1-T(I))**2/T(I)/(4.0*VESS))
      A3=0.5+(3.0+4.0*T(I))/(2*VESS)+(1.0+T(I))**2/(4.0*VESS*VESS)
      A4=EXP(1.0/VESS)
      E(I)=1-0.5*YHxA1*A2+A3*A4*Y2
      WRITE (*,*) I,T(I),E(I)
20    CONTINUE
      DO 30 I=1,100
      WRITE (2,40) T(I),E(I)
30    CONTINUE
40    FORMAT (3X,2(F8.4,2X))
      STOP
      END
C
```

```
      SUBROUTINE SIMPS(X,Y)
      IMPLICIT REAL(A-Z)
      INTEGER I,J,K
      F=0.0
      DO 10 I=1,10000
      XX=0.005*I+X
      TERM=EXP(-XX**2)
      F=F+2*TERM
      IF (I.NE.I/2*2) F=F+2*TERM
      IF (I.NE.2000) GOTO 10
      IF (ABS(TERM).LE.1E-16) GOTO 20
10    CONTINUE
20    Y=0.005/3.0*(EXP(-X**2)+F)*2/3.1415926**0.5
      RETURN
      END
```

Figure 4.13 is calculated using this program.

APPENDIX 8

SOLUTION TO THE TANKS-IN-SERIES MODEL AND CALCULATION OF VESSEL DISPERSION NUMBER

Theoretical RTD is easily computed from the tanks-in-series model. The $\gamma(n)$ function is calculated using Simpson's Rule. The variance of the theoretical RTD curve is the inverse of N value (the number of well-mixed equal tanks), which is related to the vessel dispersion number. This program written in FORTRAN calculates a theoretical RTD curve and the vessel dispersion number for a given number of tanks.

```
C
C     THIS PROGRAM COMPUTES THE RTD IN A CONTINUOUS
C     SYSTEM USING TANKS IN SERIES MODEL
C           program: tanks1.for
C
      IMPLICIT REAL*8(A-Z)
      INTEGER I,J,K,M
      DIMENSION T(100),EMODEL(100)
      OPEN (2,FILE='B:COMD3.PRN')
      N=10.52632
C
```

```
C       CALCULATE THE DISPERSION NUMBER
C
        I=1
        X1=0.005D0
        X2=0.2D0
10      F1=2.0*X1-2.0*X1*X1*(1.0-DEXP(-1.0/X1))-1.0/N
        F2=2.0*X2-2.0*X2*X2*(1.0-DEXP(-1.0/X2))-1.0/N
        X=(X1*F2-X2*F1)/(F2-F1)
        I=I+1
        FX=2.0*X-2.0*X*X*(1.0-DEXP(-1.0/X))-1.0/N
        A=DABS(FX)
        IF (A.LT.1.0E-10) GOTO 20
        IF (I.GT.100) GOTO 20
        X1=X2
        X2=X
        GOTO 10
20      WRITE (*,30) N
30      FORMAT (15X,'NUMBER OF TANKS   =',F12.4)
        WRITE (*,40) X
40      FORMAT (15X,'DISPERSION NUMBER =',F12.4)
C
C       USING SIMPSON'S METHOD TO CALCULATE INTEGRATION
C
        F=0.00
        DO 50 J=1, 10000
        XX=0.005*J
        TERM=2*XX**(N-1)*EXP(-XX)
        F=F+TERM
        IF (J.NE.J/2*2) F=F+TERM
        IF (J.LE.5000) GOTO 50
        IF (DABS(TERM).LE.1E-10) GOTO 60
50      CONTINUE
60      F=0.005/3.0*(F+1.0)
C
C       CALCULATE THE THEORETICAL RTD
C
        DO 70 I=1,70
        T(I)=0.05*I
        EMODEL(I)=1.0/F*N*(N*T(I))**(N-1)*DEXP(-N*T(I))
70      CONTINUE
        DO 75 I=1,70
        WRITE (2,80) T(I),EMODEL(I)
75      CONTINUE
80      FORMAT (5X,3(F12.4,5X))
        CLOSE(2)
        STOP
        END
```

Figure 4.16 is calculated using this program.

APPENDIX 9

NUMERICAL SOLUTION TO BACKFLOW COMPARTMENT MODEL

Theoretical RTD is computed from the backflow compartment model using finite difference method. The age distribution inside the column can be obtained just by taking value of concentration in the required compartments.

```
C
C     THIS PROGRAM SOLVES THE BACKFLOW MIXING
C     MODEL USING FINITE DIFFERENCE METHOD
C     PROGRAM: backflow.for
C
      IMPLICIT REAL*8(A-Z)
      INTEGER I,J,K,N
      DIMENSION E(61),E0(61),F(35000)
      OPEN(2,FILE='B:A1.PRN')
C
C     parameter definitions
C
C     N      : NUMBER OF THE SECTIONS FOR A TOTAL LENGTH, L
C     DT     : TIME INTERVAL < 0.001
C     PHI    : THE BACKFLOW RATIO
C
      N=20
      DT=0.001D0
      NT=3500
      PHI=5.0
      DO 10 I=1,N
      E0(I)=0.0D0
      E(I)=0.0D0
10    CONTINUE
      DO 40 K=1,NT
      A1=1.0-(1.0+PHI)*N*DT
      B1=PHI*N*DT
      IF (K.EQ.1) THEN
      E0(1)=N
      ENDIF
      E(1)=A1*E0(1)+B1*E0(2)
      DO 20 I=2,N-1
      A=(1.0+PHI)*N*DT
      B=1.0-(1.0+2.0*PHI)*N*DT
      C=N*PHI*DT
      E(I)=A*E0(I-1)+B*E0(I)+C*E0(I+1)
20    CONTINUE
      AN=1.0-(1.0+PHI)*N*DT
```

```
      BN=(1.0+PHI)*N*DT
      E(N)=AN*E0(N-1)+BN*E0(N)
      DO 30 I=1,N
      E0(I)=E(I)
30    CONTINUE
      F(K)=E(N)
      IF (K.EQ.K/50*50) THEN
      WRITE (*,*) K*DT,F(K)
      ENDIF
40    CONTINUE
      DO 60 K=1,NT
      IF (K.EQ.K/50*50) THEN
      WRITE (2,70) K*DT,F(K)
      ENDIF
60    CONTINUE
70    FORMAT (5X,2(F8.4,3X))
      CLOSE(2)
      STOP
      END
```

Figures 4.18 and 4.19 are calculated using this program.

APPENDIX 10

EXAMPLE OF MOMENTS AND RTD CALCULATION

Pulse Tracer Signal (Dirac Delta function)

In theory, a pulse tracer signal means an input into a vessel over an infinitely small or zero time. In practice, this can not be realized. Nevertheless, if the time required to inject the tracer is very small in comparison with the mean residence time of the fluid in the vessel, we can safely treat this input as a pulse signal. A special function, called Dirac Delta function, δ, is defined to describe this discontinuous signal. Thus, $\delta(t-t_0)$, is a distribution curve which is zero everywhere except at $t=t_0$ where it is infinite. Figure A.1 graphically shows the δ function. The area under the curve is unity and the width of the curve is zero, or,

$$\delta(t-t_0) = \infty, \quad at\ t=t_0$$
$$\delta(t-t_0) = 0, \quad elsewhere \tag{A.16}$$

Thus,

$$\int_{-\infty}^{\infty} \delta(t-t_0)\,dt=1 \tag{A.17}$$

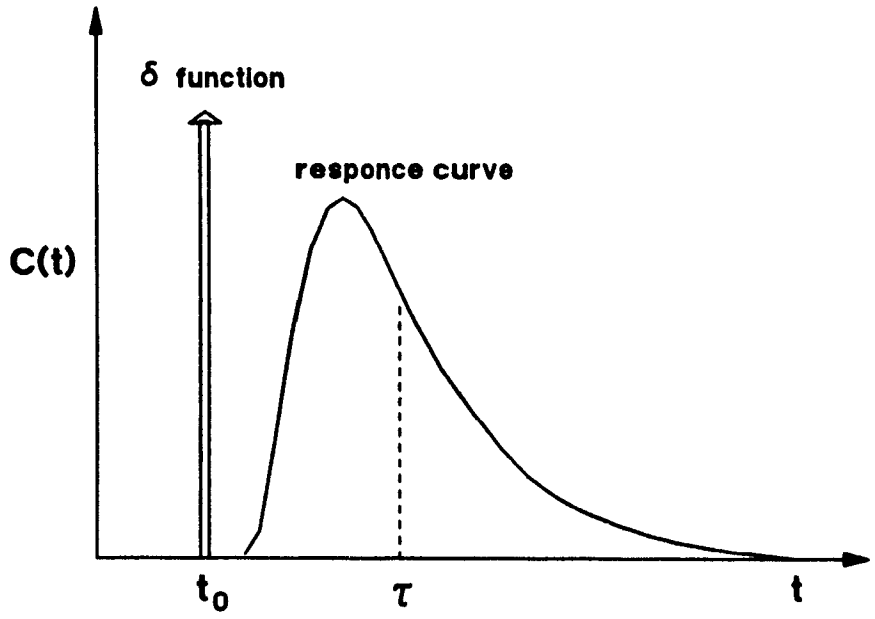

Figure A.1 Dirac delta function and response curve

Moments calculation from Raw Data

Several mathematical concepts which are essential in RTD studies are introduced here. These concepts are mainly used to normalize the RTD curves and to calculate the mean residence time and extent of mixing from the RTD data.

The tracer concentration vs. time curve (C vs. t) is called C-curve. The mean residence time of the vessel can be calculated from a C-curve, and given by,

$$\tau = \frac{\int_0^\infty tC\,dt}{\int_0^\infty C\,dt} \tag{A.18}$$

If the distribution curve is measured only at a number of discrete time values t_i, then

$$\tau = \frac{\sum_{i-1}^{n} t_i C_i \Delta t_1}{\sum_{i-1}^{n} C_i \Delta t_i} \tag{A.19}$$

The next important descriptive quantity is the spread of the distribution. This is commonly measured by the variance σ^2, defined as,

$$\sigma^2 = \frac{\int_0^\infty (t-\tau)^2 C\,dt}{\int_0^\infty C\,dt} \tag{A.20}$$

Once again, in discrete form,

$$\sigma^2 = \frac{\sum_{i-1}^{n} (t_i-\tau)^2 C_i \Delta t_i}{\sum_{i-1}^{n} C_i \Delta t_i} \tag{A.21}$$

The variance represents the squares of the spread of the distribution and has the unit of (time)^2. The dimensionless variance (σ_θ^2) is σ^2/τ^2. It is particularly used for matching experimental curves to one of the theoretical curves.

After the mean residence time of the curve is obtained, it is easy to normalize the distribution curve (C_θ vs t), given by,

$$C_\theta = \frac{C_i}{\sum_{i=1}^{n} C_i \Delta t_i} \tag{A.21}$$

which has the unit of (1/time). A dimensionless time is defined as,

$$\theta = \frac{t}{\tau} \tag{A.22}$$

Thus, the dimensionless RTD curve (E vs θ) is obtained by,

$$E = C_\theta \tau \tag{A.23}$$

Then area under the dimensionless RTD curve should be unity, that is,

$$\int_0^\infty E(\theta)\, d\theta = 1 \tag{A.24}$$

or

$$\sum_{i=1}^{n} E(\theta_i)\, \Delta\theta = 1 \tag{A.25}$$

For the RTD measurement technique commonly used in flotation column studies, the flotation column can be treated as a closed vessel. A closed vessel means that once the tracer has entered the vessel it does not move upstream from the entrance, and once it leaves the vessel, it does not return to the vessel. In this case, the dimensionless variance is related to the vessel dispersion number from the moments matching,

$$\sigma_\theta^2 = 2N_d - 2N_d^2[1-\exp(\frac{-1}{N_d})] \tag{A.26}$$

The vessel dispersion number N_d is the dimensionless variable indicating the degree of mixing, and is often used for design and scale-up.

Example Calculation

Table 1 presents the raw data (time vs. the voltage signal) obtained using the a pulse tracer input into a flotation column. The tracer injected was 20 ml KCl solution (20% wt., or 4g KCl). The volumetric discharge flowrate is 0.6 liter/min.

Step 1: Converting Voltage Signal to KCl Concentration

By calibration, a relationship was established between KCl concentration and relative voltage (voltage of solution - voltage of pure water). The calibration curve was,

$$KCl\ (\%) = 0.05\ (relative\ voltage)$$

Using the above correlation, Kcl concentration (%) is calculated and given in Table 1. Figure A.2 presents the concentration curve vs. time curve.

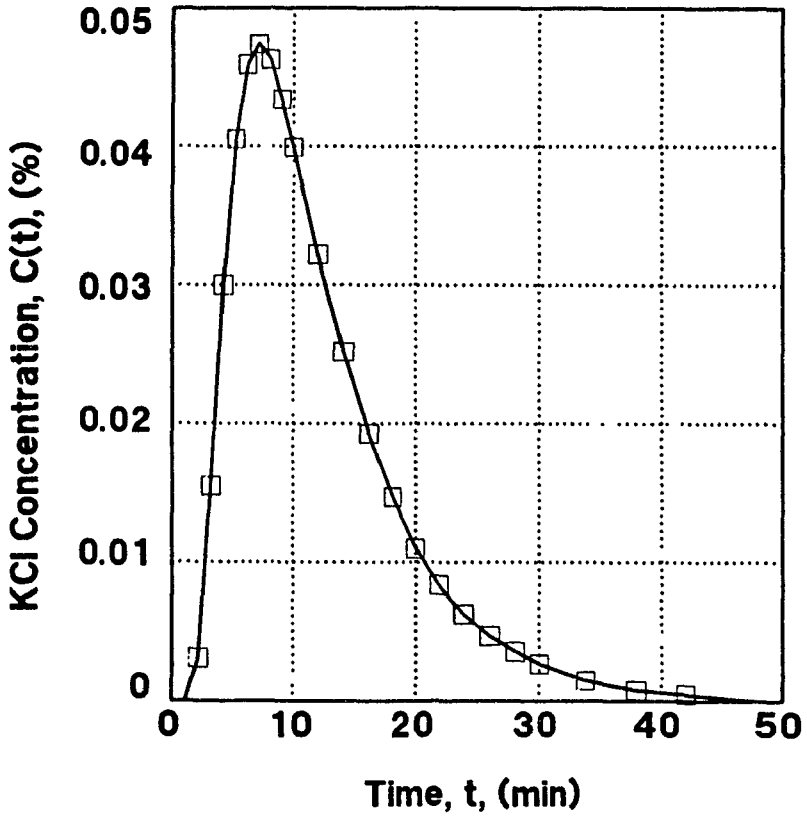

Figure A.2 Kcl concentration-time response curve

Step 2: Checking the Mass Balance

The area under the KCl concentration vs. time curves is,

$$I_1 = \sum_{i=1}^{25} C_i \Delta t_i = 0.6256 \ (\%\,\text{min})$$

The total mass of KCl detected at the exit,

$$G = Q_t I_1 = 0.6 X 0.6256 = 0.3754 (\%\cdot liter) = 3.754 (g)$$

This is sufficiently close to the amount injected and thus this test is valid. It is essential to check the mass balance before proceeding.

Step 3: Calculating the Mean Residence Time

$$I_2 = \sum_{i=1}^{25} t_i C_i \Delta t_i = 7.4972 (\text{min}\cdot\%\,\text{min})$$

$$\tau = \frac{I_2}{I_1} = 11.9840 (\text{min})$$

Step 5: Calculating the Variance and Vessel Dispersion Number

$$I_3 = \sum_{i=1}^{25} (t_i - \tau)^2 C_i \Delta t_i = 31.4602 (\text{min}^2\cdot\%\,\text{min})$$

$$\sigma^2 = \frac{I_3}{I_1} = 50.2853 (\text{min}^2)$$

$$\sigma_\theta^2 = \frac{50.2853}{11.9840^2} = 0.3501$$

The vessel dispersion number, N_d=0.224, is obtained by solving Equation (A.26). The vessel dispersion number obtained using this method is subject to the choice of cut-point of the RTD tail. The best method is to use least squares fit.

Step 6: Calculating Dimensionless RTD Curve

Dimensionless time θ vs. E is presented in Table A.1. Figure A.3 presents the dimensionless RTD curve.

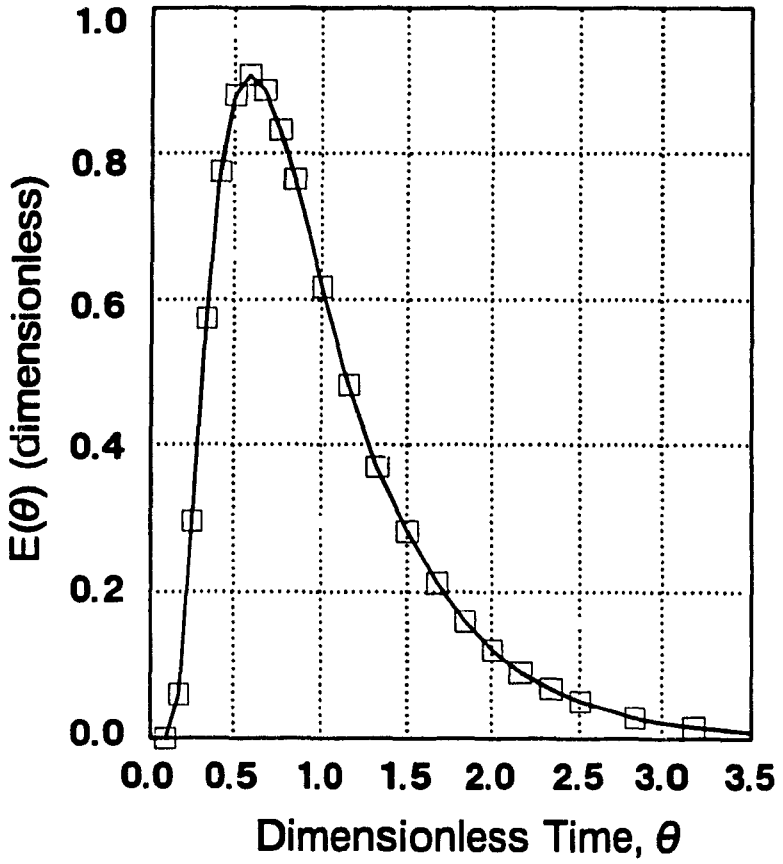

Figure A.3 Dimensionless RTD curve

Table A.1 RTD calculation

time (t, min)	KCl concentration		Dimensionless RTD	
	(volts)	(%)	θ	E
0	0.000	0.0000	0.000	0.000
1	0.000	0.0000	0.083	0.000
2	0.063	0.0031	0.167	0.060
3	0.309	0.0155	0.250	0.296
4	0.600	0.0300	0.334	0.575
5	0.810	0.0405	0.417	0.776
6	0.919	0.0459	0.501	0.880
7	0.948	0.0474	0.584	0.908
8	0.926	0.0463	0.668	0.887
9	0.869	0.0434	0.751	0.832
10	0.799	0.0399	0.835	0.765
12	0.644	0.0322	1.001	0.617
14	0.504	0.0252	1.168	0.482
16	0.385	0.0193	1.335	0.369
18	0.294	0.0147	1.502	0.281
20	0.221	0.0110	1.667	0.212
22	0.167	0.0084	1.836	0.160
24	0.126	0.0063	2.003	0.121
26	0.094	0.0047	2.170	0.090
28	0.071	0.0036	2.337	0.068
30	0.054	0.0027	2.504	0.051
34	0.030	0.0015	2.837	0.029
38	0.017	0.0008	3.171	0.016
42	0.009	0.0005	3.505	0.009
48	0.000	0.0000	4.006	0.000

APPENDIX 11

FUNCTION MINIMIZATION
(Least Squares Fit to Experimental RTD)

Problems that require minimization or maximization of a function $F(x)$ subject to certain constraints on the search parameter x are frequently encountered in model fitting. The function minimization used in this work is called Fabonacci Search. The basic principle of the Fabonacci search is to minimize the maximum interval of uncertainty on the search parameter x (in this case, x is the vessel dispersion number N_d). This method is very powerful and widely used for unimodal functions, that is, functions having a single maximum or minimum within the given interval.

Consider the interval (a, b) containing the search locations l_i and r_i, given by,

$$l_i = b - \tau_i (b-a) \tag{A.6}$$

$$r_i = a + \tau_i (b-a) \tag{A.7}$$

It is clear that, for $\tau_i > 0.5$, l_i and r_i are left and right points in the interval equidistant from the opposite end. Then, the minimum of the function $F(x)$ lies in the interval,

$$(l_i, b), \text{ if } F(l_i) > F(r_i) \tag{A.8}$$

$$(a, r_i), \text{ if } F(l_i) < F(r_i) \tag{A.9}$$

$$(l_i, r_i), \text{ if } F(l_i) = F(r_i) \tag{A.10}$$

Since $F(l_i)$ and $F(r_i)$ may satisfy any one of the above possibilities, the new maximum interval of uncertainty is either (a, r_i), (l_i, r_i) or (l_i, b). In any one of the above cases, the interval (a,b) is reduced into a new interval (a_i, b_i). The quantity τ_i is given by,

$$\tau_i = \frac{F_{n-i-1}}{F_{n-i}}, \quad i = 0, 1, 2, \cdots \tag{A.11}$$

$$\tau_{n-2} = \frac{1 \pm \epsilon}{2} \tag{A.12}$$

$$F_0 = F_1 = 1,\ F_{j+1} = F_j + F_{j-1},\quad j = 1,2,\cdots \tag{A.13}$$

The quantity ϵ is arbitrarily small and can be set to zero. From equations (A.12) and (A.13), it follows that,

$$(b_i - a_i) = \frac{F_{n-1}}{F_n}(b-a) \tag{A.14}$$

In each interval reduction step, a single function evaluation is required except the first where two searches have to be made in the interval (a, b). Thus, with n function evaluations, (n-1) reduction steps are executed. From equation (A.14), the final interval is,

$$b_{n-1} - a_{n-1} = \frac{b-a}{F_n} \tag{A.15}$$

In general for n=21, the interval (b, a) is reduced to 0.000056(b-a). The following program written in FORTRAN is to fit the experimental RTD to the numerical solution to axial dispersion model (closed-closed boundaries) using Fabonacci search to minimize the sum of the deviations between experimental RTD and model RTD. The search parameter is N_d. Similar programs are available for fitting experimental data to the other solutions of the axial dispersion model, the tanks-in-series model, and the backflow compartment model.

```
C
C       THIS PROGRAM SOLVES THE AXIAL DISPERSION
C       MODEL USING FINITE DIFFERENCE METHOD AND
C       FITS IT TO THE EXPERIMENTAL DATA AND
C       ESTIMATES THE VESSEL DISPERSION NUMBER
C       USING FABONACCI SEARCH
C       PROGRAM: numerfit.for
C
C       parameter definitions:
C
C       M       : number of data points
C       DL      : vessel dispersion number
C       X       : to be searched  X=DL
C       PUL     : upper limit of DL
C       PLL     : lower limit of DL
C       SSD     : sum of squares of deviations
C       NSM     : maximum number of searches
C
        IMPLICIT REAL(A-Z)
        INTEGER I,J,K,M,NSM
        COMMON /RTD/ T(100),EEXP(100),EMODEL(100),M
        DIMENSION T1(100),Y(100)
        OPEN (1, FILE='A:RTD4.PRN')
        OPEN (2, FILE='A:DRTD4.PRN')
        NSM=20
        M=51
        PUL=1.2
        PLL=0.6
        READ (1,*) (Y1,Y2,T1(I),Y(I),I=1,M)
C
C       LINEAR INTERPOLATION
C
        DO 10 K=1,70
        T(K)=0.05*K
        DO 5 I=1,M-1
        IF (T1(I).LT.T(K)) THEN
        IF (T1(I+1).GT.T(K)) THEN
        EEXP(K)=Y(I)+(Y(I+1)-Y(I))/(T1(I+1)-T1(I))*(T(K)-T1(I))
        WRITE(*,*) K,T(K),EEXP(K)
        PAUSE
        WRITE (*,4)
4       FORMAT (20X,'WORKING ------ WAIT')
        ENDIF
        ENDIF
5       CONTINUE
10      CONTINUE
C
C       EEXP(20)=EEXP(21)/2+EEXP(19)/2.0
C
C       using Fibonacci search routine
C
```

```
      CALL FIBO(NSM,PUL,PLL,X,RSSD)
      WRITE (2,20) (T(I),EEXP(I),EMODEL(I),I=1,70)
20    FORMAT (5X,3(F12.8,5X))
      WRITE (*,30) RSSD
      WRITE (2,30) RSSD
30    FORMAT (25X,'RSSD  =',F12.8)
      WRITE (*,40) X
      WRITE (2,40) X
      PAUSE
40    FORMAT (10X,'DISPERSION NUMBER  =',F12.8)
      CLOSE(1)
      CLOSE(2)
      STOP
      END
C
C     function minimization by FIBONACCI search
C
C     NSM    : NUMBER OF SEARCHES
C     X      : DISPERSION NUMBER TO BE SEARCHED
C     BETA   : VALUE OF OBJECTIVE FUNCTION
C
      SUBROUTINE FIBO(NSM,XUL,XLL,X,BETA)
      IMPLICIT REAL(A-Z)
      INTEGER I,J,K,NSM,NP1,JFLAG,ITER
      DIMENSION F(25),TAU(25)
      NP1=NSM+1
C     generate FIBONACCI number F(I)
      F(1)=1.0
      F(2)=1.0
      DO 20 I=3,NP1
20    F(I)=F(I-1)+F(I-2)
      DO 30 I=1,NSM
      J=NP1-I
30    TAU(I)=F(J)/F(J+1)
      ITER=0
      JFLAG=3
40    DIFF=XUL-XLL
      IF (ITER.GT.NSM) GOTO 120
      GOTO (50,60,70), JFLAG
70    ITER=1
50    XP=XUL-TAU(ITER)*DIFF
      FUNL=OBJFUN(XP)
      IF (JFLAG.EQ.1) GOTO 80
60    XP=XLL+TAU(ITER)*DIFF
      FUNU=OBJFUN(XP)
80    ITER=ITER+1
      IF (FUNL.LE.FUNU) GOTO 100
      XLL=XUL-TAU(ITER-1)*DIFF
      FUNL=FUNU
      IF (JFLAG.LT.2) GOTO 90
      X=XP
```

```
      BETA=FUNU
90    JFLAG=2
      GOTO 40
100   XUL=XLL+TAU(ITER-1)*DIFF
      FUNU=FUNL
      IF (JFLAG.EQ.2) GOTO 110
      X=XP
      BETA=FUNL
110   JFLAG=1
      GOTO 40
120   RETURN
      END
C
C     subprogram to evaluate the objective function
C     residual sum of squares of the deviations between
C     experimental RTD and that calculated by the model
C
      FUNCTION OBJFUN(X)
      IMPLICIT REAL(A-Z)
      INTEGER I,J,K,M,N,M1,M2
      COMMON /RTD/ T(100),EEXP(100),EMODEL(100),M
      DIMENSION E(201),E0(201),F(4001)
C
C     parameter definitions
C
C     M2    : NUMBER OF THE SECTIONS FOR A TOTAL LENGTH, L
C     DX    : WIDTH OF EACH SECTION
C     DT    : TIME INTERVAL < 0.001
C     X     : VESSEL DISPERSION NUMBER
C     A,B,C : CONSTANTS MUST BE NONNEGATIVE
C
      M1=21
      M2=M1-1
      DX=1.0/FLOAT(M2)
      DT=0.001
      N=3500
      A=X*DT/DX/DX+DT/DX/2.0
      B=1-2.0*X*DT/DX/DX
      C=X*DT/DX/DX-DT/DX/2.0
      DO 40 I=1,M1
      E0(I)=0.0
      E(I)=0.0
40    CONTINUE
      DO 60 J=1,N
      IF (J.EQ.1) THEN
      E(1)=DX*M/(DX+X)
      ELSE
      E(1)=X*E0(2)/(DX+X)
      ENDIF
      DO 50 I=2,M2
      E(I)=A*E0(I-1)+B*E0(I)+C*E0(I+1)
```

```
50      CONTINUE
        E(M1)=E0(M2)
        DO 55 I=1,M1
        E0(I)=E(I)
55      CONTINUE
        F(J)=E(M1)
60      CONTINUE
        SUM=0.0
        DO 70 J=1,N
        SUM=SUM+F(J)*DT
70      CONTINUE
        DO 80 J=1,N
        IF (J.EQ.J/50*50) THEN
        EMODEL(J/50)=F(J)/SUM
        ENDIF
80      CONTINUE
C
        RESIDU=0.0
        DO 100 I=1,70
        RESIDU=RESIDU+(EEXP(I)-EMODEL(I))**2
100     CONTINUE
        WRITE (*,101) X
101     FORMAT (15X,'Nd =',D20.8)
        WRITE (*,102) RESIDU
102     FORMAT (15X,'RESIDU =',D20.8)
        OBJFUN=RESIDU
        RETURN
        END
```

Appendix 12

COMPUTER DATA ACQUISITION PROGRAM

A computer data acquisition system (Figure 5.21) was used to measure radial local gas holdup profiles and to determine liquid RTD. The following the data acquisition program written in QuickBASIC can be modified for various purposes. The program was compiled into DOS executable software.

```
'=========================================
'       DATA ACQUISITION PROGRAM (DT2801+RELAY)
'       written by MANQIU XU used for column
'       studies. The total channels are 20,
'       and can be modified for various studies
'                       McGill University
'               November, 1988 (gas20.bas)
'=========================================
'       program identification
'=========================================
```

```
        DECLARE SUB delay (ti)
        CLS : SCREEN 2
        DIM gain(4)
        LINE (210, 90)-(430, 120), , B, &HCCCC
        LOCATE 13, 30: PRINT "Data Acquisition Program"
        LOCATE 14, 38: PRINT "Manqiu Xu"
        LOCATE 15, 38: PRINT "Nov. 1988"
'=======================================
'       input A/D board operation conditions
'=======================================
        CLS
        LOCATE 8, 25: PRINT "for one hour test, the number"
        LOCATE 9, 28: PRINT "of conversions is 400"
        LINE (60, 83)-(550, 132), , B, &HCCCC
        LINE (95, 83)-(95, 132), , , &HCCCC
        LINE (430, 83)-(430, 132), , , &HCCCC
        LOCATE 10, 55: PRINT DATE$
        LOCATE 12, 10: PRINT "1"
30      LOCATE 12, 15: PRINT "Enter A/D Gain Code (0,1,2 or 3)"
        ADGAIN = 0
        LOCATE 12, 56: PRINT ADGAIN
        IF ADGAIN > 3 THEN GOTO 30
        ADCHANNEL = 0
        LOCATE 13, 10: PRINT "2"
        LOCATE 13, 15: PRINT "Enter the Total Loops to Be Done"
        NCONVERSIONS# = 10
        LOCATE 13, 56: PRINT NCONVERSIONS#
        LOCATE 14, 10: PRINT "3"
        RELAYS# = 20
        LOCATE 14, 15: PRINT "Enter the Total Channels of Relay"
        LOCATE 14, 56: PRINT RELAYS#
        LOCATE 15, 10: PRINT "4"
        LOCATE 15, 15: PRINT "The Time Interval between Each Sample"
        ti = 3
        LOCATE 15, 56: PRINT ti
        LOCATE 16, 10: PRINT "3"
        LOCATE 16, 15: PRINT "The Time Interval between Each Scan"
        TT# = 5
        LOCATE 16, 56: PRINT TT#
'=======================================
'       start A/D process or end program
'=======================================
        LOCATE 23, 35: INPUT "Enter Y to Start Reading A/D  ", y$
        IF (y$ = "y" OR y$ = "Y") THEN GOTO 20
        CLS : LOCATE 12, 25: PRINT "User Terminate the Program"
        END
20      LOCATE 25, 36: INPUT "Enter Data File Name  ", ne$
        CLS : SCREEN 2
'=======================================
'       graphics display 3 channels
'=======================================
        START.TIME# = 0
        END.TIME# = NCONVERSIONS# * (ti * RELAYS# + TT#)
        LOCATE 3, 32: PRINT "data file:"
        LOCATE 3, 43: PRINT ne$
        LINE (230, 30)-(630, 150), , B
```

```
        LOCATE 4, 28: PRINT "5"
        LOCATE 19, 28: PRINT "0"
        LOCATE 7, 28: PRINT "4": LINE (228, 54)-(232, 54)
        LOCATE 10, 28: PRINT "3": LINE (228, 78)-(232, 78)
        LOCATE 13, 28: PRINT "2": LINE (228, 102)-(232, 102)
        LOCATE 16, 28: PRINT "1": LINE (228, 126)-(232, 126)
        LINE (628, 54)-(632, 54)
        LINE (628, 78)-(632, 78)
        LINE (628, 102)-(632, 102)
        LINE (628, 126)-(632, 126)
        LOCATE 2, 6: PRINT "1"
        LOCATE 3, 6: PRINT "2"
        LOCATE 4, 6: PRINT "3"
        LOCATE 5, 6: PRINT "4"
        LOCATE 6, 6: PRINT "5"
        LOCATE 7, 6: PRINT "6"
        LOCATE 8, 6: PRINT "7"
        LOCATE 9, 6: PRINT "8"
        LOCATE 10, 6: PRINT "9"
        LOCATE 11, 6: PRINT "10"
        LOCATE 12, 6: PRINT "11"
        LOCATE 13, 6: PRINT "12"
        LOCATE 14, 6: PRINT "13"
        LOCATE 15, 6: PRINT "14"
        LOCATE 16, 6: PRINT "15"
        LOCATE 17, 6: PRINT "16"
        LOCATE 18, 6: PRINT "17"
        LOCATE 19, 6: PRINT "18"
        LOCATE 20, 6: PRINT "19"
        LOCATE 21, 6: PRINT "20"
        LOCATE 20, 30: PRINT "0"
        FOR i = 1 TO 4
        LINE ((230 + 80 * i), 148)-((230 + 80 * i), 152)
        NEXT i
        FOR i = 1 TO 4
        LINE ((230 + 80 * i), 28)-((230 + 80 * i), 32)
        NEXT i
        LOCATE 20, 75: PRINT END.TIME#
        LOCATE 21, 50: PRINT "time(seconds)"
'=========================================
'       dimensions the arrays
'=========================================
        DIM LOW(NCONVERSIONS#, RELAYS#), HIGH(NCONVERSIONS#, RELAYS#)
        DIM data.volts#(NCONVERSIONS#, RELAYS#)
        DIM time.seconds#(NCONVERSIONS#, RELAYS#)
```

```
'=========================================
'       initializing the DT2801 board
'=========================================
        BASE.ADDRESS = &H2EC
        COMMAND.REGISTER = BASE.ADDRESS + 1
        STATUS.REGISTER = BASE.ADDRESS + 1
        DATA.REGISTER = BASE.ADDRESS
        COMMAND.WAIT = &H4
        WRITE.WAIT = &H2
        READ.WAIT = &H5
        CCLEAR = &H1
        CADIN = &HC
        CSTOP = &HF
        BASE.FACTOR# = 4096
        RANGE.VOLTS# = 10
        gain(1) = 1
        gain(2) = 2
        gain(3) = 4
        gain(4) = 8
'=========================================
'       initializing the relay
'=========================================
        TIME$ = "00:00:00"
        OUT &H303, &H80
'=========================================
'       start the loops
'=========================================
        FOR lps = 1 TO NCONVERSIONS#
        FOR lp = 1 TO RELAYS#
        LOCATE 3, 65: PRINT TIME$
        IF lp > 8 AND lp < 17 GOTO 11
        IF lp > 16 GOTO 15
        i = 2 ^ (lp - 1)
        OUT &H301, 0
        OUT &H300, i
        GOTO 22
11      OUT &H300, 0
        i = 2 ^ (lp - 9)
        OUT &H302, i
        GOTO 22
15      OUT &H302, 0
        i = 2 ^ (lp - 17)
        OUT &H301, i
22      CALL delay(3)           'pause for 3 seconds
'=========================================
'       stop and clear the A/D board
'=========================================
        OUT COMMAND.REGISTER, CSTOP
        TEMP = INP(DATA.REGISTER)
        WAIT STATUS.REGISTER, WRITE.WAIT, WRITE.WAIT
        WAIT STATUS.REGISTER, COMMAND.WAIT
        OUT COMMAND.REGISTER, CCLEAR
'=========================================
'       write command byte into
'       command register
'=========================================
```

```
        WAIT STATUS.REGISTER, WRITE.WAIT, WRITE.WAIT
        WAIT STATUS.REGISTER, COMMAND.WAIT
        OUT COMMAND.REGISTER, CADIN
'
'=========================================
'       write A/D gain byte into
'       data in register
'=========================================
        WAIT STATUS.REGISTER, WRITE.WAIT, WRITE.WAIT
        OUT DATA.REGISTER, ADGAIN
'=========================================
'       write A/D channel byte into
'       data in register
'=========================================
        WAIT STATUS.REGISTER, WRITE.WAIT, WRITE.WAIT
        OUT DATA.REGISTER, ADCHANNEL
'=========================================
'       read A/D high and low byte
'       from data in register
'=========================================
        WAIT STATUS.REGISTER, READ.WAIT
        LOW(lps, lp) = INP(DATA.REGISTER)
        WAIT STATUS.REGISTER, READ.WAIT
        HIGH(lps, lp) = INP(DATA.REGISTER)
'=========================================
'       check the error register
'=========================================
        WAIT STATUS.REGISTER, WRITE.WAIT, WRITE.WAIT
        WAIT STATUS.REGISTER, COMMAND.WAIT
        STATUS = INP(STATUS.REGISTER)
        IF (STATUS AND &H80) THEN GOTO 100
'=========================================
'       calculate and display the D/A
'       reading in volts
'=========================================
        DATA.VALUE# = HIGH(lps, lp) * 256 + LOW(lps, lp)
        FACTOR# = (10 / BASE.FACTOR#) / gain(ADGAIN + 1)
        VOLTS# = DATA.VALUE# * FACTOR#
        data.volts#(lps, lp) = VOLTS# * 2 - (10 / gain(ADGAIN + 1))
        time.seconds#(lps, lp) = TIMER
        xx = 230 + INT(400 / END.TIME# * time.seconds#(lps, lp) + .5)
        yy = 150 - INT(24 * data.volts#(lps, lp) + .5)
        LINE (xx, yy)-(xx + 1, yy)
        IF lp = 1 THEN
        LOCATE 2, 12: PRINT USING "##.####"; data.volts#(lps, 1)
        ELSEIF lp = 2 THEN
        LOCATE 3, 12: PRINT USING "##.####"; data.volts#(lps, 2)
        ELSEIF lp = 3 THEN
        LOCATE 4, 12: PRINT USING "##.####"; data.volts#(lps, 3)
        ELSEIF lp = 4 THEN
        LOCATE 5, 12: PRINT USING "##.####"; data.volts#(lps, 4)
        ELSEIF lp = 5 THEN
        LOCATE 6, 12: PRINT USING "##.####"; data.volts#(lps, 5)
        ELSEIF lp = 6 THEN
        LOCATE 7, 12: PRINT USING "##.####"; data.volts#(lps, 6)
        ELSEIF lp = 7 THEN
```

```
            LOCATE 8, 12: PRINT USING "##.####"; data.volts#(lps, 7)
            ELSEIF lp = 8 THEN
            LOCATE 9, 12: PRINT USING "##.####"; data.volts#(lps, 8)
            ELSEIF lp = 9 THEN
            LOCATE 10, 12: PRINT USING "##.####"; data.volts#(lps, 9)
            ELSEIF lp = 10 THEN
            LOCATE 11, 12: PRINT USING "##.####"; data.volts#(lps, 10)
            ELSEIF lp = 11 THEN
            LOCATE 12, 12: PRINT USING "##.####"; data.volts#(lps, 11)
            ELSEIF lp = 12 THEN
            LOCATE 13, 12: PRINT USING "##.####"; data.volts#(lps, 12)
            ELSEIF lp = 13 THEN
            LOCATE 14, 12: PRINT USING "##.####"; data.volts#(lps, 13)
            ELSEIF lp = 14 THEN
            LOCATE 15, 12: PRINT USING "##.####"; data.volts#(lps, 14)
            ELSEIF lp = 15 THEN
            LOCATE 16, 12: PRINT USING "##.####"; data.volts#(lps, 15)
            ELSEIF lp = 16 THEN
            LOCATE 17, 12: PRINT USING "##.####"; data.volts#(lps, 16)
            ELSEIF lp = 17 THEN
            LOCATE 18, 12: PRINT USING "##.####"; data.volts#(lps, 17)
            ELSEIF lp = 18 THEN
            LOCATE 19, 12: PRINT USING "##.####"; data.volts#(lps, 18)
            ELSEIF lp = 19 THEN
            LOCATE 20, 12: PRINT USING "##.####"; data.volts#(lps, 19)
            ELSEIF lp = 20 THEN
            LOCATE 21, 12: PRINT USING "##.####"; data.volts#(lps, 20)
            END IF
            LOCATE 23, 45: PRINT "Press S to stop A/D process"
            IF (INKEY$ = "s" OR INKEY$ = "S") THEN GOTO 85
            NEXT lp
80          NEXT lps
'===========================================
'           compute the average values
'===========================================
            FOR i = 1 TO NCONVERSIONS#
            data1# = data1# + data.volts#(i, 1)
            data2# = data2# + data.volts#(i, 2)
            data3# = data3# + data.volts#(i, 3)
            data4# = data4# + data.volts#(i, 4)
            data5# = data5# + data.volts#(i, 5)
            data6# = data6# + data.volts#(i, 6)
            data7# = data7# + data.volts#(i, 7)
            data8# = data8# + data.volts#(i, 8)
            data9# = data9# + data.volts#(i, 9)
            data10# = data10# + data.volts#(i, 10)
            data11# = data11# + data.volts#(i, 11)
            data12# = data12# + data.volts#(i, 12)
            data13# = data13# + data.volts#(i, 13)
            data14# = data14# + data.volts#(i, 14)
            data15# = data15# + data.volts#(i, 15)
            data16# = data16# + data.volts#(i, 16)
            data17# = data17# + data.volts#(i, 17)
            data18# = data18# + data.volts#(i, 18)
            data19# = data19# + data.volts#(i, 19)
            data20# = data20# + data.volts#(i, 20)
```

```
        NEXT i
        LOCATE 2, 12: PRINT USING "##.####"; data1#
        LOCATE 3, 12: PRINT USING "##.####"; data2#
        LOCATE 4, 12: PRINT USING "##.####"; data3#
        LOCATE 5, 12: PRINT USING "##.####"; data4#
        LOCATE 6, 12: PRINT USING "##.####"; data5#
        LOCATE 7, 12: PRINT USING "##.####"; data6#
        LOCATE 8, 12: PRINT USING "##.####"; data7#
        LOCATE 9, 12: PRINT USING "##.####"; data8#
        LOCATE 10, 12: PRINT USING "##.####"; data9#
        LOCATE 11, 12: PRINT USING "##.####"; data10#
        LOCATE 12, 12: PRINT USING "##.####"; data11#
        LOCATE 13, 12: PRINT USING "##.####"; data12#
        LOCATE 14, 12: PRINT USING "##.####"; data13#
        LOCATE 15, 12: PRINT USING "##.####"; data14#
        LOCATE 16, 12: PRINT USING "##.####"; data15#
        LOCATE 17, 12: PRINT USING "##.####"; data16#
        LOCATE 18, 12: PRINT USING "##.####"; data17#
        LOCATE 19, 12: PRINT USING "##.####"; data18#
        LOCATE 20, 12: PRINT USING "##.####"; data19#
        LOCATE 21, 12: PRINT USING "##.####"; data20#
'=============================================
'       save data into disk file
'=============================================
85      LOCATE 24, 42: INPUT "Do you want to save the data"; y$
        IF (y$ = "Y" OR y$ = "y") THEN GOTO 90
        GOTO 110
90      LOCATE 25, 42: PRINT "Data File Name: "; ne$
        OPEN ne$ FOR OUTPUT AS #1
        FOR lps = 1 TO NCONVERSIONS#
        PRINT #1, USING "##.####"; data.volts#(lps, 1);
        PRINT #1, USING "##.####"; data.volts#(lps, 2);
        PRINT #1, USING "##.####"; data.volts#(lps, 3);
        PRINT #1, USING "##.####"; data.volts#(lps, 4);
        PRINT #1, USING "##.####"; data.volts#(lps, 5);
        PRINT #1, USING "##.####"; data.volts#(lps, 6);
        PRINT #1, USING "##.####"; data.volts#(lps, 7);
        PRINT #1, USING "##.####"; data.volts#(lps, 8);
        PRINT #1, USING "##.####"; data.volts#(lps, 9);
        PRINT #1, USING "##.####"; data.volts#(lps, 10);
        PRINT #1, USING "##.####"; data.volts#(lps, 11);
        PRINT #1, USING "##.####"; data.volts#(lps, 12);
        PRINT #1, USING "##.####"; data.volts#(lps, 13);
        PRINT #1, USING "##.####"; data.volts#(lps, 14);
        PRINT #1, USING "##.####"; data.volts#(lps, 15);
        PRINT #1, USING "##.####"; data.volts#(lps, 16);
        PRINT #1, USING "##.####"; data.volts#(lps, 17);
        PRINT #1, USING "##.####"; data.volts#(lps, 18);
        PRINT #1, USING "##.####"; data.volts#(lps, 19);
        PRINT #1, USING "##.####"; data.volts#(lps, 20)
        NEXT lps
        CLOSE
        GOTO 110
'=============================================
'       print error message
'=============================================
```

```
100     CLS
        PRINT
        PRINT "error"
        PRINT
110     END
'=======================================================
'       subroutine for time delay
'=======================================================
        SUB delay (ti) STATIC
        CONST SecondsInday = 24& * 60& * 60&
        LoopFinish = TIMER + ti
        IF LoopFinish > SecondsInday THEN
        LoopFinish = LoopFinish - SecondsInday
        DO WHILE TIMER > LoopFinish
        LOOP
        END IF
        DO WHILE TIMER < LoopFinish
        LOOP
        END SUB
```

APPENDIX 13

COMPUTER DATA PROCESSING AND REDUCTION PROGRAM

The following program first converts the voltage-time signal into KCl concentration vs. time data, then calculate the mass of KCl injected from the data. Then, the mean residence time and variance are computed. At last, the data file is reduced to about 100 points.

```
C       ************************************************
C       RTD DATA PROCESSING AND REDUCTION PROGRAM
C               name: datapro2.For
C               original datafile: a:old.Prn
C               new datafile name: a:new.Prn
C       1.      Transfer voltage signal into
C               concentration as a funcion of time
C       2.      Compute the dimensionless rtd data
C       3.      Compute the mean residence time
C       4.      Compute the dimensionless variance about
C               the mean residence time
C       5.      Check the mass balance
C               parameter definitions:
C       S(I),T(I),TH(I)  time,sec.,min.,dimensionless
C       V(I)             voltage signal
C       C(I)             normalised concentration
C       E(I)             dimensionless rtd
```

```
C       TAU             mean residence time
C       VW              voltage signal of water only
C       SIGMA1          variance about the mean
C       SIGMA           dimensionless variance
C       AREA1           mass of tracer injected
C       AREA            mass balance, the integration
C       FACTOR          voltage to KCl concentration conversion
C       M               number of total data points
C       QL              measured liquid volumetric flowrate
C       ***************************************************
C
        IMPLICIT REAL*8(A-Z)
        INTEGER I,J,K,M
        DIMENSION T(500),TH(500),D(500),C(500),E(500)
        OPEN (1,FILE='A:OLD.PRN')
        OPEN (2,FILE='A:NEW.PRN')
        M=500
        FACTOR=0.050
        READ (1,*) (T(I),V(I),I=1,M)
        DO 5 I=1,M
        C(I)=V(I)*FACTOR
        T(I)=T(I)/60
5       CONTINUE
C
C       estimate the mean residence time TAU
C
        D(M)=10.0
        DO 10 I=1,M-1
        D(I)=T(I+1)-T(I)
10      CONTINUE
        SUM1=0.0D0
        SUM2=0.0D0
        SUM3=0.0D0
        DO 20 I=1,M
        SUM1=SUM1+C(I)*D(I)
        SUM2=SUM2+C(I)*T(I)*D(I)
        SUM3=SUM3+C(I)*T(I)*T(I)*D(I)
20      CONTINUE
        AREA1=SUM1*QL
        TAU=SUM2/SUM1
        SIGMA1=SUM3/SUM1-TAU*TAU
        SIGMA=SIGMA1/TAU/TAU
        DO 25 I=1,M
        C(I)=C(I)/SUM1
25      CONTINUE
C
C       compute the dimensionless RTD
C
        DO 30 I=1,M
        E(I)=TAU*C(I)
        TH(I)=T(I)/TAU
30      CONTINUE
C
C       check mass balance
C
        AREA=0.0D0
```

```
      DO 40 I=1,M
      AREA=AREA+E(I)*D(I)/TAU
40    CONTINUE
C
      WRITE (*,50) AREA1
      WRITE (*,60) TAU
      WRITE (*,70) SIGMA
      WRITE (*,80) AREA
50    FORMAT (15X,'THE TOTAL MASS OF TRACER =',F20.8)
60    FORMAT (15X,'THE MEAN RESIDENCE TIME =',F20.8)
70    FORMAT (15X,'THE DIMENSIONLESS VARIANCE =',F20.8)
80    FORMAT (15X,'THE RTD MASS BALANCE =',F20.8)
C
C     data reduction by 50
C
      DO 90 I=1,M
      IF (M.EQ.M/50*50 ) THEN
      WRITE (2,100) TH(I),E(I)
      END IF
90    CONTINUE
100   FORMAT (1X,2(F8.4,2X))
110   CLOSE(1)
      CLOSE(2)
      STOP
      END
```